PROXIMAL AND REMOTE SENSING FOR EARLY DETECTION AND ASSESSMENT OF HERBICIDE DRIFT DAMAGE ON COTTON CROPS

A Thesis submitted by

Luz Angelica Suarez Cadavid

BEng. Land Surveying, M. Adv. Mult. Cadastre

For the award of

Doctor of Philosophy

2017

Abstract

The herbicide 2,4-dichlorophenoxyacetic acid (2,4-D) is one of the most successful selective herbicides used in agriculture to control broadleaf weeds. Unfortunately, cotton crops are highly susceptible to 2,4-D, and they are often damaged by the off-target movement of the active ingredient when sprayed as a herbicide on surrounding farms. This action, referred to as herbicide drift, affects the cotton industry every season, causing losses of millions of dollars. Although the economic repercussions on the industry are high, the traditional (visual) assessment of damage is often imprecise and inaccurate. Crop sensing tools can offer alternative and reliable methods to overcome the typical limitations of visual assessments by providing accurate estimations of crop performance. The aim of this research project was to assess the capabilities of crop sensing techniques of providing spatial and quantitative information of cotton yield after being affected by 2,4-D herbicide drift. This information is valuable to agronomic planners for evaluating their crop management strategies in order to maximise cotton production while safeguarding the environment in the affected area.

The research area was located in a cotton-growing region in Jondaryan, Queensland, Australia. Two study cases and three remote/proximal sensing approaches were tested. The first study case consisted of controlled doses to simulate accidental exposure to 2,4-D, where three doses (D) and three timing of exposures (S) were examined at four different dates after the exposure (DAE): 2, 7, 14 and 28 DAE. In this case, a hyperspectral sensor and a terrestrial laser scanner (TLS) were evaluated to assess their ability to predict yield loss, dose and canopy structure variability. The second case examined the potential capabilities of satellite imagery for yield loss assessment in an uncontrolled exposure of cotton crops to 2,4-D. For this case, several multispectral (Landsat 8 Operational Land Imager - OLI) images were analysed and a comprehensive approach was developed to overcome the potential limitation of moderate resolution imagery at the field level.

The controlled case revealed that hyperspectral data can be used to predict yield loss with high accuracy ($R^2 = 0.88$) regardless of the timing of exposure and dose, and that 7 DAE and 28 DAE (RMSECV: 2.6 bales/ha; $R^2 = 0.88$ and RMSECV: 3.2 bales/ha;

R^2 = 0.84, respectively) were the best times for data collection purposes. The main difference in the model performance between the best (7 DAE) and the worst (14 DAE) prediction model was the inclusion of the NIR range, as the 14 DAE was the only model with no significant wavelengths in this range.

Through this case, it was possible to better understand how the internal changes of the contaminated leaves, that is photosynthesis, stomatal conductance and hormone contents, influenced their spectral response and the lint quality of the cotton. Most of the variables analysed in this study manifested a significant relationship with hyperspectral data (p-value < 0.05). The harvested yield was severely affected by the herbicide, with losses recorded as high as 98%, while the fibre quality remained relatively unaffected. The prediction capabilities for the simulated dose were also tested by implementing Canonical Powered PLS (CPPLS) and Sparse PLS Discriminant Analysis (sPLS-DA). High accuracies (> 70%) were obtained regardless of the method, D or S. However, the timing of exposure (S) resulted in being a determinant to improve the classification accuracy to more than 90%.

The analysis of laser scanner-derived data provided accurate information about the canopy height and canopy volume that could be strongly correlated (r > 0.88) with yield at different times of assessment (2 DAE, 7 DAE and 14 DAE). High R^2 (> 0.90) between measured and estimated canopy height validates the height values estimated from the TLS-derived data. Furthermore, the weak relationship (R^2 =0.39, p-value > 0.05) between point density and estimated canopy volume provided an insight that the approach implemented to estimate cotton canopy height and volume overcame the reported limitations of terrestrial laser scanners in the field.

The uncontrolled case (i.e. Landsat 8 imagery) tested six different dates for optimal data collection purposes. The results demonstrated that traditional vegetation indices (VI) and individual multispectral bands were incapable of predicting yield in neither affected nor unaffected cotton areas (R^2 < 0.27). However, PLS-R models optimised the information provided by the multispectral bands. As a result, the R^2 increased, in some cases, by more than 60%. From the PLS- model results, it was determined that one week after the exposure was the best time for the prediction of yield in affected areas (RMSEP = 1.19 bales/ha and R^2 = 0.60). Satellite imagery could be then implemented to support targeted monitoring programs in 2,4-D-injured areas.

The technologies implemented in this study were proven to be reliable for damage assessment after an accidental spray drift by accurately predicting yield and dose and also by estimating canopy structure variables strongly correlated with yield in 2,4-D-affected areas. These comprehensive analytical approaches also provided information on temporal windows for optimal data collection after an incident, and also on less-recommended dates for the same purpose. These methods indicated an optimal window between seven and 14 days, or more than 28 days after the exposure, for the prediction of damage. However, as soon as two days after the cotton plant was exposed, hyperspectral measurements and TLS-derived data recorded significant differences in comparison with unaffected control plants.

Certification of thesis

This thesis, ideas, experimental work, results, analysis, conclusions and recommendations are entirely the work of *Luz Angelica Suarez Cadavid* except where otherwise acknowledged. The work is original and has not previously been submitted for any other award, except where acknowledged.

Student and supervisors signatures of endorsement are held at USQ.

Prof. Armando Apan

Principal Supervisor

Dr. Troy Jensen

Associate Supervisor

Publications and awards

Peer-review journal papers

Suarez, L. A., Apan, A., & Werth, J. (2016). Hyperspectral sensing to detect the impact of herbicide drift on cotton growth and yield. ISPRS *Journal of Photogrammetry and Remote Sensing*, 120, 65-76. doi: 10.1016/j.isprsjprs.2016.08.004.

Suarez, L. A., Apan, A., & Werth, J. (2017). Detection of phenoxy herbicide dosage in cotton crops through the analysis of hyperspectral data. IJRS *International Journal Remote Sensing*, 8(23), 6528-6553. doi:10.1080/01431161.2017.1362128.

Conference presentations

Suarez, L. A., Apan, A., Werth, J. Neale, T., & Jensen, T. (2015). Discrimination of Herbicide Drift Damage in Cotton Crops under Varying Stages of Growth and Chemical Dosages. *In: 2nd Australian Cotton Research Conference, 8-10 September 2015*. Toowoomba, University of Southern Queensland. Australia.

Suarez, L. A., Apan, A., & Werth, J. (2016). Prediction of Yield Loss in Cotton Crops Caused by Herbicide Drift Through the Analysis of Hyperspectral Data. *In: World Cotton Research Conference, 2-6 May 2016*. Goiás, Convention Center. Brazil.

Suarez, L. A., & Apan, A. (2017). Crop sensing technologies for herbicide drift assessment in cotton. *In: 3rd Australian Cotton Research Conference, 5-7 September 2017*. Canberra, CSIRO Discovery. Australia

Grants

Project "USQ1404 Quantifying and Mapping the Impacts of Herbicide Drift on Cotton (Non-Target Crop)" (2014-2017) founded by the Cotton Research and Development Corporation (CRDC).

Travel, Conference & Scientific Exchange Participation. *The World Cotton Conference 6 – Goiania Brazil 2016*, funded by the Cotton Research and Development Corporation (CRDC). Presentation titled: "Prediction of Yield Loss in Cotton Crops Caused by Herbicide Drift through the Analysis of Hyperspectral Data".

Acknowledgments

I dedicate this work to my beloved kids, Juan Felipe and Lucianna, and to my husband, Luis Fernando. There are no words to express my gratitude for their infinite love and patience. I also dedicate this work to my parents, Jorge and Alicia, whom from the distance sent me all their love.

To my supervisor Professor Armando Apan, for his teachings and committed dedication to this research project. For his guidance and wisdom and his sincere words when most needed.

To my family (Jorge, Alicia, Cesar and Liliana) for believing in me and to my "compadres" Yelitza and Ray, and to my friends Mafe and Yira (and their respective families) for their support.

Profound gratitude to Jeff Werth, Michelle Keenan and Luke Szaban for their altruistic and generous training and support. Without them, the story of this research project would be completely different.

Special thanks to my supervisory team Professor Armando Apan, Dr Troy Jensen, and Tim Neale for their ideas, support and opportune feedback. Also, thanks to Dr Sir Anthony Done for proofreading this thesis.

To the University of Southern Queensland (USQ) and to the Queensland Department of Agriculture and Fisheries (QDAF) for providing research facilities and equipment, to Professor John Ross from University of Tasmania (UTAS) for facilitating the hormone analysis, and to the farmer, Mac Baartz, for allowing me to expose part of his cotton crops to 2,4-D, and for providing land and services for growing the trials.

To the Cotton Research and Development Corporation (CRDC) for believing and for funding this research project and the activities related to it.

Finally, thanks to the Australian Commonwealth Government for the contribution to this research study through the Research Training Program (RTP).

THANK YOU ALL. Luz Angélica Suárez Cadavid

Table of contents

List of figures

List of tables

Abbreviations

ABA	Absicic Acid
ABARES	Australian Bureau of Agricultural and Resource Economics and Science
ABS	Australian Bureau of Statistics
APVMA	The Australian Pesticide and Veterinary Medicines Authority
BNDVI	Blue-Normalized Difference Vegetation Index
CPPLS	Canonical Powered Partial Least Square
CRDC	Cotton Research and Development Corporation
CSM	Canopy Surface Model
DAF	Department of Agriculture and Food
DDT	The Australian Cotton Industry Development and Delivery Team
DEDJTR	Department of Economic Development, Jobs, Transport and Resources
DEPI	Department of Environment and Primary Industries
g a.i	Grams of active ingredient
GNDVI	Green-Normalized Difference Vegetation Index
GRDC	Grain Research and Development Corporation
IAA	Indole Acetic Acid
ITF	Industry Task Force
kg a.i	Kilograms of active ingredient
LAI	Leaf Area Index
LiDAR	Light Detection and Ranging
NCEA	National Centre for Engineering in Agriculture
NDVI	Normalized Difference Vegetation Index
NOAA	National Oceanic and Atmospheric Administration
PCM	Precision Crop Management
PES	Pesticide Environmental Stewarding
PSM	Phase-shift method
sMC	Significant Multivariate Correlation
sPLS-DA	Spearse Partial Least Square Discriminant Analisys
TLS	Terrestrial Laser Scanner
TOF	Time-of-flight
UAV	Unmanned Aerial Vehicle
VI	Vegetation Indices

Chapter 1

INTRODUCTION

1.1. Introduction

The need for herbicide use causes several numbers of incidents of spray drift affecting non-target crops every season with consequences that vary from yield delays to yield reductions (Cowell, 2007). Furthermore, lawsuits and expensive fines may be involved, because herbicide drift events are generally considered illegal. These spray drifts can result in prohibited residues present in adjacent areas, environmental concerns, and human exposure (Clemson University Cooperative Extension, 2013b; Department of Economic Development, 2016; Rhodes et al., 2012).

Damage caused by herbicide drift on non-target crops cannot be accurately related to yield reduction by applying traditional (visual) assessments as they relay in the physical appearance of the crop without taking in consideration the recovery capabilities of the plants. Sub-lethal doses capable of causing yield loss might only be evident 2-3 weeks after the event. The time lost, between the spray drift event and the appearance of symptoms, could have been used to mitigate injuries that may affect the expected yield by properly adjusting crop management practices. In addition, traditional or visual assessment does not to supply comprehensive spatial information about the distribution and degree of the damage in the field (Cotton Australia, 2012, p. p. 4; Cowell, 2007). It would, therefore, be of value to implement new technologies capable of providing reliable information about the condition of crops exposed to, and injured by, unintentional herbicide damage. A new method of damage estimation that allows the information to be available as soon as the event happens could be of great benefit, in order to maximise the opportunity to minimise damage to the crop, as the movement and translocation of herbicides in crops is rapid (Munk et al., 2014).

Cotton crops are highly susceptible to phenoxy herbicide drifts, and particularly to 2,4-D, a herbicide widely used in other agricultural crops to control broadleaf weeds. Phenoxy herbicide drifts onto cotton still occur, despite many efforts having been

made to minimise this risk. These drifts result in industry losses of millions of dollars every season, as the assessment of damage to the cotton crop remains unreliable and the damage cannot be economically mitigated due to the lack of accurate information on degree of damage and potential yield loss.

Over the past several years, remote sensing techniques have had extensive use in agriculture (Goel, Prasher, Landry, et al., 2003; Mewes et al., 2009; Moran et al., 1997). Specifically, it has been shown that these techniques can detect changes in stressed crops following a herbicide drift incident, when external symptoms were not yet evident. Yield variability has also been estimated to a high degree of accuracy (Buehring, 2004; Henry et al., 2004). *It is therefore pertinent to test these tools to accurately and rapidly assess, quantify and detect damage caused by sub-lethal doses of 2,4-D on cotton crops*.

Recent improvements in hyperspectral, multispectral and LiDAR sensors could allow enhanced detection and assessment of such damage. The improvements also include the reduced cost of some of these technologies. There are currently multispectral satellite sensors with high spatial resolution and free access, while hyperspectral imagery is becoming commercially accessible. Similarly, LiDAR, which is highly applicable in research, is tending to become commercially available due to its enormous potential in crop structural estimations. Individually, these techniques have been shown to be precise and reliable. Hyperspectral sensors are capable of detecting changes in plant pigment (Blackburn, 2007), moisture content (Chen et al., 2011), and leaf internal structure (Martinez-Morales, 2012), all of which are potentially affected by 2,4-D herbicide drift, while multispectral satellite sensors, in addition to the benefits of hyperspectral sensors, have the capability to monitor the crop regularly and provide spatial information on yield variability (Yang et al., 2009). LiDAR scanners, on the other hand, have the ability to quantify canopy attributes, such as canopy height, percent crown cover, vegetation density and canopy volume, which are also expected to change after a herbicide drift event (Sun et al., 2017).

The proposed methodology for this study has been designed to examine different alternatives for 2,4-D damage assessment, from the reflectance-based and canopy structure perspectives. This study therefore applied different approaches to assessing damage and to documenting the internal and canopy structural changes that could

occur in the plant after a 2,4-D drift event, in order to understand how these changes are reflected in:

- the spectral response,
- the growth regulator hormones,
- the biophysical and the physiological changes, and
- yield.

Specific analyses of leaf tissues are desirable to characterise changes in the plant in relation to dosage rates of the chemical and the growth stage of the crop at the time of exposure. This is in addition to measuring physiological variables (e.g. photosynthesis and stomatal conductance) and biophysical attributes (e.g. canopy height, canopy volume and yield). The objectives proposed for this research are steps towards being able to map and quantify 2,4-D damage in cotton crops, which will help to anticipate and estimate yield loss in relation to the spectral changes and canopy variability observed over the time after exposure.

1.2. Statement of the problem

Crops are susceptible to unintentional damage caused by management practices in surrounding farms as particles of chemicals can drift or produce volatile vapours, and move through the air far from the target site. Soybean, corn or wheat can, for example, be injured by glyphosate or paraquat, while cotton can be damaged by 2,4-D, glyphosate, glufosinate, dicamba or bromoxynil (Buehring, 2004; Clemson University Cooperative Extension, 2013a; Everitt & Keeling, 2009; Henry et al., 2004; Huang & Thomson, 2010; Liu et al., 2013). Such management practices can be controlled or regulated but it is unlikely that accidents will never happen due to the difficulties encountered in controlling every factor that interferes with "good" management practices. Sensitive crops subjected to sub-lethal doses of herbicides are, in addition, at high risk of commercially significant damage as even the smallest dose can cause considerably injuries (Birch & Moree, 2004; Munk et al., 2014). All agrochemicals, including herbicides, are regulated in Australia, and some states prohibit the application of specific chemicals, as they can cause harm to humans and/or the environment (Australian Pesticides and Veterinary Medicines Authority [APVMA], 2005).

The chemical 2,4-D is a phenoxy herbicide that can be used to control broadleaf weeds species at low cost. Industries such as horticulture, rangeland and food crop systems (corn and other small grains) have widely adopted this chemical due to its high effectiveness in controlling weeds (Industry Task Force II on 2-4-D Research Data, 2013; Munk et al.). Broadleaf crops such cotton, grapevines and many tree crops are, however, affected every season by 2,4-D applied in surrounding farm systems. The Australian Pesticides and Veterinary Medicines Authority (APVMA), in an effort to find a balance between the interests of conflicting industries, and also to protect humans against potential exposure and reduce its impacts on waterways, cancelled the registration of selected 2,4-D high volatile esters (HVE). The de-registered esters have particles that produce a vapour that can drift many kilometres away from the target crop and reach susceptible systems (APVMA, 2013; Department of Economic Development, Jobs, Transport and Resources [DEDJTR], 2016). 2,4-D products still represent between 7-8% of all herbicides sales in Australia, even with this cancellation, a situation that illustrates the need for action to prevent and mitigate its impacts (APVMA, 2013).

Cotton, the summer crop most susceptible to 2,4-D, grows at the same time that this herbicide is used to control weeds in cereals during warmer months. Cotton regions in Australia are mainly located in New South Wales (NSW) and Queensland (QLD), where there are restrictions on herbicide uses, specifically to 2,4-D. However, these are only based on temperature, wind speed, size of nozzles and other specifications, which are insufficient to prevent all drift (APVMA, 2005; 2013; Cotton Australia, 2012). Genetic improvements to cotton's resistance to sub-lethal doses of 2,4-D are being investigated (Charles et al., 2007), but have so far had no practical outcome and the annual cost resulting from cotton's susceptibility to 2,4-D is very high (Cotton Australia, 2013c, 2015b; Cotton Australia & Grains Growers, 2016). There are also limitations to current ability to detect damage soon after an accident in the field. Inaccurate predictions of yield loss based on traditional visual assessments is another aspect of a group of problems that exacerbate the impacts of herbicide drifts on cotton crops claiming to the cotton industry losses of millions of dollars every season not only in Australia but around the world (Charles, 2011; Charles et al., 2007; Pimentel et al., 1998; Rhodes et al., 2012).

There is currently a lack of research exploring a method that is different from visual assessments based on external symptoms, to detect and assess the damage (yield reductions) due to 2,4-D herbicide drift on cotton crops. Relatively new remote sensing techniques have proven their potential for assessing injuries caused by other herbicides such as glyphosate, glufosinate, paraquat and many others on corn, soybean, wheat and even cotton (Buehring, 2004; Everman et al., 2008; Henry et al., 2004; Trenton, 2012). 2,4-D damage has, however, yet to be explored using those techniques. Multispectral, hyperspectral and LiDAR sensors can supply useful information about the internal structure of the leaf and canopy structure through the measurement of radiance captured in broadband or narrowband spectra, and three-dimensional (3D) readings, respectively (Hosoi & Omasa, 2009; Tian et al., 2005). Small atypical changes in radiance or canopy structure are indicative that something is happening within the plant and these sensors are able to capture such small changes. The potential applicability, accurate results, and the ability to detect small changes even if the external damage is not evident (Everman et al., 2008) are the main reasons to explore those techniques in this research study, and hopefully, resolve the problems associated with traditional assessments of crop injuries caused by herbicide drifts.

This research project addresses the question of how to detect, assess and map damage caused by 2,4-D drift over cotton crops soon after the drift has occurred, taking into consideration internal changes in the plant and their relationship with yield, spectral responses and canopy structure, using remote sensing techniques.

1.3. Significance of the study

Technological developments have impacted the way in which society interacts and resolves problems within itself. Such developments are in a continuous state of evolution but are not necessarily being utilised by all sectors of society in which they have potential benefits. This project explored different remote sensing technologies to resolve a major problem: detection and quantification of damage caused by 2,4-D herbicide drift in cotton as a non-target crop. One incentive for this project is that the technology has been available, but unused, for many decades, to potentially resolve a problem that has existed since the early 1940s (Charles et al., 2007; Price, 1998). The outcomes of this research could provide useful information to various users in the following ways:

- *Scientists* – The technical knowledge will be of value in a) improving or designing new sensors better suited to the detection of herbicide spray drift in cotton, regardless of what platform is to be implemented and b) providing a better understanding of the response of the non-target cotton plant to herbicide drifts over time.

- *Farmers* – The knowledge will be useful in a) assessing the damage caused by herbicide spray drift, for various crop management purposes, b) documenting the damage if compensation for loss is to be pursued and c) understanding when it is possible for neighbouring farms to spray with a lower risk of damage.

- *Extension agents* – The information will be useful in providing advice with regards to designing management plans, crop protection, yield optimisation, etc.

- *Other related industries* (aerial spraying companies, crop insurance, among others) – Relevant to the conduct of their particular business, e.g. awareness to better flight planning to avoid crop damage; providing an objective tool to crop loss assessors, etc.

Overall, this study is not only geared to "*improving farmers' capacity, knowledge & adoption of techniques to successfully protect the cotton crop*" (Cotton Research and Development Corporation [CRDC], 2013), but also to generating knowledge for other users contributing to the cotton industry in Australia and the entire world.

1.4. Research questions

This research project sought to answer the research questions listed below in order to supply scientific knowledge and different tools to approach the problems stated above:

a) Is it possible to detect herbicide-damaged cotton plants using hyperspectral data? What spectral bands maximise the chance of detection considering the variation in the degree of injuries at different crop growth stages? What is/are the plant variable(s) that best explains spectral variability in affected cotton?

b) Can satellite imagery accurately detect cotton crops damaged by 2,4-D herbicide drift? What spectral bands or indices will optimise detection?

c) Is it possible to detect changes in the cotton canopy caused by 2,4-D herbicide drift using LiDAR-derived metrics? Are the canopy structure variables estimated using LiDAR-derived metrics related to cotton yield?

1.5. Research aim and objectives

The aim of this study was to assess the utility of hyperspectral, multispectral and LiDAR sensors in detecting and assessing injuries or damage caused by 2,4-D herbicide drift on cotton as a non-target crop. The following specific objectives have been defined to achieve the proposed aim:

1. To understand the variability in the hyperspectral response of cotton plants affected by 2,4-D drift, in varying doses and at different crop growth stages.

2. To assess the accuracy of multispectral satellite imagery in detecting herbicide drift damage to cotton crops.

3. To identify and assess the effect of 2,4-D on the cotton canopy using terrestrial LiDAR sensors, with varying amounts of chemical and at different crop growth stages.

The underlying assumptions of the approach are the following:

i. The integration of multiple wavelengths is a powerful tool to accurately predict yield (Plant et al., 2000; Suarez et al., 2016; Thenkabail et al., 2000).

ii. Yield can be predicted from vegetation indices (VI) due to their direct relationship to water or nutrient stress, canopy structure and pigment concentrations (Zarco-Tejada et al., 2005).

iii. There is a spatial-temporal relationship between yield and reflectance data (Zarco-Tejada et al., 2005; Zhao, Reddy, et al., 2007).

iv. LiDAR data supplies valuable information to analyse diverse architectural parameters as indicators of crop performance and yield (Confalonieri et al., 2011; Friedli et al., 2016; Zub et al., 2011).

1.6. Scope of project and limitations

The objective of this project was to examine the use of hyperspectral, multispectral and LiDAR sensors for the early characterisation, detection and quantification of damage of cotton crops due to 2,4-D herbicide spray drifts. The deployment of LiDAR scanners and hyperspectral sensors for this study was ground-based, i.e. as “proximal sensing” devices, while multispectral imagery was satellite-based, i.e. a “remote sensing” system. Recognising the lack of tools for assessing 2,4-D herbicide damage, this study aimed to provide different alternatives, from within the crop sensing options, that do not rely on the physical appearance of the crop. The methods implemented and

described in the following sections were designed in relation to the technology and case under study.

Crop injuries could vary due to chemical dose and timing of exposure. The rationale and main considerations in the experimental design for the timing of exposure and dose were based on the most susceptible stage of growth for the production and development of cotton bolls. The rates of the chemical were selected based on the essential need to capture changes caused by herbicide in the controlled sub-study discussed below.

Two sub-studies (controlled and uncontrolled) were designed in order to get a comprehensive understanding of spectral and canopy changes in the plant, and also to include one of the most common remote sensing techniques, multispectral satellite imagery, in the development of remote sensing methods to predict potential yield loss. The controlled sub-study used an experimental design with three different doses (0%, 5% and 50% of the recommended commercial label rate) and three different times of exposure (4-5 nodes, 7-8 nodes and 11-12 nodes) as factors analysed during four different sampling dates after exposure (two, seven, 14 and 28 days after exposure – 2 DAE, 7 DAE, 14 DAE and 28 DAE, respectively). The uncontrolled sub-study, on the other hand, had one timing of exposure and dose rate, but six sampling dates relative to the single day of the exposure (-42 DAE, -10 DAE, 6 DAE, 38 DAE, 54 DAE, and 70 DAE).

This approach allowed the development of models for each reflectance-based technique, that is, hyperspectral and multispectral, to be constructed to quantify and map the yield as a function of damage. The three sensors were treated statistically as being independent and separate from each other, i.e. they can be used independently to acquire the necessary data, with their respective data processing workflow. This approach was advantageous insofar as it allowed more alternatives for assessing the damage to cotton crops, according to available resources.

Measurements of physiological aspects and hormone contents, such as photosynthesis, stomatal conductance, indole acetic acid (IAA) and abscisic acid (ABA), were taken to understand what was happening internally in the 2,4-D-contaminated plants and consider discuss how these changes affected spectral responses, canopy structure, and

yield. One of the potential limitations of the proposed analyses of the IAA and ABA hormone contents was the limited number of plant physiology laboratories in Australia that could process the samples. A laboratory at the University of Tasmania was willing to analyse the leaf samples from this project.

Environmental conditions during the summer of 2014-2015 caused, in some cases, delays of up to five days in the proposed field work schedule in the controlled sub-study. The delays were, however, always considered to be in the acceptable range, except for the LiDAR experiments where it was only possible to do field work for the first two out of three proposed timings of exposure, and the first three dates out of four after exposure.

A substantial effort went into looking for real cases of 2,4-D-herbicide drifts between 2009 and February 2015, after which the data collection stage of this research study ceased. Unfortunately, there was insufficient information available to assess the capabilities of multispectral satellite imagery for the detection and mapping of the degree of herbicide drift damage in cotton crops across a range of farms or locations during this period. However, there was a reported accidental exposure to 2,4-D in a commercial cotton farm in January 2015, on which the Objective 2 of this thesis could be developed. There were massive drifts reported in three other growing regions across Australia during the following growing season, in January 2016, but the data collection stage of this thesis was completed by then, and there was insufficient time remaining to process and analyse the new satellite data from these events. It was therefore not possible to include them in this research project.

The spatial resolution of the multispectral sensor Landsat-8 Operational Land Imager (OLI) is 30 m by 30 m, potentially imposing a limitation when examining the relationships between multispectral bands and canopy reflectance. The statistical approach used in this study was, however, able to overcome this potential limitation.

1.7. Thesis organisation

This thesis presents different alternatives for assessing damage to 2,4-D-contaminated cotton crops from the agricultural remote sensing perspective. The organisation of this thesis is as follows, and is summarised in Figure 1-1.

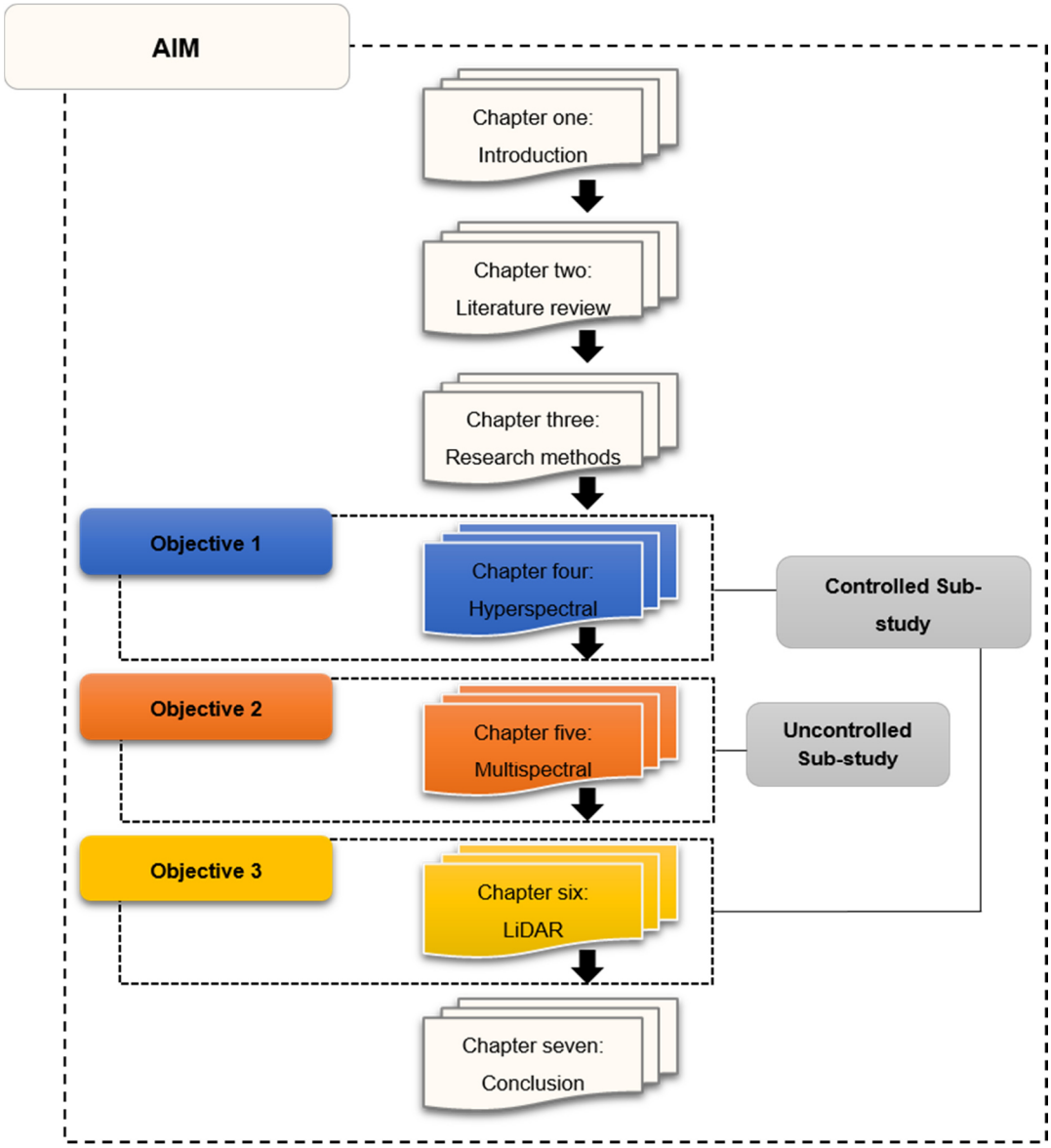

Figure 1-1. The schematic layout of the thesis

Chapter one discusses the background to the research study, reviewing the extent of the problem, and its agronomic and economic significance, and the scope and limitations of the methods implemented in this study.

Chapter two describes the cotton industry and the significant aspects of yield production, the implications of crop stress caused by herbicide drifts in agricultural crops, particularly in cotton crops affected by off-target movements of the phenoxy herbicide 2,4-D. The traditional assessment of 2,4-D spray drift in cotton and its limitations are also discussed. Agricultural remote sensing or crop sensing are also reviewed.

Chapter three describes the general aspects of the research methods used in this study.

Chapter four is the first technical chapter and covers the use of hyperspectral sensors for the detection and prediction of yield loss caused by herbicide drift. It also presents a comprehensive description and analysis of the physiological and hormone content changes in relation to the timing of exposure, the dose and the time after the exposure, and their relationship with reflectance changes. This chapter addresses the first objective of the research study presented in this thesis.

Chapter five, the second technical chapter, covers the use of multispectral satellite sensors and the analysis of their data in unaffected and 2,4-D-affected areas. It explores the applicability of individual multispectral bands, vegetation indices and the integration of all multispectral bands in the prediction models of yield in both unaffected and affected areas. The content of this chapter covers the second objective.

Chapter six explores the capabilities of LiDAR for the characterisation of canopy structure in different treatments of cotton plants affected by 2,4-D. Canopy height and canopy volume are analysed and the potential limitations of LiDAR are also presented. This chapter covers the third objective of this study.

Chapter seven concludes the main results and discusses their relevance in the context of the traditional methods of assessing crop damage, followed by recommendations for the implementation of each technique. Their potential limitations are also discussed.

Chapter 2

LITERATURE REVIEW

2.1. Introduction

This chapter reviews the state-of-the-art technologies available for the detection of herbicide drift by the use of remote and proximal sensing. Herbicide drift or spray drift is defined by the APVMA as *"the physical movement of spray droplets (and their dried remnants) through the air from the nozzle to any non- or off-target site at the time of application or soon thereafter"* (APVMA, 2008). Herbicide drift, therefore, can cause damage to crops that are susceptible to the active ingredient of the sprayed chemical.

This chapter presents basic information on remote sensing of crop growth and productivity (Section 2.2), the different aspects impacting crop performance (Section 2.3), the consequences of herbicide drift in agricultural crops (Section 2.4), while the specific effects of 2,4-D contamination in cotton crops are presented in Section 2.5. The applicability of remote sensing to agricultural crops, and in particular to those crops affected by herbicide drift is discussed in Sections 2.6 and 2.7, respectively. Specific and more detailed literature reviews are presented in chapters 4, 5 and 6, according to the objectives defined in each of those chapters.

2.2. Agriculture remote sensing

Precision Crop Management (PCM) or Precision Agriculture (PA) practices reduce inputs, maximise profitability, and tend to protect the environment (Barnes et al., 2000; János, 2011). Detailed information about crops, including the spatial variability of physiological status, healthiness and stress conditions, is required to implement PCM or PA, and remote sensing techniques are one of the effective approaches that can be used to supply that information, due to their capacity to integrate spatial variability into crop status analysis (Huang & Thomson, 2010; Zhao, Huang, et al., 2007). It is possible, using remote sensing data, to measure canopy structure, estimate yield, and detect stress (caused by different factors) many times during the growing season, supplying detailed information to farmers that can be used to improve the effectiveness of their crop management strategies (Jensen et al., 2008; Liu et al., 2013). Early

detection of crop stress offers the opportunity to mitigate losses and secure profitability for farmers. This study examined three remote sensing techniques to detect, assess and map the extent of crop stress caused by herbicide drift, as a potential tool to detect damage as soon as an accident has occurred, and particularly before any visual symptoms are evident.

2.3. Cotton crops and yield production

Good lint quality and high yield depend on specific agricultural management practices tailored to the unique characteristics of the growing areas. Achieving a successful cotton crop, that is good quality and quantity, is challenging. Such cotton crops depend to a large extent on specific conditions of temperature, water and soils; these are environmental variables that, with the possible exception of water in irrigated crops, can be predicted to some extent, but not controlled. (National Cotton Council of America, 2013a; Ritchie et al., 2004). Small changes in these variables can, additionally, affect yield and have a significant impact on expected profitability (Cotton Australia, 2013b; Ritchie et al., 2004). Much research has been undertaken to understand and optimise the production of cotton crops. Some studies, for example, have concluded that planting should be done when the minimum soil temperature is around 16°C for three consecutive days at sunrise and through the growing season (Quinn & Kelly, 2011). Temperatures lower than 12°C and higher than 30°C can adversely affect yield, (Quinn & Kelly, 2011; Ritchie et al., 2004).

Water is also a major factor affecting crop yield. Water stress causes stomatal closure and thereby reduces transpiration and causes an elevation of leaf temperature, and these effects are directly related to flower production (Detar et al., 2006). Research conducted by Perumal et al. (2006) support those findings when it was possible to correlate transpiration rate changes with the shedding of squares and bolls in stressed cotton plants. Significant reductions in photosynthesis, stomatal conductance and transpiration rates were identified. Physiological shedding was highly positively correlated with transpiration rate and flower production, and significantly negatively correlated with stomatal resistance. The temperature of leaves also increased, as stomatal conductance decreased and stomatal resistance increased for comparatively less effective photosynthesis, and concomitantly affecting boll retention (Perumal et al., 2006; Sullivan et al., 2007). *This present study analysed photosynthesis and*

stomatal conductance, as they are also strongly affected by phenoxy herbicides (Perumal et al., 2006)*, and identified their relationship to the spectral response of the plant and yield. These results are presented in Chapter 4 as part of the Objective 1 of this thesis.*

2.4. Crop stress caused by herbicide spray drifts

Crop stress can be caused by lack of water and/or nutrients, but it can also be caused by management practices in surrounding farms, such as those resulting in herbicide drifts. Herbicide drift is the movement of pesticides into non-target areas; in other words, drifts happen when the herbicide leaves the intended target site and moves to other places (Figure 2-1). There are two different types of drift: a) vapour and b) particle or droplet drift (Ball et al., 2014; Wilson, n.d.). The second type is the most common cause of off-target movement, but both are highly dependent on environmental conditions. Particle drift depends on several variables, such as wind speed, droplet size, nozzle type, sprayer pressure and formulation (DEDJTR, 2016). Vapour drift happens when particles of the active ingredient evaporate or volatilize during application and depends mainly on the temperature in addition to the variables affecting particle or droplet size (Clemson University Cooperative Extension, 2013a; DEDJTR, 2016).

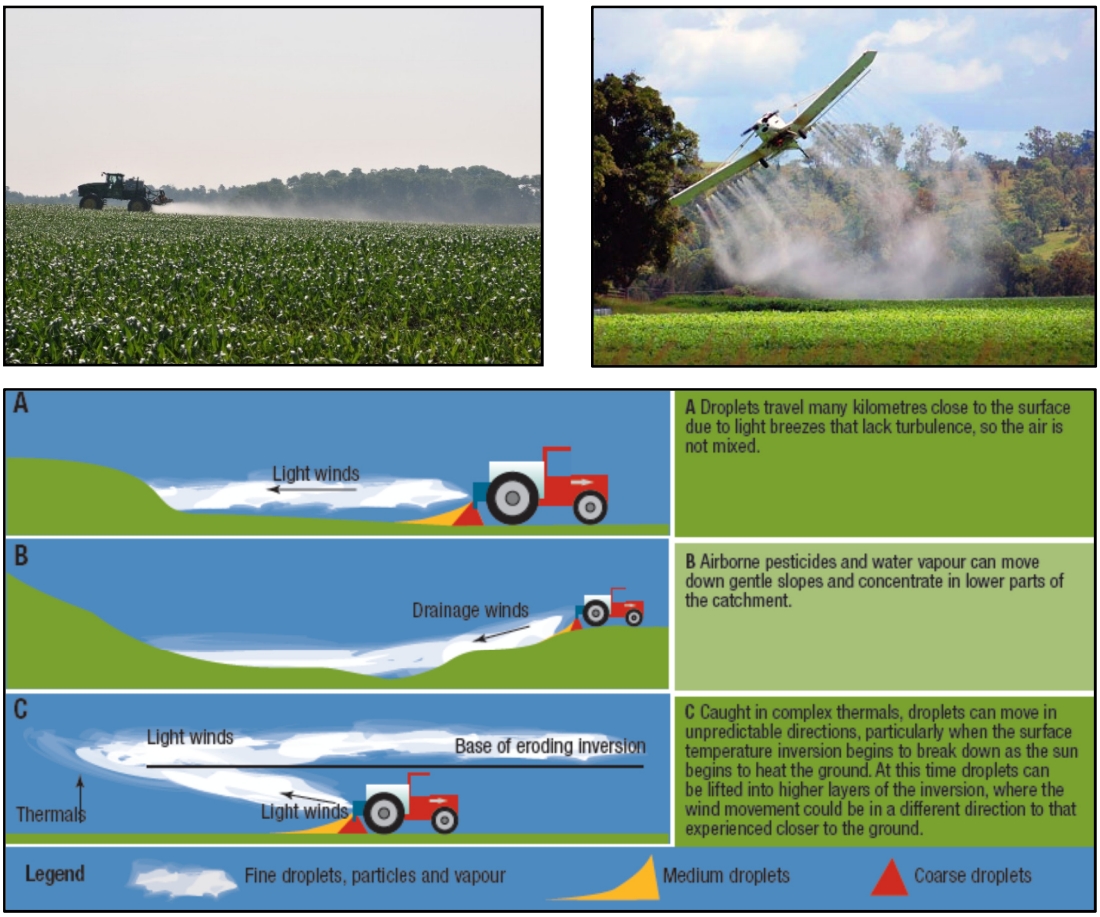

Figure 2-1. Potential movement of droplets to non-target areas.
Source : (GRDC, 2013; Nicolai et al., 2015; Roseboro, 2014)

Certain environmental conditions have to be satisfied to avoid herbicide drifts, more rigorously when highly volatile formulations are to be applied. Some specific optimal conditions are: a) wind speed higher than 3 km/h and less than 15 km/h (DEDJTR, 2016) but some other organizations like Pesticide Environment Stewardship (PES) recommend not to spray if the wind speed is higher than 16 km/h because of the increased risk to downwind areas adjacent to the target site; b) moderate humidity and c) absence of temperature inversions in the atmosphere (DEDJTR, 2016; Grain Research and Development Corporation [GRDC], 2013; Wilson, n.d.).

The effects in contaminated plants depend on the mode of action of the chemical (Table 2-1), as different herbicides affect the biochemistry of the plant in different ways. Photosynthetic inhibitors gradually block the photosynthetic process (carbohydrate production) causing slow starvation manifested by chlorosis and posterior necrosis within susceptible species (University of Minnesota, 1999) (Figure 2-2, left). The photosynthetic pigment inhibitors do not allow the production of

compounds that protect chlorophyll from destruction (Figure 2-2, right), while the plant growth regulators disrupt hormone balance and protein synthesis at multiple sites in the plant, causing rapid or uncontrolled growth abnormalities (University of Minnesota, 1999) (Figure 2-3).

Table 2-1. Herbicide classification based on the mode of action.

Class	Sub-classes	Description
Modes of action	Plant growth regulators	Referred as auxins. They mimic the action of naturally-occurring auxins causing rapid or uncontrolled growth.
	Photosynthesis inhibitors	Inhibit photosynthesis in the plant.
	Photosynthetic pigment inhibitors	Prevent the plant from forming photosynthetic pigments.
	Lipid synthesis inhibitors	Inhibit the production of lipids causing disruption in the production of cell membranes until plant growth stops.
	Amino acid synthesis inhibitors	Simulate specific enzymes to prevent the production of amino acids essential for plant growth and development.
	Seedling growth or plant growth inhibitors	Interrupt new plant growth and development.
	Cell membrane disruptors	Form compounds such as superoxides and hydroxyl radicals that destroy the cell membrane of the plant.
	Unknown	Herbicides whose mode of action is not well understood.

Note: 2,4-D herbicide is classified as a plant growth regulator. *Source*: (Kappler & Namuth, 2004)

Figure 2-2. Effects of herbicide's mode of action in susceptible plants.
Left: photosynthetic inhibitor and right: photosynthetic pigment inhibitor. *Source*: (Kappler & Namuth, 2004; North Carolina State University, 2015)

Figure 2-3. Effects of herbicide in susceptible plants: growth regulators.
Source: (Kappler & Namuth, 2004; North Carolina State University, 2015)

Herbicide drifts can cause damage not only to crops but also to animals, the environment and humans, as effective active ingredients of the formulation leave the attempted target, reaching areas susceptible to those chemicals (DEDJTR, 2016; Wilson, n.d.). 2,4-D is an effective phenoxy herbicide that is used to control weeds at low cost when it is used properly, but it has a history of causing drift problems. These two main characteristics, low cost and high effectiveness, saw the adoption of 2,4-D as one of the most common herbicides, not only in the cereal cropping sector but in many forage, forestry and food crop systems. The high and constant demand for this herbicide has created serious problems due to a high risk of environmental contamination, soil-degradation and effects on crops that are not the target (Department of Agriculture and Food [DAF], 2016; Industry Task Force II on 2-4-D Research Data, 2013; Munk et al.).

The herbicide 2,4-D is a selective plant growth regulator designed to attack broadleaf weeds by causing uncontrolled growth by simulating the effects of indole acetic acid (IAA), which is the main hormonal growth regulator of the plant (DEDJTR, 2014). It is a systemic herbicide, and therefore affects only parts of the plant with which it is in direct contact. (Figure 2-3 and Figure 2-4). Particles with sub-lethal doses of the chemical can reach the non-target crops from any direction, increasing the difficulties in accurately locating damage in the entire potentially affected area. *This research project aimed to develop approaches for applying remote sensing techniques in order to map damage caused by herbicide spray drift without restrictions on the size of the potentially affected area. These approaches are presented in Chapter 5 of this thesis; they address Objective 2.*

Figure 2-4. 2,4-D-contaminated cotton crop.
Source: (Ballew, 2015; Cotton Australia, 2017)

Herbicide drifts of 2,4-D are common in Australia and around the world. Industries such as grapevines, tomatoes and cotton have been facing drift occurrences since 2,4-D was first introduced in the 1940's (Munk et al., 2014). Cotton plants are particularly susceptible to 2,4-D herbicide drifts, as they are broadleaf and perennial plants with a complex structure and well-defined patterns of growth (Cotton Australia, 2013b; Kantartzi & Stewart, 2013; North Carolina State University Extension Service, 2010). The cotton industry in particular, due to its proximity to cereal grain producing areas, has had to deal with 2,4-D damage every season. Effects vary from non-yield damage to severe yield loss, with significant negative impact on incomes (Cotton Australia, 2012, 2013c; Munk et al.; H. Zhang et al., 2013). Exposure of cotton crops to 2,4-D is thought to have caused more than 10 million dollars loss due to damage in an area of

approximately 200 km^2 during the 2015-16 growing season. Common sense was urged when applying this chemical (Cotton Australia & Grains Growers, 2016). Millions of dollars were also reported lost during the 2012-13 and 2014-15 seasons due to 2,4-D damage in cotton crops in Australia, with more than 12,000 ha being affected (Cotton Australia, 2013d, 2015b).

2.5. Cotton crops, 2,4-D herbicide drift and traditional assessment

Cotton growing areas in Australia are located in two of the six states. The major area is located in New South Wales, and the second one in Queensland (Figure 2-5). The cotton industry is one of the largest export earners, with more than 1000 cotton farms reported by Cotton Australia (2016). The cotton industry was the only major industry reporting growth in production (tonnes), area (ha) and value ($) during the 2015-16 season, compared to 2014-15 (48%, 41% and 58.6%, respectively) (Australia Bureau of Statistics [ABS], 2017a, 2017b).

Cotton is a comparatively small field crop in terms of harvested hectares in Australia, but of the major crops, it is also the industry with the highest return per produced hectare (approximately A$5,410/ha). Cotton was the second highest commodities earner during 2009-2012 and 2013-14 in NSW. It has been the highest in Queensland since 2009, although there was a dramatic drop in 2012-2013 because global prices fell and production was higher than the years before, oversupplying the market (Australian Bureau of Statistics, 2013). The highest cotton commodity values in Australia were more than 2300 million dollars during the 2011-2012 season. The gross value was just above A$1900 million in the 2012-13 season, lower than the previous season in spite of increased production. A similar value was achieved during 2010-2011, representing 261% more than the previous season (2009-2010) (ABS, 2013; Cotton Australia, 2016).

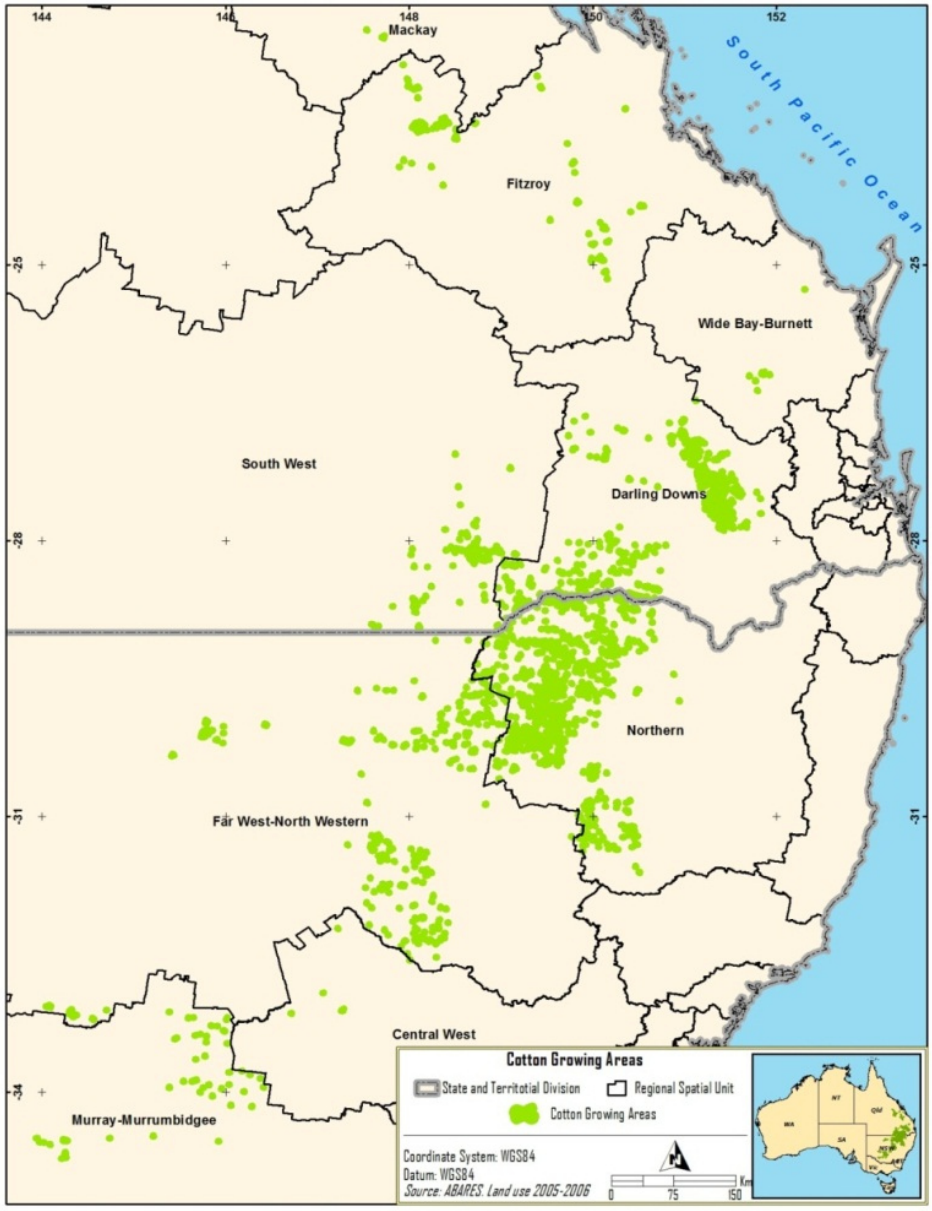

Figure 2-5. Cotton growing areas in Australia.
Source: Land use 2005-2006 (Australian Bureau of Agricultural and Resource Economics and Sciences [ABARES], 2010); Australian Standard Geographical Classification (ASGC) Digital Boundaries (ABS, 2011)

There have been many efforts to improve the inherent resistance of the plant to 2,4-D herbicide, given the importance of this crop to the Australian economy. Charles et al. (2007) compared non-modified cotton with transgenic cotton, and although resistance to unintentional damage increased, effects were still evident in the transgenic cotton. Regulations and annual campaigns by Cotton Australia to educate 2,4-D users have also reduced herbicide drifts from more than 10% in 2008 to just 3% in 2012-2013 (Cotton Australia, 2013a). Unintentional phenoxy herbicide drifts can nevertheless still occur at any time, and cotton growers lack the appropriate information to detect damage to their crops soon after the event, to allow rapid re-designing of management

plans and mitigate loss. The present research project was applied to cotton because of the economic magnitude of the problems caused by accidental 2,4-D drift in this industry.

Traditional methods for the detection of 2,4-D injuries depend on the visual evaluation of symptoms, and can usually be applied no earlier than two to four weeks after the event, depending on the quantity of chemical that reaches the plants. There is, therefore, a substantial time interval in which mitigation plans could have been implemented if there were suitable early detection techniques. Many research studies have supplied information about physical or external changes of the plant caused by 2,4-D drift. Some examples are Al-Khatib et al. (2004), Everitt and Keeling (2009) and Charles et al. (2007) where cotton plants were sprayed with 2,4-D and other herbicides at rates that simulated spray drift; cotton showed injuries at all proposed timings, even with the lowest rates of 2,4-D (0.28 g a.i/ha – 4 g a.i/ha). However, their results illustrate the potential inaccuracies of yield loss estimates based on visual symptoms. Doses as low as 0.28 g a.i/ha could visibly injure the crop in 50% of cases according to visual assessments 14 days after treatment (DAT), but yield was reduced in less than 1% of cases. Visual assessment at the end of the season (120 days after planting) with a higher dose (28 g a.i/ha) only detected damage in 18% of cases, with an accompanying yield loss of 50% (Everitt & Keeling, 2009).

The problem related to accuracy in visual estimations can be due to three variables that pertain to: a) the capacity of the plant to recover as the plant continues to grow after unintentional damage; b) how much herbicide reaches the leaves -as injuries increase when the dose is higher; and c) the timing of a herbicide drift in relation to key stages in reproductive development (Munk et al.; National Cotton Council of America, 2013b). Remote sensing techniques are potential tools to resolve those limitations since visual assessment is not able to supply accurate information on potential losses or spatial variability in the crop status. *This research used three different alternatives to traditional assessment equivalent to Objectives 1, 2 and 3, respectively: a) hyperspectral proximal sensor; b) multispectral remote sensor and c) LiDAR scanner. The first objective of this thesis also provides a better understanding of the internal response of the plant and how this affects yield and quality.*

2.6. Sensing technologies for agricultural crops

2.6.1. Reflectance-based sensors

Remote sensing techniques are widely applied in the agriculture sector due to their ability to provide information about biophysical and physiological variables without the need to take destructive samples, and their ability to integrate the concept of spatial distribution, environmental conditions and soils with high accuracy (Tian et al., 2005). Accurate results were obtained to identify disease or stress caused by pesticides (Henry et al., 2004), water (Detar et al., 2006) (Figure 2-6), nitrogen (Schlemmer et al., 2013) and other nutrient insufficiencies (Chen et al., 2011; Tian et al., 2012) (Figure 2-7a).

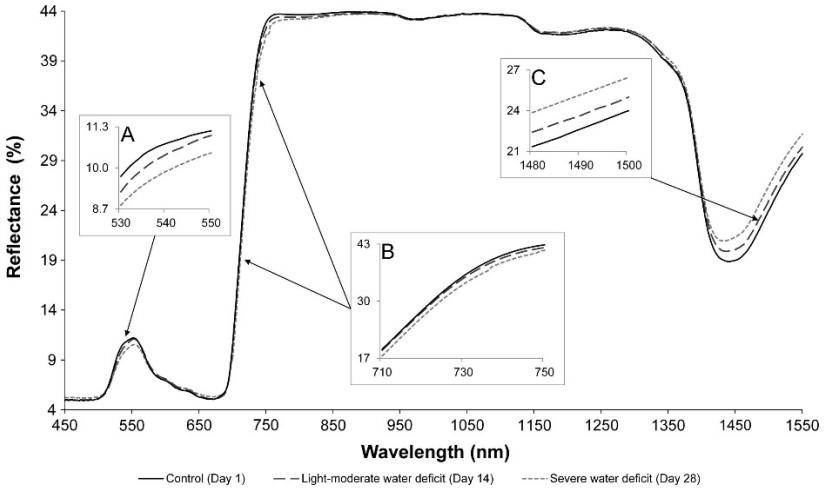

Figure 2-6. Spectral responses of a grapevine crop due to water deficiency.
Source: (Rapaport et al., 2015)

Remote sensing data have also been used to discriminate species (Ghosh et al., 2014; Zainol Abdullah et al., 2014) (Figure 2-7, D), canopy variables and structure (Lefsky et al., 2002; Rama Rao, 2008) (Figure 2-7, B and C), estimate different biophysical and physiological variables (Figure 2-7, A) and pigmentation contents of vegetation over large number of crops as indicators of healthiness (Barnes et al., 2000; Li et al., 2001; Pinter et al., 2003) (Figure 2-7, A). Although several studies have implemented and tested remote sensing techniques to estimate different crop variables based on spectral responses over crops*, the potential of these techniques for the detection and assessment of herbicide drift damage on cotton has yet to be explored. Objectives 1 and 2 explored reflectance-based sensors for detection of 2,4-D-injured cotton plants.*

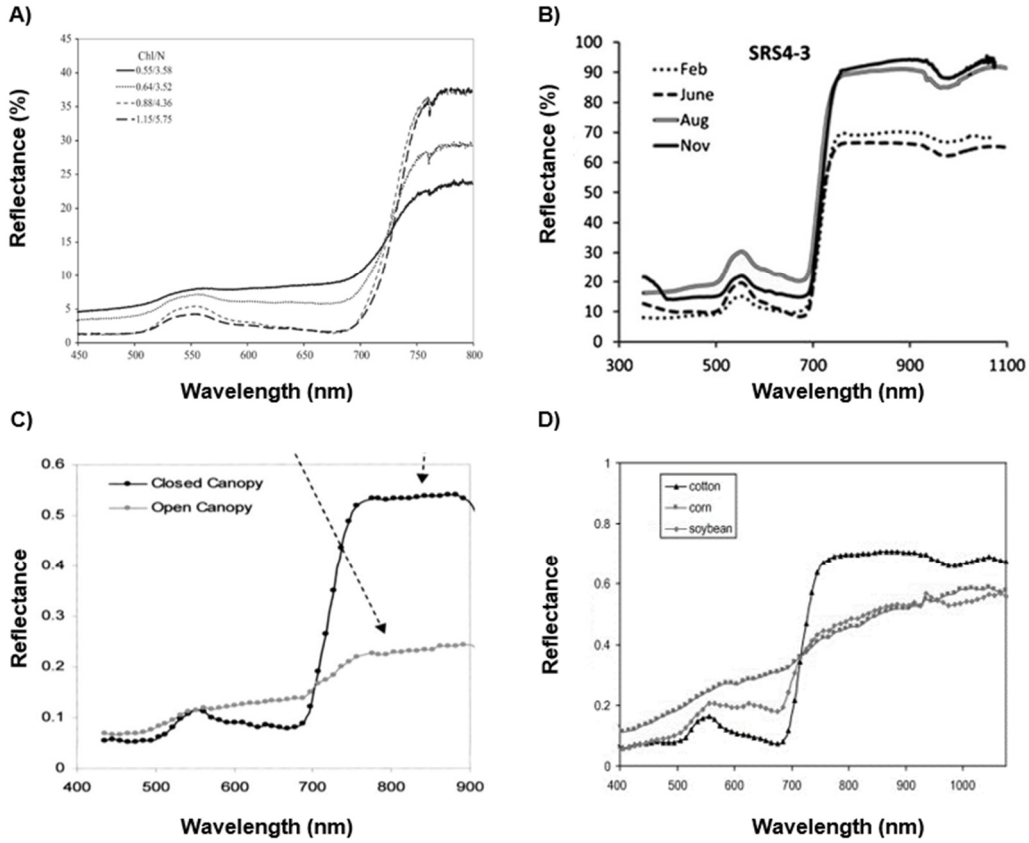

Figure 2-7. Spectral response variability due to different crop conditions.
a) Variation in nitrogen and pigment concentrations in maize; b) maturity of red mangrove leaves; c) canopy structure of cotton crops and d) different crop types.
Source : (Lagomasino et al., 2014; Schlemmer et al., 2013; Zarco-Tejada et al., 2005; H. Zhang et al., 2013)

Different remote sensing approaches have been developed to monitor crop variables, including vegetation indices or models that integrate the most suitable bands to discriminate specific variables; different approaches with highly applicable results confirm the potential use of those techniques. Photosynthesis is a key consideration when evaluating biomass production as most of the dry matter is produced by plant photosynthesis, so it can be used to monitor growth status (Tian et al., 2005). Carter (1998) estimated photosynthetic capacity-A_{max} based on reflectance of a mixed stand of loblolly pine (Pinus taeda *L*) and slash pine (P. elliottii *Engelm*. var elliottii), using hyperspectral imagery with a bandwidth of 1.0 nm. The best relationship between A_{max} and spectral responses was the ratio Near-infrared (NIR) to red edge at R_{820} and R_{701}, and they also found that the red edge inflection point at R_{701} is more important than the NIR range, as the variability of NIR between R_{750} and R_{850} did not change the relationship between the ratio and A_{max}. Tian et al. (2005), in other research that supports the above findings, developed and tested a ratio vegetation index $R_{(810/680)}$ to estimate the leaf net photosynthesis and canopy leaf photosynthetic potential in rice,

with a close linear relationship between the index and the photosynthesis measures. It was also possible to demonstrate that the first two leaves at the top of the rice canopy are the best for monitoring photosynthesis and crop status. Both the experiments described above agree that reflectance near to R_{700} and R_{800} can be used to estimate photosynthetic capacity and other highly correlated variables such as stomatal conductance and chlorophyll content. *Photosynthesis, stomatal conductance and hormone contents are variables that were measured and analysed as part of the aim of this study and presented in Chapter 4.*

Crop sensing techniques have also been used to assess water content or water stress in situations where these factors can affect yield. Short-wave near-infrared (SWNIR) range has a high correlation with water status in the plant. Tian et al. (2005) found that R_{810} and R_{1500} were strongly affected by leaf structure and water status, respectively, when rice crops were exposed to different water regimes. Detar et al. (2006) estimated water stress based on temperature changes in cotton canopies. Multiple regression techniques were applied to estimate the increase in temperature above the temperature baseline. Several strong relationships between two or three combinations of bands were found ($R^2 > 0.93$) between un-stressed and stressed crops around 750 nm and 960 nm, which can be explained by the stability of the spectral differences in that range of the spectrum. The technology that was used in Detar et al. (2006) (including the SWIR bands) can be used to explain the level of crop stress after a spray drift event. It will be possible to detect water stress in the crop and relate this to photosynthesis, canopy temperature and conductivity as affected by an accidental spray drift.

The time at which the imagery is captured is an important aspect to consider when estimating yield using remote sensing data. Zarco-Tejada et al. (2005) demonstrated that there is a temporal and spatial relationship between NDVI – a structural vegetation index - and cotton yield variability associated with the time at which the imagery was captured. Correlation coefficients decreased significantly from $r = 0.61$ to $r = 0.06$, and k-mean clustering techniques used to segment the imagery into low, medium and high potential yield decreased from 0.36 to -0.01, with percentage of accuracy from 58.60% to 31.73%, from images captured at an early stage of crop growth as compared to those captured close to harvest. Those results can be explained by the influence of canopy stage over spectral responses, and NDVI should therefore only be used to estimate

yield at specified stages in crop growth (Figure 2-7, B). Yang et al. (2004), in other research, tested narrow and broadband vegetation indices, and individual narrow bands, to predict yield. Individual narrow bands were better able to explain yield variability ($0.61 \leq R^2 \leq 0.69$) compared to narrow vegetation indices such as BNDVI, GNDVI and NDVI, where the R^2 values were between 0.06 and 0.65. The first approach had better results than the second one, but both were significant. Images were captured when the crop reached its maximum canopy cover, which can explain the results on the basis of any of the structural indices used. *The research described in this thesis used spectral responses from a hyperspectral sensor and multispectral imagery (narrow bands and broadband vegetation indices) to estimate cotton yield after an unintentional injury caused by 2,4-D. The above is approached in* ***Objectives 1 and 2****.*

2.6.2. Laser-based sensors

Leaf area density (LAD) in individual horizontal layers can be used to represent vertical canopy structure in crop canopies and it has been related to yield, growth rate and nitrogen allocation (Hosoi & Omasa, 2009). Other structural canopy variables can be calculated based on LAD, such as Leaf Area Index (LAI). Limitations to calculating LAD occur when it is not possible to distinguish between leaves, stems and other parts of the plant that are not part of the canopy structure. It is necessary in those cases to represent the canopy structure based on Plant Area Density (PAD) or Plant Area Index (PAI).

LiDAR technologies have active sensors and scanners that use a laser beam to measure the distance between the target and the device, from which a 3-D surface can be created. They have been widely applied in forestry to accurately measure variables related to the horizontal and vertical structure of canopies (Coops et al., 2007; Ediriweera et al., 2011). These include vegetation height (Figure 2-8), diameter at breast height (DBH), biomass, LAD, PAD and LAI (Coops et al., 2007; Jensen et al., 2008). Agricultural applications of LiDAR are relatively new and limited in scope. Research in wheat (Hosoi & Omasa, 2009) and oil palm plantations (Tan et al., 2012) have demonstrated the potential use of this technique to estimate canopy structure under different management conditions or growth stages. Hosoi and Omasa (2009) demonstrated a near-perfect linear relationship between PAD directly measured in the field with LiDAR-derived PAD (R^2=0.95), and also a strong correlation between the

dry weight of stems and leaves and LiDAR-derived area of stems and leaves (R^2=0.94).

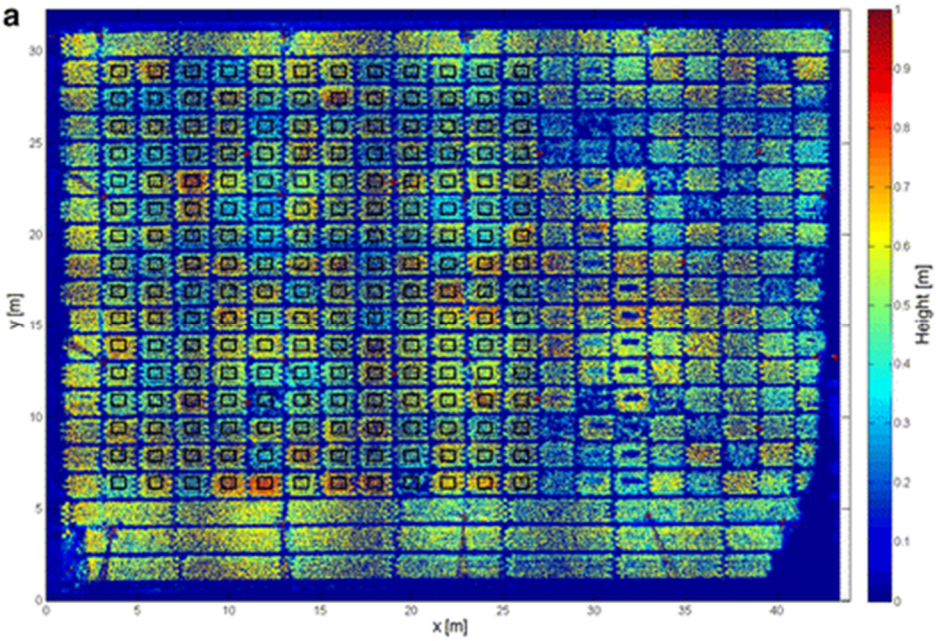

Figure 2-8. Plant height maps computed from LiDAR scans in wheat fields.
Source: (Friedli et al., 2016)

Canopy structure variables vary depending on management conditions and stress or disease, and they are highly correlated with yield in crops. Measuring those variables can, therefore, provide valuable information to monitor growth rates and health. *State-of-the-art LiDAR techniques in agriculture are well-defined and their potential value has been proved. The third objective of this thesis, therefore, addressed the use of LiDAR sensors to capture canopy structure variability after herbicide drift, in order to understand the behaviour of the canopy once it has been affected by unintentional injury and speculate on how this behaviour was related to yield.*

2.7. Remote sensing techniques and detection of herbicide drifts

Remote sensing tools have also been applied to detect herbicide drift on crops with promising results. Moreover, it has been possible to map and classify damage with high accuracy. Robles et al. (2010) used multispectral imagery to estimate phytotoxicity caused by two different herbicides (glyphosate and imazapyr) on water hyacinth (*Eichhornia crassipes*). They found close linear relationships between phytotoxicity and spectral responses, from 760 nm to 900nm, one week after the event.

However, when the phytotoxicity level was very low the prediction equations tend to underestimate or overestimate phytotoxicity. The limitation of this study is that the variable used to assess the damage (phytotoxicity) was based on visual estimation. Changes in the colour of the leaves could additionally be associated with causes other than to herbicide damage. Henry et al. (2004) tested the potential use of hyperspectral sensors to determine the type and degree of unintentional injury caused by glyphosate and paraquat on corn and soybean that had been treated at an early growth stage. It was possible to distinguish between healthy and unhealthy plants with classifications accuracy higher than 92% of corn. They also concluded that the most useful technique to distinguish between different rates or doses is wavelet analysis and the best ten bands between 600 nm and 670 nm, and 770 nm and 950 nm were chosen.

The mode of action of a herbicide (Table 2-1) causes differences in spectral responses that can be detected by proximal sensors. Buehring (2004) tested the accuracy of classification methods using hyperspectral imagery as a function of herbicide damage based on a percentage of visual injury, yield reduction, herbicide rate and mode of action. They tested herbicides with three different modes of action in cotton and corn and found that early detection increased the accuracy of prediction of the percentage of yield reduction and discrimination between herbicides. However, they also demonstrated that the optimum vegetation index and the best spectral bands to estimate yield reduction varied according to the herbicide. That can be explained as being due to the herbicides tested in this research having different modes of action in the plant. Henry et al. (2004) tested two different herbicides: Glyphosate (plant growth regulator) and paraquat (photosynthetic inhibitor). Their study also demonstrated accuracy fluctuations due to the mode of action, the affected crop and the days after exposure (DAE) with classifications results higher than 92% for herbicide rates as low as 3% of the recommended label rate.

Different studies have then demonstrated high prediction capabilities of spectral-based remote/proximal sensing for detection of herbicide drift damage in several crops and herbicide modes of action, but none of them has explored these techniques in 2,4-D-injured cotton. Furthermore, the literature review highlighted the capabilities of LiDAR in characterising crop canopy structure but no research study has been found

testing the capabilities of LiDAR in 2,4-D-injured cotton. *Objectives 1, 2 and 3 of this thesis addressed this particular issue.*

2.8. Summary

This review examines the problems caused by 2,4-D and discusses how the traditional assessment of damage (based on visual assessment) could be improved. Remote and proximal sensing are tools that capture information of the objects under study without direct contact. The review has provided evidence regarding the potential uses of remote sensing techniques to assess several variables associated with crop status under different management and stress conditions. There is, however, a lack of research into the assessment of 2,4-D drift over susceptible crops using remote sensing techniques. The aim of this research project was to fill this information gap in the use of remote sensing to detect, assess and map 2,4-D herbicide drift in cotton crops using three methods: hyperspectral, multispectral and LiDAR sensors (Objective 1, 2 and 3, respectively). Factors such as growth stage of the crop, yield reduction and doses of 2,4-D were also analysed to understand their influence on remote/proximal sensing data.

Chapter 3

RESEARCH METHODS

3.1. Introduction

This chapter describes general aspects of the research methods used in this thesis, including the location of the study area (Section 3.2) and methods of data capture and acquisition (Section 3.3). This study comprised two sub-studies: a) controlled exposure and b) uncontrolled exposure to 2,4-D. The present chapter also describes how each sub-study area contributed to the objectives of this research as presented in Section 1.4.

Objectives 1 and 3 are addressed in the controlled contamination sub-study and the Objective 2 is addressed in the uncontrolled sub-study. Descriptions and more detailed information pertaining specific methods, study area and data collection are presented and discussed in Chapters 4, 5 and 6 which corresponded to Objectives 1, 2 and 3, respectively.

3.2. Study area

The study area for both sub-studies was located in Jondaryan, a rural town in the Darling Downs region, about 140 km west of Brisbane and midway between Toowoomba and Dalby, Queensland, Australia. The Darling Downs has horticultural, oilseed, cereals and cotton industries that compete with each other for natural resources (Cotton Catchment Communities CRC, 2009). Jondaryan is currently part of the Toowoomba Regional Council (Figure 3-1) but was one of the 23 local government areas where cotton was grown in Queensland in 2008 (ERIN, 2008). It had a population of 377 according to the 2011 census. The largest part of the shire comprises black soil alluvial plains, with undulating basaltic uplands (Centre for the Government of Queensland, 2015). The general soil type is black self-mulching cracking clays with dominant principal profile form as uniform fine cracking, smooth faced peds, and dark clay horizon underlain by brown/mottled clay (Department of Natural Resources and Mines [DNRM], 2015).

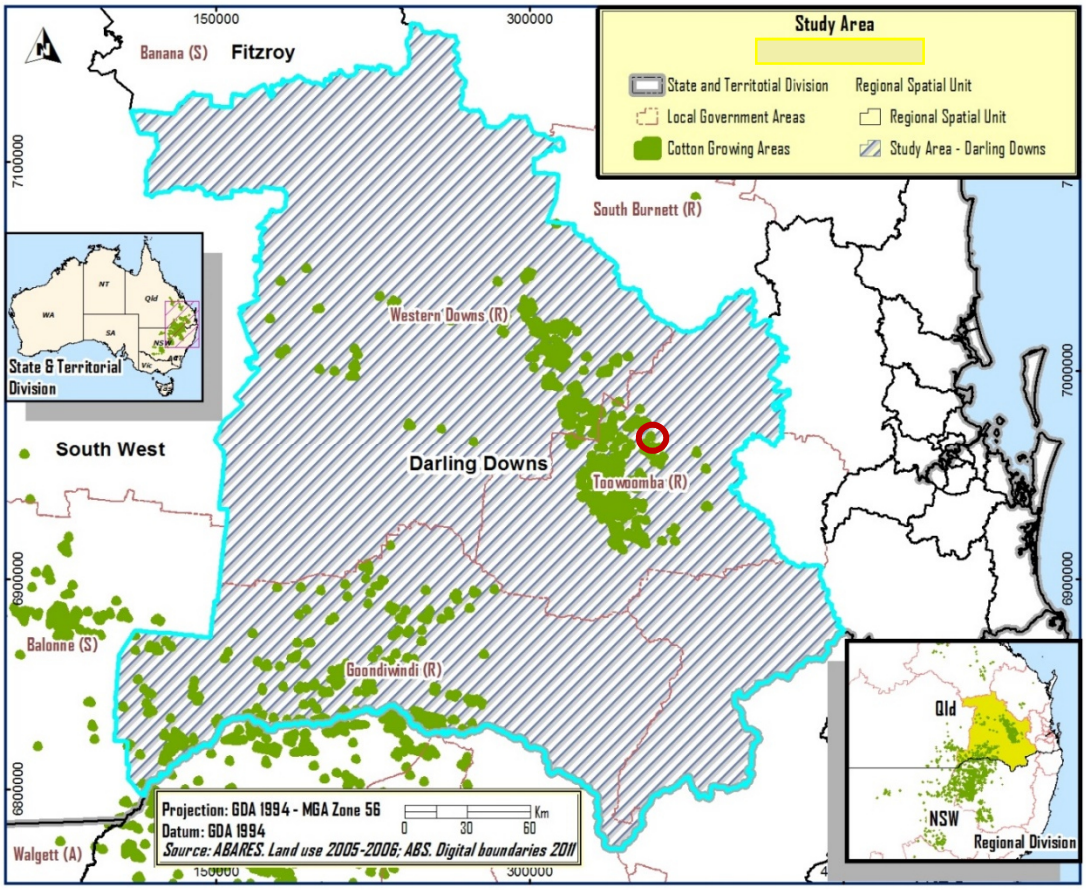

Figure 3-1. General location of the study area.
The red circle marks the location of the Jondaryan shire. *Source*: (Australian Bureau of Agricultural and Resource Economics and Sciences, 2010; ABS, 2011)

The main industries of employment in Jondaryan are sheep, beef cattle and grain farming (Figure 3-2) which in total represent 20.1% of the employed people aged 15 years and over (ABS, 2017). The grain farming systems surrounding the cotton crops spray 2,4-D as an effective method to control summer weeds (Cotton Australia & Grains Growers, 2016). The cotton crops are usually reaching key maturity stages for development of fruits when 2,4-D spray activity occurs. This activity, in some environmental conditions, results in potential risk for cotton farmers, because the chemical can move tens of kilometres away from the target cereal crops.

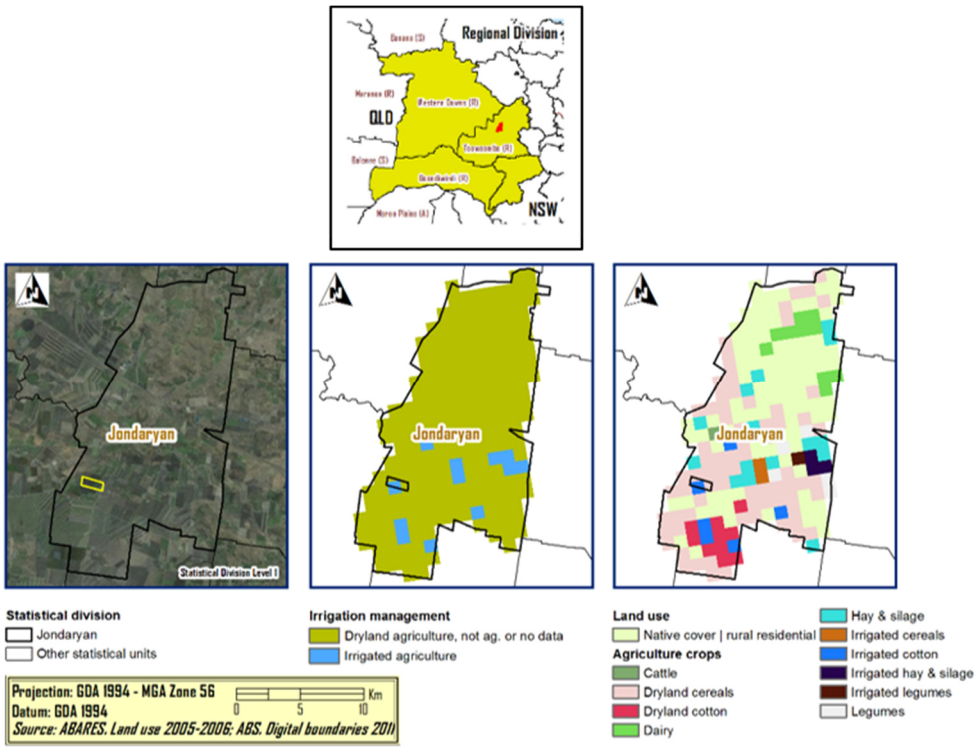

Figure 3-2. Study area location, irrigation management and land use.
The yellowish area indicates the general location of the study area. The background on the bottom-left image is a true colour composite of a Worldview-3 image (red, green, blue bands in the RGB colour channel). *Source*: (ABS, 2010; 2011)

The cotton growing season in Australia starts in September-November for planting and goes until March-June for harvesting (Cotton Australia, 2015a). In total, the growing period can last for up to 6 months and it follows a complex but well-defined and consistent pattern of growing under optimal conditions (National Cotton Council of America, 2013a). Cotton is a perennial plant, so it can survive year after year. This characteristic allows the plant to activate a defence mechanism to improve its chances of survival under stress conditions by dropping or "shedding" some flowers or small bolls, allowing the plant to maintain vegetative growth. Once the plant has recovered sufficiently, it resumes reproductive growth (CottonInfo, 2016). The growing cycle has four main stages (Figure 3-3) that overlap over time:

1. germination and emergence,
2. vegetative growth and canopy development,
3. flowering and development, and
4. maturation

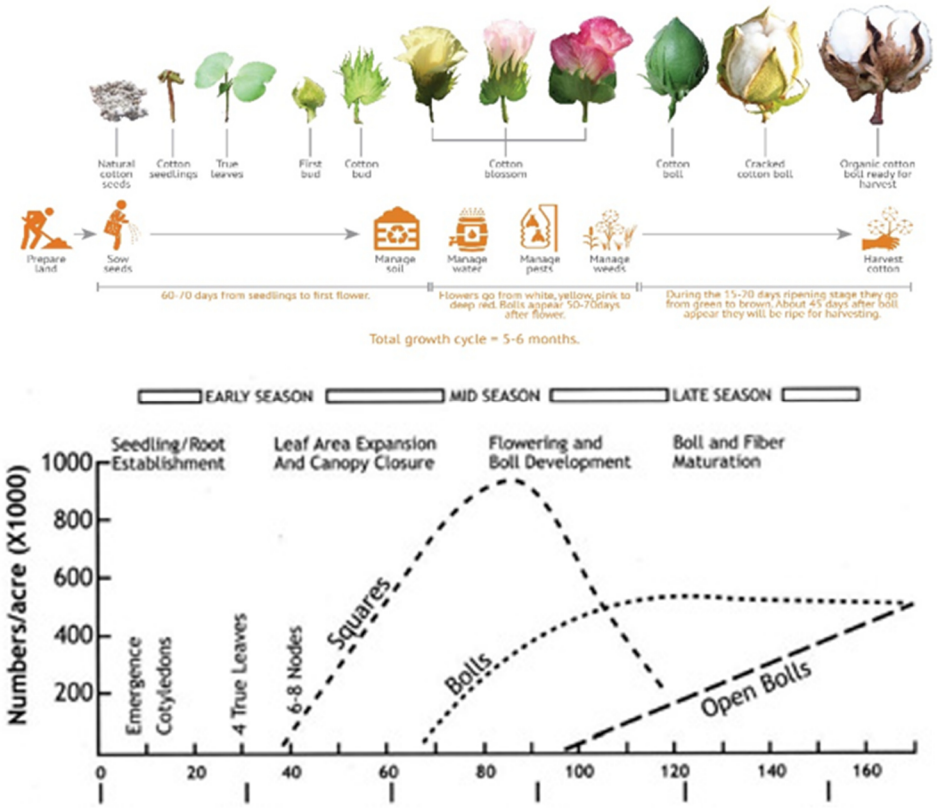

Figure 3-3. Growing and development cycle of cotton plants.
Source: (About Organic Cotton, 2016; National Cotton Council of America, 2013a)

Germination and emergence include root development, which under optimal soil temperature and moisture conditions can result in emergence five to 10 days after sowing (**DAS**) (Cotton Australia, 2015a). Vegetative growth is defined as starting as soon as the cotton seedlings emerge and the cotyledons are stable. The main stem consists of a series of internodes and nodes to which vegetative branches are attached. The vegetative branches and main stem can also produce fruit branches that will generally arise from nodes 6 or 7 on the main stem. The fruiting branch grows in a zig-zag pattern with multiple fruiting positions. Flowering can last approximately seven days after three weeks of squaring (that is, the beginning of the flowering and boll development stage). A small green boll is exposed once the flower has desiccated. During the maturity stage, the boll will continue to grow until it matures (after 20-25 days) and opens, approximately 50 days from flowering. This growing cycle from flowering to boll opening will continue in a pattern up to the plant. Crops are ready for defoliation applications once the last white flower is about four to five nodes from the terminal (that is, the top of the plant) (CottonInfo, 2016).

Once the flowering and development stage starts, some four to five weeks after planting, the vegetative growth of the plant slows down, as much of its resources are then put into reproductive growth. Good management strategies aim at maintaining a balance between vegetative and fruit development (CottonInfo, 2016) to maximise boll load. The period between squaring and flowering, is not affected by external factors or plant stress. However, a vigorous vegetative growth, after the sixth node, and between 40 to 90 DAS, is important as it supports the future boll load.

The growing season in this study area started on the 27th October 2014 and finished on the 24th April 2015. The crop management in both the sub-study areas was dryland cotton (Figure 3-2) with three irrigations scheduled during the growing season. Standard management practices such as control of weeds, pests and refuge cotton paddocks were used in the study area as part of the normal commercial management plan.

3.2.1. Controlled sub-study

The study area (Figure 3-4) for this case (Chapters 4 and 6) was located on a commercial cotton farm (151°32'40.0"E, 27°25'47.5"S; and 376.8 meters above sea level). Three doses were investigated: Nil, 28 g a.i/ha and 280 g a.i/ha of 2,4-D (*Amicide Advance 700*®; 700 g/L 2,4-D) at three different timings of exposure: 4-5 nodes (S1), 7-8 nodes (S2) and 11-12 nodes (S3). Data was collected at two, seven, 14 and 28 days after each exposure (days after exposure, DAE), for each timing of exposure and herbicide rate. Table 3-1 summarises the treatment combinations.

Table 3-1. Controlled sub-study treatment combinations.

Timing of exposure *(S)*	Percentage of recommended label rate (%)	Herbicide dose (g a.i/ha - 2,4-D)	Day for collecting data (Days after exposure – DAE)
4 – 5 nodes (S1)	0	Nil – D0	2 DAE
7 – 8 nodes (S2)	5	0.028 – D1	7 DAE
11 – 12 nodes (S3)	50	0.28 – D2	14 DAE
			28 DAE

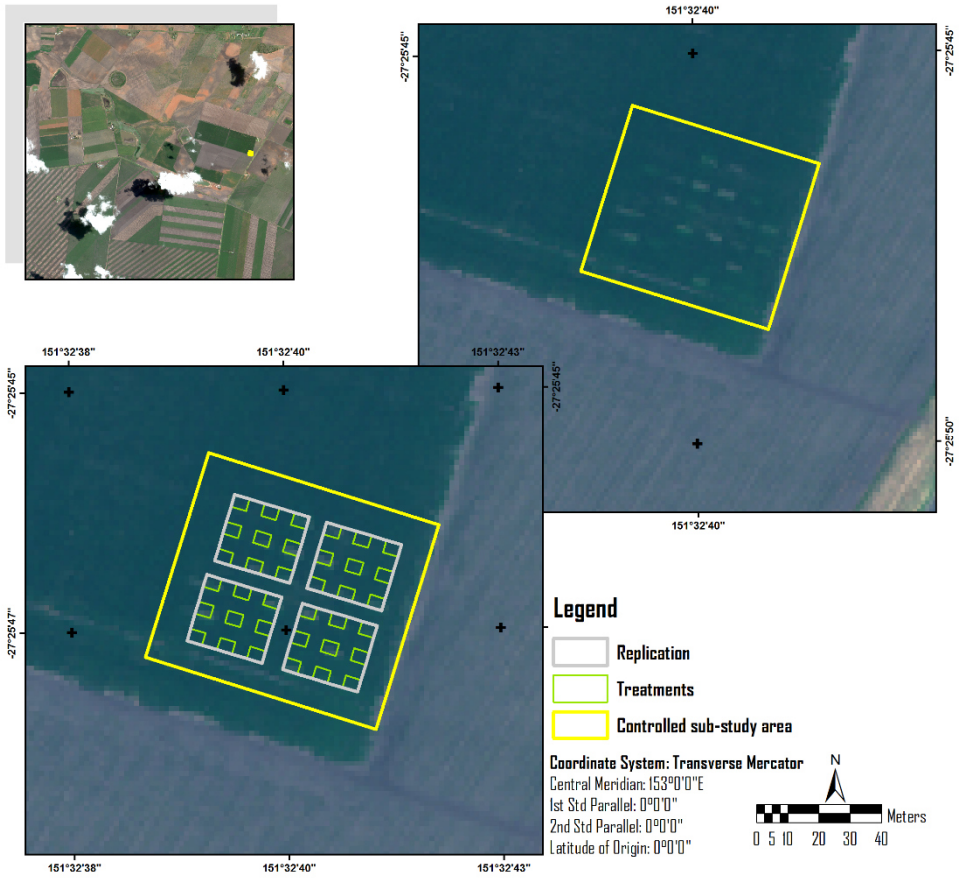

Figure 3-4. Geographic location of the controlled sub-study.
The background on the image is a true colour composite of a Worldview-3 image (red, green, blue bands in the RGB colour channel).

Each treatment plot comprised five rows, each 5.0 m long, at 1.0 m row spacing. A buffer zone of five rows by 5 m was established between plots to reduce the risk of drift between treatments (Figure 3-5). The herbicide was applied when plants reached the stage of growth defined as a factor, under optimal environmental conditions between 9 am and 10 am local time. Plants were treated only once and directly sprayed in two rows of the 5 rows available with a CO2 Research Sprayer provided by the Queensland Department of Agriculture and Fisheries (QDAF) at Toowoomba. The walking speed was set at 1 m/s for all treatments. The pressure was 2 bar, the nozzle size TTI110015, and the water volume was set at a constant rate of 143 L/ha (Figure 3-6).

Figure 3-5. Controlled sub-study: an overview of the study area.
The figure presents the rows included in a treatment (top part) and the marks delimiting the initial and final point of each treatment (bottom part).

Figure 3-6. Sprayer setup (top) and spraying activity in the field (bottom).
The equipment and application method includes an accurate mix of chemical and water to simulate the proposed dose, and a constant walking speed for a homogeneous cover of the rows.

3.2.2. Uncontrolled sub-study

The study area comprised 37 ha of dryland cotton (Figure 3-7) of the high yielding variety Sicot 74BRF (*CSIRO Cotton breeding team*), located in a commercial cotton farm (151°32'30" E, 27°25'35"S). Cotton was planted between the 27th and the 29th October 2014. Approximately 38% of the area was accidentally sprayed with a phenoxy herbicide 2,4-D (*Amicide Advance 700®; 100 ml/ha 2,4-D*) on approximately the 27th January 2015, three months after planting. This uncontrolled sub-study is

addressed in Chapter 5 and examines the effect of one dose at one timing of exposure (93 DAS) and six different times in relation to the exposure.

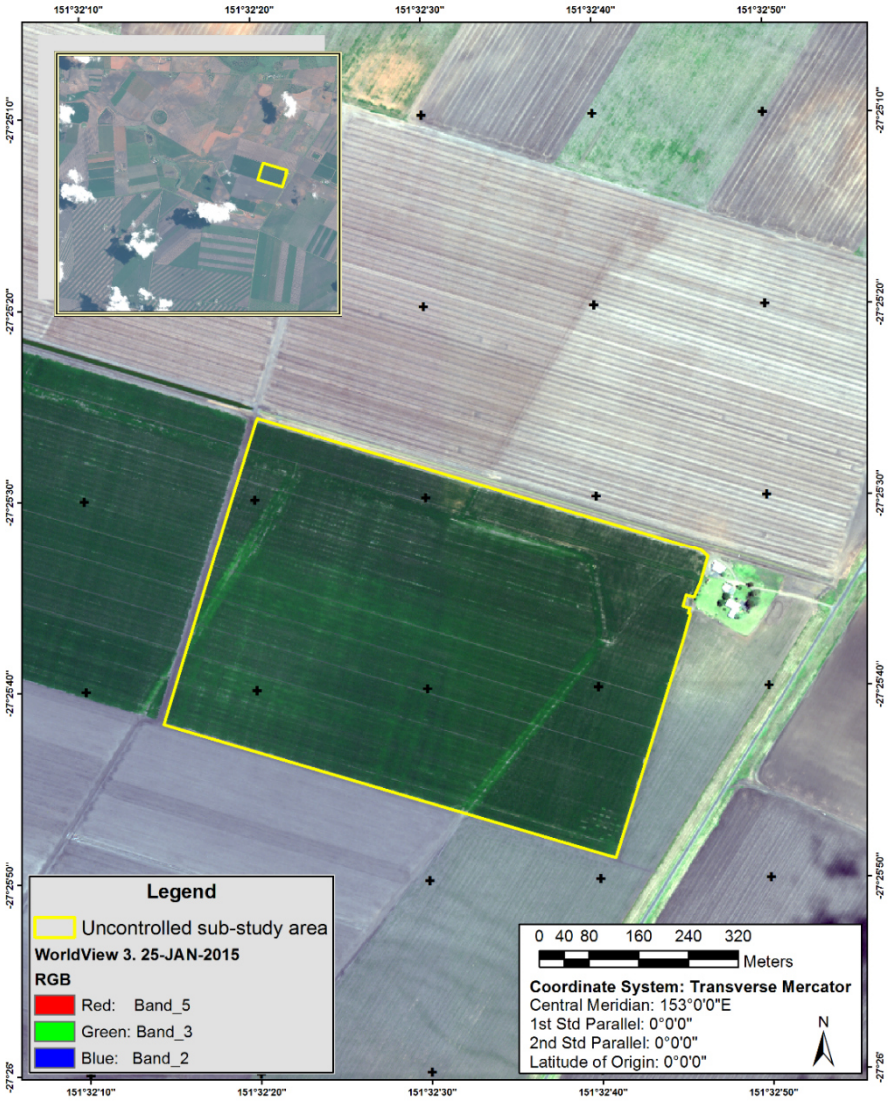

Figure 3-7. Geographic location of uncontrolled sub-study.
The background on the image is a true colour composite of a Worldview-3 image (red, green, blue bands in the RGB colour channel).

3.3. Data capture and acquisition

Data capture and acquisition dates varied according to the sub-study and the instrument to be used. Table 3-2 summaries the different sensors, platforms and variables analysed in this study, in relation to the study area and the objectives listed in Section 1.4.

Detailed descriptions of the data capture and acquisition methods are presented in sections 4.3, 5.3 and 6.3. Hyperspectral measurements and LiDAR data were collected in the controlled experiment for each of the treatments and multispectral satellite data

was acquired in the uncontrolled case. Figure 3-8 presents the research framework as it relates to the objectives of this research project.

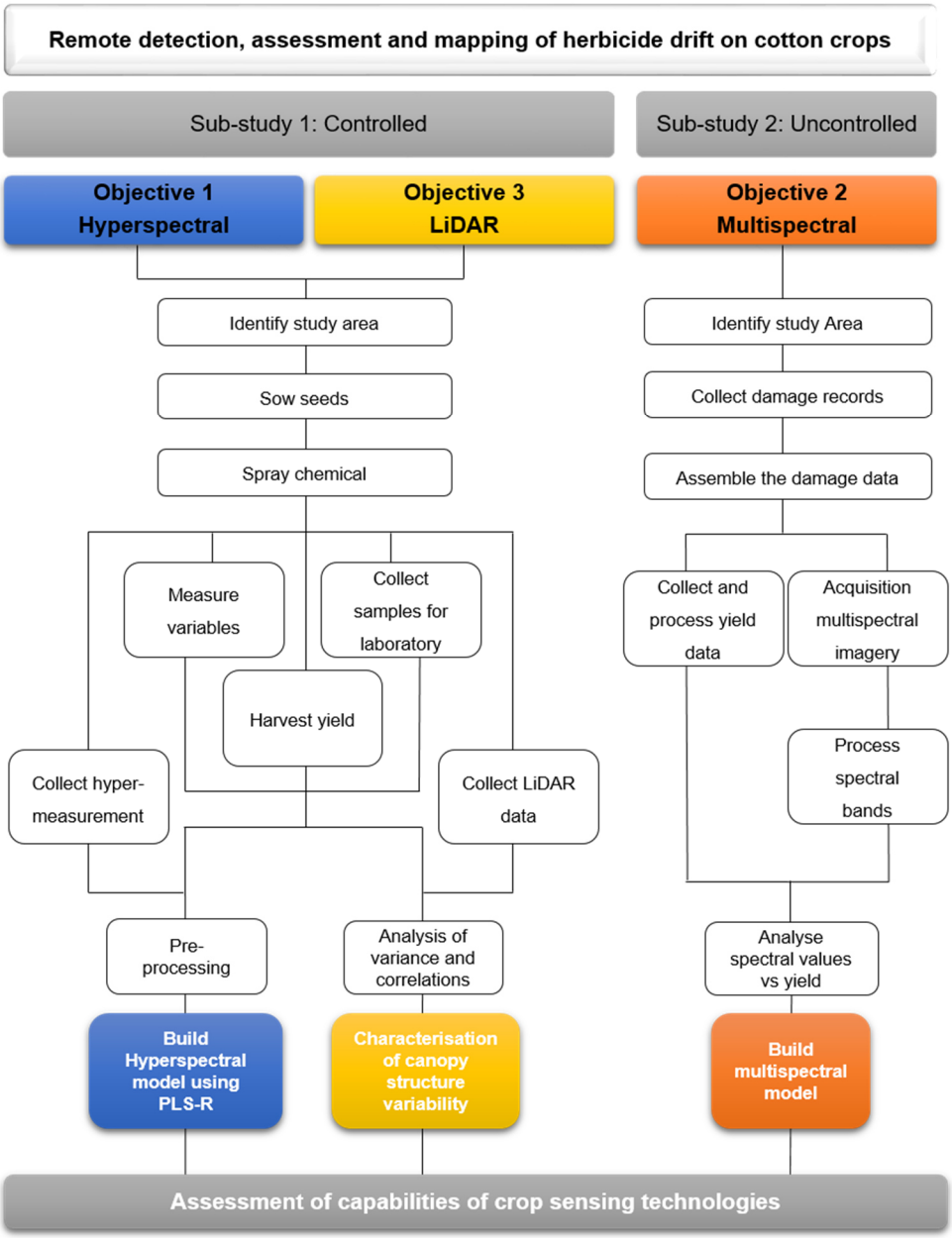

Figure 3-8. Research framework listing the main activities.

Table 3-2. Sensors, platform and attributes measured in this study.

Objective	Sensor and platform	Sub-study	Attributes to measure
1	Handheld hyperspectral sensor (Proximal)	Controlled	Reflectance variability associated with 2,4-D contamination and internal changes in leaves.
2	Multispectral satellite sensor (Landsat-8 OLI)	Uncontrolled	Reflectance changes under the influence of 2,4-D
3	Terrestrial LiDAR sensor (Proximal)	Controlled	Changes in canopy attributes (canopy height and canopy volume).

3.3.1. Controlled sub-study

Fieldwork started soon after planting and finished with hand harvesting at 169 days after sowing (Table 3-3). The date for harvesting was established on the basis of the maturity status of the control treatments. Chemical defoliation was applied to facilitate the harvesting process and was successful in control treatments, however, the 2,4-D-treated treatments manifested some resistance to the chemical defoliant (Figure 3-9).

Figure 3-9. Influence of 2,4-D dose in the efficacy of defoliation applications in plants treated at the latest stage (S3).
Note the significant amount of green and dried leaves still in the plants after the defoliation applications. Left: lower dose (D1); right: higher dose (D2).

It was not always possible to collect data or samples on the dates specified in the design schedule due to environmental conditions or commercial activities, such as irrigation and pest control, in the field. Data collection and sampling were executed a few days later in those instances, as indicated in Table 3-3, which lists the dates and details of the field activities of this sub-study.

Table 3-3. Dates for data collection purposes according to days after the exposure (DAE) and instruments.

Stage	Date	Activity	Description
Planting	**27/10/2014**		
---	31/10/2014	Delimitation of treatments	
4 nodes	**19/11/2014**	**Spraying**	Wind direction ENE
	21/11/2014	Destructive sampling Hyperspectral LiCOR-6400	2 DAE
	26/11/2014	Hyperspectral LiCOR-6400 LiDAR	7 DAE
	8/12/2014	Destructive sampling Hyperspectral LiCOR-6400 LiDAR (4/12/2014)	16 DAE (Cancelled), 19 DAE
	16/12/2014	Hyperspectral LiCOR-6400	28 DAE
8 nodes	**1/12/2014**	**Spraying**	**Wind direction ENE**
	3/12/2014	Destructive sampling Hyperspectral LiCOR-6400 LiDAR (4/12/2014)	2 DAE
	8/12/2014	Hyperspectral LiCOR-6400	7 DAE
	16/12/2014	Destructive sampling Hyperspectral LiCOR-6400	15 DAE
	9/01/2015	Hyperspectral LiCOR-6400	40 DAE
12 nodes	**10/12/2014**	**Spraying**	**Wind direction NE**
	15/12/2014	Destructive sampling Hyperspectral LiCOR-6400	2 DAE (Cancelled), 5 DAE
	17/12/2014	Hyperspectral LiCOR-6400	7 DAE
	23/12/2014	Destructive sampling Hyperspectral LiCOR-6400	14 DAE
	9/01/2015	Hyperspectral LiCOR-6400	30 DAE
14/04/2015	**Full growth**	**Hand harvesting**	**169 days after planting**

3.3.2. Uncontrolled sub-study

Landsat-8 Operational Land Imager (OLI) images of the affected and unaffected areas of the crop from various dates before and after the spray damage event were downloaded and analysed (Table 3-4). The experimental area was harvested using a four-row picker supplied by the grower. A yield monitor, equipped with a GPS tracker was installed in the picker, calibrated in a refugee paddock prior to harvesting (Figure 3-10), and implemented to record yield every three seconds. More details are provided in Chapter 5.

Figure 3-10. Uncontrolled sub-study: calibration process of yield monitor in a refugee paddock.

The entire paddock was sprayed two weeks before harvest with chemical defoliant to accelerate defoliation and facilitate mechanical harvesting. This process was successful in the area of the paddock that was not contaminated by 2,4-D, but the defoliation rate was slower and less homogeneous in the 2,4-D-affected area, as in the controlled sub-study. (Figure 3-11).

Figure 3-11. Visual assessment of defoliation effectiveness in the paddock.

Table 3-4. Uncontrolled sub-study: data acquisition schedule for Landsat-8 OLI, as days after sowing (DAS) and days after exposure (DAE).

				Area	
	Date	DAS	DAE	Unaffected	Affected
27th-29th Oct 2014			Planting		
Acquisition Date	17/12/2014	51	-42	x	x
	18/01/2015	83	-10	x	x
	3/02/2015	99	6	x	x
	7/03/2015	131	38	x	x
	23/03/2015	147	54	x	x
	8/04/2015	163	70	x	x
24th April 2015			Harvesting		

3.4. Summary

The two sub-studies or cases have different approaches but seek to achieve similar outputs, that is, models to predict cotton yield under the influence of *2,4-D* herbicide drifts.

The controlled sub-study was designed to:

i. assess the internal responses of the plant to different doses of the chemical at specific times of exposure throughout the growing season.

ii. provide a better understanding of how these biological effects (internal changes) at the cell level were associated with treatments, yield, spectral variability and canopy structure.

The second sub-study (uncontrolled) is designed to:

i. test the usefulness of multispectral imagery in detecting and assessing damage in the field caused by sub-lethal doses of herbicide.

ii. identify the potential and the respective limitations of medium spatial resolution satellite imagery.

Chapter 4

HYPERSPECTRAL SENSING FOR PROXIMAL DETECTION OF HERBICIDE DRIFT DAMAGE ON COTTON CROPS

4.1. Introduction

The first objective of the research project is covered in this chapter, where the potential uses of proximal hyperspectral sensors on the detection of 2,4-D herbicide drift on cotton crops are explored. The potential uses of hyperspectral data focused on the prediction capabilities of 2,4-D herbicide reaching the crop and the yield loss caused by the contact with the chemical. The temporal variability of hormone contents (i.e. Indole Acetic Acid – IAA and Abscisic Acid – ABA) and the physiological variables defined by photosynthesis and stomatal conductance are analysed to understand the spectral changes as a function of the internal variations within the plants. Different pre-processing methods for hyperspectral noise removal and filtering were tested to investigate their influence on the prediction capabilities of the models.

This chapter is divided into six sections starting with an introduction in Section 4.1 about the objective of this study, after which a literature review section is presented (Section 4.2). Materials and Methods comprise Section 4.3 where the different instruments and procedures used to reach the proposed objectives are documented. Results are presented in the fourth section (4.4), while a comprehensive and detailed discussion is presented in Section 4.5. Finally, section 4.6 presents a summary of this chapter.

This chapter explores the capabilities of the hyperspectral proximal sensor as an alternative method for assessing herbicide drift damage in cotton crops caused by the herbicide 2,4-D. Six specific objectives were defined:

i) to analyse the amount and quality of yield variability due to the timing of exposure and dose;

ii) to understand the influence of dose in the temporal variability of photosynthesis, conductance and two hormones - IAA and ABA;

iii) to assess if spectral pre-processing techniques can improve the robustness of the models;

iv) to predict models of yield at four different time periods after the exposure to herbicide;

v) to examine if herbicide dose can be accurately predicted from field measurements of hyperspectral reflectance; and

vi) to determine whether prediction models can be improved by establishing the optimum data collection time after the exposure.

4.2. Proximal sensors for the detection of herbicide drift

Cotton crops are highly susceptible to 2-4-dichlorophenoxy acetic acid (2,4-D). This chemical is a derivative of indole acetic acid (IAA) which elicits the same type of plant responses as IAA, but with stronger intensity and higher stability in the plant (Grossmann, 2010). 2,4-D, as a selective synthetic auxin herbicide, is often referred to as phenoxy class herbicide. The mode of action of 2,4-D is to disrupt the plant cell growth by an uncontrolled production of simulated IAA in broadleaf plants (Bondada, 2011). IAA is considered as a master hormone because it influences every aspect of plant growth and development such as cell division and elongation, floral meristem differentiation, leaf initiation, senescence, apical dominance and root formation (Grossmann, 2010). Synthetic auxins, applied as herbicide, mimic the deformation and growth-inhibiting effects caused by IAA at a very constant and increasing concentration until the growth causes plant death. The biosynthesis of the phytohormone abscisic acid (ABA) is also over-stimulated by herbicide 2,4-D causing growth inhibitors, morphological abnormalities and senescence (Teixeira et al., 2007). ABA is an important plant hormone for adjusting to environmental stress, seed development and dormancy (Straub et al., 1994). *This study explores the temporal variability of these two hormones and their relationships with hyperspectral data under the effect of 2,4-D*.

Several efforts to remediate cotton from spray drifts have been limited mainly because the extent of injury depends upon the climate and proximity to thousands of cereal and fallow fields where 2,4-D is sprayed to control broad-leaved weeds (Bondada, 2011)

while significant inconsistencies in the traditional assessment of damage have been proven in several studies (Charles et al., 2007; Everitt & Keeling, 2009). These limitations prevent farmers from optimising management practices and mitigating losses while reinforcing the need for more precise techniques for prediction of cotton damage.

Remote sensing techniques are widely applied in agriculture due to their capability to provide significant information about the health of crops. Biophysical and physiological variables are analysed through the visible (VIS)-to-shortwave infrared (SWIR) wavelengths without the need to implement destructive sampling. The ability to integrate the concept of spatial distribution, environmental conditions and soils, with high accuracy, has turned remote sensing techniques into a valuable tool for crop assessment (Clevers, 1999; Suarez et al., 2016; Tian et al., 2005). Hyperspectral sensors are able to detect small variations in the biophysical and physiological characteristics of the plants (Rapaport et al., 2015). Accurate prediction results (i.e. prediction accuracy = 92%) were obtained in predicting the grain protein content of wheat (*Triticum aestivum*) (Apan et al., 2006) through the implementation of hyperspectral data and partial least squares regression (PLS-R) analysis.

Hyperspectral sensors have been also used in a variety of detection of plant disease or stress applications caused by pesticides (Henry et al., 2004), water (Detar et al., 2006), nitrogen (Schlemmer et al., 2013), and other nutrient deficiencies (Chen et al., 2011; Tian et al., 2012). Effects on carotenoids, an important pigment of green leaves, were accurately predicted by different statistical approaches applied to hyperspectral data in cotton crops (Yi et al., 2014). These techniques included stepwise multiple linear regression (SMLR), band selection indices, partial least squares regression (PLS-R) and linear regressions using published vegetation indices such as NDVI and red-edge chlorophyll index.

Remote sensing data has been also used to discriminate species (Ghosh et al., 2014), canopy variables and canopy structures (Lefsky et al., 2002; Marshall & Thenkabail, 2015; Rama Rao, 2008). This technology has been further applied to estimate different biophysical and physiological variables and pigment contents of vegetation over a large number of crops (Barnes et al., 2000; Li et al., 2001; Pinter et al., 2003) with the objective of examining the healthiness of vegetation. Other remote sensing studies

have analysed the relationship between cotton reflectance and lint yield under variable Nitrogen and irrigation treatments (Li et al., 2001). In another study, cotton yield was found to be highly correlated with stomatal conductance and transpiration rate, as they are positively correlated with flower production (Perumal et al., 2006).

Studies on the effects of 2,4-D on cotton crops demonstrated that photosynthesis was highly affected by this herbicide leading to ineffective photosynthesis processes, affecting boll production and development (Perumal et al., 2006; Sullivan et al., 2007). Perumal et al. (2006) reported a reduction of 23% in stomatal conductance and 70% in photosynthesis when cotton plants were exposed to 2,4-D at 5 ppm. Spectral bands in the green, red and NIR regions have been identified as good predictors of yield and they are also associated with the health condition of the plants (Plant et al., 2000; Zhao et al., 2005). Photosynthesis has a strong relationship with the spectral bands around 700 nm, which is also related to physiological stress (Merton et al., 2004; Zhao, Reddy, et al., 2007). As the visible and NIR bands respond to different conditions of the crop, it may be possible to determine yield based on those responses (Pinter et al., 2003; Thulin et al., 2012; Zarco-Tejada et al., 2005).

Several narrow and broadband vegetation indices have been developed in order to minimise the influence of soil (Yu et al., 2015), pigments, moisture, and the general variability of external factors on leaf and canopy reflectance (Cyr et al., 1995; Zhao, Huang, et al., 2007). However, their applicability may be limited by the pigments' variability per unit leaf area and potential saturation at medium-to-high leaf area index (LAI), which are related to spatial and temporal situations (Blackburn, 2007; Carter, 1998; Zarco-Tejada et al., 2005). On the other hand, hyperspectral sensors may allow the detection of very small changes within the plant due to reflectance changes on the electromagnetic spectrum, which often consist of hundreds of highly correlated wavelengths (Figure 4-1). These sensors rely on the efficiency of the processing and analysis techniques to isolate one single response variable with a sample size greatly smaller than the number of predictors (Rapaport et al., 2015; Wold et al., 2001).

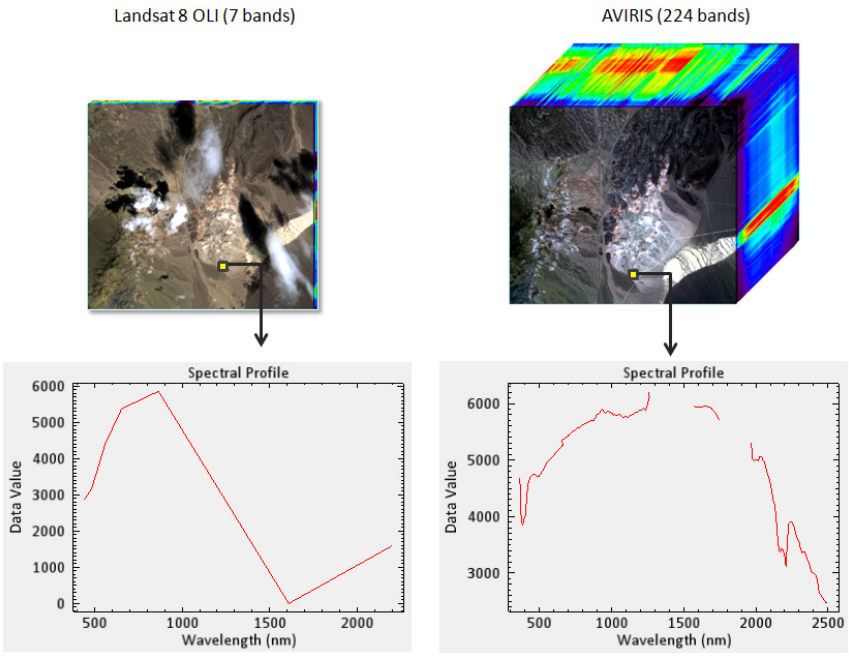

Figure 4-1. Comparison of the spectral profile generated by a multispectral sensor and a hyperspectral sensor.
Source: (Harrys Geospatial Solutions, 2017)

Signal noise is a documented limitation of hyperspectral data, caused by instrument and atmospheric conditions (Vaiphasa, 2006). Noise in the spectral data has to be removed with caution due to a high correlation between discrimination capabilities and bandwidth (Schmidt & Skidmore, 2004). Noise removal decreased the predictive capabilities of models in Barbin et al. (2012), while Vaiphasa (2006) demonstrated the negative effects of smoothing techniques in the outcomes of subsequent analysis when statistical characteristics of spectral data were required. Smoothing techniques should be objectively selected rather than ad hoc as many studies have previously done (Chen et al., 2011; Helland et al., 1995; Swatantran et al., 2011).

Partial least squares regression (PLS-R) is an algorithm that deals with hundreds of highly correlated variables that is commonly used and considered as a powerful tool in spectroscopy (Indahl & Næs, 2004). Furthermore, PLS-R optimises the resulting model by reducing the dimensionality of the electromagnetic spectrum (Mevik & Wehrens, 2007; Wold et al., 2001). While various statistical methods are available for quantitative studies, such as neural networks (de Castro et al., 2012; Goel, Prasher, Patel, et al., 2003), PLS-R has proven to be optimal as the first-step approach for supervised classifications (Indahl et al., 2009), and it is also one of the most effective methods for quantitative predictions (Mevik & Wehrens, 2007).

Successful yield prediction studies and discrimination of healthy from unhealthy plants damaged by herbicide drifts can be found in the literature. A research gap still exists to accurately model 2,4-D herbicide drift damage, in cotton crops, using hyperspectral data as a function of three factors: a) dose (**D**), b) timing of exposure (**S**), and c) days after the exposure (**DAE**).

4.3. Materials and methods

A complete description of the experimental design was described in section 3.2. This design was composed of three timing of exposures: 4-5 nodes (**S1**), 7-8 nodes (**S2**) and 11-12 nodes (**S3**) and three doses of 2,4-D (*Amicide Advance* 700®; 700 g/L 2,4-D) according to the recommended label rate as Nil (0%), 28 g a.i/ha (5%) and 280 g a.i/ha (50%) (Figure 4-2). Plants were treated only once and directly sprayed in two rows of the 5 rows available as presented in Figure 4-3.

Figure 4-2. Set up of equipment and preparation of simulated dose.

Standard management practices were applied to all treatments before and after the spray activity. In two replications, some treatments were required to be relocated as some rows looked slightly affected by drift from a neighbouring treatment. Figure 4-3 shows the treatments locations and the treatments subjected to relocations.

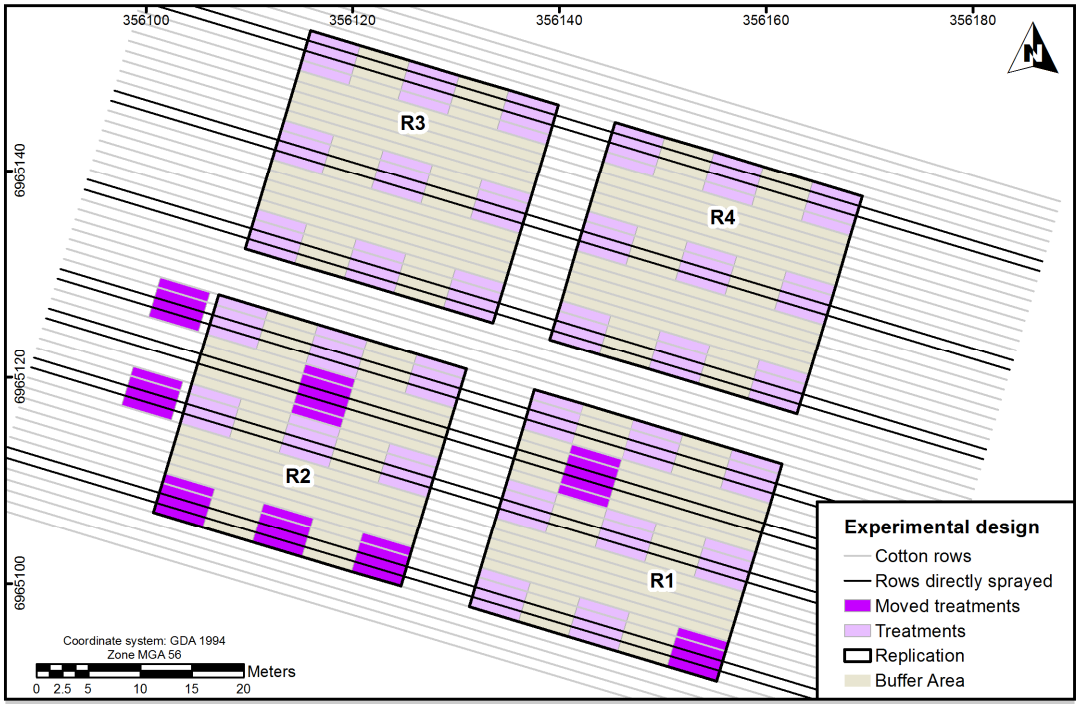

Figure 4-3. Layout of the experimental design.

The herbicide was applied under optimal environmental conditions between 9 am and 10 am local time once the plants reached the timing of exposure previously defined (Figure 4-4). The spray treatment area of each plot was clearly marked to avoid spraying outside this area, with consequent possible exposure of other plots to the herbicide (Figure 4-5).

Figure 4-4. Spraying activity at 4-5 nodes.

Figure 4-5. General view of the experimental area and treatment set-up.
The initial and final point of each treatment is defined by the white and yellow markers in the ground, respectively.

Table 4-1 summarises the frequency, the instruments and the variables implemented in this study while Figure 4-6 summarises the approach implemented in this chapter.

Table 4-1. List of frequency, variables and instruments analysed in this study.

			Days after exposure (DAE)				
Variables		**Instrument**	**2**	**7**	**14**	**28**	**Harvest**
Hormones	Indole Acetic Acid (IAA)*	Laboratory	x		x		
	Abscisic Acid (ABA)*		x		x		
Physiology	Photosynthesis	LiCOR	x	x	x	x	
	Stomatal Conductance		x	x	x	x	
Spectral data	Spectral response	Hyperspectral	x	x	x	x	
Yield	Quality						x
	Quantity						x

* Destructive sample

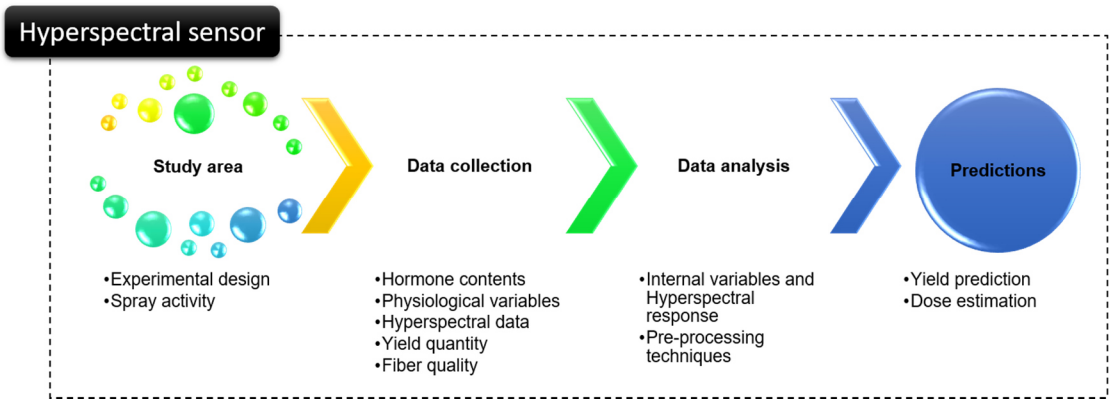

Figure 4-6. Flowchart of the main activities undertaken for the analysis of hyperspectral data.

4.3.1. Data collection

Data collection was performed at four specific days after the exposure (DAE) to analyse the temporal changes to the variables listed in Table 4-1, and to establish the optimum data collection date after the exposure. Five uppermost fully expanded leaves were sampled from five plants randomly selected in each treatment at 2, 7, 14 and 28 days after exposure (2 DAE, 7 DAE, 14 DAE and 28 DAE, respectively). Destructive sampling was necessary for IAA and ABA analysis. Hormone content analysis was performed only at 2 DAE and 14 DAE due to the high cost of the laboratory analyses, while the physiological variables were measured at the same proposed dates as the hyperspectral measurements: 2, 7, 14 and 28 DAE. For each DAE, all the measurements were collected in the same leaf, clearly identified on the plants (Figure 4-7). The labels were moved to the top node after destructive sampling to identify and exclude these plants from further analysis.

Figure 4-7. Plants were marked to be excluded from further analysis after destructive sampling.

4.3.1.1. Hyperspectral data

Leaf spectral reflectance was measured using a portable spectroradiometer *FieldSpec HandHeld2* (Analytical Spectral Devices Inc., Colorado USA) which acquires continuous spectra from 325 nm to 1075 nm, with an accuracy of ± 1nm and resolution of < 3nm at 700 nm. The instrument was configured to calculate each reflectance as an average of ten repeated scans on cloudless and sunny days between 9h00 and 15h00 during the 12 data capture campaigns. The weather and sunlight conditions were generally stable. Calibration and optimisation procedures with a *Spectralon*® white reference panel were performed per treatment and for every time slight changes in environmental conditions were observed. These procedures were implemented to maximise the signal-to-noise ratio without saturation and to ensure that the different spectral reflectance measurements were comparable (ASD Inc, 2010; Liu et al., 2013; Yi et al., 2014) (Figure 4-8).

Figure 4-8. Calibration and optimisation procedure with a *Spectralon*® white reference panel.

The standard field-of-view of the instrument was 25° so the instrument head was placed approximately 2.25 cm above the leaf to get a circular view area of 1 cm diameter. As cotton is a broadleaf plant, this facilitates a clear spot size of 1cm on the leaf without soil and background effects. Leaves were positioned horizontally to simulate Lambertian surfaces and reduce any possible backscattering and solar

illumination effects (Figure 4-9). The horizontal position also allows the device to detect the same magnitude of radiance at any angle of field-of-view of the instrument relative to the leaves (ASD Inc, 2010; Vigneau et al., 2011). Furthermore, the instrument was placed above the leaf in such position that no shadow was generated from the device or from the person collecting the data. These sampling techniques were previously used in measuring reflectance from mangrove (Lagomasino et al., 2014) and corn leaves (Wang et al., 2012).

Figure 4-9. Collection of hyperspectral data in the field.

4.3.1.2. Photosynthesis and stomatal conductance

A portable photosynthesis system Li-6400 (Li-Cor, Lincoln, NE, USA) was used to take instantaneous measurements of photosynthesis (umol/m^2/s) and stomatal conductance (mol/m^2/s) in the same leaves sampled for hyperspectral measurements. Li-6400 is an open system where photosynthesis and transpiration are computed on the differences in CO_2 and H_2O in an air stream that is flowing through the leaf cuvette or chamber (LiCOR, 1999) (Figure 4-10). The photosynthesis and stomatal conductance calculations were based on the chamber area (see Figure 4-10) which is equal to 6 cm^2. Some leaf areas were smaller, so the calculations were performed based on the percentage of the area exposed inside the chamber (LiCOR, 1999). This situation occurred a few times during the early stage of growth, as the leaf area was

not big enough to completely cover the leaf cuvette. Measurements were performed at intervals of 2, 7, 14 and 28 DAE. Data was imported and combined with hyperspectral data into R software to create hyperspectral objects for posterior analysis. Figure 4-11 shows the functionality of the Li-6400 in the field.

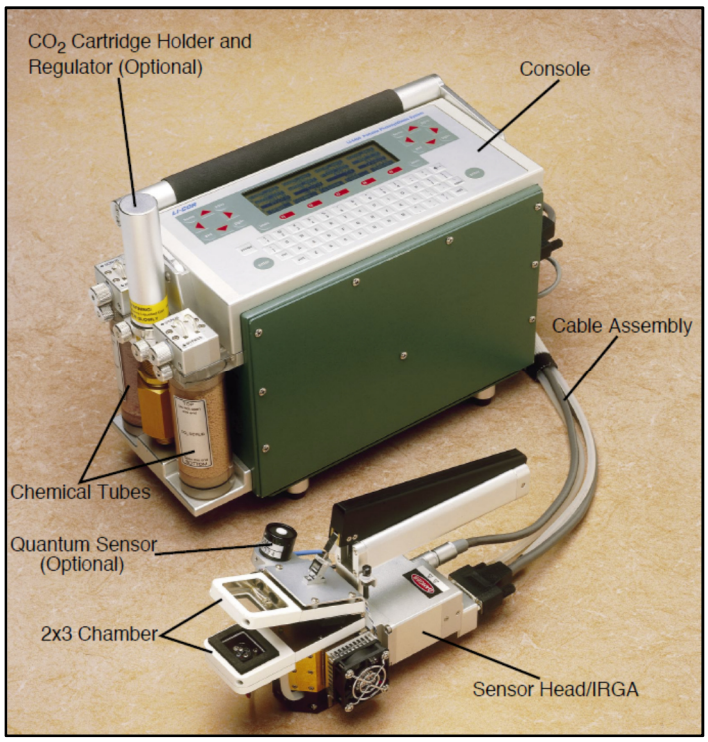

Figure 4-10. Main parts of the Li-6400 portable photosynthesis system.
Source: (LiCOR, 1999)

4.3.1.3. IAA and ABA estimations

The IAA and ABA responses during the growing season were analysed at 2 DAE and 14 DAE. In the field, five leaves per treatment were sampled after the respective hyperspectral and physiological measurements. A total of 72 samples, representing all treatments and replications for 2 DAE and 14 DAE were analysed. Before the extraction of IAA and ABA, the samples were stored in liquid nitrogen during transportation and kept frozen in a -80°C freezer until the freeze-dried procedures were undertaken to remove or extract all water content from the leaves. Hormone extraction was then performed following the procedure described by Tivendale et al. (2012).

Figure 4-11. Measurement of physiological variables.

4.3.1.4. Harvested yield (including quality and quantity)

Cotton was manually harvested over three consecutive days during April 2015. Yield, as well as a count of immature bolls, were recorded for each treatment (Figure 4-12). Only the two rows directly sprayed with the chemical were harvested and weighed. Three of the 5 m per row available were harvested resulting in an equivalent area of 6

m^2 picked at each treatment. The three meters were measured one meter after the starting point of each treatment. Quality characteristics of the yield samples were also measured. Table 4-2 summarises the quality variables investigated in this study and their corresponding description. From this analysis, lint yield percentage (Lint) was calculated and yield was estimated in the units of bales/ha using the equation 1, where W is the weighted yield projected in bales units (1 bale = 227 kg):

$$Yield_{(Bales/ha)} = Lint \cdot W^{-1} \qquad \textbf{(Equation 1)}$$

Table 4-2. Cotton fibre quality variables measured in this study

Variable	Description	Acronym
Gin turnout	Percentage of lint compared to total sample weight	Lint
Staple length	Length of fibre expressed as 36/inch	Length
Micronaire	Factor based on fibre maturity and fibre thickness	M
Fibre uniformity	How uniform the fibre sample is	Uni
Fibre strength	Strength of the fibre	Strength
Short Fibre Index	Percentage of short fibre within each sample	SFI
Fibre elongation	Percentage of the starting length	Elon

Figure 4-12. Manual harvesting in a control treatment.

4.3.2. Data processing

The reflectance data (751 wavelengths) was exported into ASCII format using *ViewSpec Pro* (Analytical Spectral Devices Inc., Colorado USA). The data was then imported into R software (R Core Team 2014) and converted to hyperspectral objects using *hyperSpect* package to conveniently manage the hyperspectral data (Beleites, 2015). A cleaning process took place to exclude the noisy wavelengths of two regions (i.e. 325 nm - 399 nm and 901 nm - 1075 nm) from data analysis (Apan et al., 2006). Outliers or anomalous reflectance data were also omitted from the remaining reflectance data from 400 nm to 900 nm, as they tend to increase the error in statistical models (Wold et al., 2001; Zainol Abdullah et al., 2014). Although the *hyperSpect* package provides different approaches for pre-processing techniques, the *prospectr* package was implemented in this study as it supplies functions that work independently from the object class (vector, data frame or matrix) in R (Stevens & Ramirez-Lopez, 2014); this facilitates data manipulation while applying the pre-processing algorithms.

4.3.2.1. Noise removal and filtering of hyperspectral data

Different pre-processing techniques were applied after the cleaning process. These techniques are commonly used in spectroscopy to remove or minimise light scattering effect by removing the noise and normalizing the data (Stevens & Ramirez-Lopez, 2014). Pre-processing algorithms can change the spectral characteristics of the data which could lead to inaccurate results (Vaiphasa, 2006). Selecting the pre-processing technique is a task that involves continuous testing and there is no standard procedure to define it (Barbin et al., 2012). A range of different pre-processing algorithms was performed to reduce the spectral variation and noise generated by light scattering effects with data collected at 2 DAE. Raw spectral data were analysed to compare the influence of pre-processing techniques in the prediction ability of regression models.

Pre-processing filters of hyperspectral data include smoothing, derivatives and scatter correction. Smoothing techniques are mathematical approaches that alter original data to remove or minimise noise originated by the instrument or environmental conditions. Derivatives of the first (**FD**) and second order (**SD**), have the potential to remove additive (offset) and multiplicative (slope) effects, enhance small spectra absorptions and resolve overlapping absorption. However, there are negative impacts associated

with these filters, as they increase the noise and the risk of overfitting the calibration model (Barbin et al., 2012; Stevens & Ramirez-Lopez, 2014). Savitzky-Golay (**SG**) is another smoothing technique that smooths the reflectance signature while conserving the relative information of minima, maxima and width (Barbin et al., 2012; Luo et al., 2005).

Relatively new spectral transformations, such as Fourier transformation and empirical mode decomposition, have been proven to produce reliable results. However, the former has been mainly developed to reduce the full-column atmospheric effects or the stripping effects from satellite imagery (Rama Rao, 2008) while the latter has been applied to analysing the properties of time series (Wang et al., 2016). Wavelet transform has been implemented with limitations, especially in cases with high background influences (Hai-bin et al., 2005).

Scatter corrections remove the light scatter effects and variations in effective path length. Standard Normal Variate (**SNV**) is a way to normalize spectra by removing the light scattering effect. SNV establishes a common scale for all spectra as each individual spectrum is divided by its standard deviation. Multiplicative Scatter Correction (**MSC**) is another mathematical treatment that uses the mean spectrum of the data set (Barbin et al., 2012). SNV or MSC only take into consideration the spectral information of the sample. Other scatter corrections not only take the information of the sample but they also take the chemical variation within the sample as a source of scattering (Helland et al., 1995).

The two scatter correction methods, of Multiplicative Scatter Correction (MSC) and Standard Normal Variate (SNV), were performed in this study. Furthermore, first and second derivatives (**FD** and **SD**), as well as Savitzky-Golay (**SG**) filtering with 11 local polynomial regression, were also investigated.

4.3.3. Statistical analysis

Classical Partial Least Square Regressions (PLS-R) analysis is the most used regression technique in chemometrics and spectroscopy. It can be performed to obtain *Y*-variable responses indicating continuous data or classes or categories. The influence of pre-processing techniques was tested, in this study, by comparing five PLS-R models with raw or transformed spectral data as *X*-variables, and yield as *Y*-variable.

Furthermore, four PLS-R models were built to investigate the temporal variability of the models with hyperspectral data collected at 2, 7, 14 and 28 DAE. Likewise, Two PLS-R methods for predicting categorical variables (**D0**, **D1**, and **D2**) were tested: Canonical Powered PLS-R (**CPPLS**) and Sparse PLS Discriminant Analysis (**sPLS-DA**).

New and promising non-parametric and machine-learning algorithms have been used in recent years for spectral regression applications such as estimation of nitrogen, phosphorus and potassium (Zhai et al., 2013; X. Zhang et al., 2013).). However, from a statistical perspective, linear models should be the calibration tool of choice (Olivieri, 2015) as non-parametric algorithms can only be implemented in a limited way, and only non-linear relations can be modelled. Furthermore, the effect of each predictor, in this case, the wavelength, can be less easy to understand intuitively than in linear models such as PLS-R.

The calibration performance of PLS-R has been compared with sophisticated non-linear models, such as least-squared support vector machines, perception networks and kernel PLS-R in some studies (Thissen et al., 2004). The comparisons are often based on the error of prediction and the coefficient of determination (R^2). However, these parameters, particularly R^2, are inadequate to assess the prediction performance of these models (Olivieri, 2015; Spiess & Neumeyer, 2010). It is not possible to calculate the R^2 in a non-linear regression, since the Total Sum of Squares of the Response (SST) minus the Sum of Squared of the Regression (SSR) is not equal to the Sum of Squared Errors (SSE) as it is in a linear model. Hence, the R^2 cannot be estimated as the ratio of SSR and SST (Frost, 2014; Spiess & Neumeyer, 2010). An adequate and carefully defined statistical procedure should be implemented to test whether the performances of these methods are significantly different (Olivieri, 2015). *Based on the lack of proper analysis and interpretation of results in the literature, this study implemented the most common, reliable and extensively investigated prediction algorithm to analyse the hyperspectral data: PLS-R.*

The identification and selection of the most significant wavelengths can be performed with different algorithms. This is a critical stage in modelling as it is being used not only to optimise and simplify the model but also for interpretation purposes (Suarez et al., 2016; Yi et al., 2014). Two methods for the selection of the most significant

wavelengths were applied according to the response (Y) variable: yield or dose. Weighted regression coefficients (**Bw**), resulting from the optimal yield prediction models, where plotted across all wavelengths. The higher the value obtained for Bw, the more significant the wavelength was for the model (Garrido Frenich et al., 1995; Olivieri, 2015) therefore peaks of Bw were indicators for the contribution of each wavelength (Barbin et al., 2012) into the resulting model. The Significant Multivariate Correlation (**sMC**) algorithm was implemented for extracting information regarding the most significant wavelengths in the models with dose as a response variable. sMC is reported as an algorithm that corrects the limitations of the variable selection method Variable Importance in the Projection (VIP) (Tran et al., 2014).

4.3.3.1. Testing pre-processing techniques and predicting yield with PLS-R

PLS-R is a multivariate procedure for modelling the relationship between a set of independent variables or predictors *X* and a set of dependent variables or responses *Y* (Wold et al., 2001). PLS-R is commonly used in spectroscopy for the following main reasons: 1) it deals with a high amount of correlated *X*-variables and relatively few samples; and 2) it reduces hundreds of potentially correlated predictors into a new small set of orthogonal variables (also called components or latent variables - LV) which carry most of the information. PLS-R incorporates the information of predictors and response variables optimising prediction capabilities (Mevik & Wehrens, 2007).

The optimal number of latent variables (**LV**) is referred as the one with the highest significance for prediction purposes (Mevik & Wehrens, 2007). The set of predictor ***X***-variables ($N_{samples}$ x $W_{wavelengths}$) was composed of 36 initial samples **N** with 501 wavelengths from 400 nm to 900 nm. On the other hand, the dependent variable ***Y*** was yield expressed in bales/ha (Equation 1). The resulting PLS-R equation is:

$$\boldsymbol{Y} = X \times B + \varepsilon \qquad \textbf{(Equation 2)}$$

where ***B*** is the matrix of regression coefficients *b* and ε the matrix of residuals. The determination of wavelength's importance or influence within the model is complex because it is necessary to consider not only the magnitude of b-coefficient but also a variable with small absolute value and a large variance (Garrido Frenich et al., 1995). To identify the most significant wavelength and to ensure the same variance for each

variable, the data has to be standardised ($X_{standarised}$) by weighting the *X*-variables with the inverse of the standard deviation (See Equation 3). The resulting *Bw*-matrix is used to predict new *Y*-values from $X_{standarised}$. A large absolute coefficient (*bw*) is indicative of an important *X*-variable while large *Y*-residuals from the F residual matrix are indicative of poor performance (Wold et al., 2001). The new equation would be:

$$\boldsymbol{Y} = X_{standarised} \times Bw + F \qquad \textbf{(Equation 3)}$$

The resulting prediction models used a maximum number of 10 latent variables (LV), while the leave-one-out (LOO) method was implemented as the cross-validation (CV) algorithm and normalized reflectance per band was used as the predictors. Cross-validation has been reported as an optimum and reliable way to test the predictive significance of the models when highly correlated data is included as predictors, and when an independent and representative set of validation data is not available (Olivieri, 2015; Wold et al., 2001). CV splits the available dataset into *v* groups of approximately the same size (usually 10 groups). The PLS-R algorithm is then run *v* times using (*v* - 1) groups as training sets and one group as a validation set, with a different group being used as the validation set each time. In the case of v equals to N, one object or sample is left out at a time, turning CV into LOO-CV, and CV is then designed to simulate how well the model predicts new data by running the algorithm leaving one object out at a time rather than one larger group.

The coefficient of determination (R^2) in a multiple regression, is defined as:

$$\boldsymbol{R^2} = \frac{SSR}{SST} = \frac{SST-SSE}{SST} = 1 - \frac{SSE}{SST} = 1 - \frac{\sum_{i=1}^{n}(Y_i - \hat{Y}_i)^2}{\sum_{i=1}^{n}(Y_i - \bar{Y})^2} \qquad \textbf{(Equation 4)}$$

Where SST is the Total Sum of Squares of the Response $SST = \sum_{i=1}^{n}(Y_i - \bar{Y})^2$, the Sum of Squared of the Regression (SSR) is equal to SST – SSE, and $\bar{Y}$ is the mean of the measured response. Because the calibration model applied in this study was LOO, the explained variance for the cross-validation model (R_{cv}^2) is defined based on the Prediction of Sum of Squares (PRESS) rather than the SSE. PRESS residuals are the difference between the measured value Y_i and the predicted value $\hat{Y}_{i,-i}$. The stand for $i, -i$ indicates that it is the residual for the ith sample based on the ith point removed from the model (Smith, 2005). In this way, PRESS is defined by:

$$\boldsymbol{PRESS} = \sum_{i=1}^{n}(Y_i - \hat{Y}_{i,-i})^2 = \sum_{i=1}^{n} {e_{i,-i}}^2 \qquad \textbf{(Equation 5)}$$

The PRESS residuals $e_{i,-i}$ can be calculated using the expression:

$$\boldsymbol{e_{i,-i}} = \frac{e_i}{1-h_{ii}} \qquad \textbf{Equation 6)}$$

Where the leverage of the ith sample, h_{ii}, is the distance of the predicted sample i to the centre of the data set (i.e. training or test data set) (Bellon-Maurel et al., 2010). Replacing the SSE factor by PRESS in the Equation 4, the explained variance of a cross-validated (R_{cv}^2) corresponds to:

$$\boldsymbol{{R_{cv}}^2} = 1 - \frac{PRESS}{SST} \qquad \textbf{(Equation 7)}$$

R_{cv}^2 was calculated using the datasets into the LOO-CV models. Because the PRESS can be higher than SST, R_{cv}^2 can yield negative values (Smith, 2005).

The selection of the best performing PLS-R model was based on the minimum number of LV, the ability to explain LOO-CV yield variance (R_{cv}^2) and the minimum absolute root square mean error of the LOO-CV (RMSECV). Also, the fitted values were plotted against the measured values, and the regression coefficient was used as an additional indicator of fit. RMSECV is given as (Mevik & Cederkvist, 2004):

$$\boldsymbol{RMSECV} = \epsilon = \sqrt{\frac{SSE}{n}} = \sqrt{\frac{(\sum \hat{\epsilon}_i^2)}{n}} = \sqrt{\frac{\sum(Y_i - \hat{Y}_i)^2}{n}} \qquad \textbf{(Equation 8)}$$

Assessments of collinearity between scores per LV were performed to avoid model overfitting and support the selection of LVs (Garrido Frenich et al., 1995; Mevik & Wehrens, 2007; Zhao et al., 2013).

Figure 4-13 shows the flowchart of the process followed to test pre-processing techniques and assessing model capabilities for predicting yield (bales/ha) from hyperspectral data.

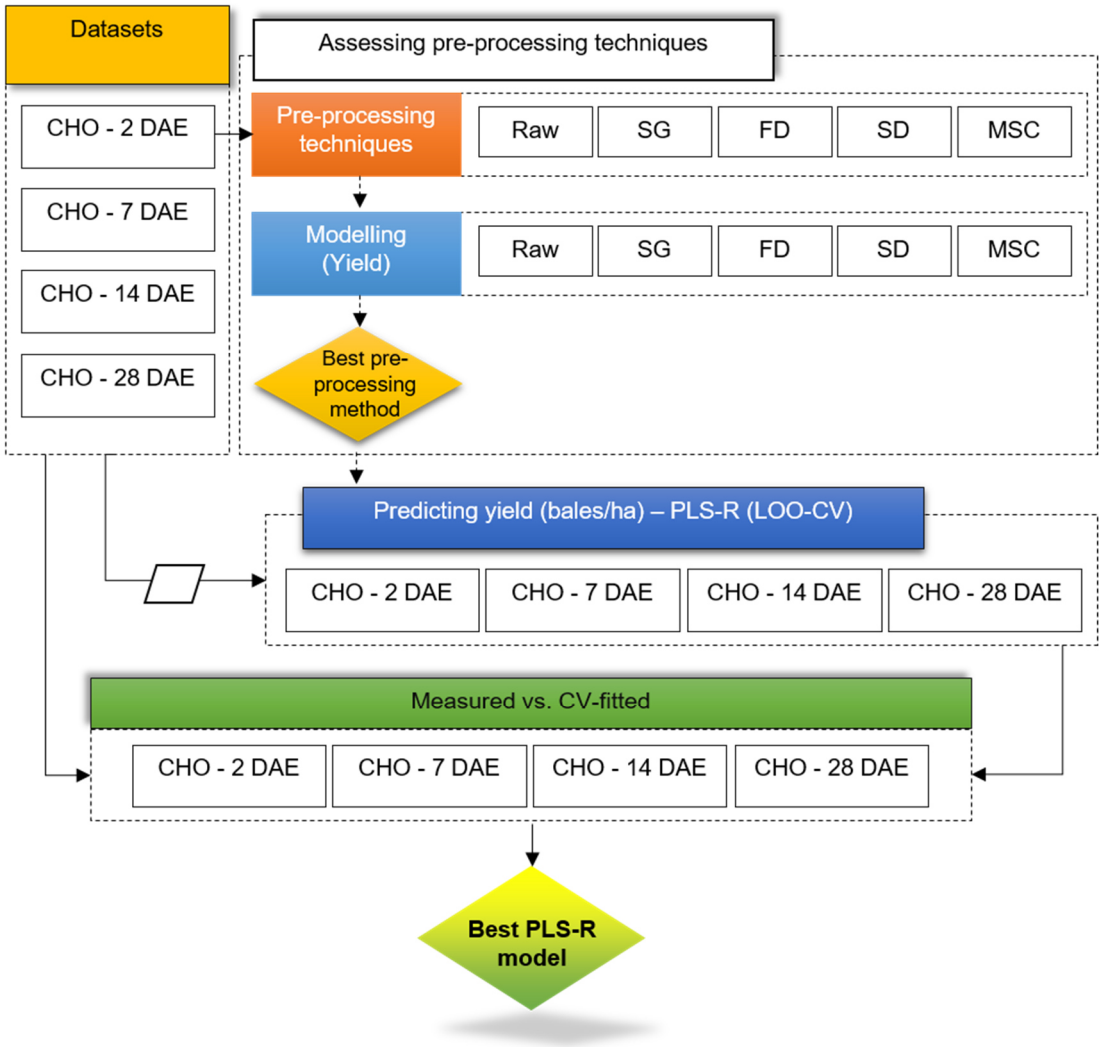

Figure 4-13. Flowchart for assessing pre-processing techniques and prediction of yield applying PLS-R.

4.3.3.2. Estimating Dose with Canonical Powered (CPPLS) and Sparse Discriminant Analysis (sPLS-DA)

Canonical powered (**CPPLS**) and sparse discriminant analysis (**sPLS-DA**) are classical PLS models (supervised classification) but the main difference is that the response *Y*-variate is qualitative indicating classes or categories. CPPLS integrates canonical correlation analysis and the parameterisation of loading weights optimised over a given interval (Indahl et al., 2009). In this study *cppls.fit* function from the *pls* R-package was implemented (Mevik & Wehrens, 2007) and linear discriminant analysis was applied for classification purposes. CPPLS has demonstrated the ability to extract more information in the first LVs and it is appropriate when: a) classification problems related to group priors occur and/or b) regression and classification problems with an individual weighting of the observation occur (Indahl et al., 2009).

sPLS-DA is a one-step approach where building model and classification are performed under the same algorithm. Three different methods for classification are available (Centroid, Maximum and Mahalanobis distance) under the *mixOmics* (González et al., 2011) package in R. More information about these methods is available in Indahl et al. (2009); Jiang et al. (2014) and Mevik and Wehrens (2007).

Figure 4-14 presents the main processes implemented for the estimation of dose. The datasets collected during each DAE were combined after the cleaning process (CHO, cleaned hyperspectral data). From this combined dataset (CHO), a training and a test dataset were generated using the *createDataPartition* function available in the *caret* R-package with a proportion of 75% for the training dataset and 25% for the test dataset. This function is used to create stratified random splits of a dataset while maintaining a balanced ratio of the factor classes (i.e. Dose) so that the overall class distribution is preserved as far as possible (Kuhn, 2008). *From this analysis, it is possible to determine whether dose can be estimated regardless of DAE and timing of exposure (S).*

To identify the influence of DAE, the initial CHO was segregated by DAE. This resulted in four datasets (CHO-DAE): 2 DAE, 7 DAE, 14 DAE and 28 DAE. Training and test sets were generated for each of these datasets, using the procedure described above. Subsequently, each CHO-DAE was segregated by S (CHO-DAE-S). The same procedure was applied to generate the training and test datasets. This level of segregation was used to identify the influence of S.

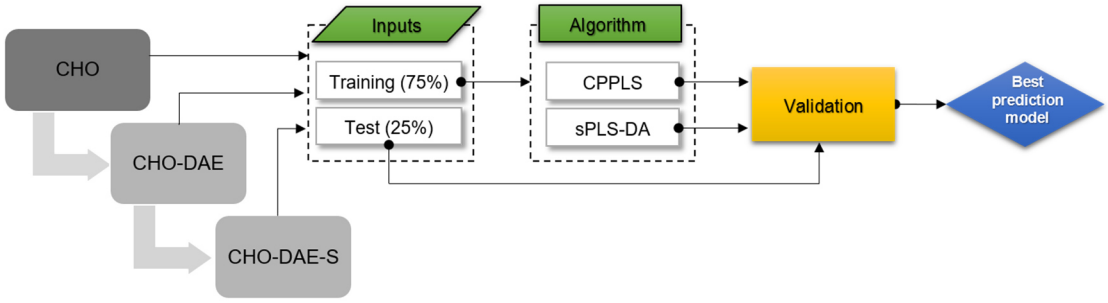

Figure 4-14. Flowchart of main processes to assess prediction capabilities of hyperspectral data to estimate dose.

4.4. Results

4.4.1. Yield, timing of exposure and dose

The timing of exposure is an important factor in determining the final damage to the crop. The highest recovery capabilities were evident when the crop was exposed to 2,4-D at early stages of growth (Figure 4-15). Few recovery signs were evident within the first two months after exposure. However, as the crop got nearer to harvest, the treatments had significantly recovered especially those treatments sprayed at very early stage (S1). The main stem of plants exposed at the early stage (S1) appeared to have died, but the plant kept growing in a horizontal trend where the main stem tended to be replaced by several thickened lateral branches. Early visual assessment (within three weeks) suggested a complete mortality of the plants. After 30 days, visual assessment suggested an initial recovery of plants sprayed with the lowest dose (D1) starting from the bottom of the plant while the plants treated with the highest dose (D2) had no visual evidence of recovery. In general, early exposure to the herbicide caused visual symptoms as soon as 2 DAE regardless the dose.

Figure 4-15. The visual appearance of 28 g a.i./ha of 2,4-D herbicide drift 74 days after sowing (DAS).
Top-left: control plants (D0); top-right: plants treated at 4-5 nodes (S1); bottom-left: plants treated at 7-8 nodes (S2); bottom-right: plants treated at 11-12 nodes.

Plants sprayed at 7-8 nodes (S2) only showed slight curls at the edge of the leaf and discolouration within the first days of assessment. At this stage, the recovery was slower than S1 and the plant did not grow significantly. Visual symptoms, when assessing the middle stage (S2) with the highest dose (D2), included necrotic patches in leaves and branches as soon as 2 days after the exposure (2 DAE). After 28 DAE plants had shown two different recovery patterns according to the dose applied. S2 plants affected by the lowest dose (D1) grew more than the D2 dose but several younger nodes and leaves looked more affected. With D2, the plants did not grow much after the spray but the younger nodes and leaves looked less affected. For the last stage (S3), the symptoms were similar to S2: when plants were sprayed with the highest dose, fewer young leaves looked affected than when they were sprayed with D1, while those plants sprayed with the lowest dose grew more than the plants sprayed with D2.

Cotton yield (bales/ha) was highly affected by 2,4-D. The yield was documented to be reduced by more than 90% when the plants were treated with the highest dose (280 g a.i/ha). The timing of exposure was an important factor in the recovery capabilities of the plants. The yield was relatively higher when the plants were exposed at an early stage (S1) as the plants had more time to recover, but the impact of dose was greater; treatments sprayed with D1 produced, on average, 5.29 bales/ha more than those treatments sprayed with D2.Yield reduction, on the other hand, was higher in those treatments sprayed at a late stage (11-12 nodes) (Figure 4-16 and Figure 4-17) and the average difference on the final yield between D1 and D2 was lower (less than 1.37 bales/ha).

The early stage was the only timing of exposure able to produce yield higher than 2.16 bales/ha and 7.49 bales/ha, under the influence of the highest and lowest dose, respectively (D2 and D1), hence S1 had the highest yield possible for both doses (Figure 4-17). S3 had the highest losses as yield in those treatments were reduced between 87% and 98% (Figure 4-18). Yield reduction of treated plants at S2 with the highest dose was similar to S3 (97%) but much lower with D1 (53%) (Figure 4-18). These findings generally agree with other studies which found that yield was significantly reduced by phenoxy herbicide regardless of variety, dose or application (Everitt & Keeling, 2009; Smith & Wiese, 1972).

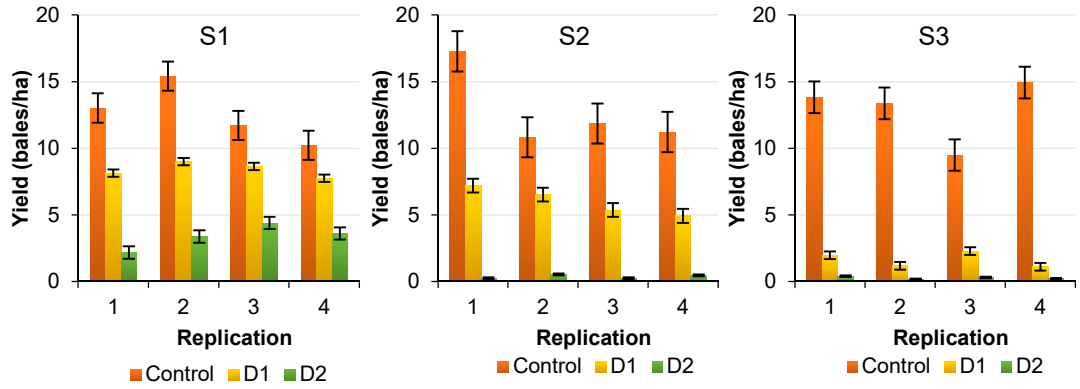

Figure 4-16. Yield (bales/ha) by replication (1 to 4): influence of dose (D) at different timing of exposure (S). Error bars represent the standard error of the mean.

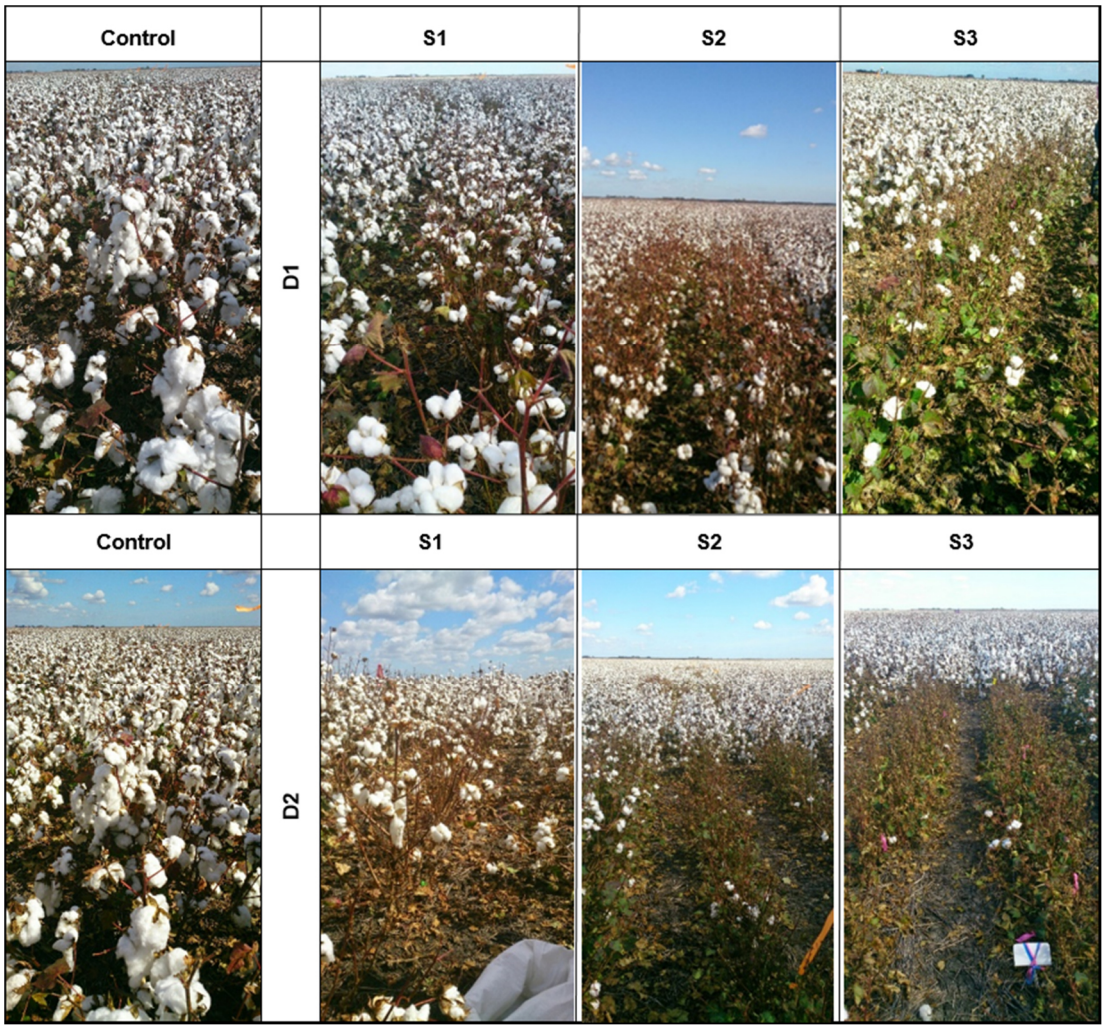

Figure 4-17. Yield variability according to the timing of exposure and dose.

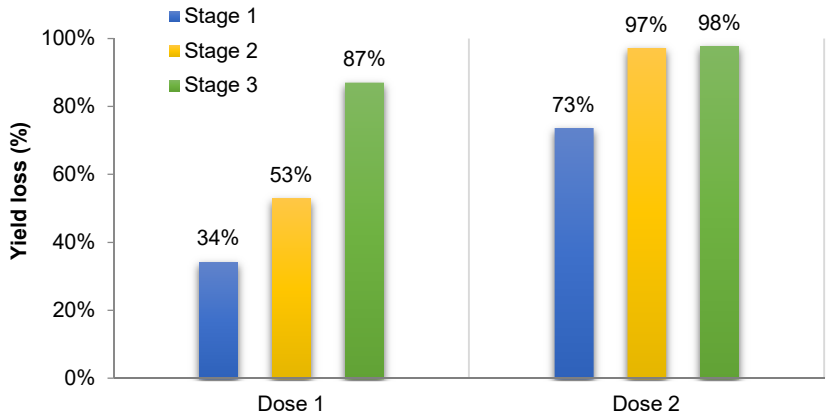

Figure 4-18. Percentage of yield reduction as compared with control treatments.

Correlation analysis provided a better understanding of the relationship between yield and the reflectance of the plants. The significant bands (p-value $\leq$ 0.05) were mainly located around the green peak (~550 nm) and NIR (between 719 nm and 767 nm) wavelengths (Figure 4-19). However, the significance varied through time. The green peak had a significant relationship with yield within the first 14 days after the exposure while the NIR wavelengths had more variability and only at two specific dates were correlated: 7 DAE and 28 DAE. While the entire NIR region (except for the small window from 700 nm to 718 nm) had a significant relationship with yield at 7 DAE, only the first 67 wavelengths (from 700 nm to 767 nm) were correlated with yield at 28 DAE. Apart from the wavelengths between 525 nm and 575 nm, the visible range did not provide information about the yield variability of the different treatments at any date after the exposure.

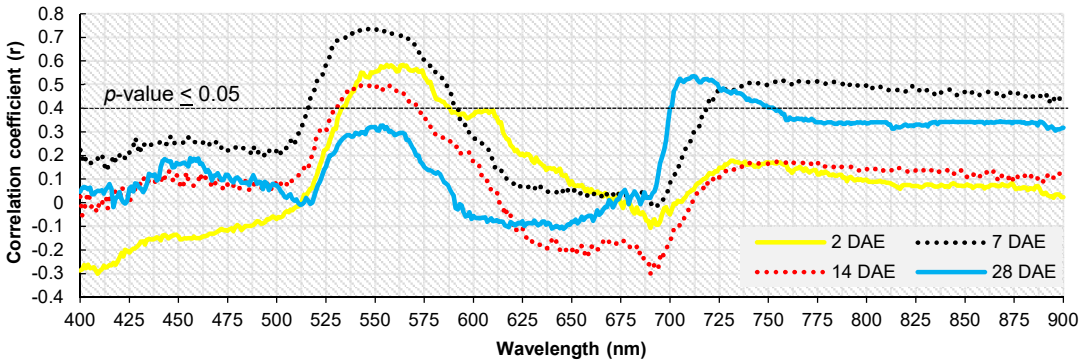

Figure 4-19. Temporal variability of the relationship between yield and spectral reflectance.

Table 4-3 presents the quality variables assessed in this study for all treatments. Only two of these variables reacted to dose: lint turnout (which is more related to quantity) and micronaire (r = -0.73 and r = -0.61, respectively with p-value < 0. 001). Among

the others quality variables, there was no apparent variability or reduction of quality in relation to the herbicide (see Figure 4-20 and Figure 4-21).

Table 4-3. Mean, median and mode of cotton fibre quality variables.

	Lint	Length	Micronaire	Uniformity	Strength	SFI	Elongation
Mean	45.4	1.3	4.1	84.1	34.2	8.0	5.4
Median	46.3	1.3	4.0	83.9	34.2	8.1	5.3
Mode	47.2	1.2	4.3	83.5	33.8	8.3	5.2

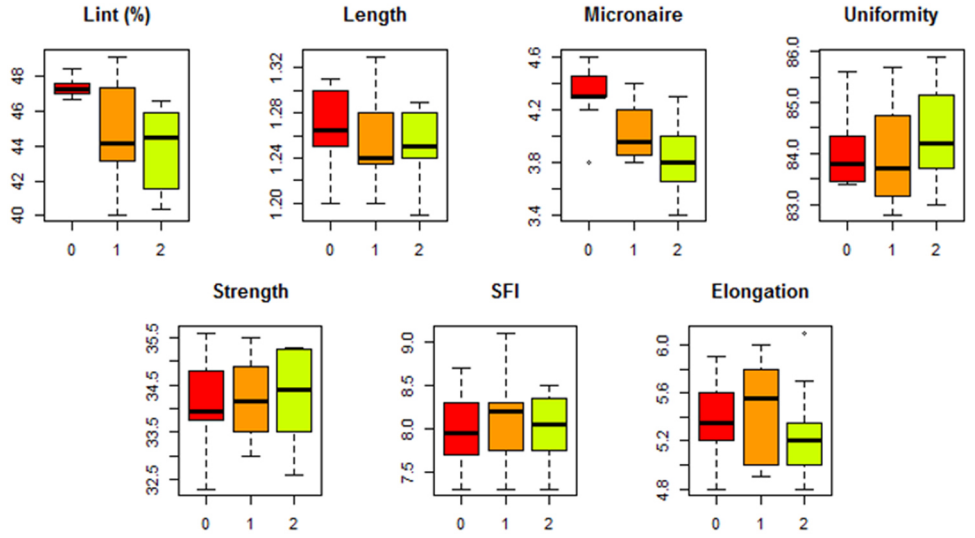

Figure 4-20. Quality variables grouped by dose.
Control: "0", D1: "1"; D2: "2".

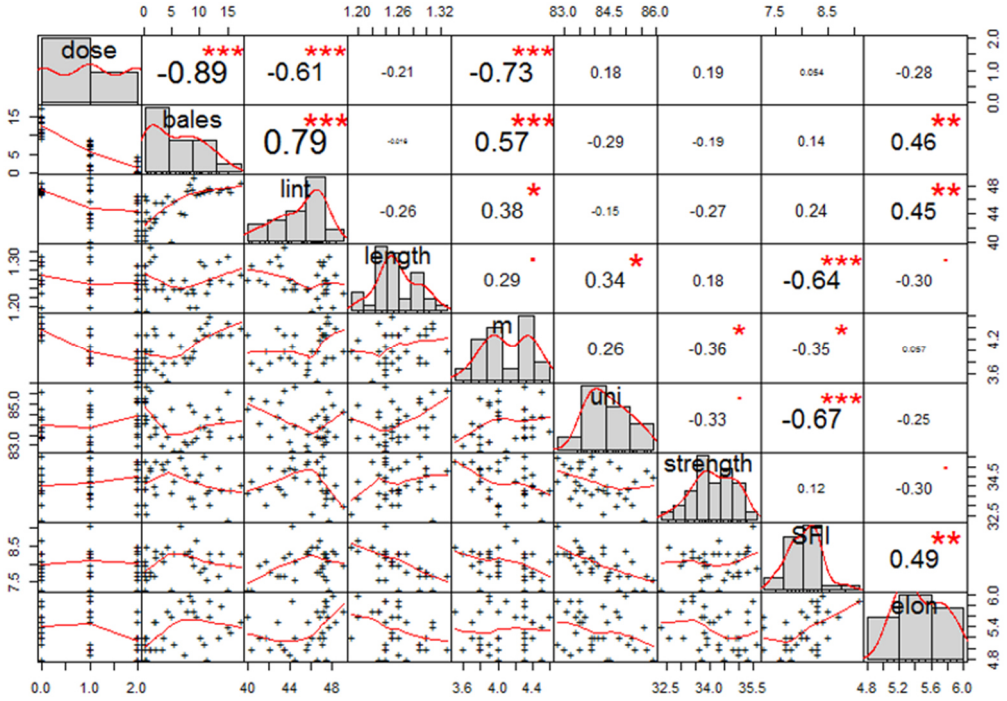

Figure 4-21. Correlation matrix: dose vs. yield and quality variables.
dose: Dose; bales: yield (bales/ha); lint: lint turnout percentage, length and strength of fibre, m: micronaire, uni: uniformity; SFI: short fibre index; elon: elongation.

4.4.2. Internal changes of cotton plants after the exposure to 2,4-D

4.4.2.1. Physiological changes in cotton after exposure to 2,4-D

Photosynthesis and stomatal conductance were highly affected by the simulated spray drift in each treatment. These variables exhibited a reduction in measured values as the dose was increased regardless of the timing of exposure. However, when plants were sprayed at 4-5 nodes (S1) and 7-8 nodes (S2) with the lowest dose, photosynthesis was only slightly different from control plants. On the other hand, when plants were treated at 7-8 nodes (S2) and 11-12 nodes (S3) with the highest dose, photosynthesis was reduced by more than 75% and 64%, respectively (Figure 4-22). A similar situation occurred with stomatal conductance: the plants treated with the highest dose (D2) had, at those timings of exposure (S2 and S3), the highest variability (more than 75%). Stomatal conductance and photosynthesis were the second and third variables highly negatively correlated to dose (r = -0.81 and r=-0.79, respectively), which indicates that stomatal conductance was more sensitive to the dose (Figure 4-23) but it was also more sensitive to the timing of exposure (Figure 4-22).

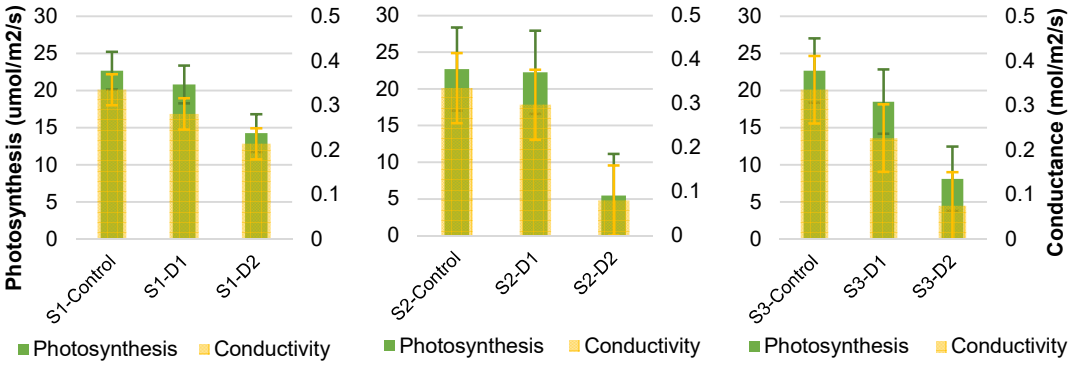

Figure 4-22. Relationship of photosynthesis and stomatal conductance rates with treatments.
Error bars represent the standard error of the mean.

Yield was further investigated to understand its relationship with internal variables such as hormones, photosynthesis and stomatal conductance. Correlations coefficients manifested between moderate and high positive relationship with IAA, photosynthesis and stomatal conductance, with r coefficients equal to 0.52, 0.79 and 0.85, respectively (Figure 4-23).

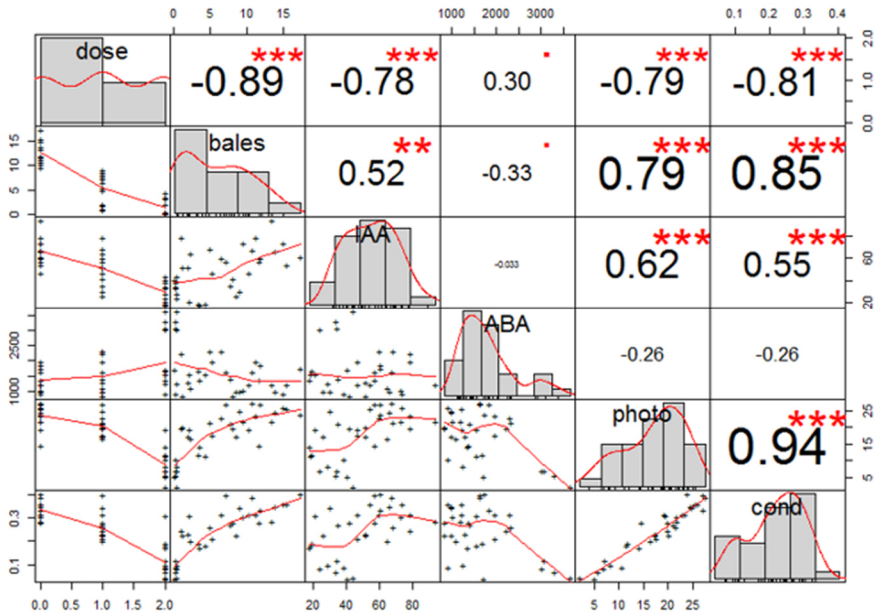

Figure 4-23. Correlation matrix: dose vs. yield and internal variables (IAA, ABA, photosynthesis and stomatal conductance).
bales: yield (bales/ha); dose: dose; photo: photosynthesis and cond: stomatal conductance.

4.4.2.2. Hormone content variability in cotton crops affected by 2,4-D

Figure 4-24 shows the relationship between Indole acetic acid (IAA) concentrations and the different treatments. Untreated plants during the early stage of growth (S1) manifested an IAA increment through time that stabilised around 7-8 nodes (S2) when the IAA increment still occurred at a reduced rate. A decrease in the values of IAA was evident when the crop reached 12 nodes. The IAA content of plants was significantly reduced soon after 2 DAE, with the highest dose causing a greater reduction. IAA reduction was the usual response when it was measured at 14 DAE (with the exception of those plants treated with the lowest dose at S2 and S3). Grossmann (2010) reported that plants were lethally damaged with increasing concentration and auxin activity after the application of 2,4-D. The author's finding is in accordance with the results reported in this study where the decrement of IAA was associated with high concentrations of 2,4-D (i.e. auxin concentrations).

Spearman correlation was used to investigate the temporal relationship of IAA and hyperspectral data and the internal variables explored in this study (Figure 4-23). IAA content was positively and highly correlated to photosynthesis and stomatal conductance while it was strongly and negatively correlated with dose (Figure 4-23).

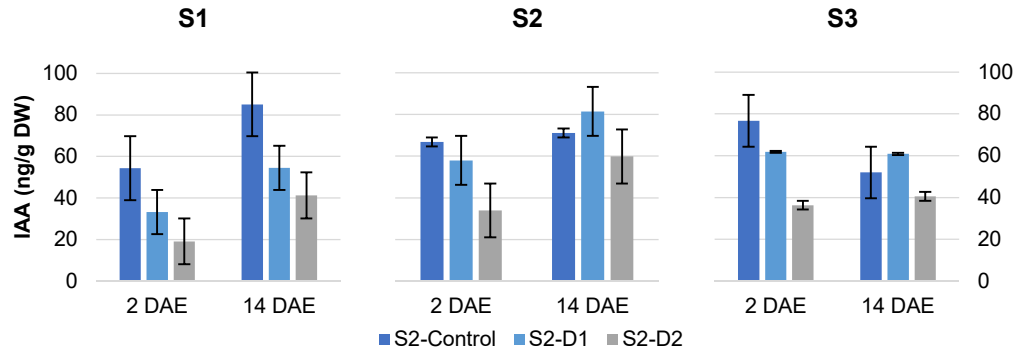

Figure 4-24. IAA concentrations measured for all treatments.
Error bars represent the standard error of the mean.

The lack of IAA caused by the auxin (2,4-D) overdose, leading to disruption of membranes and necrosis of tissues (Grossmann, 2010) which could explain the strong correlation between IAA and NIR wavelengths (i.e. $r > 0.70$ at 760 nm) (Figure 4-25). However, the relationship's magnitudes were different at each DAE. The green peak (550 nm $\pm$ 5 nm) had a significant and positive relationship with IAA regardless of the DAE ($0.4 \leq r \leq 0.7$). Particularly, moderate correlations were obtained between reflectance from 541 nm to 574 nm at 2 DAE ($r > 0.6$, p-value ≤ 0.05). High reflectance in the green peak is associated with lower rate of photosynthesis and pigments (Blackburn, 2007; Yi et al., 2008). Grossmann (2010) reported that within the first 24 h, the physiological processes caused by auxin overdose included an intensified green leaf pigmentation, which could explain the higher correlation at 2 DAE than 14 DAE with the green peak.

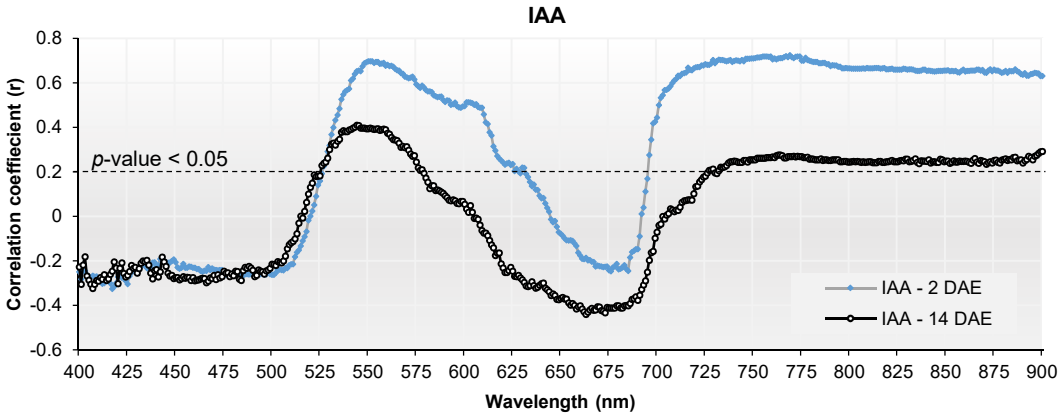

Figure 4-25. Correlation coefficients (r) of IAA and hyperspectral data after exposure to 2,4-D.

ABA content did not show a clear pattern after exposure to 2,4-D (Figure 4-26). In control plants, ABA reached the highest values around 7-8 nodes (S2). Treatments sprayed at S2 with the highest dose (D2) displayed a large but non-significant

increment in the ABA content soon after spraying. This non-significant increment was observed in all of the treatments sprayed with D2 at 2 DAE. At fourteen days after exposure, there was a drastic fall in ABA in all treatments compared with levels measured at 2 DAE, except when plants were treated at a late stage (S3), where the decrease still occurred, but at a lower rate. At the early stages (S1 and S2) with the lowest dose (D1), ABA decreased at 14 DAE but rose at the latest stage (S3) while when ABA was measured at 2 DAE, the only fall was presented at S1. In the middle and late stage (S2 and S3), the ABA, under the D1-influence, rose in comparison with control plants.

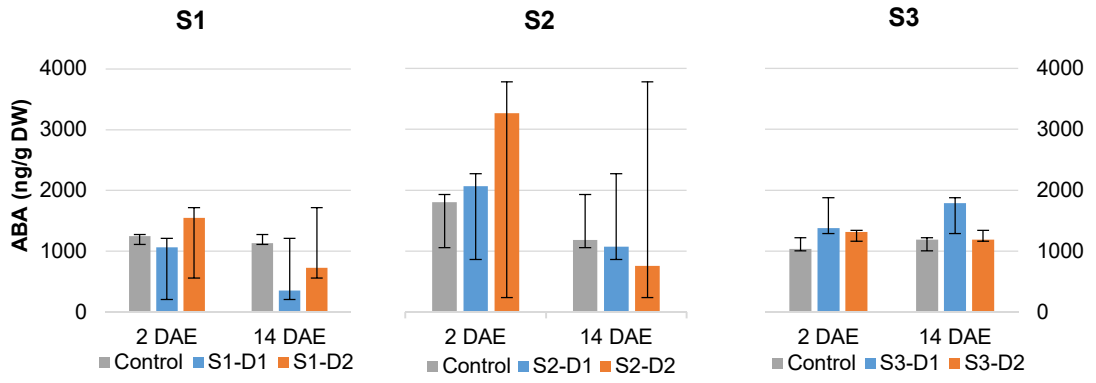

Figure 4-26. ABA concentration for different treatments measured 2 DAE and 14 DAE.
Error bars represent the standard deviation of the samples.

The ABA values in treated plants decreased through time (14 DAE vs. 2 DAE), except at the latest stage (S3), regardless of the dose. S3 treatments sprayed with D1 exhibited an increment in measured values from 2 DAE to 14 DAE (see Figure 4-26).

This study has shown that a significant overproduction of ABA was presented when plants were treated at 7-8 nodes (S2) and 11-12 nodes (S3) and other studies have shown that overproduction of ABA was a crucial factor in growth inhibition (Grossmann, 2010). Hence, the high levels of ABA in S2 and S3 treatments can explain the lower regrowth rate of the plants in comparison with the regrowth rate of treated plants with the lowest dose (i.e. lower ABA values).

While the ABA content after the exposure could not be directly correlated to any physiological variable (see Figure 4-23), there was a moderate correlation ($r = 0.4$) between ABA and the blue range (450 nm to 499 nm) and the early green range from the 500 nm to 525 nm, and a stronger relationship with the NIR particularly from the 740 nm to 810 nm ($0.58 < r < 0.60$, p-value ≤ 0.05) (Figure 4-27). Blue light has an

important role in photomorphogenic in plants including stem elongation (Cosgrove, 1981) and stomatal control (Schwartz, 1984) which influences water relations and CO_2 exchange. However, there was not a strong relationship between ABA and red wavelengths, indicating that ABA did not have a significant impact on pigment concentrations but it did have in cell structure. During the first days of the exposure (~ 2 DAE), only the visible range (long blue and short green) manifested a positive relationship with ABA. On the other hand, the only significant relationship (p-value $\leq$ 0.05) with ABA with the NIR range was at 14 DAE.

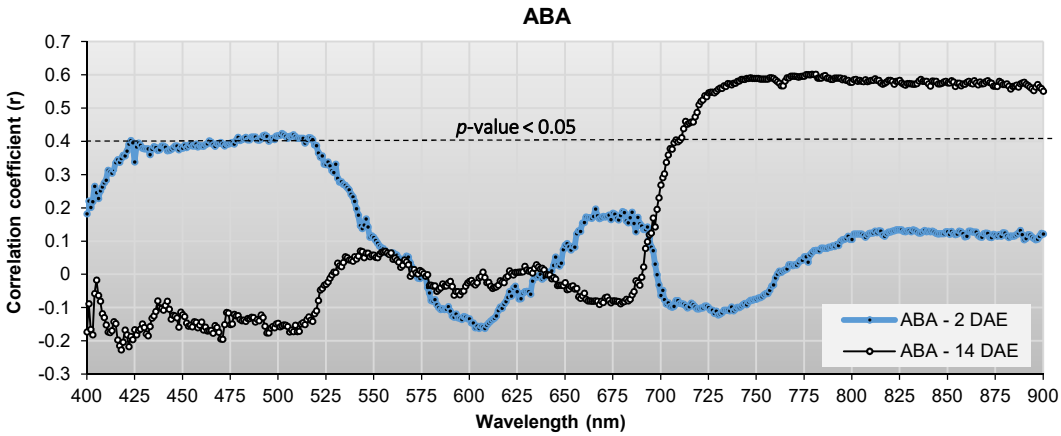

Figure 4-27. Temporal relationship between ABA and reflectance data in 2,4-D injured leaves.

4.4.3. Hyperspectral data analysis

A change in the spectral variability of the crop foliage occurred throughout the entire growing season. Figure 4-28 shows the spectral changes from 4 nodes to 12 nodes in non-treated plants. Controls exhibited higher NIR reflectance and lower visible reflectance as they became mature. Varying the exposure dose from 0% to 5% of the recommended label rate reduced the reflectance in the NIR from higher than 0.6 to nearly 0.4 (Figure 4-29). The amount of NIR reflectance variability due to different doses was nearly the same in S2 and S3 (~ 0.03). Although treatments sprayed at S1 with D1 and D2 presented changes in the reflectance, the curve from 400 nm to 900 nm did not tend to vary greatly through time. In the green peak (550 nm), there was no major change for D1 at S2 and S3 (Figure 4-29). However, when these treatments were compared with controls and S1, the reflectance for both S2 and S3 was the lowest of the treatments (Figure 4-29).

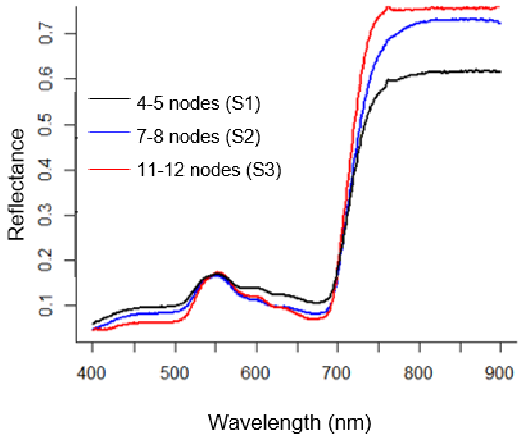

Figure 4-28. Reflectance average at different growing periods of control plants.

When the crop was treated at S2 and S3, they had comparatively similar curves as with non-treated plants in the visible range from 400 nm to 700 nm (except in the green peak), i.e. at some point after the exposure, the treatments S2 and S3 did not show significant visual changes in comparison with non-treated plants. On the other hand, a completely different shape (from 400 nm to 500 nm and from 600 nm to 700 nm) was obtained for treatments at S1 regardless of the dose. S1 had the highest reflectance values in the red range tending towards more redness. In general, the spectral curve of S1 was highly different from the other stages in the entire region from 400 nm to 900 nm. This supports the visual symptoms evident in the field, as it looked "highly damaged" in comparison with the other two timings of exposure (S2 and S3).

The visible wavelength range (400 nm to 700 nm) presented different patterns in treated plants than in controls. However, the similarities within this range were higher than in the NIR (700 nm to 900 nm). High NIR reflectance is associated with healthy leaves due to a better leaf internal structure, higher LAI, and biomass (Schlemmer et al., 2013). In this study, controls had the highest NIR reflectance which suggests that they were the healthiest plants in the experimental plots. Results in the NIR have shown a decrease in reflectance values irrespective of the timing of exposure, suggesting that the cell structure abnormalities of the 2,4-D injured leaf are the most determinant variables (rather than pigment) for accurately assessing the damage caused by 2,4-D phenoxy herbicide in cotton crops.

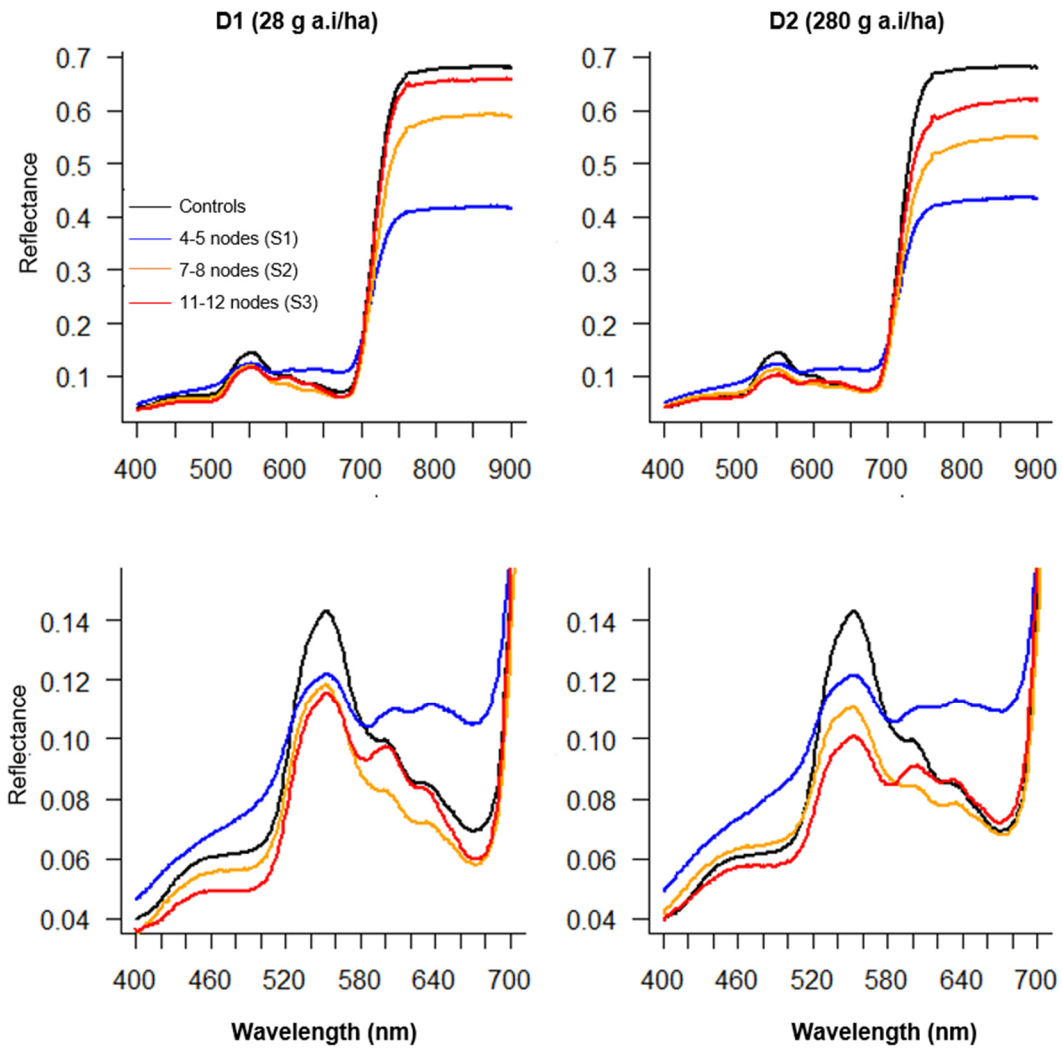

Figure 4-29. Influence of dose at different timing of exposure.

Early detection of damage was possible due to the variability in the reflectance as soon as 2 days after the exposure (2 DAE) even for the lowest dose. Figure 4-30 shows the difference of means in the spectral responses of controls and all treatments collected at 2 DAE, 7 DAE, 14 DAE and 28 DAE. Treatments sprayed at 4-5 nodes (S1) showed a clear different shape from 600 nm to 900 nm in comparison with other stages, and a major difference from control plants in the NIR range (700 nm to 900 nm). The differentiation in the NIR range at different doses was clear while the visible (from 400 nm to 700 nm) wavelengths did not show such difference within doses, except when data was collected 14 days after the exposure (14 DAE) in the green and red range (i.e. from 500 nm to 700 nm) (Figure 4-30).

When sprayed at 7-8 nodes (S2), the visible range had very similar differences (i.e. similar shapes) for the lowest dose (D1) and the highest dose (D2), i.e. the visual aspect

of the plants did not vary significantly (for data collected at 14 DAE, Figure 4-29). Soon after the spray, D1 did not show a major spectral change in comparison with control plants (except at the green peak around 550 nm) but D2 manifested changes also in the red range (at 7 DAE, Figure 4-30). At this stage (S2), the major changes between doses (Nil - D0, 5% - D1 and 50% - D2) were observed 14 DAE in the NIR range. When plants were treated at a late stage (S3), the behaviour of the visible was similar to the pattern described above for S2. The green peak (in the visible range) and the NIR (around 750 nm) were the major points of spectral variability within doses through time, except for 28 DAE where the variability between D1 and D2 was nearly null (Figure 4-30).

At the end, when plants were treated at the earliest stage (S1), the reflectance in the visible range did not change between doses but NIR exhibited the highest variability for all of the treatments through time. At S2, the differences between doses in the visible wavelengths were not so evident after 14 DAE. However, soon after the exposure, spectral changes manifested with the highest dose (D2) were different. The lowest dose (D1) tended to not vary in the same range (from 400 nm to 700 nm) in comparison with controls (except at 550 nm). At the late stage, the peaks around 550 nm and 750 nm were clearly differentiated from doses at any time between 2 DAE and 14 DAE. The spectral variability of S3 after 28 days of the exposure (28 DAE) was not evident when comparing doses (except at the red edge from 700 nm to 730 nm) which may explain the visual similarities between treatments regardless of the dose. As expected, NIR was the most constant range showing clear differences for all of the treatments.

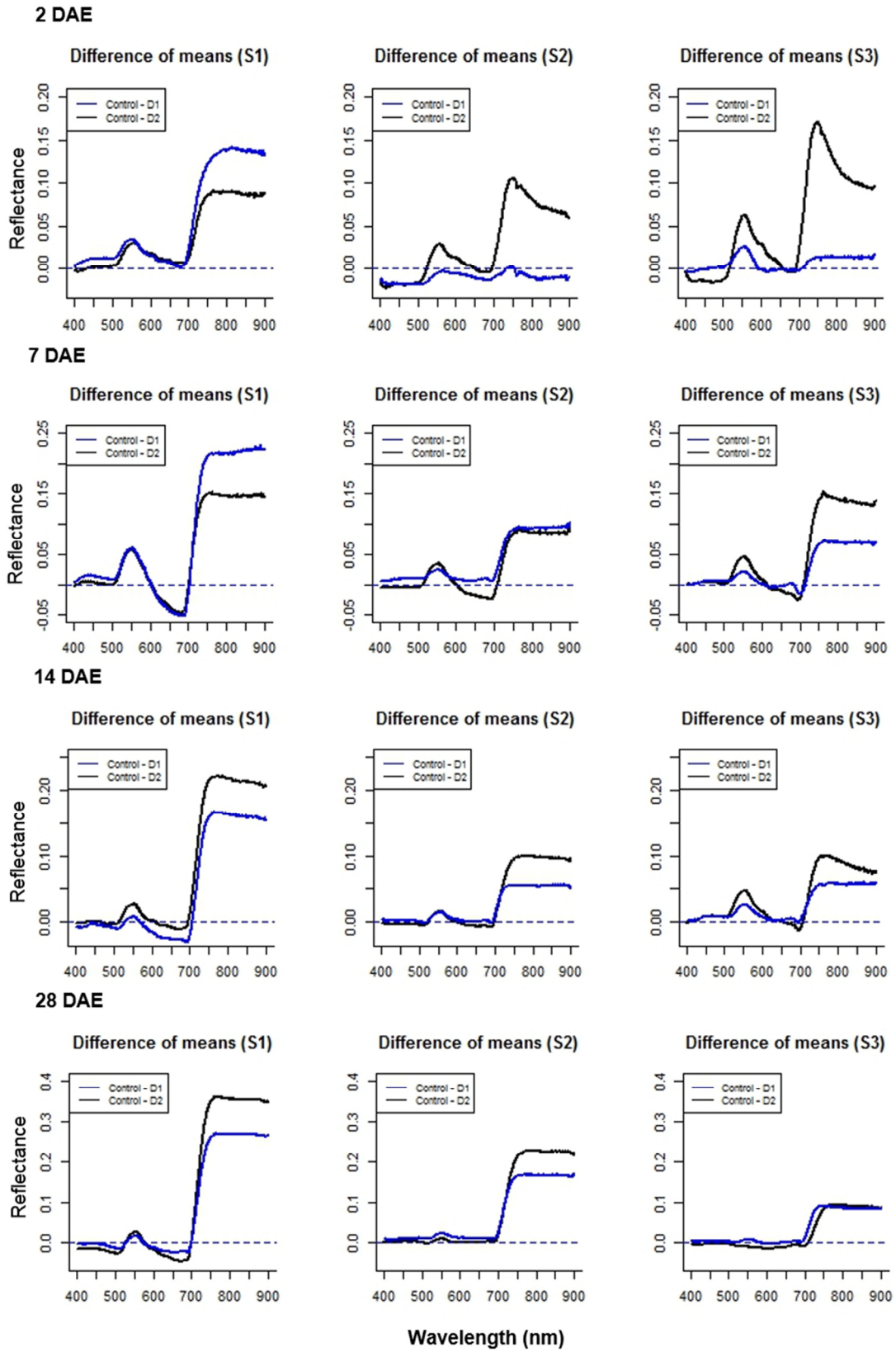

Figure 4-30. Temporal reflectance changes according to dose (D), timing of exposure (S) and days after the exposure (DAE).

4.4.3.1. Pre-processing techniques and their impact on prediction capabilities

Raw spectral data and five pre-processing techniques were assessed. Derivatives and smoothing filters eliminated the number of wavelengths at the beginning and/or the end of the range. Application of the Savitzky-Golay (SG) filter has reduced the total number of wavelengths by 10: 5 wavelengths from 400 nm to 404 nm, and another 5 wavelengths from 896 nm to 900 nm. The first derivative (FD) filter reduced one wavelength at the beginning of the range, while the second derivative (SD) reduced two wavelengths also at the beginning of the range. Multiplicative scatter correction (MSC) and standard normal variation (SNV) filters kept the original number of resulting wavelengths (Table 4-4).

Table 4-4. Hyperspectral data pre-processing techniques used in this study.

Pre-processing filter	Acronym	No. of bands	Initial – final band
Raw spectra	RAW	501	400 - 900
Savitzky-Golay	SG	491	405 - 895
First derivative	FD	500	401 - 900
Second derivative	SD	499	402 - 900
Multiplicative scatter correction	MSC	501	400 - 900
Standard normal variation	SNV	501	400 - 900

Source: (Suarez et al., 2017)

The scatter filters increased the noise of the spectral curves and the original reflectance characteristics exhibited changes (except for Savitzky-Golay filter - SG). MSC and SNV incremented the slope of the original spectra in the red edge range (from 700 nm to 750 nm) (Appendix 4-10). Furthermore, MSC' shape looked similar than raw reflectance in the VIS range but with higher magnitude through all the NIR, while SNV accentuated the reflectance through all the spectrum. SG transformation properly reduced the spectral noise of the raw data and kept the shape of the original reflectance (See Appendix 4-10). On the other hand, derivatives changed the corresponding value significantly in each wavelength (Appendix 4-11). The highest value for First Derivative (FD) was 0.06 but most of the values were below 0.02. For Second Derivative (SD), the resulting values are even lower and the noise is higher than all techniques assessed in this study.

Different factors can be integrated to assess the impact of pre-processing techniques (as described in section 4.3). In this particular case, results were compared based on the root mean square error of LOO-CV (RMSECV) and R_{cv}^2. The lower RMSECV and the higher R_{cv}^2 the better the model was. The dataset collected at 2 DAE was implemented to build the models.

Table 4-5 presents the results according to each pre-processing technique. The best performing models were those that used raw spectral data and the Savitzky-Golay (SG) filter. Both models were composed of the same number of LV (=4), R_{cv}^2 (X = 99.7% and Y = 64.6%) and RMSECV equal to 3.7 bales/ha. The poorest performance occurred when the data was converted into derivatives. With other pre-processing techniques such as MSC and SNV, the RMSECV was nearly the same with only 0.01 bales/ha difference. However, with derivatives, that error increased to 5.99 bales/ha (more than 61% higher than the best prediction model).

Table 4-5. Influence of pre-processing techniques in PLS-R models performance.

DATA	Pre-processing filter	LV	RMSECV	X-R^2 (%)	Y-R^2 (%)
2 DAE	RAW	4	3.70	99.68	64.57
	SG	4	3.70	99.68	64.57
	FD	5	4.00	68.33	94.53
	SD	1	5.99	21.29	20.15
	MSC	2	3.84	88.32	61.34
	SNV	2	3.83	88.18	61.38

4.4.3.2. Assessing hyperspectral capabilities by predicting yield under 2,4-D-influence

The analysis of the pre-processing techniques demonstrated that these techniques did not improve the prediction performance of the models. As a result, the PLS-R models for prediction of yield were developed with raw spectral data. Four prediction models were analysed to determine the best time to collect data in the field. The relationship between the root mean square error of prediction (RMSECV) of the leave-one-out cross-validation predictions and the number of latent variables is shown in Figure 4-31.

The optimal number of LV was selected based on RMSECV, the highest R_{cv}^2 and the resulting scores (data not presented). Scores were analysed to detect any significant outlier among the samples. The results show that data collection can be done anytime

after exposure with good prediction capabilities (except for 14 DAE, see Table 4-6), particularly for the model composed of 7 DAE data. This model appeared to be the best time for modelling with the lowest RMSECV (= 2.6 bales/ha) and the highest Y-R^2 (= 0.88). This corresponds to prediction error of 16.9%, which represents more than 80% correct predictions (Table 4-6).

Table 4-6. Performance of PLS-R models on yield (bales/ha).

DAE	LV	RMSECV	X- R^2	Y- R^2	RMSECV of yield (%)
2	4	3.7	0.98	0.65	21.66
7	6	2.56	0.99	0.88	16.91
14	3	4.68	0.96	0.37	27.39
28	6	3.16	0.99	0.84	18.48

DAE: Days after exposure. LV: Optimal number of latent variables (LV). RMSECV: Root mean square error of LOO-CV. R^2: variance explained of LOO-CV (R_{cv}^2).

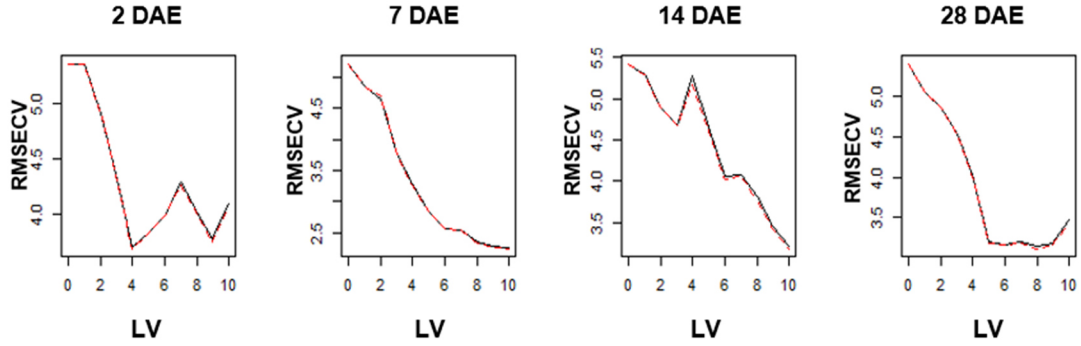

Figure 4-31. Relationship between RMSECV and the number of PLS-R LV.

The contribution of each wavelength can be visualised by the analysis of weighted regression coefficients (*Bw*) of the models (Figure 4-32). Weighted regression coefficients are more informative and easier to interpret (Barbin et al., 2012; Garrido Frenich et al., 1995; Yi et al., 2014). In general, all models contained at least one wavelength in the green range (Table 4-7) which can be explained due to the high correlation between healthy plants and chlorophyll fluorescence with this spectral region (Rama Rao et al., 2008; Rapaport et al., 2015).

Blue wavelengths (400 nm, 414 nm and 498 nm) had an important contribution in 7 DAE and 28 DAE models which were the best prediction models based on RMSECV and R^2 values. This is an interesting finding, as the blue region is not commonly associated with healthy plants or other physiological variables as demonstrated in a

study on the detection and prediction of herbicide injury on water hyacinth using remote sensing techniques (Robles et al., 2010).

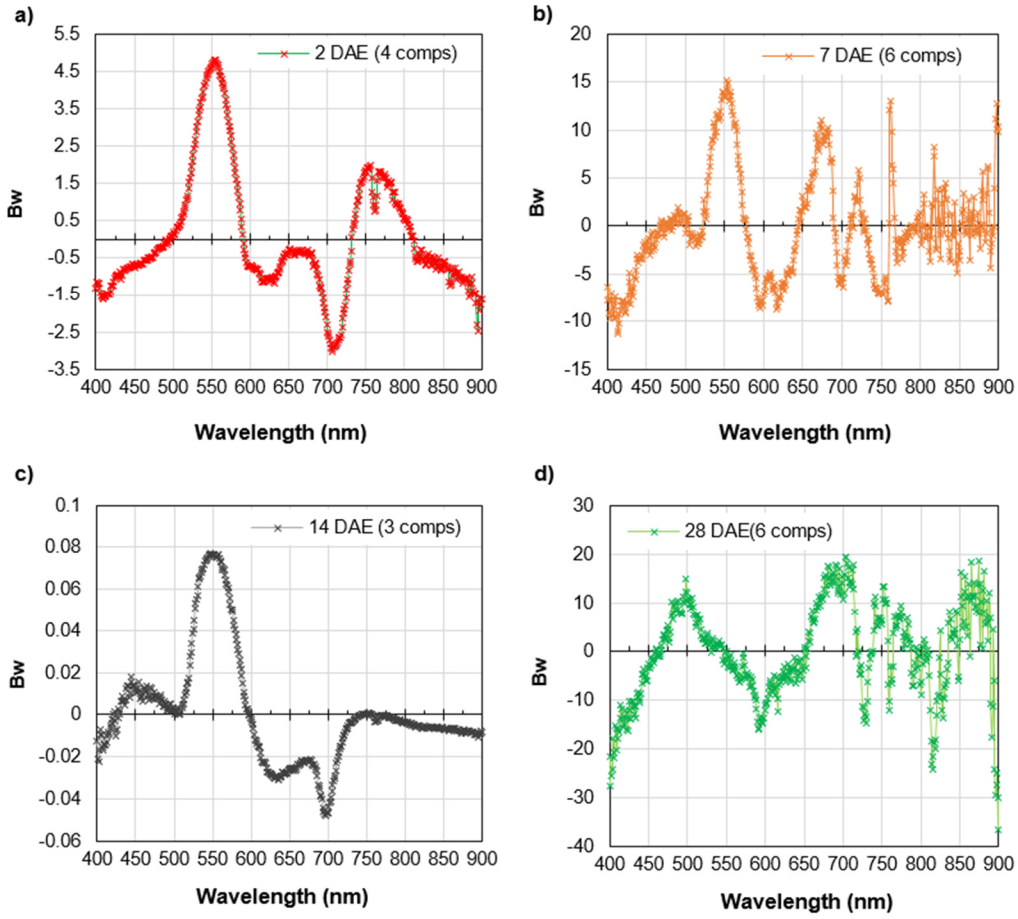

Figure 4-32. Weighted regression coefficients (Bw) from the yield prediction models.

Table 4-7. Significant wavelengths according to peaks of weighted regression coefficients of PLS-R models.

	Spectral range				
Model	**Blue**	**Green**	**Red**	**Red-edge**	**NIR**
2 DAE		554		706/756	895
7 DAE	414	553/595	617/673	762	897
14 DAE		548	636/700		
28 DAE	400/498		616/681	704	815/899

The red range (636 nm, 673 nm, 677 nm, 681 nm and 700 nm) contributed in three models: 7 DAE, 14 DAE and 28 DAE. Red edge, specifically at 704 nm, 706 nm, 756 nm and 762 nm, and the NIR range at 815 nm, 895 nm, 897 nm, 899 nm, had important contributions in all models except for 14 DAE. This could explain the poor results of the model (RMSECV = 4.7 bales/ha) in comparison with the others. The wavelengths

around 550 nm (± 4 nm) were highly important for all models except for 28 DAE. The contribution of 895 nm (± 4 nm) was significant for all models except for 14 DAE. The significance of green, red, red edge and NIR observed in the prediction models agrees with several studies related to photosynthesis capacity, physiological stress, pigment concentration and, in general, different conditions of the crop (Merton et al., 2004; Pinter et al., 2003; Zhao, Reddy, et al., 2007).

Integration of results in Table 4-6 and Figure 4-33 indicated that the best prediction performance was obtained when data was collected at 7 DAE. The highest regression coefficient value of measured vs. predicted yield (R^2 = 0.74) corresponded to the minimum RMSECV of the PLS-R models (RMSECV = 2.6). The second best model (28 DAE) corresponded to the second lowest RMSECV (= 3.2) and the second highest values R^2 (= 0.64). According to the significant wavelengths included on each of these two models, the presence of the blue, red, red edge and NIR wavelengths was a common factor (Table 4-7). On the other hand, the worst performance occurred when only two regions of the spectrum (green and red) were significant (data collected 14 DAE, RMSECV = 4.68 and Y-R^2 = 0.37) which coincided with the lowest R^2 of the linear regression of predicted vs. measured yield (R^2 = 0.21) (See Table 4-6).

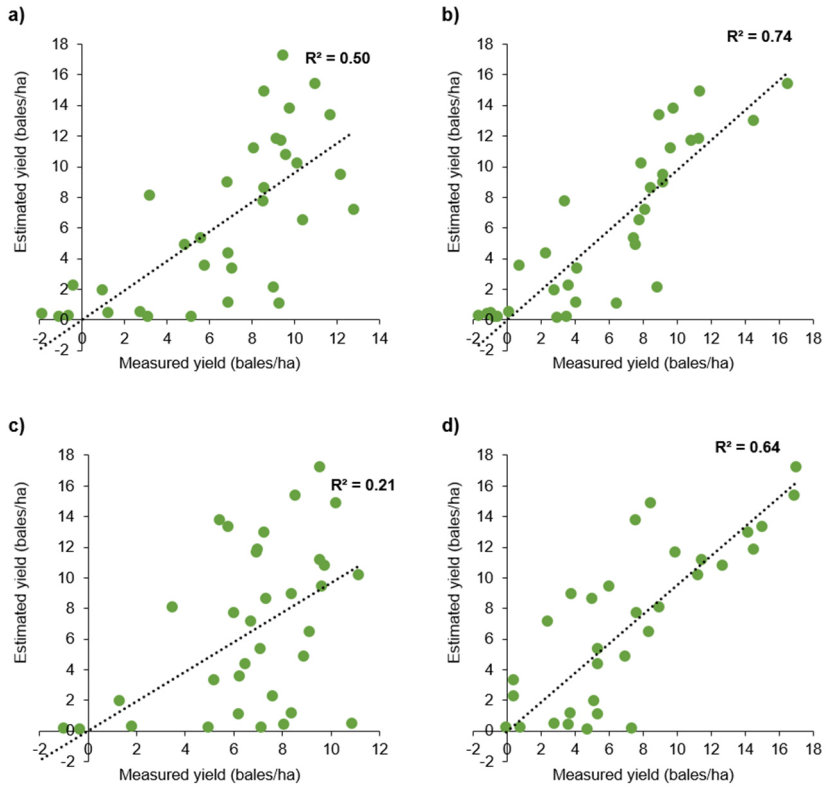

Figure 4-33. Scatter plots of measured vs. estimated yield (bales/ha) derived from PLS-R.
a) 2 DAE, b) 7 DAE, c) 14 DAE and d) 28 DAE.

4.4.3.3. Assessing hyperspectral data for estimating 2,4-D dose

Two different approaches were tested to establish the best method for the estimation of dose. Canonical powered partial least squares (CPPLS) and sparse partial least squares discriminant analysis (sPLS-DA) were tested at three grouping levels (D0, D1 and D2).

CPPLS

This approach was implemented in two steps: development of prediction models and classification. Linear discriminant analysis (**LDA**) was performed as a classification tool for all groups. Each group was divided into training and test datasets composed of 75% and 25% of the samples, followed by outlier's removal. The first group (level 1) was composed of all data pooled across with a total of 697 samples (Table 4-8).

Table 4-8. Sample size per group of analysis of CPPLS and sPLS-DA.

Sample/Group		Sample size	No. of training samples (75%)	No. of test samples (25%)
All data		697	523	174
2 DAE		172	130	42
	S1	56	42	14
	S2	58	45	13
	S3	58	44	14
7 DAE		171	129	42
	S1	56	43	13
	S2	55	42	13
	S3	60	45	15
14 DAE		175	132	43
	S1	54	41	13
	S2	59	45	14
	S3	56	43	13
28 DAE		176	133	43
	S1	58	44	14
	S2	60	45	15
	S3	57	44	13

Classification accuracy results range from 47% with only one LV to 72% with 10 LV. (Figure 4-34). The second group (level 2) was composed of data grouped by days after the exposure (DAE). Four resulting groups (2 DAE, 7 DAE, 14 DAE and 28 DAE) were analysed in order to determine the impact of DAE in the prediction capabilities

of the models. The highest classification performance was between 30% and 53% with 7 and 9 LVs, respectively. The classification accuracy was lower than the first group (all data) (Figure 4-34). The prediction capabilities increased to more than 90% in the classification accuracy with just one LV when the level 2 was subdivided by the timing of exposure (S) (Figure 4-35).

The data grouped by DAE and timing of exposure (S) manifested more variability in prediction performance (Figure 4-35). However, the classification accuracy improved considerably with less LV. Plants sprayed at the earliest stage (S1) produced the best classification accuracy (> 90%) with 3 LV at 2 DAE. It appeared that as soon as the event occurred, it is more likely to predict accurately the dose that reached the crop. At 28 DAE was also a good time to predict dose with the same accuracy but it needed more LV (between 7 and 10). 7 DAE and 14 DAE predictions are still good but with lower accuracy (≤ 85%). When plants were treated at S2, the worst time for data collection was at 2 DAE while 28 DAE was the best time as it only required two LV to reach 100% of correctly classified data. The best time for data collection at S3 was 7 DAE with one LV and 93% of correctly classified data.

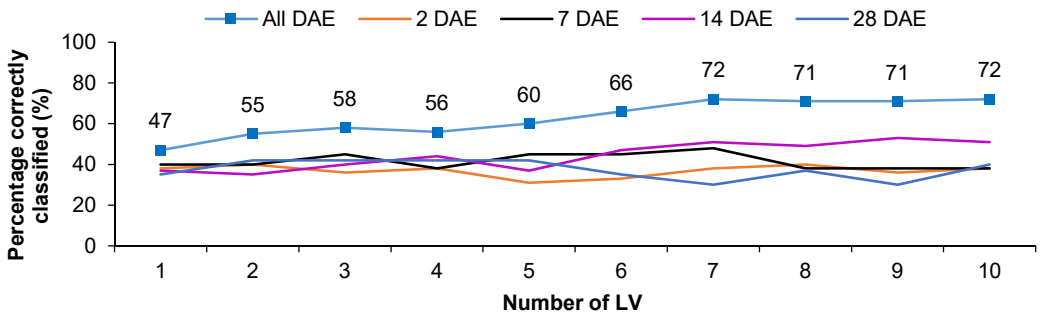

Figure 4-34. Comparison of classification accuracy of CPPS for all data (All DAE) and grouped by DAE.

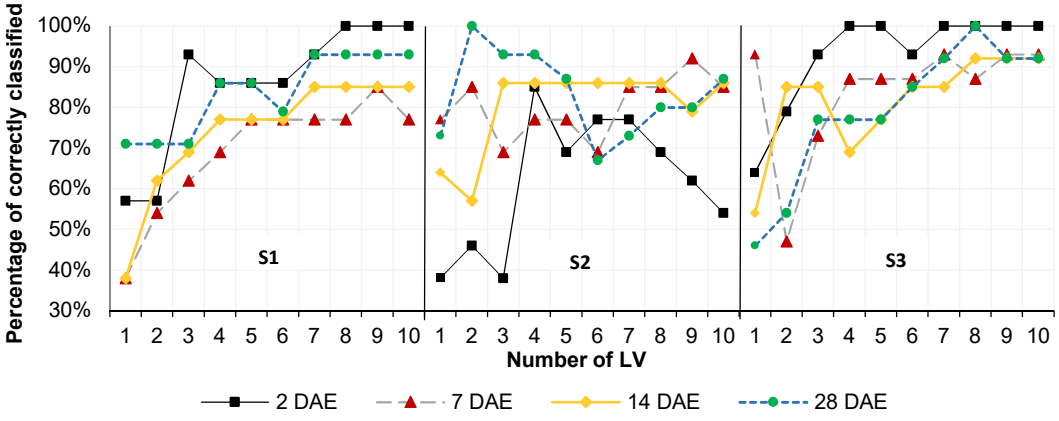

Figure 4-35. Classification accuracy of CPPLS for level 3: Data grouped by DAE and timing of exposure.
Source: (Suarez et al., 2017)

Although the *X*-variance explained by the models with data grouped by DAE and S (level 3) was, in many cases, low, good classification accuracies were achieved, for example, 2 DAE-S3, 7 DAE-S3 and 28 DAE-S2 (Table 4-9). On the other hand, there were also models that reached more than 90% of *X*-variance explained but with poor classification results, for example, 28 DAE, level 2. The algorithm CPPLS only required 27.3% of variance explained for yielding good classification results (> 90%) (7 DAE-S3) (Table 4-9 and Figure 4-35).

Table 4-9. Percentage of X-variance explained at different grouping levels with CPPLS algorithm.

		Number of LV									
Level	**Group**	**1**	**2**	**3**	**4**	**5**	**6**	**7**	**8**	**9**	**10**
1	All DAE	34.9	37.9	46.8	47.6	48.1	48.7	48.8	48.9	49.1	49.2
2	2 DAE	41.9	50.5	52.9	54.6	57.5	58.0	58.3	58.3	58.4	58.6
	7 DAE	44.7	46.5	51.0	52.3	55.7	56.6	56.6	56.6	56.6	56.9
	14 DAE	50.9	56.3	60.7	61.1	62.3	62.9	63.3	63.5	63.6	64.2
	28 DAE	40.1	45.6	51.0	92.2	93.3	93.4	94.8	94.8	94.9	95.0
3	2 DAE-S1	73.2	86.7	87.0	90.0	91.1	91.1	91.2	91.4	91.4	91.4
	2 DAE-S2	50.9	52.0	54.6	54.9	61.8	66.4	66.7	66.8	67.3	67.5
	2 DAE-S3	43.1	49.2	56.5	57.9	60.5	60.7	60.8	60.9	61.0	61.1
	7 DAE-S1	30.1	33.6	35.8	35.9	36.3	36.4	36.7	36.7	36.7	36.7
	7 DAE-S2	16.8	20.8	65.2	67.4	68.7	69.4	71.7	74.5	75.8	77.2
	7 DAE-S3	27.3	30.6	35.1	38.2	38.7	39.5	40.5	40.5	43.6	46.4
	14 DAE-S1	34.7	53.3	56.3	57.8	58.0	60.6	61.0	61.3	61.7	61.9
	14 DAE-S2	27.3	54.1	54.7	59.8	60.0	60.1	60.7	61.5	62.2	62.8
	14 DAE-S3	17.8	20.3	28.8	30.1	30.9	31.3	32.4	33.6	33.9	35.6
	28 DAE-S1	58.5	69.8	71.6	73.1	73.2	73.6	73.7	73.7	73.8	73.8
	28 DAE-S2	42.2	50.1	57.6	58.0	59.5	59.6	60.3	60.4	60.9	61.0
	28 DAE-S3	13.6	86.7	87.2	96.6	96.7	96.8	96.9	97.0	97.0	97.0

The identification and selection of the most significant wavelengths are critical stages in modelling. These procedures can be implemented with different algorithms. The Significant Multivariate Correlation (***sMC)*** algorithm was applied for extracting information regarding the most significant wavelengths in the resulting models, as it corrected the limitations of the variable selection method Variable Importance in the Projection *(VIP)* (Tran et al., 2014).

The model built with data at level 3 (28 DAE and S2) was significantly improved with the addition of the second LV. Figure 4-36 shows the most significant wavelengths for both LV 1 and LV 2. The difference between those LVs is the participation of the

wavelengths around 550 nm ± 12nm in the second LV, which also included a few more bands from 442 nm to 449 nm and from 595 nm to 612 nm. The inclusion of those bands increased the classification performance from 73% to 100% of correctly classified cases.

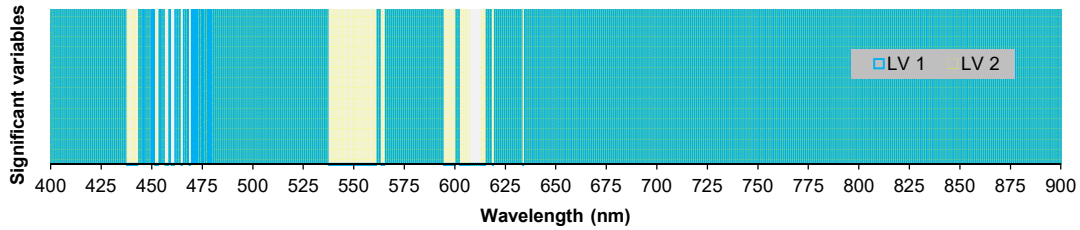

Figure 4-36. Significant Multivariate Correlation (sMC) for the first two LVs of the CPPLS approach: 28 DAE-S2 model.

sPLS-DA

For this approach, same levels of analysis were performed as CPPLS while three different algorithms for classification purposes were tested: Centroid distance, Maximum distance and Mahalanobis distance. In contrast with CPPLS, the classification accuracy increased as the number of LVs increased. Centroid distance was the worst classification algorithm which was slightly higher than 60% of properly classified samples in a few specific cases (Figure 4-37 and Figure 4-38). Maximum and Mahalanobis distance performed similarly in most of the scenarios. Grouping the data into DAE improved the classification results for 7 DAE and 28 DAE after 6 LVs (Figure 4-37).

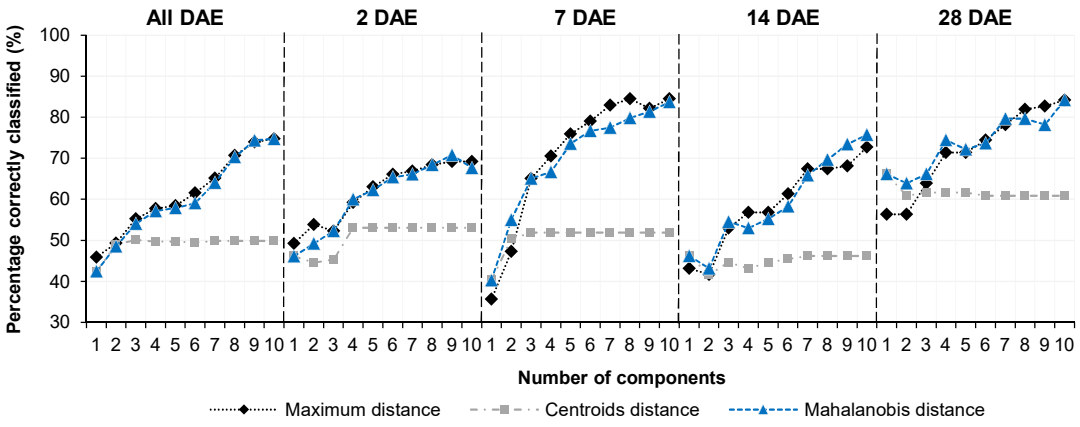

Figure 4-37. Classification accuracies for estimation of dose with all data pooled across (All DAE) and grouped by days after the exposure (DAE).
Source: (Suarez et al., 2017)

When comparing levels 2 and 3 (Figure 4-38), some cases resulted in improved classification accuracy. Collecting data at 2 DAE did not perform well for any of the timing of exposure with the exception of S3 when 91% of the cases were properly classified. At this stage, it was possible to reach more than 90% of samples correctly classified by grouping the data 7 DAE.

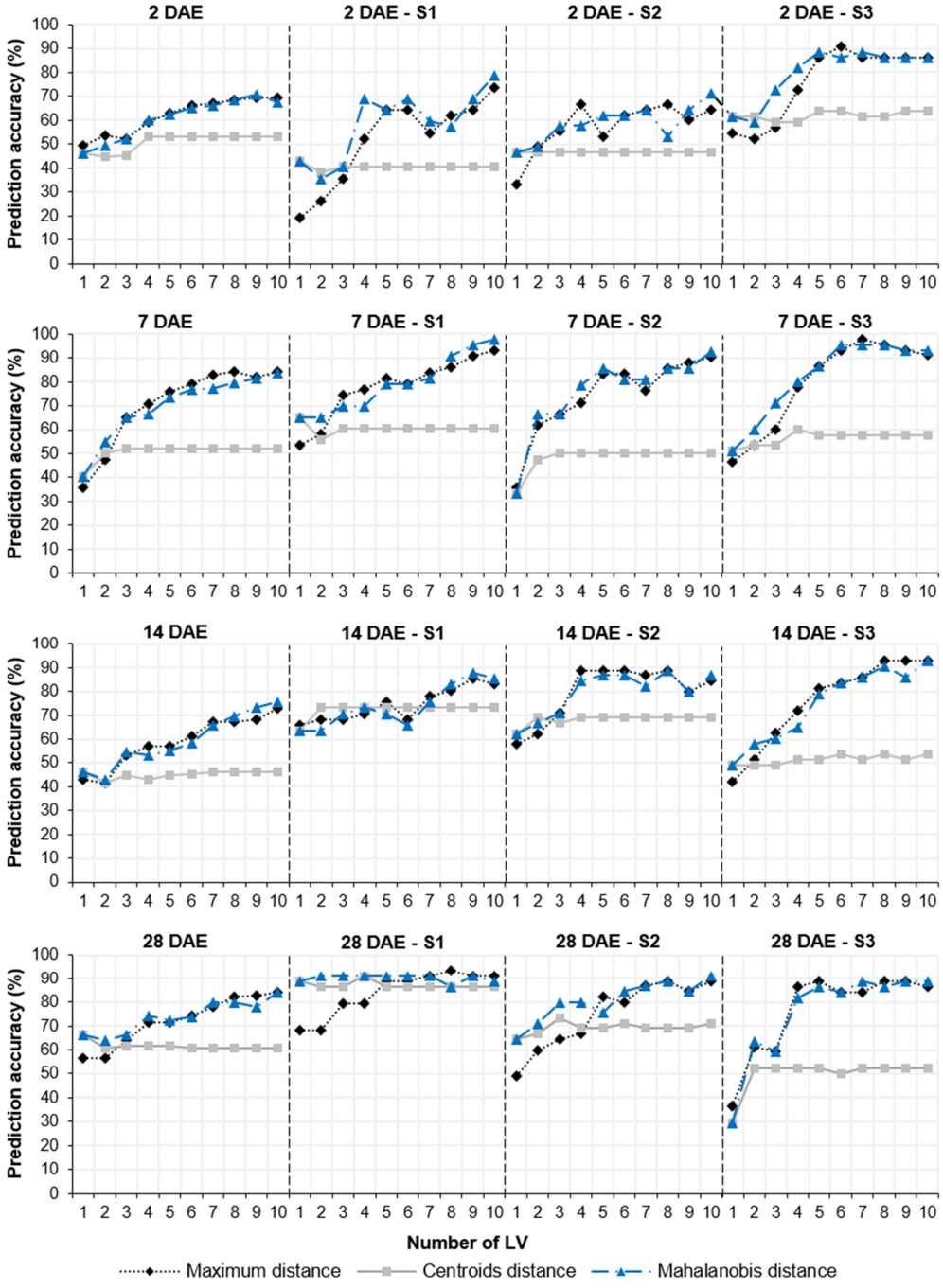

Figure 4-38. sPLS-DA prediction accuracy with data grouped by days after exposure (DAE) and timing of exposure (S) with one to ten LVs and for three different classification methods.
Source: (Suarez et al., 2017)

It was also possible to reach accuracy levels higher than 90% for the timing of exposure S1 and S2 but with more LV (8 and 10, respectively). For 7 DAE, the subdivision by the timing of exposure (S) (Figure 4-38) increased the accuracy levels. A similar situation occurred with the 14 DAE grouping factor when the accuracy increased from less than 80% to more than 90%. Predicting dose at 14 DAE was particularly good for the timing S2 (> 90% and 4 LVs). Data collection conducted 28 DAE increased the classification accuracies for all of the different timings of exposure. This was especially true for S1 when the internal changes were clearly identified by the hyperspectral sensor. Two LVs were able to properly classify 91% of the samples. Similar results were obtained for S3 (> 86%), although more LVs were needed (5 and 7 to 10 LV).

Table 4-10 summarises the best time for data collection according to the timing of exposure and classification method. When the timing of exposure was late, the best time for collecting data was within the first 14 days after the incident (2 DAE and 7 DAE and up to 14 DAE with less accuracy). When the plants were exposed to the chemical at 7-8 nodes (S2) (and the data was grouped by 28 DAE), the CPPLS could predict dose with 100% accuracy and with only two LV. As a result, 28 DAE was the best time for data collection purposes for cotton plants affected at the middle stage (S2). However, in general, this timing of exposure was the most difficult to properly classified as indicated by the lowest classification accuracy (usually below 90%).The methods performed differently at the very early stage of exposure (S1): based from CPPLS analysis, the best classification accuracy was attained with data collected at 2 DAE (> 90%) while sPLS-DA results showed that the best time was 28 DAE.

Table 4-10. Summary of optimal number of LVs as per classification approach, timing of exposure (S) and days after exposure (DAE).

	CPPLS				sPLS-DA			
S	**2 DAE**	**7 DAE**	**14 DAE**	**28 DAE**	**2 DAE**	**7 DAE**	**14 DAE**	**28 DAE**
S1	3 LV			4 LV*				2 LV
S2			3 LV*	2 LV			4 LV*	
S3	3 LV	1 LV	2 LV*		6 LV	6 LV	5 LV*	

Results only show the optimal number of LVs for classification accuracies higher than 90% and * accuracies between 80% and less than 90%.

The correlations between reflectance and yield after contact with the chemical clearly support the results of the classification methods, in the way that the optimal time for

data collection purposes (7 DAE for S3 and 28 DAE for S1) coincided with the highest differences that occurred in the NIR and green peak. Two and fourteen days after the exposure (2 DAE and 14 DAE) did not present such significant correlations but they resulted to be the best time for collecting data if the incident occurred at the early stage (S1) (in addition to 28 DAE) and the middle stage (S2), respectively. The NIR range and some of the visible wavelengths (i.e. blue range for S1 and green and red range for S2) manifested the biggest differences between varying doses at these times (2 DAE and 14 DAE).

The classification methods (CPPLS and sPLS-DA) tested in this study for estimation of dose provided good classification accuracies. The main difference was the optimal number of LVs. CPPLS performed better in most of the cases and required less LV to reach the same classification accuracy than sPLS-DA. However, both classification approaches highlighted the importance of knowing the stage of the crop when the incident occurred as the plants reacted differently at every timing of exposure (Everitt & Keeling, 2009). Based on the results, the time (DAE) by itself did not improve the prediction capabilities. However, when the data was segregated by the timing of exposure (S), the accuracy was substantially improved suggesting a higher influence of (S) in the model performance. *The best time for data collection purposes, after the exposure, depended on the stage of growth of the plants*.

The analytical techniques and results presented in this study provide valuable information for a better understanding of cotton crop variability due to herbicide drift. The findings related to fibre quality (e.g. gin turnout, micronaire, fibre length, elongation, uniformity, and strength, and percentage of short fibre within the sample) reduces the possible negative consequences associated to 2,4-D damage allowing farmers to focus on the maximisation of yield recovery by applying mitigation management practices. Most of the findings agreed with previous work, however, a significant disparity was observed in Abscisic Acid (ABA) content of treated plants, which could explain the plant growth inhibition according to Grossmann (2010). Another interesting finding was the inclusion of the blue spectral range (from 400 nm to 415 nm) in the prediction models in order to increase their prediction capabilities. Furthermore, the implication of the days after herbicide exposure in relation to field data campaigns was found relevant. With these findings in mind, it is possible to plan

field data collection activities in a specific period of time to make the damage assessment more accurate.

4.5. Discussion

4.5.1. Impact of 2,4-D herbicide drift on cotton yield and lint yield

The recovery capabilities of the plants exposed to 2,4-D assessed by the amount of harvested yield manifested a clear relationship with the timing of the exposure. Plants exposed at very early stage (S1) reached a harvested yield equivalent to 66% of the control treatments while plots treated at middle and late stage (S2 and S3 respectively) did not reach 50% of the controls. This is in accordance with other studies where the timing of exposure proved to be an important aspect in the recovery capabilities of the plants (Charles et al., 2007; Everitt & Keeling, 2009). The dose, on the other hand, did not show a significant difference at a late stage (S3) as the yield loss recorded was only with a difference of 11% between D1 and D2 while for other stages, the differences were higher than 39% (Figure 4-17). The resulting trend of cotton susceptibility to 2,4-D is also evidenced in the study by Charles et al. (2007). In that study, conventional cotton and transgenic 2,4-D-tolerant cotton plants were exposed to similar doses (D1 and D2). Regardless the tolerant capabilities, the plants were highly affected by the phenoxy herbicide increasing the yield loss as the dose was increased.

Lint quality was not affected by the exposure according to the standard schedule of premiums and discounts of cotton marketers (e.g. Namoi Cotton Co-operative). Correlations did not show a statistically significant relationship between these variables and dose with the exception of micronaire (Figure 4-21). Although micronaire was observed to be negatively correlated with dose ($r = -0.68$, $p < 0.05$), the minimum and maximum values (i.e. 3.4 and 4.6, respectively) were within the range of “zero” discount policy of the market standards. The lowest variability and most-consistent results were obtained in fibre uniformity, strength, and length. Micronaire, SFI and elongation presented a slightly higher variation that was not clearly associated with herbicide application. These results agree with the findings reported by Smith and Wiese (1972) where they tested different concentrations of 2,4-D on cotton crops. The results of their study concluded that micronaire was the only lint quality variable negatively affected by this herbicide. The micronaire levels in that

study were also within the base range of 3.5 to 4.9 to which discounts generally did not apply (Van der Sluijs, 2015).

4.5.2. Internal changes in cotton plants after the exposure to 2,4-D and its influence in spectral responses

4.5.2.1. Physiological changes

The direct relationship between the healthiness of the plant and photosynthesis and stomatal conductance, obtained in this study, can be confirmed by several studies where the health of the plants was affected by disease or nutrient availability reducing the stomatal conductance and, therefore, the photosynthetic capacity (Merton et al., 2004; Zhao et al., 2005). The negative relationship between the physiological variables and dose explored in this study also agrees with those findings in Perumal et al. (2006), where photosynthesis and stomatal conductance decreased due to the exposure to 2,4-D of cotton crops.

It is commonly known that healthy plants decrease the reflectance in the red region (around 670 nm) while the increase of reflectance in the green peak is associated with lower rate of photosynthesis and lower pigment content (Blackburn, 2007; Gitelson et al., 2003; Merton et al., 2004; Schlemmer et al., 2013; Yi et al., 2014). Carter (1998) demonstrated a proportional indirect relationship between photosynthesis capacity and the reflectance at the end of the red band (~ 700 nm). Additionally, in Suarez et al. (2016), 2,4-D dose was highly and negatively correlated with photosynthesis. Based on those findings, including the work of Perumal et al. (2006), it was shown that treated plants suffered a reduction of photosynthesis capacity. Gitelson et al. (2003) found that in the cases where the chlorophyll (chl) content in plants did not vary, thicker leaves presented lower chlorophyll concentration (per volume) manifesting reflectance increments in the green peak and the NIR.

These results (i.e. higher green and NIR reflectance), are in accordance with the higher reflectance values in the green peak and NIR in control plants reported in this study as they had a more homogeneous, softer texture and thicker leaves than 2,4-D-injured leaves. Hence, these results suggest a potential higher chlorophyll concentration in treated plants as consequence of the chemical contamination. Furthermore, Rapaport et al. (2015) demonstrated that the progressive reflectance decrease in the green peak

and the red edge range (710-750 nm) was as consequence of gradual water deficits. 2,4-D-injured leaves manifested a combination of these two factors (lower reflectance in the green peak and red edge region) suggesting that the effects caused by the chemical also induced water stress as consequence of the physiological changes where the youngest leaves were more likely to suffer this stress as shown in Figure 4-29.

4.5.2.2. Hormone changes

Middle and late stage of exposure (S2 and S3) produced the lowest harvested yield regardless the dose. IAA decreased through time in comparison with control treatments, in plants treated at early stage. On the other hand, an overproduction of IAA after the contact with the chemical was recorded for plants treated at S2 and S3 with the lowest dose (D1) after 14 days of the exposure (14 DAE). This overproduction could explain in some extend the significant yield loss for those timing of exposure as the overstimulation of IAA culminates in a dead plant (Bondada, 2011; Grossmann, 2010).

Overproduction of ABA content causes morphological abnormalities and plants exposed to 2,4-D experienced structural modifications in the mesophyll cells of the injured leaves (Bondada, 2011; Grossmann, 2010). These structural modifications include extra cell layers proliferated near the spongy mesophyll close to the axial leaf surface (Bondada, 2011) seriously affecting photosynthesis and stomatal functioning. Significant correlations between ABA and dose and physiological variables were not manifested in this study. However, throughout the study of the correlation coefficients of ABA and reflectance data, it was possible to indirectly relate the physiological aspects of the 2,4-D-treated plants and ABA content. ABA manifested a moderate correlation in the cell-related structure wavelengths (NIR) ($r = 0.6$, p-value < 0.05) and a moderate correlation with the longer wavelengths of the blue range (p-value < 0.05). Blue light has an important role in the inhibition of stem elongation (Cosgrove, 1981) and stomatal control (Schwartz, 1984) in plants, which at the same time also influences water relations and CO_2 exchange.

4.5.3. Hyperspectral data as a tool for prediction of damage caused by herbicide drift on cotton crops

Different spectral responses captured at three growth stages of healthy plants were expected to change due to physiological changes of the crop (Plant et al., 2000) (Figure

4-28). The change in the NIR reflectance has been correlated to different conditions of the crop, such as a) fertile soil or soil nutrient content (Merton et al., 2004); b) crop development (Merton et al., 2004) and c) stage of growth (Zarco-Tejada et al., 2005). Control plants clearly manifested NIR increments as the crop became mature. Similarly, the plants treated with 2,4-D, manifested drastic changes in the NIR range (700 nm -900 nm) (Figure 4-29) indicating morphological deformities and structural alterations (Bondada, 2011).

The results from correlations between hyperspectral data with yield confirmed the important role of the green peak and the NIR wavelengths to assess the damage caused by 2,4-D. Although the correlation coefficients slightly varied through time, the relationships kept constant. An improved yield is expected when there are better conditions within the plant (Gitelson et al., 2003; Schlemmer et al., 2013) including cell structure, leave thickness and chlorophyll concentrations (Blackburn, 2007; Grossmann, 2010; Merton et al., 2004). These conditions were manifested through the changes of the reflectance shape of treated plants: the green peak and NIR reflectance increased while the reflectance in the red range decreased in comparison with control plants.

According to the literature, transformed hyperspectral data affects the performance of prediction models. The impact of pre-processing techniques is wide but they need to keep the spectral characteristics such as the wavelength position of the inflection points, the local minima or maxima as well as the preservation of the absorption features of the original data (Schmidt & Skidmore, 2004). Moreover, the mathematical approaches alter the original data (Barbin et al., 2012) by inducing spectral variations that are related to the studied variable. For these reasons, the implementation of noise-removal or smoothing techniques needs to be addressed at each particular case of study rather than ad hoc as detailed by Chen et al. (2011) and Swatantran et al. (2011). In this study, we concluded that pre-processing techniques did not considerably improve the prediction capabilities of yield models. In fact, raw data and SG yielded the best predicting models with the same coefficients (R^2) and RMSECV. These results are in accordance with Barbin et al. (2012) and Vaiphasa (2006) where any spectral pre-processing technique increased model performance. Hence, non-transformed spectra

was implemented in all subsequent analysis, since any of the analysed techniques conceded better results than raw data.

This study has proved the potential capabilities of hyperspectral data in the accurate prediction of cotton yield under the influence of phenoxy herbicide at different rates and timing of exposure. It was also possible to identify the temporal variability of the prediction models according to days after the exposure (DAE) confirming the recovery process within the plants as reported by Al-Khatib et al. (2004); Everitt and Keeling (2009) and Everman et al. (2008). Results from the prediction models included an RMSECV of 2.56 bales/ha which represent a prediction accuracy of 83% and an R^2 equal to 0.88. Charles et al. (2007) and Everitt and Keeling (2009) reported that one of the principal limitation in the traditional assessment of 2,4-D herbicide drift on cotton crops was the temporal variability of the visual symptoms which often resulted in overestimation or underestimation of yield loss. We demonstrated that proximal remote sensing is a powerful and reliable technology to overcome the traditional limitations of visual assessment of damages. As reported in Bondada (2011), broad leaves suffered changes in the internal cell-structure, once in contact to 2,4-D, that are not necessarily physically manifested at low doses or late timing of exposure (Everitt & Keeling, 2009) but significantly influenced the harvested yield.

The analysis of the contribution of each wavelength in the resulting yield prediction models provided information of the most significant aspect for the assessment of damage (Barbin et al., 2012; Garrido Frenich et al., 1995; Yi et al., 2014). The error of the prediction accuracy between the best and the worst predicting model increased by 10%. The main difference, between these two models, is the lack of significant wavelengths in the NIR range (Table 4-7) which is recognised by its close relation to internal cell-structure changes of the leaves (Zarco-Tejada et al., 2005). In this way, *cell-related structure wavelengths resulted to be the most important range for yield assessment. Pigment variability in 2,4-D-injured leaves was then as consequence of the morphological abnormalities and structural alterations* (Bondada, 2011).

Estimation of dose as a reference of herbicide drift damage was also possible with high prediction accuracy regardless the classification method. The main difference between the classification methods was the optimal number of LVs to return a higher prediction accuracy. CPPLS is a method designed to exploit information in the predictors, so it is

expected to require less LVs (Indahl et al., 2009). This study confirmed the power of CPPLS by reducing the number of LVs. CPPLS, with only two to three LVs, performed better than sPLS-DA (Table 4-10) with prediction accuracy up to 100%.

CPPLS was able to reach 72% of properly classified cases without segregation the data into the timing of exposure (S). This result has an important impact on the realistic implementation of this technology. Usually, in the field, the timing of exposure and the dose are unknown which are also limiting factors for agronomists to have a more precise assessment. The implemented methodology improved the results presented in Henry et al. (2004) where the best prediction accuracies were not higher than 92%.

In this study, every analysed variable manifested morphological changes through time. Photosynthesis, stomatal conductance, IAA, ABA and prediction capabilities responded differently at different point of time which support the findings reported in Bondada (2011); Everitt and Keeling (2009) and Grossmann (2010) where the assessment and variable changes fluctuated according to days after the exposure.

4.6. Summary

This study demonstrated that hyperspectral sensing was capable of detecting the symptoms of internal changes occurring in the cotton plants as soon as two days after the exposure to the chemical auxin herbicide 2,4-D. The herbicide 2,4-D significantly affected cotton crops regardless of the timing of exposure and dose. Yield loss due to 2,4-D exposure was higher in more mature plants, as bolls did not have enough time to develop properly.

This study tested five different pre-processing filters and concluded that they did not significantly improve the performance of models when compared with models built with raw spectral data. Days after the exposure and timing of exposure (DAE and S, respectively) were determinant factors in the performance of model prediction capabilities. Yield prediction assessment within the first two days after exposure was not necessarily the best time. However, the evaluation conducted within a week or at more than 28 days significantly increased the prediction capabilities and performance of the models, with prediction accuracy higher than 80%. The datasets segregated into DAE and posteriorly into S increased the prediction capabilities of dose to 100% of

samples correctly classified. Days after the exposure (DAE) was the most significant variable in the prediction of the simulated dose of 2,4-D in cotton crops.

The visible (400 nm to 700 nm) and the NIR range (701 nm to 900 nm) were sufficient to predict dose of 28 g a.i./ha (5%) and 280 g a.i./ha (50%) of 2,4-D in cotton crops and the consequent yield. However, the green peak (around 550 nm) and NIR range had a significant relationship to yield and a high impact on the prediction capabilities of dose by increasing the accuracy to more than 30%. In addition to the above, the variability of the NIR range was more constant through time highlighting the significance of this range in the assessment of damages caused by 2,4-D. Instruments developed in the future for the detection of herbicide drift should include these spectral ranges as they supply information about the condition of the crop.

The analytical approaches presented in this study accurately predicted yield after a simulated herbicide drift of 2,4-D onto a cotton crop, thereby providing a reliable, effective and non-destructive alternative based on the internal response of the cotton leaves. This approach provides a reliable solution to the limitations of traditional methods, which are reliant on the visual symptoms of the plants. Moreover, the combination of physiological data and proximal/remote sensing procedures, such as those previously described in this study, can provide an integrated understanding of yield variability due to plant conditions after drift, and enable the development of better mitigation plans to reduce yield loss.

Chapter 5

MULTISPECTRAL SENSING FOR THE PREDICTION OF YIELD LOSS CAUSED BY HERBICIDE DRIFT ON COTTON CROPS

5.1. Introduction

Remote sensing tools have been proven to provide reliable solutions for the traditional inconveniences that face different industries such as grapes, tomatoes and cotton when assessing damage to 2,4-D affected crops using traditional methods or visual characteristics. This chapter explores satellite image data as an alternative tool to overcome the traditional limitations when assessing yield loss in areas where uncontrolled exposure of plants to 2,4-D herbicide has occurred.

The aim of this study was to assess the utility of the medium-spatial resolution multispectral sensor Landsat-8 Operational Land Imager (OLI) data in estimating yield in cotton crops affected by 2,4-D phenoxy herbicide. Specifically, the objectives of this study were to evaluate the temporal aspect of accuracies of a) individual multispectral bands, b) several published vegetation indices and c) the integration of all multispectral bands from Landsat-8 OLI, in the prediction of yield after an accidental spray of 2,4-D in cotton crops.

The content of this chapter is divided into six sections. Section 5.1 is an introduction to this Chapter. Section 5.2 is a brief review of the literature regarding previous successful studies where remote sensing data has played a key role in the provision of alternative methods to overcome the limitations of traditional assessment techniques. Materials and Methods are presented in section 5.3 and more information can be found in Chapter 3. The Results section is presented in section 5.4, followed by Discussion in section 5.5 while a summary is presented in section 5.6.

5.2. Multispectral sensors for predicting yield variability after a herbicide drift

Best management practices in the agriculture sector are important to optimise on-farm productivity while demonstrating responsible management to the community (MyBMP, 2016). However, some crops often suffer from accidental herbicide drifts that cause economic damage (Huang et al., 2015; Huang & Thomson, 2010). This situation is worldwide and common; nevertheless, there is still a lack of reliable tools for the estimation of yield after an accidental exposure. Cotton is one of the most vulnerable crops to herbicide drift, particularly to the phenoxy herbicide 2,4-D (Zhang et al., 2001). This crop generally grows at the same time that weed control programs are taking place in neighbouring crops such as wheat, pasture, corn and grass seed, where 2,4-D is applied to kill broadleaf weeds (Ball et al., 2014; Zhang et al., 2001). This situation not only presents one of the highest risks for cotton growers, it also affects the sustainability and security of the industry. Assessment methods for phenoxy herbicide damage in cotton are not precise, often overestimating or underestimating yield. Compensatory growth after exposure to 2,4-D and the inherent recovery capabilities of cotton plants play a major role in reducing yield losses despite the appearance of symptoms of herbicide damage (Everitt & Keeling, 2009).

Proximal and remote sensing are powerful tools to characterise crop condition and are potentially superior to subjective traditional (visual) assessment methods, as they provide a spectral characterisation of leaf and/or canopy solar radiation absorption (Suarez et al., 2016; Zhao et al., 2013). Canopy absorption properties depend on the morphological structure and biochemical content such as water, nitrogen, cellulose and foliar pigments (Bondada, 2011; Yi et al., 2014). Spectral variability can, therefore, be analysed as a consequence of biochemical concentration, biophysical changes and cell structure abnormalities caused by external factors such as herbicide drifts. Vegetation indices are simple but effective mathematical equations designed to extract information about the different factors affecting the spectral response. The structural-related Vegetation Indices (VIs) are designed to extract the green plant quantity signal from complex canopy spectra while exploiting the basic differences between soil background and canopy cover (Zarco-Tejada et al., 2005) as most of the vegetation covers can be characterised by their biomass and Leaf Area Index (LAI).

There are then several "structural" indices designed to optimise their performance according to the vegetation type and species usually involving a ratio or a linear combination of the red and the near-infrared (NIR) wavelengths (Huete et al., 1994). That is the case of the universal Normalized Difference Vegetation Index (NDVI) (Rouse et al., 1974), the Simple Ratio (SR) or the Ratio Vegetation Index (RVI) (Jordan, 1969). However, these indices tend to saturate under high biomass conditions due to the high level of chlorophyll concentrations (Pinter et al., 2003). has been proposed to overcome this potential limitation, and to minimise the impact of environmental conditions by the inclusion of the blue band. However, the blue band can restrict the EVI values when tested across different sensors, because this band is more difficult to standardise due to the atmospheric correction procedure (Pinter et al., 2003). Jiang et al. (2008)) developed a 2-band EVI, that is, removing the blue band from the equation, to be able to generate a long-term time series as the counterpart NDVI, but with the improvements to the EVI equation. More robust indices such as GEMI (Global Environment Monitoring Index) (Pinty & Verstraete, 1992), the OSAVI (Optimised Soil-Adjusted Vegetation Index) and the RDVI (Renormalised Difference Vegetation Index) (Roujean & Breon, 1995) have been designed to provide information on vegetation cover regardless of the density, while minimising soil background and atmospheric effects

In addition to the structure-related indices, chlorophyll-sensitive indices have been shown to be reliable in providing biochemical information under different physiological and stress conditions. The Green Ratio Index (GRVI) and the Green Chlorophyll Index (GCI) proposed by Gitelson and Merzlyak (1994) and Gitelson et al. (2003), respectively, were proposed to estimate chlorophyll content where there is a background of high pigment concentration. This measurement can be used as an indicator of early leaf senescence or stress conditions that can highly affect yield.

Different studies implementing proximal sensing (i.e. hyperspectral sensors) have analysed the capabilities of these technologies to discriminate between healthy and unhealthy soybean crops (exposed to paraquat herbicide), with more than 70% classification accuracy (Henry et al., 2004). More recently, hyperspectral sensors have proved their potential applicability in predicting cotton yield after three simulated doses of 2,4-D herbicide drift with promising results (Root Mean Square Errors -

RMSE = 2.6 bales/ha and R^2 = 0.88) (Suarez et al., 2016). Several vegetation indices have been tested to localise the damage caused by glyphosate in cotton and corn fields (Ortiz et al., 2011). Chlorophyll Vegetation Index (CVI), a vegetation index developed to monitor photosynthetically active biomass of plant canopies (Tucker, 1979), was identified as the most accurate index for glyphosate damage detection while leaf total chlorophyll and nitrogen content in cotton crops were analysed through the identification of the narrow wavebands and narrow spectral indices that accurately estimated these biochemical parameters (Rama Rao et al., 2008).

Successful cases of the implementation of remote sensing data for yield predicting and other agronomic variables of numerous crops are well documented (Pinter et al., 2003; Plant et al., 2000; Thenkabail et al., 2000). Normalized Difference Vegetation Index (NDVI) (Rouse et al., 1974) and Soil Adjusted Vegetation Index (SAVI) (Huete, 1988) were capable of providing information for crop monitoring after a herbicide-induced injury (glyphosate) by revealing stress at different phenological stages of cotton, corn and soybean (Huang & Thomson, 2010). Aerial multispectral sensing was implemented to predict yield as a function of dosage of glyphosate in soybean (Huang et al., 2015). It was found in that study that prediction accuracies varied according to time after exposure and that between one and three weeks after exposure resulted in the best prediction results for all of the vegetation indices analysed. Damage could be also related to plant height and successfully related to vegetation indices. Some studies, on the other hand, found that linear regressions with vegetation indices (VIs) were of limited use when compared with Partial Least Squared Regression (PLS-R) models for estimating phenomics in different water regimes of cotton. Thorp et al. (2015) assessed different statistical approaches for estimating leaf water content, specific leaf mass, leaf chlorophyll $a+b$ and leaf area index (LAI) on seven cotton cultivars growing under different water conditions. The four phenotypes were successfully estimated, with RMSEs lower than 18.5%, applying PLS-R models, while the errors of linear regressions with VIs were, on average, higher by more than 4.5%.

Landsat-8, launched on the 11th February 2013, is a satellite from a series of Earth remote sensing missions launched by NASA since 1972 (Knight & Kvaran, 2014). These moderate-resolution and free data-access missions provide one of the most historical Earth observation resources with a revisit cycle of 16 days over the entire

globe. Compared with its predecessor, the Landsat-8 Operational Land Imager (OLI) sensor has an improved signal-to-noise ratio and better spectral characteristics. OLI is a "push-broom" scanner using long detector arrays (i.e. line of sensors) that do not transmit light between each other, and they gather more light than past Landsat instruments. OLI has a four-mirror telescope and 12-bit quantization (NASA, 2017). Landsat 8 OLI has 11 narrower bands with three different spatial resolutions: 15 m (one panchromatic band), 30 m (four in the visible, one near infrared –IR and two shortwave infrared bands – SWIR bands) and 100 m (two thermal infrared –TIR bands) (NASA, 2017).

Landsat missions have more than 11 thousand users in a wide field of applications such as agriculture (i.e. agricultural forecasting, management, production and conservation), energy, environmental science and management, land use and land cover, planning and development, and human needs such as hazard insurance for crop, fire and flood (Miller et al., 2013).

The extensive and well-recognised use of Landsat sensors and their derived information, such as vegetation indices, in many different areas, presents a research opportunity in the capabilities of Landsat-8 OLI for assessing yield variations after a 2,4-D herbicide drift on cotton crops. Moreover, the use of remotely sensed data to locate and identify the degree of damage to crops may provide valuable information to producers to adjust mitigation plans and potentially locate the source of the drift.

5.3. Materials and methods

5.3.1. Overall approach

Demarcation of the area affected by the drift was followed by correlation analysis between yield records and three different kriging methods to establish the best fitting interpolation approach. The original Landsat 8 product was Level-1, that is, terrain corrected, which is the highest quality L1 Precision Terrain (L1T) product. The L1T digital numbers were transformed to top-of-atmospheric correction image and corrected, including dark pixel subtraction, after which nine vegetation indices were analysed to investigate their temporal variability in the affected area in comparison with the unaffected area. The study area was covered by 349 pixels (30 m x 30 m), in

which the training (70%) and test (30%) datasets were randomly selected and associated whether the area was affected by the herbicide or not.

Linear regression models (LRM) of vegetation indices and individual multispectral bands and yield were calculated individually for each area and then compared. Partial least squares regression (PLS-R) models were implemented, rather than the traditional multivariate linear regression modelling, because some bands in the visible, the near-infrared (NIR) and the shortwave infrared (SWIR) wavelengths are highly correlated. It was then possible to compare prediction accuracies of vegetation indices and the reflectance recorded for the seven bands of Landsat-8 OLI. The predictive accuracies of the best resulting models were verified using the test dataset. Figure 5-1 shows the schematic approach employed in this study for estimating yield after an unintentional exposure to 2,4-D herbicide.

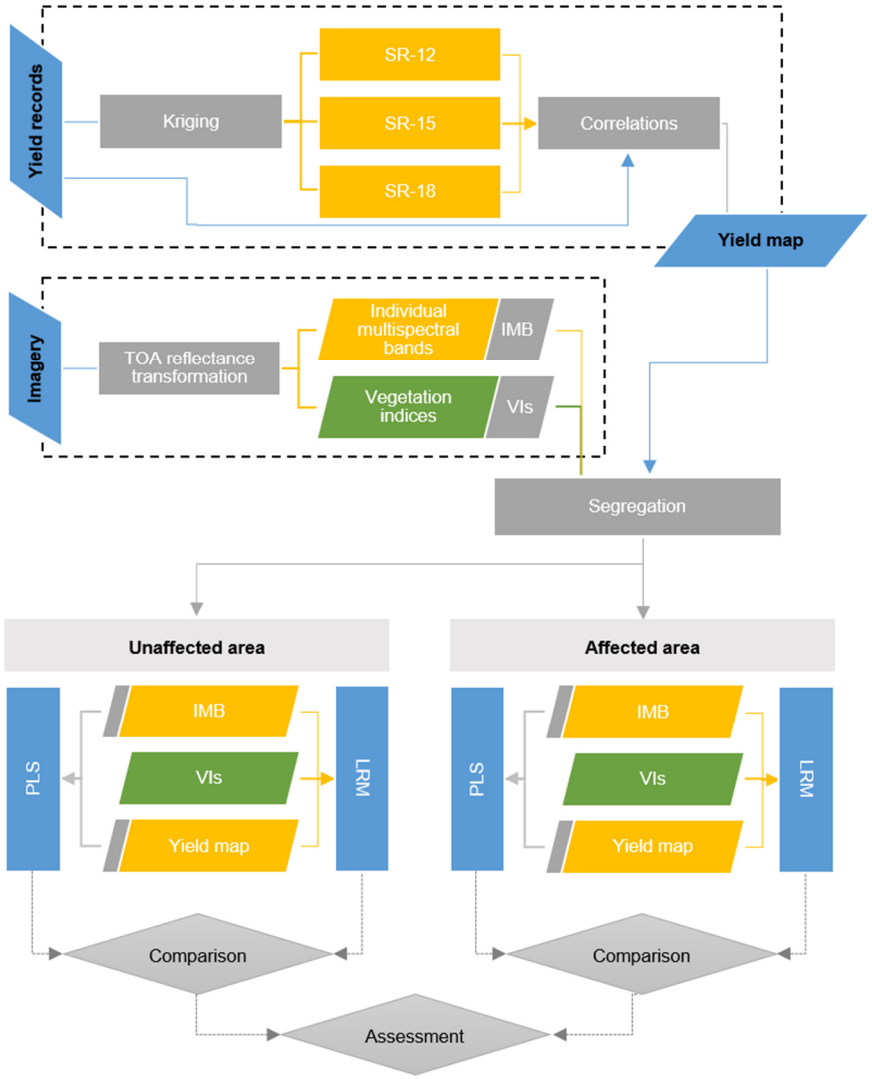

Figure 5-1. Schematic approach used for the prediction of cotton yield using Landsat data.

5.3.2. Study area

The study area covers a commercial cotton paddock comprising 37 ha (Figure 5-2) in Jondaryan, Queensland, Australia. In this region, the average size of a cotton paddock is approximately 53 ha. The unplanned exposure of the crop to the phenoxy herbicide occurred on the 28th January 2015, covering approximately 14 ha (i.e. 38% of the entire area). The weather conditions recorded on the day of exposure were 17.2°C and 23.9°C minimum and maximum temperature, respectively, and 8.6 mm of rainfall. The records came from the nearest weather station, located 19 km east of the study area (Oakey Aero station 041359; 151.74°E, 27.40°S).

A high-yielding variety Sicot 74BRF (developed by the CSIRO Cotton breeding team) was planted on the 27th October 2014 at one meter row spacing. The site was chosen because of the accidental application of the 2,4-D occurred near the peak of the growing season, and because the yield records from a yield monitor were also available.

Figure 5-2. General location of the study area.

5.3.3. Crop yield data

In this study, a four-row picker (*Case IH Cotton Picker 2555 Express Cotton)* equipped with a yield monitor (*Ag Leader PF3000 Pro)* capable of recording GPS points every

3 seconds (Figure 5-3) was implemented. Prior harvesting, the yield monitor was calibrated in a refugee paddock (see Figure 5-4) after which the cotton crop was harvested between the 24th and 25th April 2015 (Figure 5-5).

Figure 5-3. Picker and yield monitor implemented in this study.

Figure 5-4. Calibration process in a refugee paddock.

Figure 5-5. Cotton harvesting in the study area.

Much research has evaluated the relationship between yield monitor data and remote sensing imagery and found that yield maps derived from image data are correlated to those from yield monitor records (Yang et al., 2006). The correlation level was driven by the smoothing effect of the yield records rather than the resolution of the image. The above was found to be significant, especially, in those cases when the resulting yield map included more yield records (points) per pixel size (Yang et al., 2009). In this study, each yield data point represents a rectangular area of 3.8 m by 4.7 m, on average. Therefore, each pixel contained on average 42 yield points.

Yield maps are continuous surfaces generated from yield records (points) by the use of spatial interpolation methods. Several spatial interpolation methods have been tested in previous studies without an unequivocal conclusion being reached as to which is the best (Zimmerman et al., 1999). However, Zimmerman et al. (1999) used synthetic data to systematically test the statistical significance of the effect of certain characteristics such as the level of noise, surface type, sampling pattern, and the strength of the spatial correlations of four interpolation methods: ordinary kriging,

universal kriging, and two types of inversed squared-distance weighted. The authors found that the kriging methods were substantially superior to any of the inverse distance weighting (IDW) methods. This situation can be explained as being due to the advanced nature of the kriging geostatistical procedure which considers not only the distance (as in IDW) but the degree of variation (or the overall spatial arrangement) between known points when estimating values in unknown areas (GIS Resources, 2015). The direction, that is, distance, between known points indicates a spatial correlation that can be used to explain variation in the resulting surface.

Universal kriging assumes that the mean of the variable is constant in the entire area of study while ordinary kriging assumes that the mean of the variable, in this case, yield, is constant in the local neighbourhood of each estimation point (Bohling, 2005). In this way, ordinary kriging is comparable to the fact that each plant tends to respond differently to environment, so the yield of each plant can be potentially different. As a consequence, ordinary kriging methods with a spherical semi-variogram model and a variable search radius of 12, 15 and 18 points (records) (SR-12, SR-15 and SR-18, respectively) were implemented to generate yield maps.

The most accurate surface (yield map) was defined, based on its correlation coefficient with yield records. To test the correlations, the minimum, maximum and average value of the yield records contained within each (30 m x 30 m) pixel of the three resulting yield maps were extracted. Thus, the highest correlation coefficients with yield records, that is, the minimum, maximum and average value, defined the final yield map or yield surface to be implemented. The kriging interpolation methods and the spatial analysis were performed using the Spatial Analysis Tool available in ArcGIS 10.2.

5.3.4. Multispectral satellite imagery

Six dates of Landsat-8 OLI imagery from the Pre-collection Level-1 and processing level L1T were acquired from the U.S. Geological Survey Earth Explorer Viewer website. L1T is the highest quality of Level-1 Landsat products, they are radiometrically calibrated and orthorectified using ground control points and digital elevation models (DEM) to correct for relief displacement (Landsat, 2017).

The Landsat digital numbers (DN) of each date were transformed to at-sensor reflectance or Top of Atmosphere Reflectance (TOA Reflectance) by applying calibration coefficients contained in the metadata file of each capture, using the following equation (U.S. Geological Survey, 2016): $\rho\lambda = \frac{M_\rho * Q_{cal} + A_\rho}{Sin(\theta)}$ where $\rho\lambda$ is the true TOA reflectance, M_ρ is the reflectance multiplicative scaling factor for the band, A_ρ is the reflectance additive scaling factor for the band, Q_{cal} is the pixel value in digital number (DN) and θ is the solar elevation angle. All the variables, except the DN, were accessed from the metadata.

Seven structure-related vegetation indices and two chemical-sensitive indices were calculated for each date from the TOA reflectance image. These indices can be used as indicators of crop health, biomass and biochemical constituents that are closely related to yield (Zarco-Tejada et al., 2005). Therefore, as these factors are affected in 2,4-D-stressed cotton crops (Suarez et al., 2016, 2017), the VIs may serve as robust indicators of crop development and physiological status (Zarco-Tejada et al., 2005). The duration of green biomass during the boll-filling stage has a strong relationship with yield. The most common universal structural-related indices, which provide an indication of the crop's biomass, were therefore tested as indicators of crop performance after a 2,4-D herbicide drift event. Individually, these indices are useful in providing information about specific variables related to the physiological condition and stress status of the crop, but they work somewhat independently of each other, that is, each of them estimates a particular condition or set of conditions. Cotton yield is, however, influenced by the interaction of many factors, particularly when affected by 2,4-D, and its accurate estimation cannot, therefore, be expected from a single VI. Moreover, the relationship between a particular VI and yield may not be valid for others VIs (Pinter et al., 2003). *This is, therefore, the reason the proposed VIs were tested in this study; it should additionally provide further information in relation to their recognised effectiveness across different cases and scenarios.*

Table 5-1 summarises the dates of the corresponding Landsat image capture, relating them to days after sowing (DAS) and days after the exposure (DAE) and Table 5-2 summarised the multispectral bands and the spatial resolution of the imagery while

Table 5-3 lists the vegetation indices (VIs) investigated in this study.

Table 5-1. Chronology of Landsat image acquisitions used in this study.

	Acquisition Date					
	17/12/2014	18/01/2015	3/02/2015	7/03/2015	23/03/2015	8/04/2015
DAS	51	83	99	131	147	163
DAE	-42	-10	6	38	54	70

DAS = Days after sowing; DAE = Days after exposure

Table 5-2. Multispectral bands and spatial resolution of the imagery implemented in this study.

	Coastal	Blue	Green	Red	NIR	SWIR 1	SWIR 2
Wavelength (nanometer)	430–450	450–510	530–590	640–670	850–880	1570–1650	2110–2290
Resolution	30 meters spatial resolution						

Table 5-3. Vegetation indices investigated in this study.

Structural-related indices		
Vegetation Index	**Formula**	**Reference**
▪ Enhanced Vegetation Index (EVI) or soil and atmospherically resistant vegetation index (SARVI2)	**EVI** = 2.5*[(R_n – R_r)/(R_n + 6*R_r – 7.5*R_b + 1)]	Huete et al. (2002); Huete et al. (1997)
▪ Enhanced Vegetation Index 2 (EVI2)	**EVI2** = 2.5*[(R_n – R_r)/(R_n + 2.4*R_r + 1)]	Jiang et al. (2008)
▪ Global Environmental Monitoring Index (GEMI)	**GEMI** = *eta**(1 – 0.25**eta*) – [(R_r – 0.125)/(1 – R_r)]; where eta = [(2*(R_n^2 – R_r^2) + 1.5 * R_n + 0.5 * R_r)] / (R_n + R_r + 0.5)	Pinty and Verstraete (1992)
▪ Normalised Difference Vegetation Index (NDVI)	**NDVI** = (R_n – R_r)/(R_n + R_r)	Rouse et al. (1974)
▪ Optimised Soil Adjusted Vegetation Index (OSAVI)	**OSAVI =** (R_n – R_r)/(R_n + R_r + 0.16)	Rondeaux et al. (1996)
▪ Renormalised Difference Vegetation Index (RDVI)	**RDVI** = $(R_n - R_r)/\sqrt{(R_n + R_r)}$	Roujean and Breon (1995)
▪ Simple Ratio (SR) or Ratio Vegetation Index (RVI)	**RVI** = R_n/R_r	Jordan (1969)
Chlorophyll-sensitive indices		
▪ Green Chlorophyll Index (GCI)	**GCI** = (R_n/R_g) - 1	Gitelson et al. (2003)
▪ Green Ratio Vegetation Index (GRVI)	**GRVI** = R_n/R_g	Gitelson and Merzlyak (1994)

R_b = Reflectance at blue range; R_g = Reflectance at green range; R_r = Reflectance at red range; R_n = Reflectance at NIR range

The study area was analysed in two different zones: unaffected and affected area. Yield map, multispectral bands and vegetation indices were segregated by area and all the statistical analysis was performed individually. Figure 5-6 shows the visual aspect of the areas in the field and their respective demarcation.

Figure 5-6. Delimited areas (affected and unaffected) as evidenced by the brown and white predominant colours of the crop.

5.3.5. Statistical analysis

The areas were analysed individually and compared (i.e. not affected and affected areas) through time to understand the variability of reflectance data when assessing yield in cotton crop areas affected by a 2,4-D herbicide drift. Training and test datasets were randomly selected within each area, representing approximately 70% and 30% of the sample size of each area, respectively ($n_{unaffected}$ = 229 and $n_{affected}$ = 120) using

the software ArcGIS. Correlations between vegetation indices and individual bands were performed to investigate their relationship with yield and two different approaches were undertaken in this study for the prediction of yield. The yield prediction capabilities of nine vegetation indices (VIs) were used in the first approach. Linear regression models were carried out for the imagery of various dates using the following expression:

$$\boldsymbol{Y} = \boldsymbol{\alpha} + \boldsymbol{\beta X} + \boldsymbol{\varepsilon} \qquad \textbf{(Equation 1)}$$

where the dependent-variable (***Y***) = yield (bales/ha) and the independent-variable (***X***) = vegetation index. The intercept of the line is defined by **α**, while **ε** represents the statistical error of the model or the *residual standard error (**RStE**)*. If Y_i denotes the measured response value for sample i, $\hat{Y}_i$ denotes the fitted value for the same sample i, and n denotes the size of the dataset, then RStE is defined by (R Core Team, 2015):

$$RStE = \varepsilon = \sqrt{\frac{SSE}{n-2}} = \sqrt{\frac{(\sum \hat{\epsilon}_i^2)}{n-2}} = \sqrt{\frac{\sum (Y_i - \hat{Y}_i)^2}{n-2}} \qquad \textbf{(Equation 2)}$$

where SSE stands for the *Sum of Square Error* (ϵ) and n-2 is the degree of freedom. In this equation, two degrees of freedom are lost because of the estimation of two parameters: α and β.

The model performance was then tested based on the maximum value of the coefficient of determination (R^2) and the minimum absolute value of the residual standard error (RStE). All the modelling and statistical tasks were performed in R software (R Core Team, 2014).

The second approach pooled the multispectral bands from each image. These bands have been reported in several studies as highly correlated in agriculture at the field level and different land cover types (Clevers, 1999; Kaufman et al., 1997). Thus, partial least squares regression (PLS-R) models were developed to assess the prediction capabilities of multispectral bands from Landsat-8 OLI.

As described previously in Chapter 4, section 4.3.3, in ordinary least-squares regression, $\boldsymbol{Y} = \boldsymbol{X} \times \boldsymbol{B} + \varepsilon$ is given by: $\boldsymbol{B} = (\boldsymbol{X^T X})^{-1} \boldsymbol{X^T Y}$**.** However, the first term $(X^T X)$ is frequently singular due to: (a) the number of variables in *X*, exceeds the

number of samples (n), or (b) high collinearity between *X*-variables, or (c): a combination of (a) and (b). PLS encompasses these limitations by decomposing *X* into orthogonal scores (S) and loadings (L) in such a way that $\boldsymbol{X} = \boldsymbol{S} \cdot \boldsymbol{L}$. The regression of *Y* is not only in *X* but on the first α columns of scores S so PLS incorporates the information of both predictor (*X*) and response (*Y*) variables in the definition of scores and loadings. The integration of *X* and *Y* optimises the prediction capabilities of PLSR models (Bouckaert et al., 2011; Mevik & Wehrens, 2007; Wold et al., 2001).

The resulting prediction models used a maximum number of seven latent variables (LVs) as seven is the maximum number of variables or multispectral bands. Leave-one-out cross-validation (LOO-CV) was also applied as the calibration algorithm with normalized reflectance per band. Two independent datasets (training and test) were implemented for cross-validation and the respective validation of the resulting models. This approach was employed because LOO has been reported as an optimum calibration algorithm when highly correlated data is included as predictors (Olivieri, 2015). The independent (test) dataset was then used to assess the transferability of the resulting models.

The selection of the best performing PLS-R model was based on the same principles as those described in Chapter 4, section 4.3: a) the optimal number of LVs, b) the minimum absolute root mean square error of the cross-validation (RMSECV), and c) the ability to explain cross-validation (training) yield variance (R_{cv}^2). Furthermore, because there was an independent dataset available for validation, the ability to explain predicted (test) yield variance (R_p^2), the minimum absolute root square mean error of the prediction (RMSEP), and the respective RMS Ratio = RMSEP/ RMSECV were also examined. R_p^2 and RMSEP were estimated using the test dataset and they are equivalent to R_{cv}^2 and RMSECV, respectively. The equations of R_{cv}^2 and RMSECV are presented in section 4.3.3.1.

5.4. Results

Each area was assessed and analysed individually and then compared to each other. This approach was implemented to characterise the crop according to the spectral response as well as the prediction capabilities of the corresponding models within each.

The herbicide 2,4-D impacted the harvested yield to a substantial extent according to the yield records. Comparing both areas, the affected area suffered a substantial reduction of more than 36%. The unaffected area had an average yield of 11.83 bales/ha, whereas the affected area only reported 7.56 bales/ha. Yield variability within the areas was not similar as the standard deviation in the affected area (*std* = 2.05) nearly doubled the standard deviation of the unaffected area (= 1.22) (Table 5-4). A clear region where the herbicide had the highest impact is shown in Figure 5-7.

The soil conditions and the management practices were standard across the two areas before and after the accidental exposure. Hence, the variability within the affected area might be attributable to the recovery capabilities of individual plants.

Table 5-4. Descriptive statistics of yield in unaffected and affected areas.

	Yield (bales/ha)	
	Unaffected	***Affected***
Mean	11.83	7.56
Standard Error	0.01	0.02
Median	11.92	7.78
Standard Deviation	1.22	2.05
Minimum	7.76	0.03
Maximum	15.00	12.00

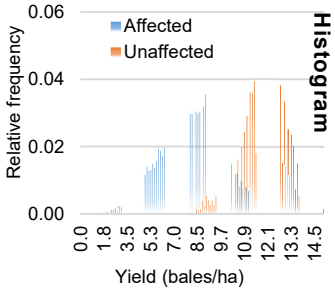

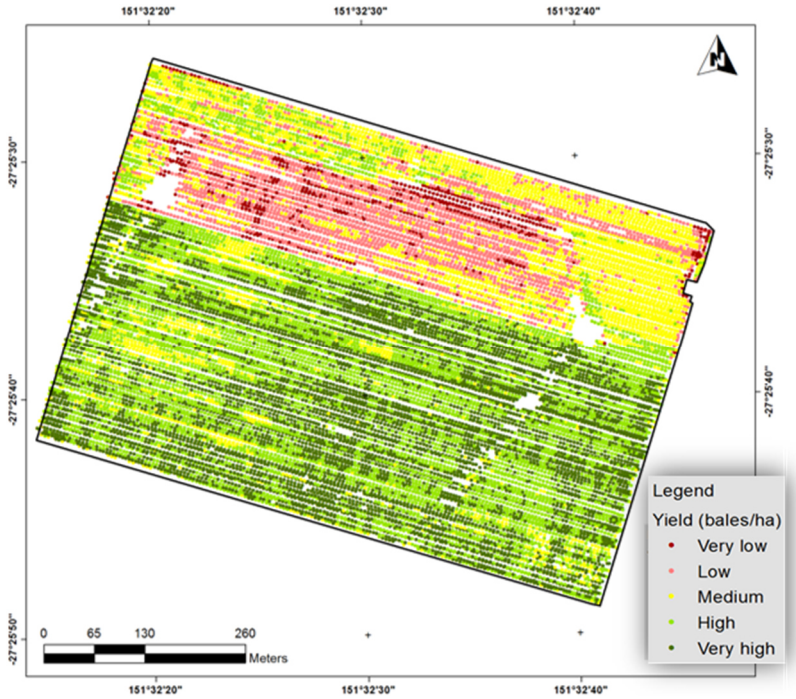

Figure 5-7. Yield point records collected from the yield monitor in the study area.

5.4.1. Yield maps

Yield maps were created through the implementation of ordinary kriging methods with three different variable search radius, and resulting pixel size of 30 m by 30 m was used to match with the spatial resolution of the satellite imagery (Yang et al., 2006).

Because the yield records were transformed into a continuous surface and resampled to a significantly coarser resolution, it was pertinent to test how consistent the resulting surface was when compared with the original records. Correlations coefficients were then calculated as indicative of the most reliable kriging approach (Yang et al., 2006). To assess this, the minimum, maximum and average of the yield records within a pixel were extracted and correlated with the pixel value. In general, only small differences occurred when comparing the search radius tested in this study. The smallest and the biggest search radius (SR-12 and SR-18, respectively) were slightly less correlated with each other while the medium search radius (SR-15) was perfectly correlated with both SR-12 and SR-18. Table 5-5 presents the descriptive statistics per pixel, and summaries the correlation coefficients from the yield records and the respective yield map.

Table 5-5. Correlation coefficients between yield records and yield maps.

		Correlation coefficient *		
		SR 12 pts	**SR 15 pts**	**SR 18 pts**
Kriging parameter (search radius SR)				
	SR-12 pts	1.000		
	SR-15 pts	0.996	1.000	
	SR-18 pts	0.995	0.998	1.000
Spatial statistics per pixel				
	Minimum yield records	0.648	0.655	***0.659***
	Maximum yield records	0.885	0.891	***0.893***
	Average yield records	0.963	0.969	***0.972***

* *p*-value $\leq$ 0.05. SR 12 pts: variable search radius of 12 points; SR 15 pts: variable search radius of 15 points; SR 18 pts: variable search radius of 12 points.

The highest correlation coefficients were between yield records and SR-18 values (*p*-value $\leq$ 0.05). Although the coefficients were similar to other kriging parameters, SR-18 was always the highest correlated with minimum, maximum and average yield records. Based on these results, the ordinary kriging method with a spherical semivariogram model and a variable search radius of 18 points (SR-18) was selected as the most accurate yield map.

5.4.2. Temporal variability of multispectral bands and vegetation indices in relation to exposure area

Raw bands in the visible range behaved similarly during the first 99 DAS when the point of maximum absorption in the coastal, blue, green and red bands was reached (Figure 5-8). The reflectance values per area started to vary after that time, where the unaffected area showed an incremental reduction of absorbance once the crop reached the peak of nodal development (Quinn & Kelly, 2011). The absorption in the visible wavelengths also started to decrease in the affected area but the rate was lower when compared with the unaffected area. The affected area barely manifested spectral changes in the green band for nearly 50 days between 6 DAE and 54 DAE. This period only had a maximum reflectance difference of 0.002 while for the same period the unaffected area manifested reflectance changes of more than 0.01.

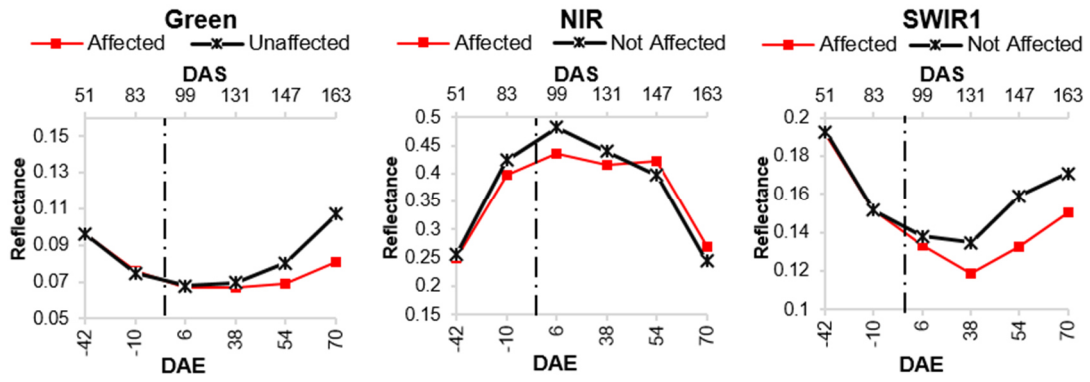

Figure 5-8. Reflectance variability through time in unaffected and affected areas.

The near infrared (NIR) band also manifested different patterns according to the area. Both areas had a reflectance peak at 99 DAS but with different magnitudes (0.48 and 0.43 in the unaffected and in the affected area, respectively). The temporal changes in reflectance in the unaffected area defined a curve which represented the structural changes at the canopy and leaf level due to the normal growing condition of the crop. This is also supported by the maximum correlation coefficient between yield and NIR which was reached after 99 DAS, at approximately 131 DAS (Appendix 5-2). Variation in NIR reflectance in the affected area tended to be less after exposure, indicating a minimum canopy development between 6 DAE and 54 DAE (Figure 5-8). In this area, NIR reflectance did not manifest correlations with yield (except at 51 DAS=-42 DAE) and only the VIS bands developed a moderate and significant (p-value ≤ 0.05) correlation with yield just before harvesting (Appendix 5-3).

The SWIR bands (SWIR1 and SWIR2) manifested the same mean reflectance at -42 DAE and -10 DAE (0.16 and 0.11, respectively). After this time, the reflectance patterns changed (Figure 5-8). The affected area manifested lower reflectance values than the affected area soon after the exposure and the difference gradually increased through time reaching a maximum of 0.026 difference at 54 DAE, after which the reflectance difference started slowly to decrease.

The VIS and SWIR bands in the unaffected area did not manifest a good relationship ($r \leq 0.4$) with yield at any time after 51 DAS, while the NIR band shown a moderate correlation ($r = 0.43$, p-value ≤ 0.05) at 131 DAS, when the crop was mature and most of the bolls were developed (Appendix 5-2). On the other hand, in the affected area, all the VIS bands were moderately correlated with yield ($r > 0.50$, p-value ≤ 0.05) at two weeks before harvesting (163 DAS and 70 DAE) (Appendix 5-3).

The temporal variability of the cell-related and the chlorophyll-related indices was calculated for both areas over the growing period analysed in this study. The VI values show a clear peak around 99 DAS in the unaffected area, whereas the indices tended to "stabilise" after exposure to the herbicide in the affected area, decreasing only close to harvest (Figure 5-9).

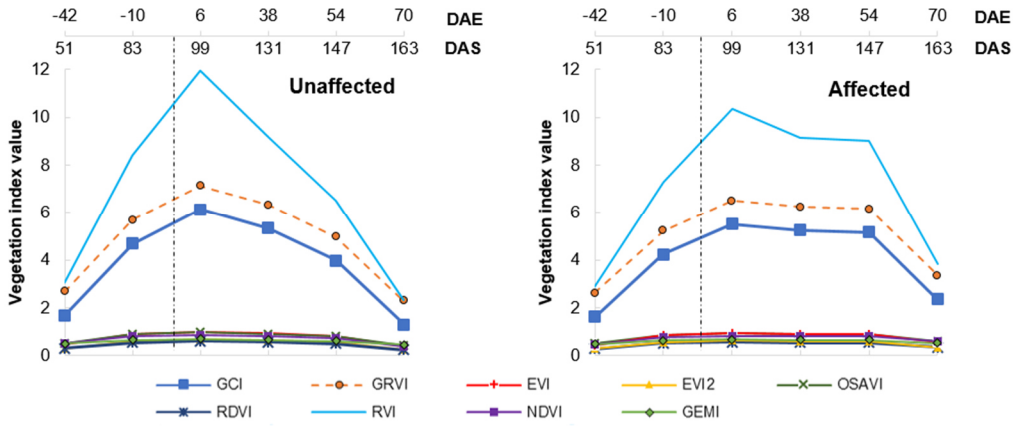

Figure 5-9. Temporal variability of the vegetation indices according to the area (unaffected or affected). Dotted line: date of exposure.

Correlations between VIs and raw bands were performed to determine their relationship with the harvested yield at the end of the season for each area individually. A peak relationship between VIs and yield, under optimal growing conditions, was expected to occur when the crop reached the maximum vegetative growth and starts fruit development. In this study, that point was reached around 131 DAS in the

unaffected crop (Figure 5-10). All VIs had their peak point of correlation at that time ($r > 0.3$) with NDVI and RVI manifesting the lowest correlation values ($r = 0.29$). An opposite situation occurred in the affected area where the maximum point of correlation was as early as 51 DAS. The moderate correlation between most of the cell structure-related vegetation indices (VIs) and yield at 131 DAS in the unaffected area can be explained by the significant correlation between the NIR band and yield, as this band is always a factor in their equations (See Table 5-2 and Figure 5-10 left). However, the moderate correlations of the NIR band with yield in the affected area were not enough to positively influence the correlations between VIs and yield.

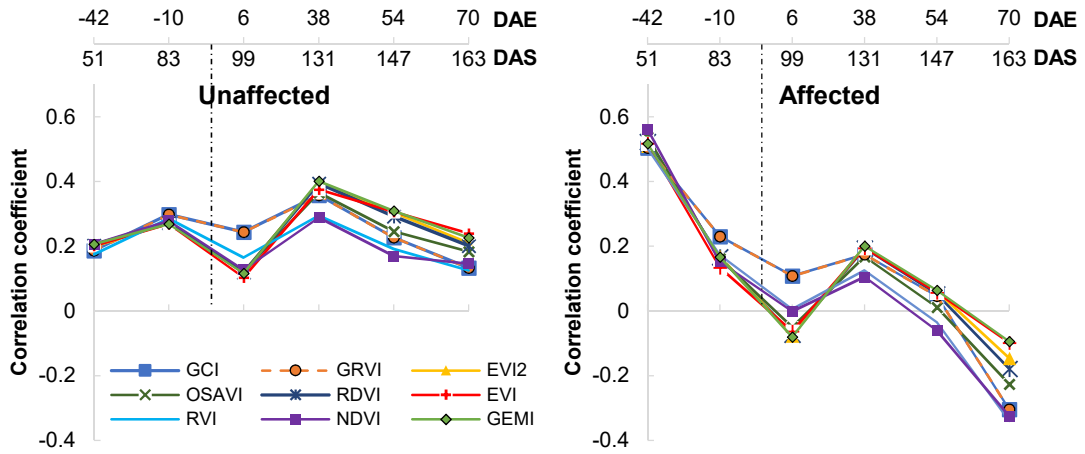

Figure 5-10. Temporal variability of the relationship between vegetation indices and yield.
Dotted line: date of exposure.

GEMI and RDVI exhibited the highest correlations with yield in the unaffected area. These indices were developed to minimise the soil background effect and reduce the atmospheric effect from the satellite data. Although the correlations were not strong, they indicated that green biomass is a good indicator of crop performance under optimal growing conditions. The highest correlation in the affected area occurred when the crop was vigorous with the canopy under development (51 DAS) but still immature and not yet under the influence of the herbicide. That could explain the positive response of all of the VIs, and particularly NDVI. To understand the spectral response, the VI values, and their consequent relationship with yield, it is important to note that the harvested yield was under the influence of the herbicide, consequently, it was very low and similar to an immature crop, since the affected area had delayed development. The high correlations in the affected area at 51 DAS can be properly interpreted from this similarity between herbicide damage and an immature crop.

5.4.3. Statistical models of crop yield estimation

Linear regression (LRM) and PLS-R models were developed to assess the capabilities of three predictor groups: 1) individual multispectral Landsat-8 OLI bands; 2) VIs and 3) the integration of all multispectral bands. Models were developed per area to identify the variability and prediction capability through time of each predictor's group.

5.4.3.1. Vegetation indices and multispectral bands

Linear regression models (LRM) were built with individual multispectral bands (IMB) and VIs for each of the dates analysed in this study. Neither the IMBs nor the VIs were sufficient to accurately predict yield under optimal agronomical conditions of the crop (*p*-value > 0.05), nor when the crop was affected by an external factor such as an accidental spray. The resulting *RStE* was within the range of 1.5 bales/ha but the R^2 was low for each LRM turning the transferability of the models into "not reliable" (Table 5-6). Yield is a complex variable that integrates not only pigment content and nutrition status but also is driven by soils characteristics, moisture and canopy structure (Domenikiotis et al., 2004). An individual band is not capable of integrating all that information, and hence it did not result into a good model performance. This situation applies to both areas analysed in this study, but it turned more complex in the affected area as the exposure to the chemical introduced more variability at physiological and biophysical levels.

Vegetation indices, although performing better than individual bands, still were not sufficiently powerful for yield prediction using linear regression methods (Table 5-6). The highest explained variability (R^2 = 0.14) and the lowest RStE (= 0.75 bales/ha) were obtained when GEMI was the predictor index at 147 DAS (*p*-value < 0.05) in the unaffected area. However, for the same date in the affected area, the GEMI index was not significant for the prediction of yield (*p*-value > 0.05, R^2 = 0.003). The affected area had, as a result, a slightly better fitting model with NDVI as the predictor index with data captured at 51 DAS, that is more than a month prior the accidental exposure (R^2 = 0.24 bales/ha and RStE = 1.33 bales/ha).

Table 5-6. Linear regression parameters of yield predicted by vegetation indices.

Unaffected area																			
		Structural-related Indices														Chlorophyll-related Indices			
		GEMI		NDVI		EVI2		OSAVI		RDVI		RVI		EVI		GRVI		GCI	
DAS	DAE	*RStE*	R^2	*RStE*	R^2	*RStE*	R^2	*RStE*	R^2	*RStE*	R^2	*RStE*	R^2	*RStE*	R^2	*RStE*	R^2	*RStE*	R^2
51	-42	0.78	0.07	-	-	0.78	0.07	0.78	0.07	0.78	0.07	0.79	0.06	0.78	0.07	0.79	0.06	0.79	0.06
83	-10	0.78	0.09	-	-	0.77	0.09	0.77	0.10	0.77	0.10	0.77	0.10	0.78	0.08	0.76	0.12	0.76	0.12
99	6	-	-	0.81	0.01	-	-	0.81	0.01	0.81	-	0.80	-	-	-	0.79	0.06	0.79	0.06
131	38	0.75	0.14	-	-	0.75	0.14	0.76	0.11	0.75	0.14	0.79	0.06	0.76	0.12	0.77	0.10	0.77	0.10
147	54	0.79	0.06	0.81	0.01	0.79	0.06	0.80	0.03	0.79	0.05	-	-	0.79	0.06	0.80	0.02	0.80	0.02
163	70	0.79	0.04	0.80	0.02	0.80	0.03	0.80	0.03	0.80	0.03	-	-	0.79	0.05	-	-	-	-

Affected area																			
		Structural-related Indices														Chlorophyll-related Indices			
		GEMI		NDVI		EVI2		OSAVI		RDVI		RVI		EVI		GRVI		GCI	
DAS	DAE	*RStE*	R^2	*RStE*	R^2	*RStE*	R^2	*RStE*	R^2	*RStE*	R^2	*RStE*	R^2	*RStE*	R^2	*RStE*	R^2	*RStE*	R^2
51	-42	1.36	0.23	1.33	0.27	1.36	0.23	1.35	0.25	1.36	0.24	1.37	0.22	1.36	0.23	1.37	0.22	1.37	0.22
83	-10	-	-	-	-	-	-	-	-	-	-	-	-	-	-	-	-	-	-
99	6	-	-	-	-	-	-	-	-	-	-	-	-	-	-	-	-	-	-
131	38	-	-	-	-	-	-	-	-	-	-	-	-	-	-	-	-	-	-
147	54	-	-	-	-	-	-	-	-	-	-	-	-	-	-	-	-	-	-
163	70	-	-	1.50	0.07	-	-	-	-	-	-	1.50	0.07	-	-	1.51	0.05	1.51	0.05

RStE units = bales/ha. * Not significant (*p*-value > 0.05)

The indices related to canopy structure or chemical content were inadequate for prediction of yield at any point during the time analysed in this study regardless condition of the area: unaffected or affected. These results indicate that the changes within the plant and at the canopy level were not properly characterised by these indices and that the results were even more limited for individual multispectral bands (see Table 5-6).

5.4.3.2. Multivariate yield prediction models

The integration of all the multispectral bands considerably increased the prediction capabilities of the regression models. The variance explained (R_{cv}^2) by the resulting models varied from 0.05 to 0.21 in the unaffected area and from 0.13 to 0.61 in the affected area. On average, the R^2 was improved by more than 61% of the LRM outputs as well as the corresponding errors. The validation of model performance was based on the minimum estimated RMSEP, maximum R_p^2 and the close-to-one RMS Ratio (Mevik & Wehrens, 2007; Rapaport et al., 2015).

The higher variance explained by PLS-R model was due to the inherent principles of this method to take into consideration the information of the predictor and estimator variables in the definition of scores and loadings (Mevik & Wehrens, 2007; Wold et al., 2001) and it was also higher due to PLS-R takes all of the available bands to build the resulting models (Garrido Frenich et al., 1995; Mevik & Wehrens, 2007) instead of using a pair of bands as performed VIs.

The data acquisition date was important for accurate yield prediction and varied according to the area (i.e. affected or not affected) (Table 5-7). The estimated error (RMSECV = 0.74 bales/ha) for the unaffected area was on average, considerably smaller than in the affected area (RMSECV = 1.20 bales/ha). However, the variance explained (R_{cv}^2) in the affected area was much higher (on average by 0.22) than in the unaffected area (Table 5-7). The results show that PLS-R models were capable of explaining the yield variability within the field caused by 2,4-D. The time for data collection influenced the model performance and which also changed according to the area or whether the crop was in contact with the chemical or not. The best model cross-validation fit, in the unaffected area, was when the crop reached the point of boll development, so the vegetative growth was slow (131 DAS) (Figure 5-11). The relationship between RMSECV and RMSEP, measured by the close-to-one RMS ratio,

started to decrease (Table 5-7) after 131 DAS while increasing the error in the LOO-CV model (Figure 5-12).

The model performance was clearly different in the affected area: higher RMSEs and as consequence, higher Ratios (Table 5-7, Figure 5-12) but better explained variances (R^2). The best model fit with the lowest RMSECV and the highest R_{cv}^2 (0.96 bales/ha and 0.61, respectively) were reached just two weeks before harvesting (163 DAS and 70 DAE). However, the Ratio was still very high (Ratio = 1.27)

Table 5-7. PLS-R parameters for yield prediction modelling.

		Unaffected						Affected					
DAE	DAS	LV	R_{cv}^2	R_p^2	RMSECV	RMSEP	RMS	LV	R_{cv}^2	R_p^2	RMSECV	RMSEP	RMS
-42	**51**	2	0.05	-0.04	0.79	0.76	0.97	5	0.46	0.29	1.13	1.58	1.40
-10	**83**	3	0.11	-0.09	0.76	0.78	1.03	6	0.44	0.60	1.15	1.19	1.03
6	**99**	3	0.16	0.20	0.74	0.67	0.91	5	0.28	0.30	1.31	1.56	1.20
38	**131**	4	0.21	0.15	0.71	0.69	0.97	3	0.13	-0.05	1.43	1.92	1.34
54	**147**	2	0.15	0.22	0.74	0.66	0.89	4	0.25	0.17	1.33	1.71	1.28
70	**163**	3	0.20	0.32	0.72	0.62	0.86	3	0.61	0.58	0.96	1.22	1.27

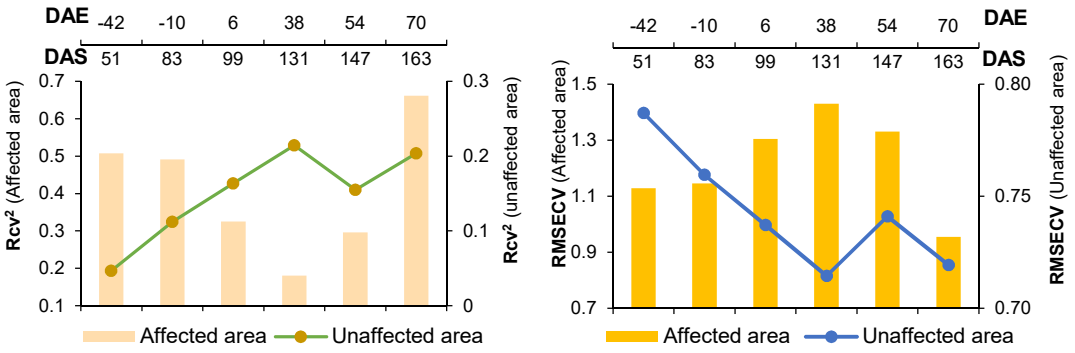

Figure 5-11. Cross-validation model parameters for the unaffected and affected area: RMSECV and R_{cv}^2. Different scales are presented to facilitate result's interpretations (points of minima and maxima per area).

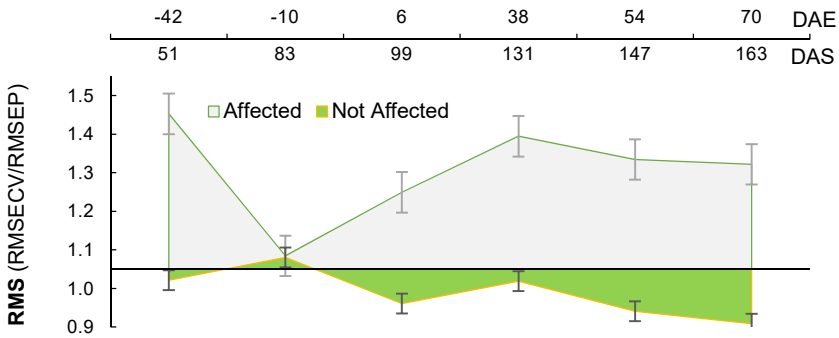

Figure 5-12. Ratio (RMSECV/RMSEP) for unaffected and affected areas.

The plant's response to 2,4-D can be interpreted based on the results of PLS-R models (see Table 5-7, Figure 5-11 and Figure 5-12). There was a drastic and incremental drop in the model performance soon after exposure until 38 DAE when the RMSECV and R_{cv}^2 changed by more than 24% and nearly 30%, respectively. The model performance started to improve significantly after this time. This curve suggests that the greatest plant damage was within the first 38 DAE after which the recovery and regrowth stage started. The model performance improved at 54 DAE by increasing the R_{cv}^2 and reducing the RMSECV, reaching the maximum point of performance at 70 DAE (RMSECV = 0.96 bales/ha and R_{cv}^2 = 0.61).

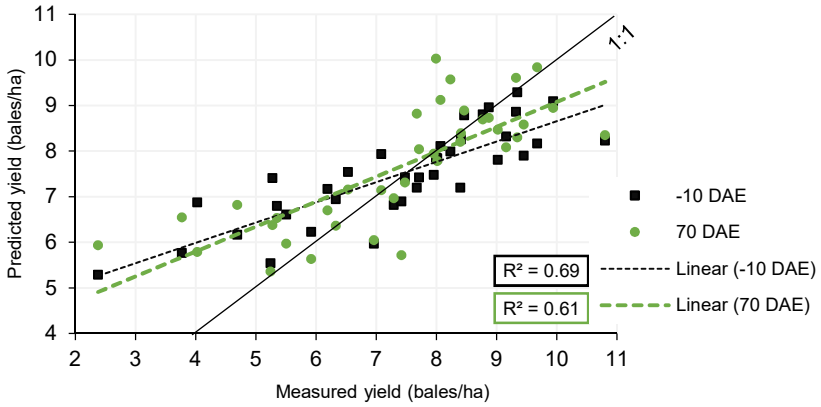

Figure 5-13. Validation performance of the best PLS-R models with test dataset in the affected area.

The validation process was carried out implementing the test dataset, which was randomly selected and extracted from each area (i.e. unaffected or affected) before modelling. Samples from each area were predicted with each model and compared against the measured yield (data not presented for the unaffected area). Parameters from the test set predictions, such as the R^2 of the prediction (R_p^2), RMSEP and RMS Ratio were estimated. Prediction parameters in both areas performed similarly to cross-validation parameters. The highest RMSEP (0.69 bales/ha) and one of the best relationships between RMSEP and RMSECV (RMS Ratio = 0.97) were reached at 131 DAS for the unaffected area (Figure 5-12). The affected area yielded the best prediction parameters (i.e. highest R_p^2, lowest RMSEP values and a close-to-one RMS ratio values) at 70 DAE and -10 DAE. The best validation fit (R^2 = 0.69) (Figure 5-13) occurred with the data acquired just before the exposure (-10 DAE and 83 DAS), followed by data collected 70 DAE (R^2 = 0.61). These validation results: a) ratify the

results from the calibration process, b) support the selection of optimal LVs, and c) provide information regarding the applicability and stability of the models.

5.5. Discussion

5.5.1. Temporal variability of multispectral bands and vegetation indices in relation to exposure area

Cotton crops, in optimal conditions, reach the peak bloom around 90 DAS and the maximum reflectance response can be found within the next 30 days (Yang et al., 2002). Furthermore, there is a reduction in pigment concentrations as the plants focus their development in reproductive growth (boll production) rather than vegetative growth (CottonInfo, 2016). The trend in the spectral response of the visible bands in the unaffected area was then expected to occur (i.e. reflectance increment after 99 DAS) as well as the peak of vegetation indices values and particularly GCI, GRVI and RVI (Zarco-Tejada et al., 2005). On the other hand, the lower reflectance in affected areas after 99 DAS (i.e. 6 DAE) and the lack of variability of the VIs after this time indicates a delay in reproductive growth, and a small variability in pigment contents indicating a lower rate of boll development.

The highest reflectance difference between the unaffected and affected area in the visible region at 70 DAE (Figure 5-8) was a consequence of a standard defoliation practice to remove the leaves from the plants. Defoliation was carried out prior to harvesting in both areas, but the defoliation rate in the unaffected area was higher due to an optimal and uniform maturity of the crop, and hence the affected area looked greener at harvesting. This situation was suggested by the green reflectance pattern in the affected area, which absorbed always more energy due to a greener appearance. This study did not provide lint quality records of the harvested yield, however, the high amount of leaves still in the plant, after the chemical defoliation in the affected area, (Figure 5-6) could potentially affect the quality of the colour reflectance and the trash content of the fibre harvested (Sluijs et al., 2015).

The NIR band, which is associated with canopy structural properties and leaf internal structure by several research studies (Huang & Thomson, 2010; Li et al., 2001), exhibited changes during the first 38 days after the exposure to the chemical (Figure 5-8). After this period, the NIR reflectance of both areas became similar. The rate of

change in the unaffected area was higher in comparison with the affected area. This could be explained by the difference in growing stages, as the affected area had delayed growth compared to the unaffected area (Everitt & Keeling, 2009). Both areas had similar structural patterns at 147 DAS (i.e. around a month before harvest), but with different pigment concentrations, as suggested by the reflectance changes in the green (Figure 5-8) and red channels. This observation is supported by the changes in plant morphology, as the unaffected area showed bolls opened, and the affected area looked greener.

The relationships between yield, VIS and NIR, that is, the high correlation with NIR and the low correlation with VIS, in the unaffected area indicate that the green biomass is a determining factor compared to nutrient content. On the other hand, in the affected area, there was no indication that green biomass had any influence over yield, while nutrients played a major role, as indicated by the higher correlation of VIS in comparison with the NIR band.

The reflectance at SWIR1 and SWIR2 bands started to vary as soon after the incident as shown in Figure 5-8 and Appendix 5-1. The variability in the SWIR needs to be contrasted with the NIR band since leaf or canopy structure also influence the SWIR reflectance (Gao, 1996; Yilmaz et al., 2008). This can also be evidenced by the moderate correlations between NIR and SWIR bands in this study. The reflectance similarities before the incident indicated similar soil conditions and crop status in both areas, affected and unaffected. The reflectance variability after the exposure could, therefore, be explained as being due to the changes in the canopy density, water-related properties or leaf area index (LAI) (Ceccato et al., 2002; Hunt & Rock, 1989; Tucker, 1979).

High reflectance at the SWIR1 band was associated with high-density canopies while low-density canopies were related to lower SWIR1 reflectance in a study developed by Khanna et al. (2007). Wang et al. (2008) demonstrated that reflectance at 1640 nm and 2130 nm decreased as the LAI increased from 0.01 up to 1 regardless surface soil moisture and Liu et al. (2015) demonstrated that all water-related properties such as the vertical distribution of gravimetric water content (GWC), relative water content (RWC), and equivalent water thickness (EWT) were highly and negatively correlated with reflectance of the SWIR region particularly around 1510 nm. The canopy density

in this study started to decrease after exposure according to the reflectance decrement in the SWIR band in the affected area, while the LAI tended to remain constant with slight variabilities. LAI in the unaffected area was expected to decrease after the crop reached the maximum maturity stage at 131 DAS and the vegetative growth started to decline, hence the reflectance in the SWIR increased through time (Quinn & Kelly, 2011; Wang et al., 2008). The 2,4-D-injured area demanded more water for a longer period in comparison with the unaffected area. The peak for water demand in cotton crops under optimal conditions coincides with the early reproductive period (The Australian Cotton Industry Development & Delivery Team, 2013) which can explain the constant drop of the reflectance until 131 DAS in the unaffected area (Liu et al., 2015). The water demand in the injured area was prolonged since the crop development rate lessened (Figure 5-8).

VIs did not manifest a distinctive and clear response due to the effects of 2,4-D in the cotton canopy. Neither the structural-related or chlorophyll-related indices were able to show a relationship between them and yield after contact with the herbicide. In fact, none of the VIs exhibited major variability after the incident for nearly 50 days (Figure 5-9). This situation can be explained by the significant damage caused by 2,4-D to the crop and by the recovery capabilities of the cotton plants through time (Everitt & Keeling, 2009; Suarez et al., 2016). The temporal dynamics of the canopy structure and pigment content at 51 DAS exhibited the highest relationship between harvested yield and VIs (Figure 5-10). However, at this time, the crop was in the middle of squaring and it had not yet reached the peak of nodal development (Oosterhuis & Kerby, 2008).

Studies have shown that cell structure-related indices such as NDVI, RDVI and OSAVI performed well for the detection of cotton yield variability within the field in normal growing conditions (Zarco-Tejada et al., 2005). Zhao, Reddy, et al. (2007) also demonstrated significant correlations between VIs and relative lint yield between 60 and 70 DAS. Contrary to those findings, we found that neither the cell structure-related band (NIR) nor the vegetation indices manifested strong correlations with yield, regardless of whether the area had herbicide damage or not. The correlation shape and peaks were different between the damaged and undamaged areas, as the crop development was dissimilar and at different rates. In particular, the area affected by

2,4-D never reached an optimal vegetative and fruit development stage, and yield was therefore considerably reduced.

5.5.2. Performance of statistical models for crop yield estimation

This study encountered serious limitations when applying VIs derived from Landsat 8-OLI as predictors of yield. Linear regression models are often implemented when applying VIs as predictors of yield, with promising results (Yang et al., 2004; Zhao, Reddy, et al., 2007). However, the VIs, tested in this study, were not able to accurately predict yield with two to three spectral bands.

The damage caused by 2,4-D affected the new foliage (i.e. top-new leaves after the incident) where the upper canopy looked seriously damaged while the middle-lower canopy appeared unaffected. The plants did not grow much after the exposure and the damaged leaves (top-canopy leaves and new leaves) were a few at canopy level (i.e. upper canopy). Due to the architectural arrangement of the canopy, the moderate spatial resolution of the satellite data impacted the prediction capability of vegetation indices and individual bands, positioned in the visible and the NIR ranges. The methods of successful examples where VIs were implemented as predictors included hyperspectral data at a low distance from the canopy or high-resolution imagery (Liu et al., 2015; Yang et al., 2004), which could discriminate the architectural arrangement of the canopy at different growing conditions. Although the resampling method of the yield monitor records could affect the prediction error, Yang et al. (2009) demonstrated that when the pixel size increases from 10 m to 30 m, the R^2–values increase when predicting yield from yield monitor records. Furthermore, the strong and significant correlations ($r > 0.99$ and p-value ≤ 0.05) between the resulting yield maps and the original dataset (yield monitor records) reduce the probabilities of exaggerating the prediction error due to the resampling method.

PLS-R models performed better than multispectral bands or VIs regardless the area. The better fit of the models can be attributed to the inclusion of all the multispectral bands irrespective of multicollinearity between them, which is one of the main advantages of this statistical approach (Garrido Frenich et al., 1995; Mevik & Wehrens, 2007). These results agreed with other studies where PLS-R was the best statistical approach when VIs were insufficient to optimise prediction capabilities of variables such as carotenoids, nitrogen and yield (Bronson et al., 2005; Rapaport et al.,

2015; Yi et al., 2014). The integration of all the multispectral bands resolved the limitation of the 30-m spatial resolution of Landsat imagery by increasing the R^2 and reducing the RMSE.

This study demonstrated that the recovery capabilities of the crop after exposure to the chemical strongly influenced the fit performance of the PLS-R models, highlighting the influence of the spatial resolution and the days after the exposure. The best prediction performance was around the date of exposure (-10 DAE or 6 DAE) or when the plants stabilised the internal mechanism in response to the contamination (70 DAE). This result agrees with previous studies, where 7 DAE proved to be the best time for collection data purposes when cotton has been exposed to 2,4-D (Suarez et al., 2016). The temporal variability in the accuracy of the model in the unaffected area agreed with other studies where the importance of growth stage for the prediction performance was demonstrated (Zarco-Tejada et al., 2005; Zhao, Reddy, et al., 2007).

5.6. Summary

The methodology implemented in this study has demonstrated the capabilities of remote sensing data in providing an alternative method to address the limitations of traditional (visual) assessment of herbicide drift in cotton crops. It has also shown that the integration of all multispectral bands from Landsat-8 OLI is a powerful approach to minimise the potential limitations of Landsat's moderate spatial resolution imagery in the prediction of yield. This study has provided an understanding of the temporal implications of cotton yield assessment in areas of optimal growth conditions and in those affected by herbicide drift.

The results indicate that the relationship between yield prediction and satellite data depends on the days after sowing (for those areas not affected by the chemical) and days after exposure (for affected areas), with the best results obtained for 131 DAS and 70 DAE, respectively. Individual bands or vegetation indices had a poor performance for predicting yield after herbicide drift. However, they were useful for understanding the main factors driving yield under stressed and optimal growing conditions, that is biochemical and biophysical conditions, respectively.

Partial least squares regression (PLS-R) models performed better, as they increased the explained variance by more than 60%, on average. The time of imagery acquisition

was a key determinant in maximising the prediction capabilities of the models for both unaffected and affected area. Prediction capabilities in the unaffected area were maximised when data from 131 DAS was implemented (RMSECV = 0.71 bales/ha). The best time for prediction purposes in the affected area was at 70 DAE (163 DAS) with a prediction error of 0.96 bales/ha and a validated R^2 of 0.61. The second best date in the affected area was just before the incident at -10 DAE with a prediction error of 1.15 Bales/ha and a validated R^2 of 0.69.

The defoliation rate in the 2,4-D-injured area was reduced by the delay in the growing stage of the crop, causing more green leaves in the plant at the harvesting time. This situation can potentially affect the quality of the fibre harvested when mechanical harvesting is employed. It is therefore important that future studies assess fibre quality, to identify if there is a significant impact of the green leaves still on the plant on the colour reflectance and trash content of the fibre harvested.

Results have demonstrated the utility of remote sensing data in the prediction of yield loss caused by 2,4-D non-target spray in cotton crops. The advantage of accurately predicting the degree of damage and spatial location of potential yield loss will provide valuable information to farmers and consultants for the adjustment of mitigation plans. The localization and assessment of damage may provide direction in finding the potential source areas or responsible party. Further studies could focus on the use of higher spatial and temporal resolution imagery, including the use of airborne hyperspectral sensors, to further assess their capabilities in crop damage detection and yield prediction.

Chapter 6

ASSESSMENT OF HERBICIDE DRIFT DAMAGE ON COTTON CROPS USING TERRESTRIAL LASER SCANNER

6.1. Introduction

This chapter explores the utility of terrestrial laser scanners (TLS) in the detection of canopy structure variability caused by 2,4-dichlorophenoxyacetic acid (2,4-D) herbicide drift on cotton crops. Temporal changes to the canopy were tested based on the timing of exposure (S) and the dose (D) of the chemical in contact with the crop. Effects at two phenological stages or times of exposure were then analysed using three doses of the recommended commercial label rate as spray applications. Scan measurements took place after three different periods of exposure: a) two days (2 DAE), b) seven days (7 DAE) and c) 14 days (14 DAE).

The aim of this research was to test whether the TLS field measurements are capable of characterising the temporal changes in the 2,4-D-injured cotton canopy structure. Three specific objectives were defined:

i) to determine the limitations of TLS for assessing canopy structure variability;

ii) to provide a comprehensive approach for the estimation of cotton canopy height and canopy volume;

iii) to assess the capabilities of TLS-derived data for the provision of spatial-temporal canopy structure after simulated spray drifts onto cotton crops.

A discussion of the current applicability of terrestrial laser scanning in agriculture is presented in Section 6.2 while the methods used in this study are described in Section 6.3. In this section, detailed information about the instrument and statistical analyses implemented in this study are presented. Results are analysed in Section 6.4, and the main findings in relation to previous research studies are discussed in Section 6.5. A summary of the suitability of this technology as a possible tool for the estimation of

canopy structure variables in cotton crops affected by 2,4-D herbicide drift is presented in Section 6.6.

6.2. LiDAR scanners as a tool for herbicide damage assessment

The principal idea behind crop monitoring is to accurately estimate and/or improve crop yield. Plant height is a plant growth indicator that is related to yield (Confalonieri et al., 2011; Zub et al., 2011). This factor, when combined with other variables (Muharam et al., 2014), such as spectral reflectance of the crops or the surrogate vegetation indices, increases its relationship with yield (Huang et al., 2015; Thenkabail et al., 2000; Zarco-Tejada et al., 2005). Canopy characterisation is also important for best management practices, where, for example, the optimisation of pesticide application and nutrient content might be highly dependent on this characterisation. Structural characterisation of plants has, additionally, a significant scientific value due to its influence in different biophysical processes, including photosynthesis, CO_2 sequestration, and evapotranspiration (Rosell et al., 2009; Zheng & Moskal, 2012). However, under stress conditions, estimations of crop growth are often inaccurate (Clevers, 1999).

Spray drifts typically expose crops to stress due to their susceptibility to the chemical in contact (Suarez et al., 2016), forcing the plant's growth to be interrupted as the plant tries to recover from the stress, thus impacting on the harvested yield. During the recovery process, several internal changes within the plants can occur, limiting the correct and precise assessment of damage (Everitt & Keeling, 2009; Henry et al., 2004). The broad aim of this research was to provide reliable proximal and remote sensing techniques for the assessment of 2,4-D herbicide drift in cotton crops. In this chapter, a Terrestrial Light Detection and Ranging Sensor (LiDAR or TLS) was evaluated to meet this objective.

TLSs provide a unique opportunity to characterise plant growth and to analyse diverse architectural parameters as potentially good indicators of crop performance (Friedli et al., 2016), due to the highly detailed information provided by these devices. The point clouds resulting from the scans can be integrated and analysed to extract important characteristics of the canopy such as plant growth, biomass and leaf area index (LAI)

that are highly related to crop status and health (Hämmerle, 2013; Rosell et al., 2009; Tilly et al., 2014). These characteristics can also provide a sensitive indicator of responses to stress and adaptation of plants to their environment (Omasa et al., 2007), especially because crops and vegetables grow fast, so the growth rate is a sensitive and direct indicator of stress. Stem heights of a harvest-ready crop of *Miscanthus giganteus* were calculated by applying dynamic and static approaches with accuracies higher than 92% (Zhang & Grift, 2012).

In another study, Tilly et al. (2014) demonstrated the advantages of TLS for deriving plant height and posterior estimations of biomass. The accuracy of the scan data was tested by correlations between TLS-derived and manual plant height measurements ($R^2 = 0.91$) and by regressing biomass measurements from the field with the calculated plant height ($R^2 = 0.86$). The transferability of the data was tested, correlating the measured against the estimated biomass samples ($R^2 = 0.90$). Architecture differences between maize, soybean and wheat genotypes were tested in a study conducted by Friedli et al. (2016), where it was also possible to determine the temporal variability of the canopy and the maximum temporal resolution for each crop.

Rosell Polo et al. (2009) demonstrated the applicability of LiDAR system and concluded that it is possible to measure geometric characteristics of plants with sufficient precision for most agriculture applications ($R^2 > 0.80$). LiDAR-derived volume was highly correlated with manual volume measurements and total foliage tree area of pear trees (regression coefficient = 0.97 and 0.84, respectively). One of the main limitations of LiDAR is a significative large amount of data to be processed. Hämmerle (2013) explored the implication of reduced scanning resolutions and found that reducing the resolution to 25% still produced a coverage area of greater than 90% and mean canopy elevation greater than 96% accuracy with respect of measured crop height.

The most common LiDAR or TLS sensors calculate the distance to the object with either a) the time-of-flight technique (TOF) or b) phase-shift method (PSM) (Figure 6-1). The first method calculates the distance to the object by measuring the time between the transmitting and receiving laser signal (Tilly et al., 2014; Zhang & Grift, 2012). The second method calculates the distance by analysing the shift in the phase of the returning beam (FARO®, 2009; Friedli et al., 2016). The main trade-offs

between the systems are i) speed of acquisition and ii) dynamic range. The PSM sensors provide a more detailed coverage in shorter time, as they do 100,000's of points per second with the TOF doing 10-100 times fewer points in the same timeframe. However, TOFs are ideal when the ranges of measurement are long, as they can reach a target up to one kilometre away from the scanner, while the PSM sensors allow a maximum distance of a hundred meters (San José Alonso et al., 2011). Regardless the method implemented, TLS have demonstrated their significant impact on canopy structure estimations.

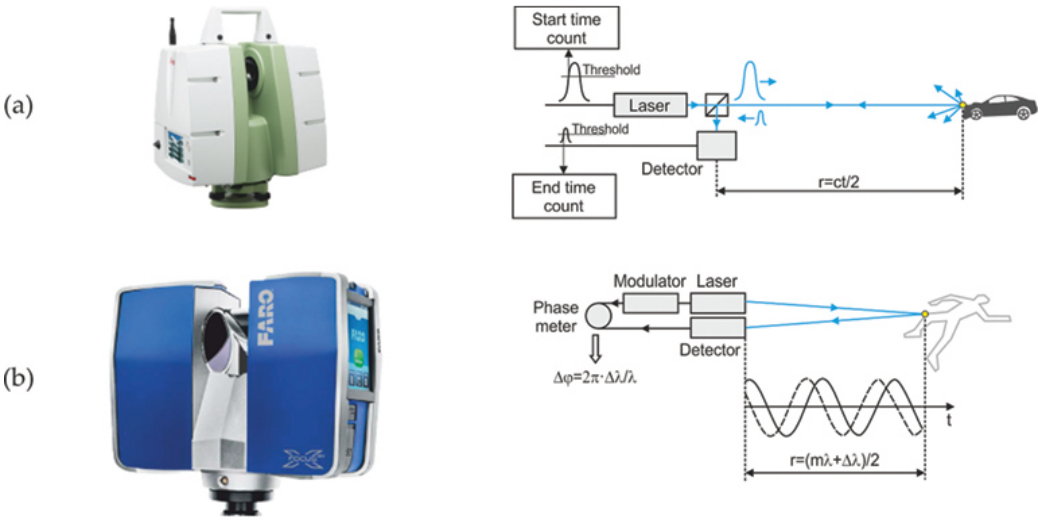

Figure 6-1. The time-of-flight (TOF) and phase-shift (PSM) principles for calculating the distance to an object.
Adapted by the author. *Source*: (Rodríguez-Gonzálvez et al., 2016)

6.3. Methods

The following sections describe the procedures used to process and analyse the terrestrial laser scanner (TLS) data collected from the trial layout explained in section 6.3.1. Four main steps undertaken to collect data include: 1) data registry; 2) edition and terrain surface generation; 3) height and volume calculations and 4) statistical analysis. Each of these steps was explained in more detail in the following sections. The methods differed based on the objective of a) calculating canopy height and b) calculating canopy volume. Figure 6-2 shows the main steps implemented in this study and each of them is described in detail in the following sections.

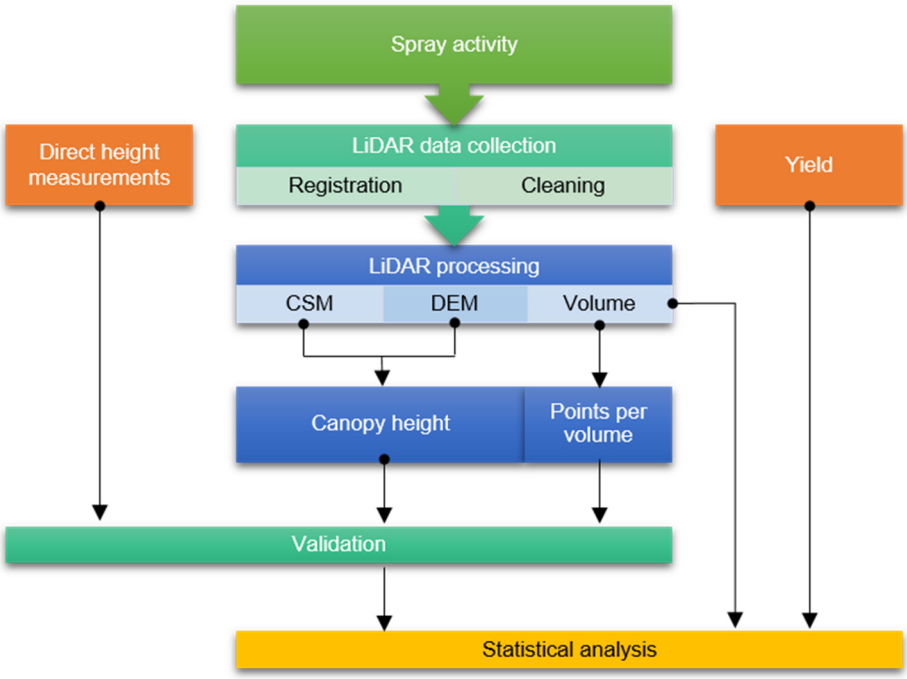

Figure 6-2. Flowchart of the main LiDAR processing steps.

6.3.1. Experimental design

The capabilities of TLSs for identifying the differences in canopy height and volume caused by simulated 2,4-D herbicide drift in cotton crops were tested as a subset of the experimental design in the controlled sub-study explained previously in Chapter 3 and 4, and reported in Suarez et al. (2016) and Suarez et al. (2017). The scanning process was undertaken only in replication four (R4) of the controlled sub-study (Figure 6-3). Six treatments corresponding to a factorial combination of two times of exposure (4-5 nodes - S1 and 7-8 nodes - S2) and three doses (Nil - D0, 5% - D1 and 50% - D2) were analysed (Table 6-1). Treatments sprayed at S1 were scanned on the 27th November and the 4th December 2014 (S1-7DAE and S1-14DAE), while treatments sprayed at S2 were scanned once on the 4th December 2014 (S2 2DAE).

Table 6-1. Factorial arrangement of scanned treatments

Timing of exposure		Dose
S1 S2	X	0% - D0 5% - D1 50% - D2

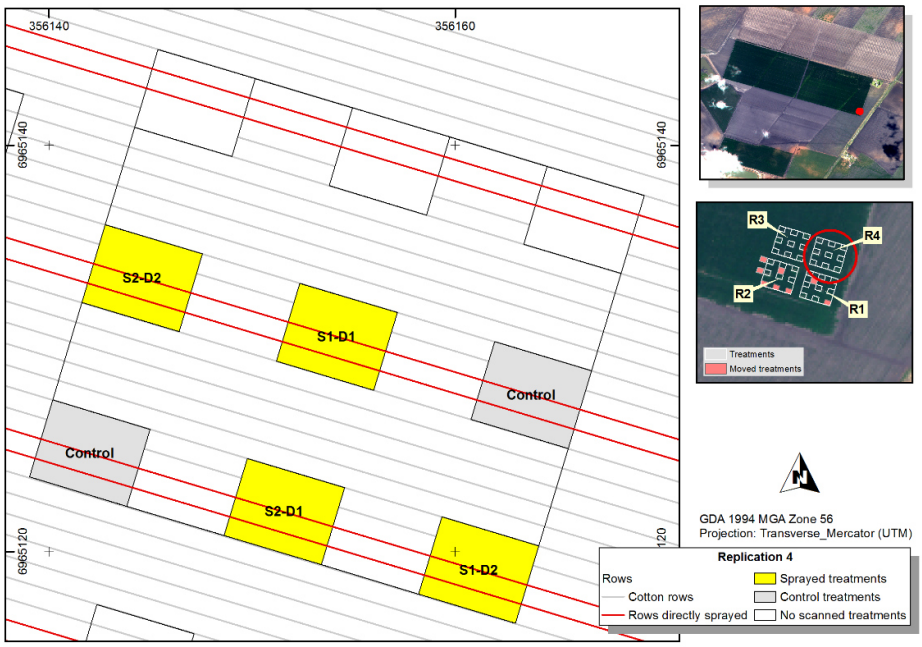

Figure 6-3. Experimental design. Replication 4 of the controlled sub-study.

6.3.2. LiDAR capture

In this study, a high-speed three-dimensional Focus3D laser scanner (Faro Technologies Inc., Lake Mary, USA) was used. The unit emits a laser beam (wavelength of 905 nm) towards the object at a fixed frequency or phase. Once the beam reaches the object, the infrared light is reflected back to the scanner at a different phase. The distance to the object is then accurately determined based on the phase-shift method (FARO®, 2011; San José Alonso et al., 2011). The distance, the vertical and the horizontal angles are encoded as polar coordinates (δ, α, β) and transformed to Cartesian coordinates (x, y, z) (FARO®, 2011).

To minimise the potential occlusion of plants or leaves by those closer to the scanner, it is imperative to combine scanning points from different view angles (Hilker et al., 2010). Five elevated scan stations were therefore established around the area of interest, that is, replication 4, where the instrument was mounted on a fixed tripod. For each scan location, the scanner height (from the ground to the instrument) varied (Figure 6-4).

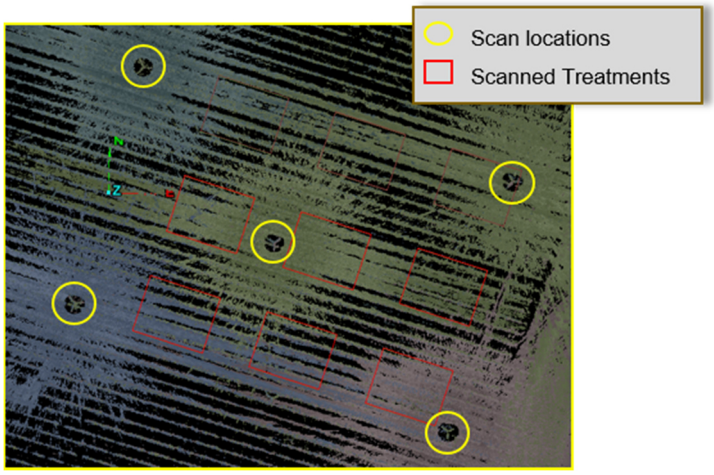

Figure 6-4. Distribution of scan locations in the scanned treatments.

The scan stations were georeferenced by the Real-time Kinematic (RTK) surveying process (a static survey process) of 15 minute static sessions to reach accurate points at the sub-centimetre level in both the X and Y positions. A minimum of four artificial reference spheres was also used prior to data collection, to establish the relative orientation between the individual scans (Hilker et al., 2010) (Figure 6-5). The quality of registration of multiple scans depends on the visibility and the spatial distribution of the spheres (FARO®, 2011). During each field session, the location of the white spheres was randomly selected at different heights, always forming an irregular polygon with unobstructed visibility. LiDAR data was collected at the centre and the four corners of replication 4 (25 x 25 m) with a scan resolution of 122,000 pts/sec (Figure 6-4 and Figure 6-6).

Figure 6-5. Northern-east scan location with white spheres around replication 4.

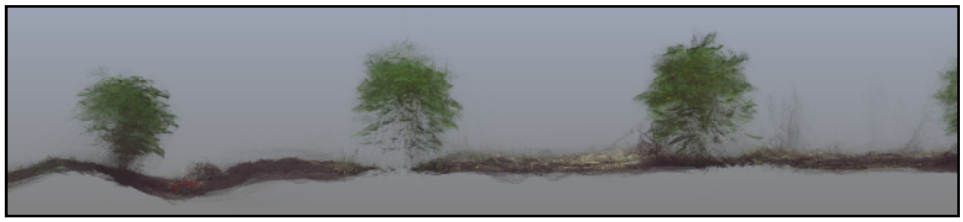

Figure 6-6. First field campaign. Frontal view of a treatment.

The treatments were scanned once or twice after the spray activity, according to the timing of exposure: a) for S1, the scan activity was performed at 7 and 14 DAE and; b) for S2, the treatments were scanned at 2 DAE. Further direct height measurements were also carried out on two randomly selected plants per treatment for S1 14DAE and S2 2DAE.

The analysis was undertaken to estimate: a) canopy height and b) canopy volume of each treatment. For both procedures, it is necessary to have a reference surface or digital elevation model (DEM) in order to remove height variability associated with the terrain conditions. The DEM was generated from scanning the experimental area with very little or no vegetation. The concept of a crop surface model (CSM)

introduced by Hoffmeister et al. (2010) (Figure 6-7) was applied to estimate the canopy height. The difference between the CSM and the DEM permits the canopy height estimation. The DEM was calculated from the scanning points acquired on the 27th November 2014, following the procedure described below (Section 6.3.2.1). The DEM was the reference surface implemented to calculate canopy height at 2, 7, and 14 DAE. The CSMs were generated for each treatment and DAE on the 27th November 2014 and 4th December (Table 6-2).

Table 6-2. Scanning dates and the corresponding scanned treatment

Date of data collection	Timing of exposure	Days after exposure	Dose
27th December 2014	S1	7 DAE	D0, D1, D2
4th December 2014	S1	14 DAE	D0, D1, D2
4th December 2014	S2	2 DAE	D0, D1, D2

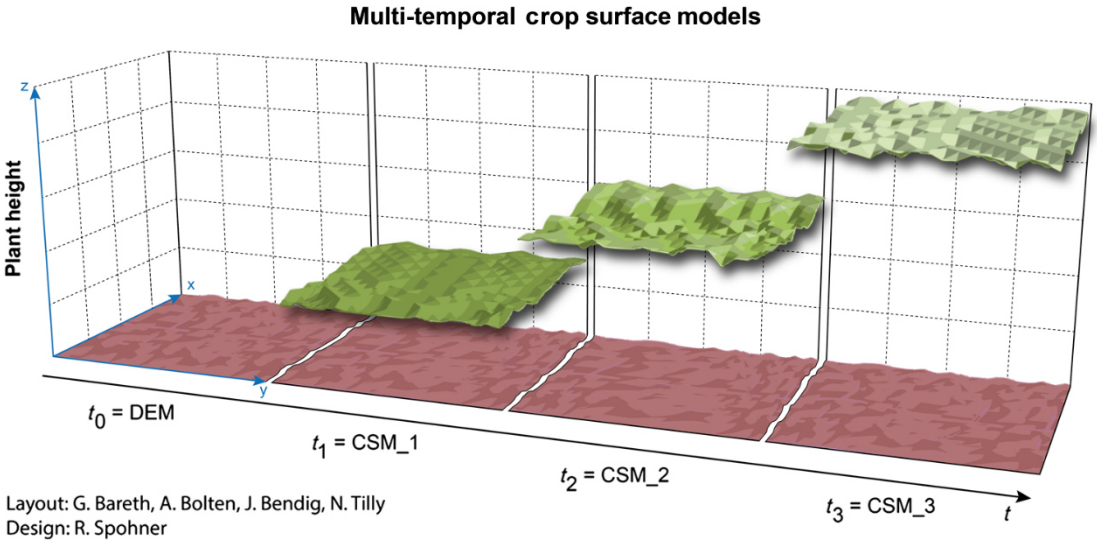

Figure 6-7. Theoretical concept of crop surface modelling (CSM).
Source: (Bendig et al., 2013).

Canopy volume, as well as the canopy height, was estimated per treated line and the lines were then aggregated by treatment and days after exposure. The volume was calculated applying the loop wrap and loop triangulation algorithms available in Maptek (Maptek™ I-Site™ Studio, 2015). The "loop function" concepts are visualised in Figure 6-8. The loop wrap function creates a polygon through a selected number of points, evenly spaced around the centre of a predetermined loop spacing, while the loop wrap triangulation algorithm creates a surface between two or more

polygons (i.e. polygons created using loop wrap function) (Maptek™ I-Site™ Studio, 2015).

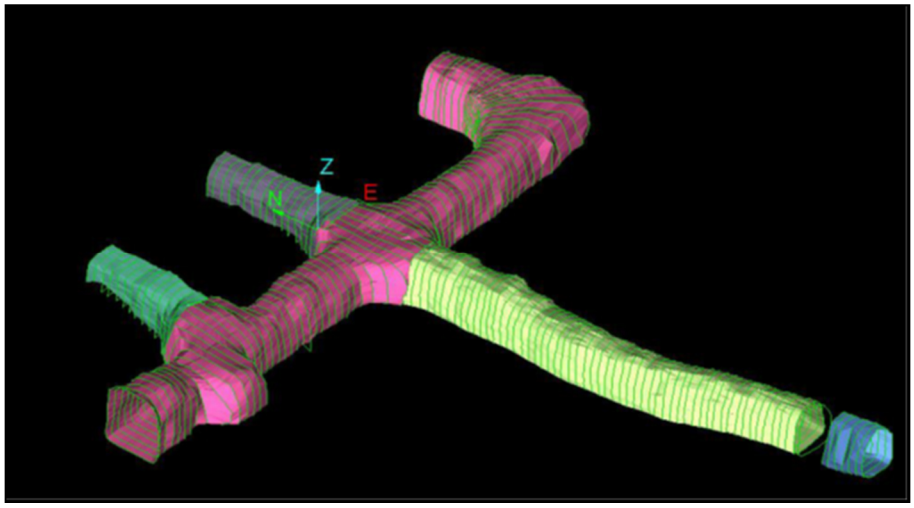

Figure 6-8. A conceptual explanation of loop functions with green lines defining loop polygons and coloured areas representing the resulting surfaces.
Source: (Maptek™ I-Site™ Studio, 2015)

The first steps, involving the geo-referencing, registration and merging of the point clouds resulting from each scan station and scan date, were executed in SCENE Software v5.2. This package is a comprehensive 3D point cloud processing and managing software tool developed by ©*FARO Technologies Inc*. A project was created in MAPTEK I-Site v6.0 (developed by *Maptek™*) where the point cloud for each DAE was imported for further analysis of volume and canopy height. Spatial analyses were conducted in ArcGIS v10.3.1 (developed by *ESRI*), and the statistical analysis was performed in R software v3.3 (developed by *R Core Team*). The general workflow for the post-processing of the TLS data is shown in Figure 6-9, with more details provided below.

Figure 6-9. Overview of the workflow for the processing and analysis of the terrestrial laser scanning data.

Initially, the scanning data was imported from the scanner to SCENE and a pre-processing activity was undertaken to a) cleaning disturbing scan points and unwanted scan points representing external objects such as vehicles, other instruments and sticks; b) identifying objects in the scans and creating reference objects for scan registration, such as the white reference spheres, and c) adding colour to the point cloud to facilitate the interpretation of the scanning points.

Following the pre-processing, the scan points were registered, applying the artificial white spheres scanned at each field day. The cloud points from each respective date were then created and exported for further analysis in Maptek, where the analysis was undertaken for each treatment at each date.

6.3.2.1. Creating the terrain surface or digital elevation model (DEM)

An iterative process integrating topography and proximity filters, and a topographic triangulation model, were implemented in order to create a precise terrain surface shown schematically in Figure 6-10. A topography filter divides the point cloud into a horizontal grid with a specific cell size, where the lowest or highest point in the cell is retained. The terrain surface was initially created searching for the lowest point in a 0.5 m cell size. The resulting filtered points were used to create an initial base surface by applying a topographic triangulation model. After restoring the initial filtering, a proximity filter was applied. This filter is recommended when a base surface is available from which the proximity rule is applied.

The first proximity range was defined as 0.05 m with the initial base surface as the reference surface. From this selection, a topography filter with a smaller cell size equivalent to 0.1 m was run. The resulting points were used to create a more accurate terrain surface from which the filtering process was repeated several times with variable search radio and cell size. The distance between the lowest points and the surface was assessed by looking for the best-adjusted surface to the points in a transversal section view and after each preliminary terrain estimate. The whole process was repeated if the surface was not well adjusted to the points, i.e. a gap between points and the terrain surface was evident. The final terrain surface was generated with a proximity filter of 0.02 m and a topography filter of 0.05 m.

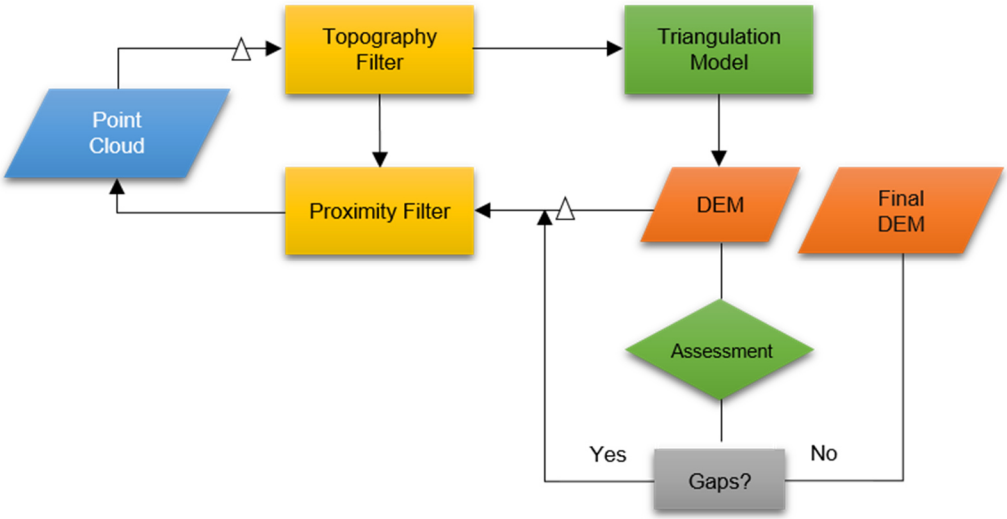

Figure 6-10. Iterative process for terrain surface modelling.

6.3.2.2. Creating crop surface models (CSM) and calculating canopy height

The canopy surfaces equivalent to the crop surface model (CSM) described by Tilly et al. (2014) were calculated after the final DEM was generated. A difference surface was subsequently calculated to measure the height of the canopy. The procedure to create the CSMs in Maptek is similar to the DEMs, the difference between the two procedures is the selection of the top points for CSM in Maptek, rather than the lower points, as for the DEM.

Due to the nature of the cotton canopy (i.e. triangular canopy structure), the area delimited by the top points is smaller than the area of the middle canopy (Figure 6-11). The canopy volume could therefore not be calculated using the same CSM as that related to the top canopy, hence a new method was proposed -loop wrap function. This function creates polygons (loop-wrap polygons) that tend to define the external shape of the canopy rather than just the top of the canopy. The CSM files and the DEM were exported from Maptek into ArcGIS once the CSMs of all treatments were finalised.

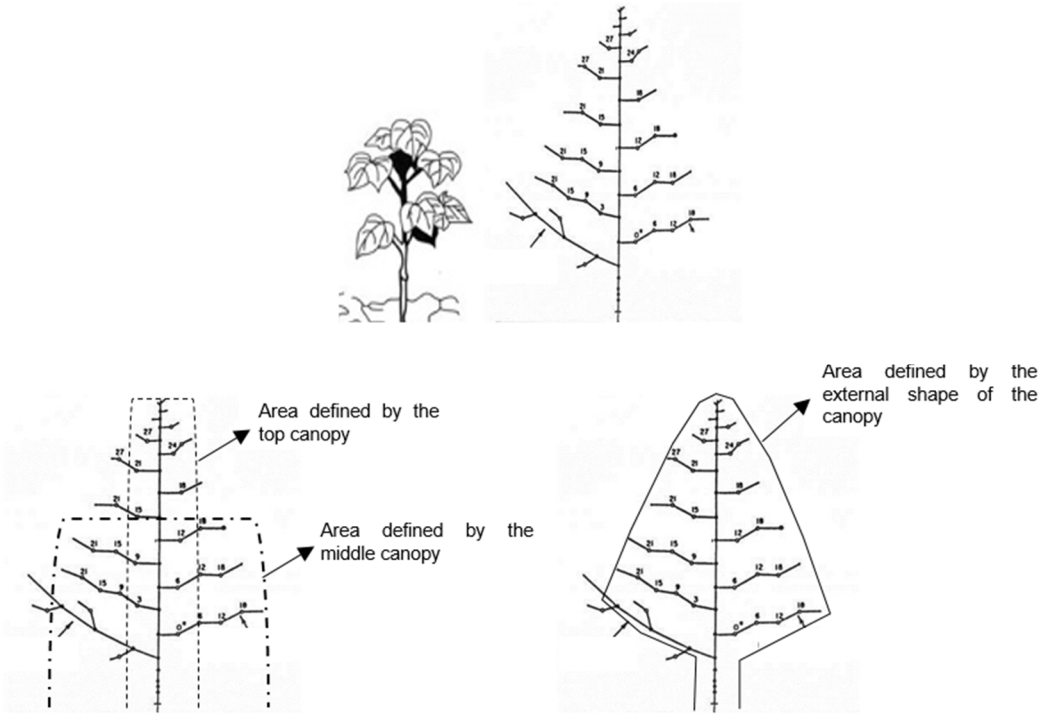

Figure 6-11. Theoretical cotton canopy structure and implications of volume estimation at different canopy positions.
Adapted by the author. *Source*: (National Cotton Council of America, 2013a; Oosterhuis, 1990).

The imported files representing the DEM and CSMs of each treatment were converted to a triangulated set of vertices which are connected with a series of edges to form a triangulated irregular network (TIN) surfaces (ESRI, 2016) with a maximum edge length between 0.5 m and 0.3 m in ArcGIS. The canopy height was then calculated, applying the Surface Distance tool available in the Triangulated Surface toolset from the 3D Analyst tool. The resulting rasters of 0.001 m pixel size contained the height of the canopy, which was exported as ASCII files to be analysed in R (Figure 6-12).

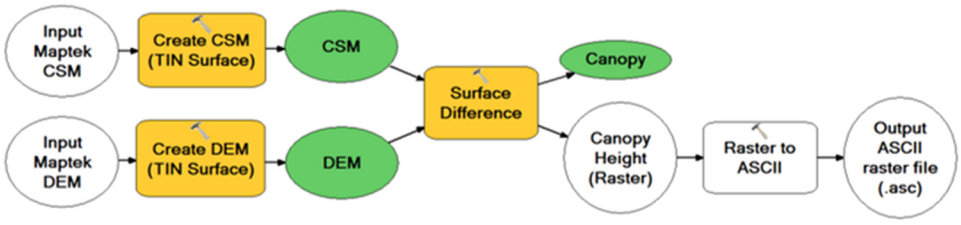

Figure 6-12. Flowchart for the calculation of canopy height in ArcGIS.

6.3.2.3. Creating canopy volume

Loop wrap polygons were generated delimiting the shape of the crop canopy with distances between 0.5 m and 1 m, prior to the loop triangulation, with between 50 and

72 points per loop, and a loop spacing between 0.005 m and 0.25 m. (Figure 6-13). Individual loop polygons were analysed implementing a transversal view. Incorrectly formed loops were edited in this view, removing invalid points or points that were outside the canopy shape. Some lines of the resulting polygons were projected into the DEM to get a more realistic transversal shape.

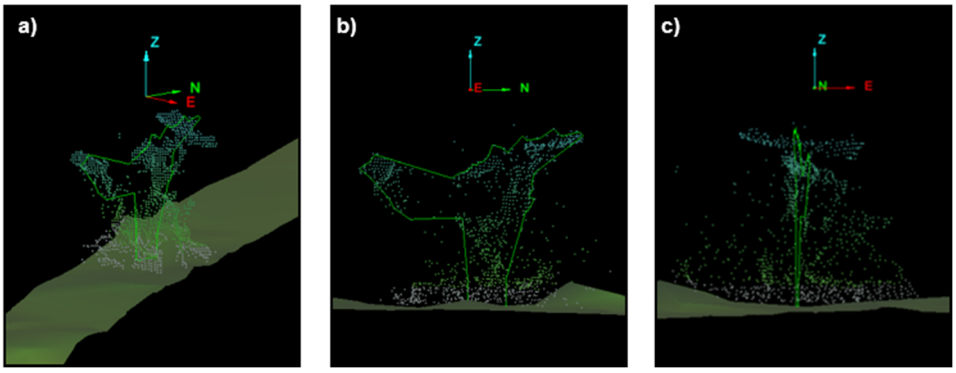

Figure 6-13. Loop wrap polygon in a section view of 0.15 m.
a) XYZ; b) YZ; c) ZX

6.3.3. Statistical analysis

Statistical analyses were performed to identify differences in 1) the canopy height and 2) the canopy volume, within each group influenced by dose (i.e. D0, D1 and D2). The previous variables were grouped by the timing of exposure (i.e. S1 or S2) and days after exposure (DAE). Each of the resulting groups was treated with D0, D1 and D2. The three groups were analysed in this assessment as:

i) S1-7DAE

ii) S1-14DAE

iii) S2-2DAE

Analysis of Variance (ANOVA) is commonly used to statistically compare the means of subsets of the data. One-way ANOVA is an extension of the traditional two-sample *t*-test where there are more than two subsets to compare in the data. Because this study was testing three doses (three subsets), it was not recommended to apply a multiple *t*-test. Applying this test, there is a 5% chance of making a Type I error; running two t-tests, the chance of making the error increases by 5%. Three t-tests on the influence of dose (i.e. D0, D1, and D2) would, therefore, increase the chance of making a Type I error to nearly 15%.

The ANOVA test indicates whether groups are significantly different from each other, but it does not indicate where the differences occur. *Post-hoc* tests, on the other hand, indicate the location of these differences, reporting whether they are significantly different or not. There were more than two doses to compare, and the data did not meet the principles of normality, homogeneity and independence, so a one-way ANOVA test and Games Howell post-hoc test were therefore applied. Correlation analyses were also performed to identify the relationships between the variables analysed in this study and harvested yield (bales/ha).

The one-way function from the *userfriendlyscience* package, available in R, was used to analyse the mean difference in the canopy height for each group. Table 6-3 summarises the groups and factors analysed in this study. The correlation analysis was run with the Data Analysis tool available in Microsoft Excel.

Table 6-3. Groups for statistical analysis.

Group	Days after exposure	Timing of exposure	Dose
1	7 DAE	S1	0% - D0; 5% - D1; 50% - D2
2	14 DAE	S1	0% - D0; 5% - D1; 50% - D2
3	2 DAE	S2	0% - D0; 5% - D1; 50% - D2

6.4. Results

The methods employed in this research were tested and evaluated in replication 4 of the controlled sub-study (Figure 6-3) in Jondaryan, Queensland, Australia. The differences in canopy height and volume will be discussed in sequence.

6.4.1. Estimation of canopy height

The canopy height surfaces for each treatment and scanning date were generated and compared with manual measurements in treatments S1-14 DAE and S2-2DAE (Figure 6-14), after the described data processing of the captured TLS point clouds. The high values of R^2 (> 0.91) validated the canopy height estimated by implementing the canopy surface model approach. The variability of canopy height caused by the different doses was much higher at the earliest timing of exposure (S1) than at the middle stage of exposure (S2), as indicated by the standard errors per group (Figure 6-14).

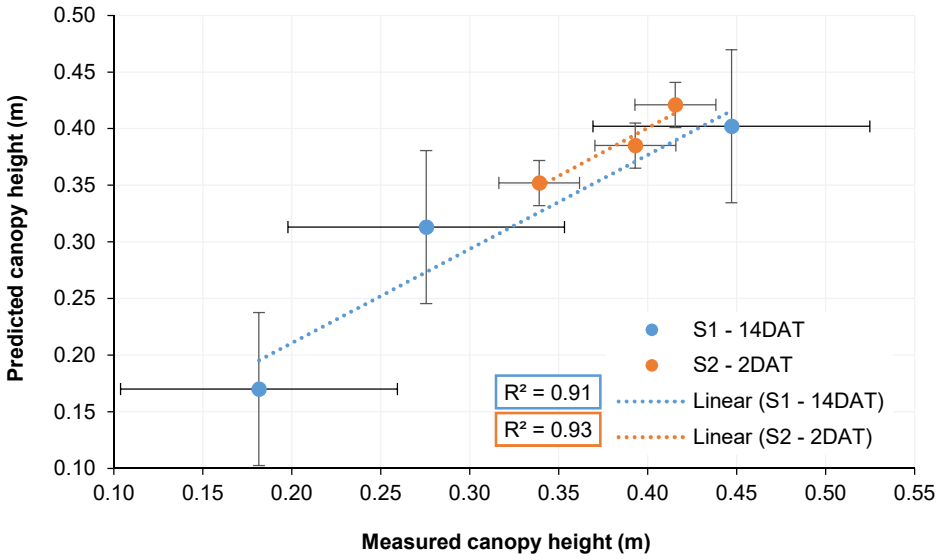

Figure 6-14. Canopy height manually measured vs. estimated by canopy surface models approaches for S1-14 DAE and S2-2 DAE.
Error bars represent the standard error.

An example of canopy height estimated by CSM is presented in Figure 6-15, which shows the mean changes in canopy height compared to control treatments through time (7 DAE and 14 DAE). At 14 DAE, the highest dose gradually affected the canopy height for plants treated at 4-5 nodes (S1) reducing plant height by 0.11 m and 0.22 m for D1 and D2, respectively (Table 6-4).

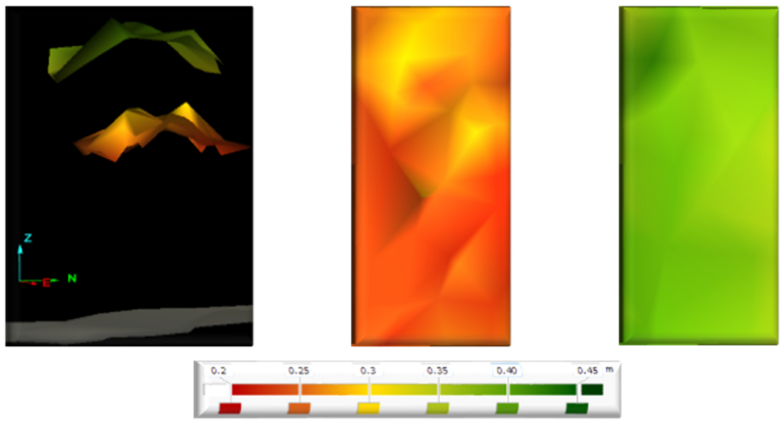

Figure 6-15. Canopy height estimation of control treatment at 7 DAE (orange) and 14 DAE (green).

Table 6-4. Measurement results for canopy height and volume of the combined experimental design.

				Canopy		Mean Difference*	
Days after the exposure (DAE)	Timing of exposure (S)	Dose (D)	Number of points	Canopy height (m) (sd)	Canopy volume (m^3)	Height (m) (ste)	Volume (m^3)
7 DAE	S1	Control	3334	***0.239 (0.018)***	***0.107***		
		D1	1776	0.119 ***(0.018)***	0.071	0.12 ***($1e^{-5}$)***	0.04
		D2	352	0.133 ***(0.019)***	0.014	0.11 ***($2e^{-5}$)***	0.09
14 DAE	S1	Control	47011	***0.357 (0.028)***	***0.388***		
		D1	6756	0.247 ***(0.036)***	0.151	0.11 ***($2e^{-5}$)***	0.24
		D2	2809	0.136 ***(0.019)***	0.057	0.22 ***($3e^{-5}$)***	0.33
2 DAE	S2	Control	7704	***0.408 (0.032)***	***0.338***		
		D1	4693	0.321 ***(0.029)***	0.329	0.09 ***($4e^{-5}$)***	0.01
		D2	7670	0.275 ***(0.044)***	0.292	0.13 ***($4e^{-5}$)***	0.05

*All mean differences are statistically different according to on-way ANOVA (*p*-value < 0.001). Standard deviation (sd) and standard error (ste) are presented in brackets (). Because canopy volume is a unique value, it did not report standard deviation.

The dose affected the canopy height of all of the treatments regardless of the amount of chemical in contact with the plants. The height reduction varied from 21% up to 62% of the control treatments. Two days after exposure (2 DAE), reductions of canopy height were calculated at 21.2% and 32.6% on treatments sprayed with the minimum and the highest dose, respectively. The minimum dose manifested the highest impact (50.2% reduction) at 7 DAE with an equivalent loss of 0.12 m. However, the maximum reduction was calculated at14 DAE with the highest dose (61.9%) (Figure 6-16).

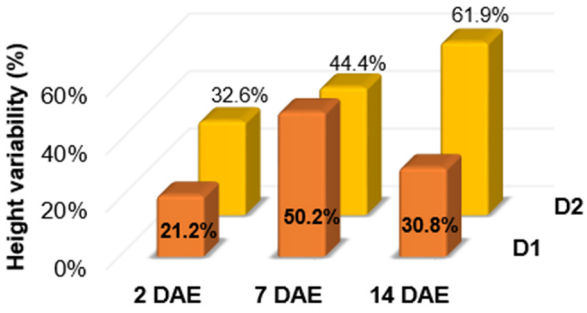

Figure 6-16. Temporal canopy height variability as a function of dose (D1 and D2).

According to the results of the one-way ANOVA (*p*-value < 0.001), there were statistically significant differences in the average canopy height between all of the

groups analysed in this study. The average difference between treated treatments with the lowest dose (D1) and their respective controls was between 0.09 m and 0.12 m. On the other hand, the mean differences of treatments in contact with the highest dose (D2) and their controls presented bigger fluctuations, between 0.11 m and 0.22 m being the most notable difference for S1 at 14 DAE (Figure 6-17).

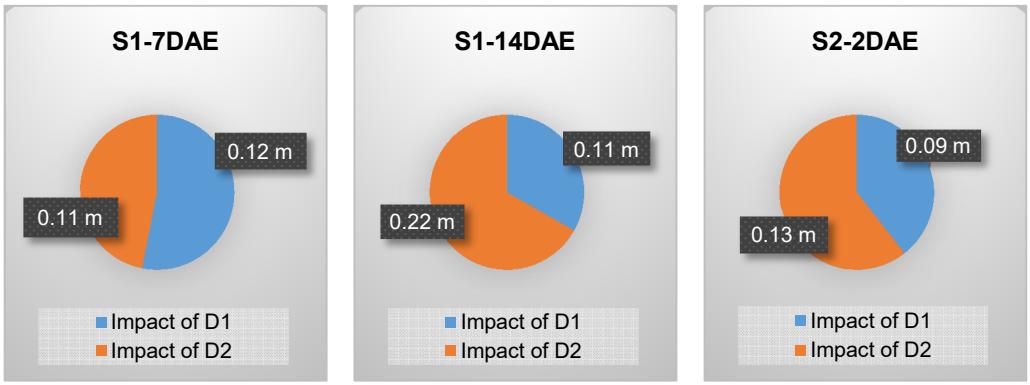

Figure 6-17. Mean differences in canopy height between treated treatments and their respective controls.

6.4.2. Estimation of canopy volume

Canopy volume, as estimated, varied according to the sprayed dose. Some areas were not properly scanned due to obstruction generated by the canopy itself, but the estimation of canopy volume was not correlated to a number of scan points (p-value > 0.05). Figure 6-18 shows the areas with good point cloud coverage and others (in the same sprayed line) with poor point cover. However, the loop wrap algorithm was able to overcome the poor point coverage and generate a volume with just a few points per area.

The volume loss ranged from 3% to 87% where the impact of the highest dose was always bigger than the lowest dose, regardless of the timing of exposure. The loss of the treatments (S2) compared to the control was nearly 14% for D2 and close to 3% for D1 soon after the exposure (2 DAE) (Figure 6-19). The volume was considerably reduced (by more than 27%) through time when treated with D1 for treatments sprayed at S1 (Figure 6-19) while the highest dose (D2) had a more constant impact through time with a high volume loss between 85.3% and 86.9% equivalent to a 0.093 m^3 and 0.331 m^3, respectively.

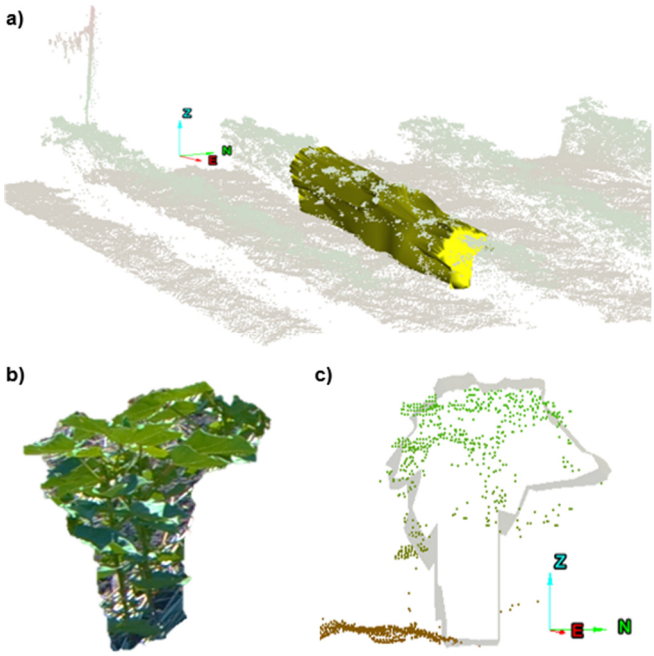

Figure 6-18. Volume of the control treatment at S2 and 2 DAE.
a) General view (XYZ) of the point cloud superimposed on volume surface; b) plant in the field; c): transversal view (YZ) of (a). Note the good cloud cover at the top of the canopy compared with the poor cover at the middle and lower canopy and the similarities between b) and c).

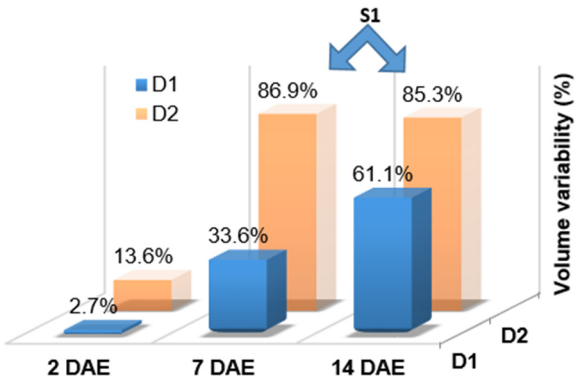

Figure 6-19. Temporal changes in canopy volume for all treatments.

An estimation of daily rate loss (DRL) was analysed to characterise the proportion of loss in terms of height or volume per day according to the timing of exposure and dose. The estimated change in a treatment was divided by the corresponding number of DAE in order to get a daily rate. Figure 6-20 shows the DRL of canopy height and volume, where D2 had a calculated DRL difference higher than D1: 5% and 2% at 2 DAE and 14 DAE, respectively. On the other hand, the DRL of volume reached a peak at 7 DAE for all the treated treatments. Differences in the DRL of volume caused by the increment of dose were calculated as 6% at 2 DAE, 7% at 7 DAE and 2% at 14 DAE.

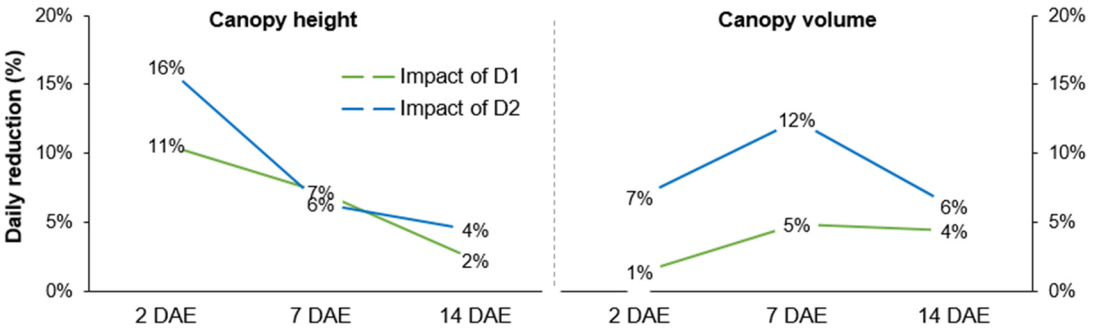

Figure 6-20. Daily rate loss (DRL) of canopy height (left) and canopy volume (right).

6.4.3. Correlation analysis of canopy structure variables and yield

Correlation analysis was implemented within each analysis group (Table 6-2) to understand the relationship between the calculated variables and yield for the specific treatment. There was a strong and significant correlation between canopy structure variables (CSV) and yield ($r > 0.88$, p-value < 0.05) for all of the groups. The direct relationships are in accordance with different studies which demonstrated that plant growth is highly related to yield (Zub et al., 2011). Yield (bales/ha) decreased as the dose increased (Figure 6-21), and yield was directly correlated to canopy volume and height (Figure 6-22). These results agree with the outcomes presented in Figure 6-19, where it was shown that the percentage of canopy volume loss increased as the dose also increased.

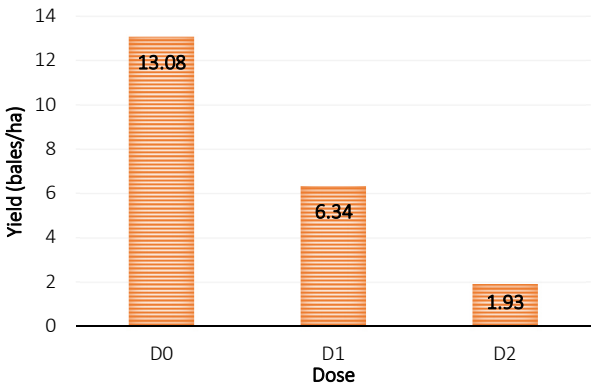

Figure 6-21. Mean of harvested yield in relation to dose.

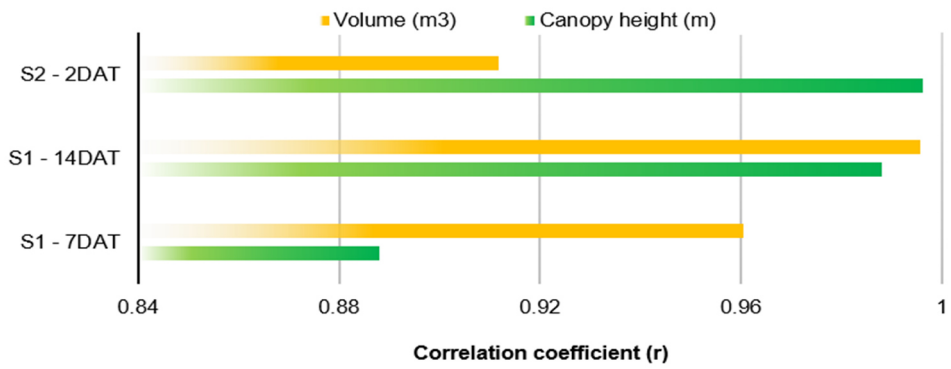

Figure 6-22. Correlations between yield (bales/ha) and canopy structure variables

6.5. Discussion

The position of the spherical targets is a major aspect in most of TLS studies. Fixed positions of the spheres during the whole season had been reported as essential for a high-accuracy setup (Friedli et al., 2016; Tilly et al., 2014), as fixed positions can reduce the potential height differences between scans and the risk propagating error when estimating canopy heights at different dates. Fixed locations are, however, not practical in agricultural fields where machinery movements are constantly needed for irrigation, pest control and other aspects of crop management. This study demonstrated that varying sphere locations and height can be implemented without affecting the accuracy of the results when the scan locations are georeferenced with high accuracy in the field.

The integration of TLS data with other remote/proximal sensing technologies may provide a more multifaceted scenario to characterise a particular situation, but many of the TLS studies available in the literature focused on a fixed coordinate system (Hilker et al., 2010; Tilly et al., 2014; Zhang & Grift, 2012) which is a potential limitation when other technologies are integrated. Special caution was taken in this study to properly register the scan locations, in order to guarantee comparisons of canopy height and volume through time and allow the potential integration with other technologies.

The concept of CSM has been widely applied for canopy height estimations (Bendig et al., 2013; Hoffmeister et al., 2010; Tilly et al., 2014; Zhang & Grift, 2012) but the selection of the points to be included in the surface model differ. Hilker et al. (2010) selected the top 40, 30, 20 and 10% of the point cloud while Friedli et al. (2016) applied

three filtering approaches based on the percentiles 100th, 99% and 90% of the highest points (P100, P99 and P90, respectively). This approach presented a limitation when assessing the P100 as all the potential outliers were included, hence that contributed to a low R^2 in relation to heights manually measured (Hilker et al., 2010). The accuracy of the canopy height estimations would, in the addition to the previous selection of the top points without prior cleaning process, depend on the canopy closure as the laser beam could penetrate and reach soil or lower areas of the plants (Friedli et al., 2016) influencing the percentiles. The iterative filtering process implemented in this study avoided the selection of lower/highest points, and hence a maximisation of the estimated canopy height. The removal of undesirable points is a fast process that did not require significant time while getting good results as demonstrated in this study.

Measuring the soil level is traditionally accomplished at the beginning of the season for later estimation of canopy height (Friedli et al., 2016). Other studies, however, obtained the ground level by subtracting the lower points at a vegetation-free stage of the study area (Andújar et al., 2013) or applied the Multi Curvature Classification (MCC) method to generate digital terrain surface layers (Jensen et al., 2008). A combined methodology was implemented in this study that did not require an additional field day for soil levelling while selecting the lower points of the scanned areas for the generation of DEM.

The results showed that the characteristics of the canopy can be captured by the TLS and compared through time. The statistically significant differences between all of the treatments analysed in this study allowed an understanding of the impact of the chemical 2,4-D on the canopy structure of the crop at a daily rate. The negative impact on canopy height and volume increased as the dose increased, regardless of the timing of exposure (except for S1 at 7 DAE where D1 had a higher impact than D2 for canopy height). The increment of the percentage of the active ingredient (dose) accounted for an additional reduction of more than 50% of canopy volume in this study. The DRL of volume increased as the dose increased, while the DRL in canopy height was usually higher soon after the incident (Figure 6-20). In this way, the DRLs of the height in treated plots with D2 were as high as 16%, 6% and 4% at 2 DAE, 7 DAE and 14 DAE, respectively. Conversely, the highest DRL of the volume was recorded at 7 DAE (irrespective of the dose).

The correlation analysis indicated how the variables analysed in this chapter changed through time. Canopy height had a higher correlation than volume with yield as soon as 2 DAE in treated plots at S2. In contrast, canopy volume had higher correlation than height with yield at 7 DAE (S1), while correlations between canopy structure variables and yield were more constant at 14 DAE (S1). These differences in the correlation coefficients, therefore, indicated that the height loss was greater than the volume loss for treatments sprayed at S2. However, the volume loss was higher than height loss for S1.

In summary, canopy height was more representative of changes at S2-2DAE while volume was more representative of yield loss for sprayed treatments at S1. This situation can be also explained by the influence of the canopy height and row spacing on laser beam obstruction (Friedli et al., 2016; Hosoi & Omasa, 2009). At younger canopy heights (S1) the laser beams can reach the lower parts of the plants turning the canopy volume estimation into a more accurate surface, hence higher correlation coefficients with yield in treated plots at the very early stage were manifested. As the canopy grew taller (S2) and became denser, it reduced the clear-row spacing. As a consequence, the single-return laser beams could not penetrate the lower part of the canopy as the upper parts obstructed the beams (Hosoi & Omasa, 2009) resulting in less accurate volume estimation evidenced by the lower correlation coefficients (in comparison to the r coefficients obtained at S1).

The proposed methodology captured the shape, area and volume of the cotton canopy that tends to be pyramidal. Due to this shape, the volume estimation directly from the CSM was limited. The calculation of canopy volume can be performed by implementing the CSM and the DEM in studies where the canopy structure of the investigated crop tends to be regular at different levels (i.e. middle and top canopy) (Bendig et al., 2013; Hoffmeister et al., 2010). However, the cotton canopy structure required a more robust method. A significant finding is that the method described in this study for the calculation of canopy volume was not affected by the amount of resulting scanned points. General TLS restrictions include the potential occlusion of plants or leaves by objects closer to the scanner (Hilker et al., 2010). The amount of scanned points per treatment had no significant correlation with the resulting volume (p-value > 0.05) while the estimated volume was statistically highly correlated with

yield ($r > 0.88$, p-value < 0.05) even though there were occlusions that could not be avoided by integrating point clouds from different scanned locations as suggested by Friedli et al. (2016) and Hilker et al. (2010).

Canopy height estimation can potentially also be affected if there is no homogenous point cloud. However, the probability of obstructions at the top of the canopy is less likely than at the middle or bottom canopy. This research study has demonstrated that although an obstruction may occur in some areas, canopy height and volume estimations are not significantly affected (p-value > 0.05). Both canopy height and volume calculated using TLS-derived point clouds were highly correlated with yield after the contact with the chemical ($r > 0.88$) regardless of any obstruction that might be present in some scanned areas.

A high location of the scanning points is needed to optimise the cover and homogeneity of the point cloud, especially when the crop is reaching maturity. A fast and applicable method is reported in Tilly et al. (2014), where the tripod and the scanner were mounted on a small trailer. This can also be achieved by mounting the instrument on the back of a utility vehicle with a cargo tray. The height of the scanner can be easily increased by a meter with this, reducing the limitations of a relatively low altitude of the scanning locations.

6.6. Summary

The results of this study demonstrated that TLS could capture the temporal changes caused by 2,4-D in cotton crops providing an alternative (to traditional visual assessment) and reliable method to characterise plant growth and production. The methodology implemented in this study also allowed the acquisition of accurate results even in those treatments, which for different reasons, such as view obstruction, could not be properly or evenly scanned. There were statistical differences in canopy height which allowed their characterisation among all groups analysed in this study. Regarding the field experiment, further studies are required to investigate other timings of exposures with shorter gaps between doses. Furthermore, the transferability of the methods into larger fields should be investigated. Nonetheless, the approach presented in this work is a promising step toward optimising the assessment of damage caused by 2,4-D in cotton crops.

Chapter 7

CONCLUSIONS AND RECOMMENDATIONS

7.1. Introduction

This study aimed at assessing the capabilities of remote and proximal sensing technologies for the accurate detection of herbicide drift on cotton crops. Three specific objectives were proposed and described previously in Section 1.4 of Chapter 1, and individually addressed in Chapter 4 through Chapter 6. The objectives were proposed to achieve the goal of this study and to answer the research questions presented in Section 1.3 of the same chapter. This final chapter presents the conclusions generated from this work, as well as the recommendations for future adoptions and operations.

7.2. Conclusions

This study provided three reliable and accessible techniques to assess herbicide drift on cotton crops. These techniques proved to be capable of overcoming the limitations associated with traditional (visual) assessment. Each technique provided accurate results, tested in both controlled and uncontrolled scenarios, and demonstrated its capabilities and potential limitations.

Proximal hyperspectral sensors, examined in *Chapter 4,* proved to be a powerful approach for the prediction of yield in contaminated cotton crops regardless of the dose or the timing of exposure. However, the prediction capabilities varied according to days after the exposure (i.e. the number of days between exposure to herbicide and the hyperspectral sensing measurements). Conversely, for the prediction of dose, the days after the exposure did not affect the accuracy of prediction models.

The timing of exposure was the factor that primarily affected the performance of the classification models of dose by increasing the prediction accuracy by more than 10%. Hence, regardless of the classification approach, it was then possible to determine the best time for data collection for each timing of exposure through the growing season.

The prediction performance of yield and simulated dose were comparable in the sense that they share similar significant wavelengths and the optimal time for data collection purposes. Therefore, these results can potentially simplify prediction models and field work campaigns.

The internal structure of the leaf, after the exposure to the chemical, was a major factor that influenced changes in the reflectance patterns in the visible and NIR range. Although the fluctuations between the physiological and the hormone content variables, particularly ABA, were not sufficient to determine a significant relationship between them, the reflectance changes were driven by both of them (i.e. physiology and hormone content variability). In particular, the structural-related wavelengths manifested stronger relationships with hormone content than the visible wavelengths.

The Multispectral satellite sensor Landsat-8 Operational Land Imager (OLI) tested in *Chapter 5* appeared to be an easily applicable and potentially useful approach at the field level to detect areas exposed to 2,4-D phenoxy herbicide. Even with the sensor's medium spatial resolution of 30 m, yield was accurately predicted in areas exposed to herbicide drift. The use of multiple image bands in a multidimensional prediction model resolved the limitations associated with the medium spatial resolution of Landsat-8 OLI for the detection of within-field variability.

The temporal reflectance changes and the variability in the accuracy of the prediction models through time were used as indicators of recovery mechanisms within the plants after the exposure. In that sense, we could surmise that the plants struggled with the impact of the herbicide during the first month after exposure.

This study concluded that the vegetation indices derived from Landsat-8 OLI, with seven of them related to canopy structure and two more related to pigment contents, were not capable of accurately predicting yield in either contaminated or healthy cropping areas. However, their temporal variability, based on their correlation coefficients in relation to the area under study, indicated that after 2,4-D exposure, nutrient/pigment availability has a relatively higher impact, while under optimal growing conditions the yield determining factors are more related to the biophysical conditions of the crop.

The multivariate approaches overcame the limitations evident in the vegetation indices by providing good yield prediction fits, particularly in the affected area. In this study, as well as in the hyperspectral study, “days after the exposure” was a determinant variable for accurately predicting yield in contaminated areas.

LiDAR-derived metrics estimated in *Chapter 6* manifested significant correlations with cotton canopy variables at different days after the exposure. Canopy height and canopy volume were accurately estimated from the LiDAR point cloud at each date of the fieldwork campaign and strongly correlated with yield as soon as two days after the exposure. The methodologies, to estimate canopy height and volume, proved to be insensitive to the common limitation caused by occlusion points during the scanning process. Significant differences in canopy height between controls and treated plants were accurately estimated with the proposed methodology. In contrast to reflectance sensing techniques, LiDAR-derived canopy variables were strongly correlated with yield regardless of the “days after the exposure”.

The preceding results help to bridge the gap between the adoptability of technology and final users, i.e. farmers, industry, consultants, etc. while providing reliable and accurate approaches for the prediction of 2,4-D herbicide drift damages in cotton crops.

7.3. Recommendations

The current lack of accurate methodologies to estimate potential yield loss and to monitor cotton crop areas that have been potentially affected by herbicide drift limits the maximisation of mitigation plans in affected areas representing millions of dollars in losses to farmers and the industry in general. This research provides three different methods to accurately predict damage caused by 2,4-D herbicide drift on cotton crops. The recommendations, provided in this section, are based on the practical applications of the methods used, and the variables that best predicted 2,4-D damage in cotton crops. As days after exposure (DAE) proved to be the most significant variable in the prediction performance of the models, it is therefore important to monitor the crop closely if any minor evidence of damage (based on spectral response) is apparent, in order to identify the timing of exposure and estimate the days after the exposure. After

which, it would be then possible to adjust the methodology described in this study to predict the dose of 2,4-D that might have affected the crop and the potential yield.

7.3.1. Recommendations for practical applications

The prediction capabilities of hyperspectral data proved to be an accurate technique for predicting yield, regardless of the timing of exposure and dose. However, days after exposure was a determining factor in model performance, which in real terms implies close monitoring of the condition of the crop. A potential limitation on practical applications is that it is a ground-based device that requires targeting and homogenous sampling within the field, and therefore, could be more limited on a larger scale.

Landsat-8 OLI, as implemented in this study, proved to be a reliable and accurate technology for the identification of contaminated zones. The continuous revisit periods allow the monitoring of extensive field areas, providing information on crop conditions and potential problems. However, in some cases where the area of the paddock is relatively small, the medium spatial resolution of Landsat-8 OLI could pose some limitations that might be remediated by the implementation of other satellite sensors with better spatial resolution.

Due to the significant impact of 2,4-D herbicide drift on cotton crops and the powerful applicability of remote and proximal sensors in the prediction of 2,4-D damage, it is highly recommended to implement a monitoring program based on remote sensing technologies at regional and field scales. The final users of this program would be regional managers, farmers and agronomists that could have access to detailed information about crop condition and potential injured areas, and distribute the information as needed to immediately activate targeting mitigation plans.

LiDAR provided valuable information in terms of canopy structure variability with relatively short processing times. Hence, it is recommended to explore different platforms for LiDAR scanners and explore practical mechanisms to incorporate this technology in the same platforms as reflectance-based sensors. Currently, the costs associated with LiDAR sensors are high so that they are mainly implemented in research settings. However, due to the accuracy of this device and the fact that the

accuracy is not affected by “days after the exposure”, the integration of this technology in practical applications should be explored further.

7.3.2. Recommendations for future research

It is recommended that the methodology be tested in different locations with varying soil and water conditions, and with lower doses during at least three growing seasons. The influence of soil and canopy structure on the prediction capabilities of the resulting models need to be explored. This can be approached by analysing the hyperspectral measurements at canopy level. Furthermore, hyperspectral imagery or hyperspectral remote sensing might resolve the issues pertaining to spatial distribution of the degree of damage across and within paddocks. The results obtained from these systems can be extrapolated to other sensors and platforms.

It is also recommended to test other satellite sensors such as Sentinel-2 and WorldView-3 (WV-3) as they provide more spatial and different spectral resolution. Because they provide smaller pixel size (20 m and 10 m for Sentinel-2 and 1.2 m for WV-3), the vegetation indices could potentially perform better for the detection of within-field yield variability and yield predictions. Testing these sensors will also provide a complete view of the implication of spatial and spectral resolutions for practical applications.

Depending on resources, a fusion of satellite multispectral imagery and ground-based hyperspectral data can potentially resolve the limitations of the ground-based measurements and the reduced accuracy of multispectral data in comparison with hyperspectral data, as well as the cost associated with very high spatial resolution sensors. For this reason, it is also recommended to explore the viability of integrating both methodologies as an improved crop sensing tool for herbicide drift damage.

Furthermore, testing of the most significant wavelengths is desirable for the development of new and simplified models. As reflectance varies according to the dose, it is recommended that other doses, especially lower ones, are tested and included in the models. Similarly, it is also recommended to test the proposed methodologies in different growing seasons and different paddocks, to further validate the transferability of the prediction models developed in this study.

References

About Organic Cotton. (2016). *Frequently asked questions*. Textile Exchange, Retrieved October 10, 2017 from http://aboutorganiccotton.org/faq/

Al-Khatib, K., Shoup, D. E., Peterson, D. E., & Claassen, M. (2004). *Cotton response to simulated drift rates of seven hormonal-type herbicides.* In International Conference on Pesticide Application for Drift Management, Hawaii. Retrieved from http://pep.wsu.edu/drift04/pdf/proceedings/pg302-308_Poster3.pdf

Andújar, D., Escolà, A., Rosell-Polo, J. R., Fernández-Quintanilla, C., & Dorado, J. (2013). Potential of a terrestrial LiDAR-based system to characterise weed vegetation in maize crops. *Computers and Electronics in Agriculture, 92*(0), 11-15. doi: 10.1016/j.compag.2012.12.012. Retrieved from http://www.sciencedirect.com/science/article/pii/S0168169913000033

Apan, A., Kelly, R., Phinn, S., Strong, W., Lester, D., Butler, D., & Robson, A. (2006). Predicting grain protein content in wheat using hyperspectral sensing of in-season crop canopies and partial least squares regression. *International journal of Geoinformatics, 2*(1), 93-108.

ASD Inc. (2010). *FieldSpec® HandHeld 2™ spectroradiometer user's manual*: ASD Inc. Retrieved from http://www.asdi.com/products-and-services/fieldspec-spectroradiometers/handheld-2-pro-vnir-hand-held-spectroradiometer

Australia Bureau of Statistics 2017a, *7111.0 - Principal agricultural commodities, Australia, Preliminary, 2015-16*, Australia Bureau of Statistics, ABS. ABS. Retrieved from http://www.abs.gov.au/AUSSTATS/abs@.nsf/Lookup/7111.0Main+Features12015-16?OpenDocument

Australia Bureau of Statistics 2017b, *7501.1 - Value of principal agricultural commodities, Australia, Preliminary, 2015-16*, Australia Bureau of Statistics, ABS. ABS. Retrieved from http://www.abs.gov.au/AUSSTATS/abs@.nsf/Lookup/7501.0Main+Features12014-15?OpenDocument

Australian Bureau of Agricultural and Resource Economics and Sciences (Cartographer). (2010). National scale land use version 4 [Raster]. Retrieved from http://www.agriculture.gov.au/abares/aclump/land-use/data-download

Australian Bureau of Statistics. (2011, 4 October). *Australian standard geographical classification (ASGC) digital boundaries*. Retrieved April 13, 2014 from http://www.abs.gov.au/AUSSTATS/abs@.nsf/Lookup/1259.0.30.001Main+Features1July%202011?OpenDocument

Australian Bureau of Statistics. (2013, November 14, 2013). *Value of principal agricultural commodities produced, Australia, Preliminary, 2012-13* Retrieved June 5, 2013 from http://www.abs.gov.au/ausstats/abs@.nsf/Lookup/7501.0main+features32012-13

Australian Bureau of Statistics. (2017, January 12). *2011 Census QuickStats, Jondaryan Code SSC30825 (SSC)*. Retrieved March, 2017 from

http://www.censusdata.abs.gov.au/census_services/getproduct/census/2011/quickstat/SSC30825?opendocument&navpos=220

Australian Pesticides and Veterinary Medicines Authority. (2005, October,). *[Archive] Status of 2,4-D products in Australia*. Retrieved March 2, 2013 from http://www.apvma.gov.au/products/review/current/2_4_d_products_status.php

Australian Pesticides and Veterinary Medicines Authority 2008, *APVMA operating principles in relation to spray drift risk*, Australian Pesticides and Veterinary Medicines Authority,. Australia: Australian Pesticides and Veterinary Medicines Authority. Retrieved from https://archive.apvma.gov.au/use_safely/docs/spraydrift_op_principles.pdf

Australian Pesticides and Veterinary Medicines Authority. (2013, August 21, 2013). *Review of 2,4-D HVE completed*. Retrieved February 2, 2014 from https://apvma.gov.au/node/11681

Ball, D. A., Corp, M., & Dami, I. 2014, *Preventing herbicide drift and injury to grapes*, E. Service, Oregon State University Extension Service. Retrieved from http://ir.library.oregonstate.edu/xmlui/bitstream/handle/1957/45880/em8860.pdf

Ballew, J. (2015). *Question of the week: 2,4-D*. Pee Dee Ag News, Retrieved April, 2017

Barbin, D. F., ElMasry, G., Sun, D.-W., & Allen, P. (2012). Predicting quality and sensory attributes of pork using near-infrared hyperspectral imaging. *Analytica Chimica Acta, 719*(0), 30-42. doi: 10.1016/j.aca.2012.01.004. Retrieved from http://www.sciencedirect.com/science/article/pii/S0003267012000189

Barnes, E. M., Clarke, T. R., Richards, S. E., Colaizzi, P. D., Haberland, J., Kostrzewski, M., . . . Thompson, T. (2000). *Coincident detection of crop water stress, nitrogen status and canopy density using ground based multispectral data.* In Proceedings of the fifth international conference on precision agriculture, Bloomington, MN. Retrieved from http://naldc.nal.usda.gov/download/4190/PDF

Beleites, C. (2015). *hyperSpect introduction*. Jena, Germany: Spectroscopy - Imaging, IPHT Jena e.V. Retrieved from https://cran.r-project.org/web/packages/hyperSpec/vignettes/introduction.pdf

Bellon-Maurel, V., Fernandez-Ahumada, E., Palagos, B., Roger, J.-M., & McBratney, A. (2010). Critical review of chemometric indicators commonly used for assessing the quality of the prediction of soil attributes by NIR spectroscopy. *Trends in Analytical Chemistry, 29*(9), 1073-1081. doi: 10.1016/j.trac.2010.05.006. Retrieved from http://www.sciencedirect.com/science/article/pii/S0165993610001585

Bendig, J., Bolten, A., & Bareth, G. (2013). UAV-based imaging for multi-temporal, very high resolution crop surface models to monitor crop growth variability. *Photogrammetrie, Fernerkundung, Geoinformation, 2013*(6), 551-562. doi: 10.1127/1432-8364/2013/0200

Birch, P., & Moree, W. R. 2004, *Understanding hormone damage*, The Australian Cottongrower. Retrieved from http://www.greenmountpress.com.au/cottongrower/Back%20issues/256oncot04/29_Understanding.pdf

Blackburn, G. A. (2007). Hyperspectral remote sensing of plant pigments. *Journal of Experimental Botany, 58*(4), 855-867. doi: 10.1093/jxb/erl123. Retrieved from http://jxb.oxfordjournals.org/content/58/4/855.abstract

Bohling, G. (2005). *Kriging*. Retrieved from http://people.ku.edu/~gbohling/cpe940/Kriging.pdf

Bondada, B. R. (2011). Micromorpho-anatomical examination of 2,4-D phytotoxicity in grapevine (*Vitis vinifera* L.) leaves. *Journal of Plant Growth Regulation, 30*(2), 185-198. doi: 10.1007/s00344-010-9183-7. Retrieved from http://dx.doi.org/10.1007/s00344-010-9183-7

Bouckaert, R. R., Frank, E., Holmes, G., & Fletcher, D. (2011). A comparison of methods for estimating prediction intervals in NIR spectroscopy: Size matters. *Chemometrics and Intelligent Laboratory Systems, 109*(2), 139-145. doi: 10.1016/j.chemolab.2011.08.008. Retrieved from http://www.sciencedirect.com/science/article/pii/S0169743911001742

Bronson, K. F., Booker, J. D., Keeling, J. W., Boman, R. K., & et al. (2005). Cotton canopy reflectance at landscape scale as affected by nitrogen fertilization. *AGRONOMY JOURNAL, 97*(3), 654-660. doi: 10.2134/agronj2004.0093

Buehring, N. W. (2004). *Alternative methods for herbicide spray drift detection in corn and cotton.* (3150631 Ph.D.), Mississippi State University, Ann Arbor. Retrieved from http://search.proquest.com/docview/305160339?accountid=14647 ProQuest Dissertations & Theses A&I database.

Carter, G. A. (1998). Reflectance wavebands and indices for remote estimation of photosynthesis and stomatal conductance in pine canopies. *Remote Sensing of Environment, 63*(1), 61-72. doi:10.1016/S0034-4257(97)00110-7. Retrieved from http://www.sciencedirect.com/science/article/pii/S0034425797001107

Ceccato, P., Gobron, N., Flasse, S., Pinty, B., & Tarantola, S. (2002). Designing a spectral index to estimate vegetation water content from remote sensing data: Part 1: Theoretical approach. *Remote Sensing of Environment, 82*(2–3), 188-197. doi: 10.1016/S0034-4257(02)00037-8. Retrieved from http://www.sciencedirect.com/science/article/pii/S0034425702000378

Centre for the Government of Queensland. (2015). *Jondaryan Shire*. The University of Queensland, Retrieved April 16, 2017 from http://queenslandplaces.com.au/jondaryan-shire

Charles, G. W. 2011, *Herbicide damage symptoms guide*, D. o. P. Industries, Cotton Catchment Communities CRC.

Charles, G. W., Constable, G. A., Llewellyn, D. J., & Hickman, M. A. (2007). Tolerance of cotton expressing a 2,4-D detoxification gene to 2,4-D applied in the field. *Australian Journal of Agricultural Research, 58*(8), 780. doi: 10.1071/ar06375

Chen, H. C., Gengxing, Z., Yinjuan, W., Long, S., & Hu, M. (2011). *Discussion on remote sensing estimation of soil nutrient contents.* In 2011 International Conference on Remote Sensing, Environment and Transportation Engineering (RSETE), Nanjing, China. Retrieved from http://ieeexplore.ieee.org/ielx5/5954011/5963913/05964963.pdf?tp=&arnumber=5964963&isnumber=5963913

Clemson University Cooperative Extension. (2013a). *2,4-D, cotton and pesticide drift*. Clemson University, Retrieved July 4, 2013 from http://www.clemson.edu/extension/pest_ed/safety_ed_prog/drift/24d_drift.html

Clemson University Cooperative Extension. (2013b). *Reducing pesticide drift*. Retrieved May 14, 2013 from http://www.clemson.edu/extension/pest_ed/safety_ed_prog/drift/reducing.html

Clevers, J. G. P. W. (1999). The use of imaging spectrometry for agricultural applications. *ISPRS Journal of Photogrammetry and Remote Sensing, 54*(5–6), 299-304. doi: 10.1016/S0924-2716(99)00033-7. Retrieved from http://www.sciencedirect.com/science/article/pii/S0924271699000337

Confalonieri, R., Bregaglio, S., Rosenmund, A. S., Acutis, M., & Savin, I. (2011). A model for simulating the height of rice plants. *European Journal of Agronomy, 34*(1), 20-25. doi: 10.1016/j.eja.2010.09.003

Coops, N. C., Hilker, T., Wulder, M. A., St-Onge, B., Newnham, G., Siggins, A., & Trofymow, J. A. (2007). Estimating canopy structure of Douglas-fir forest stands from discrete-return LiDAR. *Trees, 21*(3), 295-310. doi: 10.1007/s00468-006-0119-6

Cosgrove, D. J. (1981). Rapid suppression of growth by blue light: Occurrence, time course, and general characteristics. *Plant physiology, 67*(3), 584-590. doi: 10.1104/pp.67.3.584

Cotton Australia 2012, *Background briefing*, Cotton Australia. Retrieved from http://cottonaustralia.com.au/uploads/resources/Cotton_Australia_Background_Briefing_-_Phenoxy_Herbicides_2012.pdf

Cotton Australia 2013a, *Annual report 2012-2013*, Cotton Australia. Retrieved from http://cottonaustralia.com.au/uploads/publications/2012-13_Cotton_Australia_Annual_Report_-_FINAL.pdf

Cotton Australia. (2013b). *The cotton plant*. Cotton Australia, Retrieved July 25, 2013 from http://cottonaustralia.com.au/cotton-library/fact-sheets/cotton-fact-file-the-cotton-plant

Cotton Australia. (2013c). Rain means increased phenoxy risk to cotton [Press release]. Retrieved from http://cottonaustralia.com.au/news/article/rain-means-increased-risk-to-cotton

Cotton Australia. (2013d, 9 December). *Spray drift danger to cotton crop*. Cotton Australia, Retrieved February 7, 2014 from http://cottonaustralia.com.au/news/article/spray-drift-danger-to-cotton-crop

Cotton Australia. (2015a). *Cotton's growing cycle*. Cotton Australia, Retrieved September 6, 2013 from http://cottonaustralia.com.au/cotton-library/fact-sheets/cotton-growing-cycle

Cotton Australia. (2015b). Spray drift danger to sensitive crops follows recent rainfall [Press release]. Retrieved from http://cottonaustralia.com.au/news/article/spray-drift-danger-to-sensitive-crops-follows-recent-rainfall

Cotton Australia 2016, *Cotton annual 2016, Australian cotton industry statistics*.

Cotton Australia. (2017). *Spray drift and cottonmap*. Retrieved April, 2017 from http://cottonaustralia.com.au/cotton-growers/phenoxy-protection

Cotton Australia, & Grains Growers. (2016). Spary drift threat to cotton: Industries unite, call for common sense [Press release]. Retrieved from http://cottonaustralia.com.au/news/article/spray-drift-threat-to-cotton-industries-unite-call-for-common-sense

Cotton Catchment Communities CRC 2009, *Social and economic analysis of the Darling Downs communities*, Cotton Catchment Communities CRC. Australia.

Cotton Research and Development Corporation 2013, *Strategic R&D plan 2013–2018*. Retrieved from http://crdc.com.au/wp-content/uploads/2013/07/CRDC13004-CRDC-Strat-plan-document_WEB.pdf

CottonInfo 2016, *Australian cotton production manual*. Australia. Retrieved from http://crdc.com.au/wp-content/uploads/2013/08/2013ACPM.pdf

Cowell, B. 2007, *Your crop has just received spray drift! - What do you do now?*, The Australian Cottongrower.

Cyr, L., Bonn, F., & Pesant, A. (1995). Vegetation indices derived from remote sensing for an estimation of soil protection against water erosion. *Ecological Modelling, 79*(1), 277-285. doi: 10.1016/0304-3800(94)00182-H. Retrieved from http://www.sciencedirect.com/science/article/pii/030438009400182H

de Castro, A.-I., Jurado-Expósito, M., Gómez-Casero, M.-T., & López-Granados, F. (2012). Applying neural networks to hyperspectral and multispectral field data for discrimination of cruciferous weeds in winter crops. *The Scientific World Journal, 2012*, 630390. doi: 10.1100/2012/630390. Retrieved from http://www.ncbi.nlm.nih.gov/pmc/articles/PMC3354564/

Department of Agriculture and Food. (2016, 9 December). *Herbicides*. Goverment of Western Australia, Retrieved March 3, 2015 from https://www.agric.wa.gov.au/herbicides/herbicides

Department of Economic Development, J., Transport and Resources,. (2014, January 30, 2014). *How do selective herbicides work?* Victoria State Government, Retrieved May 20, 2013 from http://www.depi.vic.gov.au/agriculture-and-food/farm-management/chemical-use/agricultural-chemical-use/chemical-residues/managing-chemical-residues-in-crops-and-produce/how-do-selective-herbicides-work

Department of Economic Development, J., Transport and Resources,. (2016, May 17). *Spraying, spray drift and off-target damage*. Department of Environment and Primary Industries, State Government of Victoria, Retrieved May 20, 2016 from http://www.depi.vic.gov.au/agriculture-and-food/farm-management/chemical-use/agricultural-chemical-use/spraying-spray-drift-and-off-target-damage

Department of Natural Resources and Mines. (2015, March 11). *Queensland globe KML*. Queensland Government, Retrieved April 10, 2017 from https://data.qld.gov.au/dataset/queensland-globe/resource/b16dbabe-7173-45e0-94c6-fcb97998e633

Detar, W. R., Penner, J. V., & Funk, H. A. (2006). Airborne remote sensing to detect plant water stress in full canopy cotton. *TRANSACTIONS-AMERICAN SOCIETY OF AGRICULTURAL ENGINEERS, 49*(3), 655.

Domenikiotis, C., Spiliotopoulos, M., Tsiros, E., & Dalezios, N. R. (2004). Early cotton yield assessment by the use of the NOAA/AVHRR derived Vegetation Condition Index (VCI) in Greece. *International Journal of Remote Sensing, 25*(14), 2807-2819. http://www.tandfonline.com/doi/pdf/10.1080/01431160310001632729. Retrieved from http://www.tandfonline.com/doi/pdf/10.1080/01431160310001632729

Ediriweera, S., Pathirana, S., Specht, A., & Danaher, T. (2011). *Prediction of vegetation structure from LIDAR and multispectral satellite data in a topographically complex landscape, Eastern Australia.* In 34th International Symposium on Remote Sensing of Environment - The GEOSS Era: Towards Operational Environmental Monitoring, Sydney, NSW. Australia. Retrieved from http://www.isprs.org/proceedings/2011/ISRSE-34/211104015Final00172.pdf

ERIN (Cartographer). (2008). Local government areas where cotton is grown.

ESRI. (2016). *What is a TIN surface?* ESRI, Retrieved May, http://desktop.arcgis.com/en/arcmap/10.3/manage-data/tin/fundamentals-of-tin-surfaces.htm from http://desktop.arcgis.com/en/arcmap/10.3/manage-data/tin/fundamentals-of-tin-surfaces.htm

Everitt, J. D., & Keeling, J. W. (2009). Cotton growth and yield response to simulated 2,4-D and Dicamba drift. *WEED TECHNOLOGY, 23*(4), 503-506. doi: 10.1614/WT-08-061.1

Everman, W. J., Medlin, C. R., Dirks, R. D., Bauman, T. T., & Biehl, L. (2008). The effect of postemergence herbicides on the spectral reflectance of corn. *WEED TECHNOLOGY, 22*(3), 514-522. doi: 10.1614/WT-07-021.1. Retrieved from http://dx.doi.org/10.1614/WT-07-021.1

FARO® 2009, *Phase shift measurement*, FARO Technologies. Retrieved from www.faro.com

FARO® 2011, *FARO® Laser scanner Focus3D manual*, FARO Technologies Inc.

Friedli, M., Kirchgessner, N., Grieder, C., Liebisch, F., Mannale, M., & Walter, A. (2016). Terrestrial 3D laser scanning to track the increase in canopy height of both monocot and dicot crop species under field conditions. *Plant Methods, 12*, 9. doi: 10.1186/s13007-016-0109-7. Retrieved from http://www.ncbi.nlm.nih.gov/pmc/articles/PMC4731982/

Frost, J. (2014, March 6). *Why is there no R-squared for nonlinear regression?* Retrieved October 17, 2017 from http://blog.minitab.com/blog/adventures-in-statistics-2/why-is-there-no-r-squared-for-nonlinear-regression

Gao, B.-c. (1996). NDWI—A normalized difference water index for remote sensing of vegetation liquid water from space. *Remote Sensing of Environment, 58*(3), 257-266. doi: https://doi.org/10.1016/S0034-4257(96)00067-3. Retrieved from http://www.sciencedirect.com/science/article/pii/S0034425796000673

Garrido Frenich, A., Jouan-Rimbaud, D., Massart, D. L., Kuttatharmmakul, S., Martínez Galera, M., & Martínez Vidal, J. L. (1995). Wavelength selection method for

multicomponent spectrophotometric determinations using partial least squares. *The Analyst, 120*(12), 2787-2792. doi: 10.1039/AN9952002787. Retrieved from http://www.scopus.com/inward/record.url?eid=2-s2.0-0008641556&partnerID=40&md5=71e3d800eb4a9887545dd39f5d679e9b

Ghosh, A., Fassnacht, F. E., Joshi, P. K., & Koch, B. (2014). A framework for mapping tree species combining hyperspectral and LiDAR data: Role of selected classifiers and sensor across three spatial scales. *International Journal of Applied Earth Observation and Geoinformation, 26*(1), 49-63. doi: 10.1016/j.jag.2013.05.017. Retrieved from http://www.sciencedirect.com/science/article/pii/S0303243413000664

GIS Resources. (2015). *Types of interpolation methods*. Spatial Media and Services Enterprises, Retrieved October 19, 2017 from https://www.gisresources.com/types-interpolation-methods_3/

Gitelson, A., & Merzlyak, M. N. (1994). Quantitative estimation of chlorophyll-a using reflectance spectra: Experiments with autumn chestnut and maple leaves. *Journal of Photochemistry and Photobiology B: Biology, 22*(3), 247-252. doi: 10.1016/1011-1344(93)06963-4. Retrieved from http://www.sciencedirect.com/science/article/pii/1011134493069634

Gitelson, A. A., Gritz †, Y., & Merzlyak, M. N. (2003). Relationships between leaf chlorophyll content and spectral reflectance and algorithms for non-destructive chlorophyll assessment in higher plant leaves. *Journal of Plant Physiology, 160*(3), 271-282. doi: 10.1078/0176-1617-00887. Retrieved from http://www.sciencedirect.com/science/article/pii/S0176161704704034

Goel, P. K., Prasher, S. O., Landry, J. A., Patel, R. M., Viau, A. A., & Miller, J. R. (2003). Estimation of crop biophysical parameters through airborne and field hyperspectral remote sensing. *Transactions of the ASAE, 46*(4), 1235.

Goel, P. K., Prasher, S. O., Patel, R. M., Landry, J. A., Bonnell, R. B., & Viau, A. A. (2003). Classification of hyperspectral data by decision trees and artificial neural networks to identify weed stress and nitrogen status of corn. *Computers and Electronics in Agriculture, 39*(2), 67-93. doi: 10.1016/S0168-1699(03)00020-6. Retrieved from http://www.sciencedirect.com/science/article/pii/S0168169903000206

González, I., Lé Cao, K.-A., & Déjean, S. (2011). *mixOmics: Omics data integration project*. Retrieved January, 2016 from www.mixomics.org

Grain Research and Development Corporation, G. 2013, *The influence of surface temperature inversions on spray operations*, Grain Research and Development Corporation, GRDC. Retrieved from https://www.grdc.com.au/Resources/Factsheets/2013/08/Surface-temperature-inversions-and-spraying-surface-temperature-inversions-and-spraying

Grossmann, K. (2010). Auxin herbicides: current status of mechanism and mode of action. *Pest Management Science, 66*(2), 113-120. doi: 10.1002/ps.1860. Retrieved from http://dx.doi.org/10.1002/ps.1860

Hai-bin, Q., Dan-lin, O., & Yi-yu, C. (2005). Background correction in near-infrared spectra of plant extracts by orthogonal signal correction. *Journal of Zhejiang University Science B, 6*(8), 838-843. doi: 10.1007/bf02842446. Retrieved from https://doi.org/10.1007/BF02842446

Hämmerle, M. (2013. LiDAR research group completes multitemporal multisensor data for boosting quality of plant growth models. *GIScience News Blog*. Retrieved from http://k1z.blog.uni-heidelberg.de/2013/06/25/lidar-research-group-completes-multitemporal-multisensor-data-for-boosting-quality-of-plant-growth-models/

Harrys Geospatial Solutions. (2017). *Basic hyperspectral analysis tutorial*. Retrieved March, 2017 from https://www.harrisgeospatial.com/docs/hyperspectralanalysistutorial.html

Helland, I. S., Næs, T., & Isaksson, T. (1995). Related versions of the multiplicative scatter correction method for preprocessing spectroscopic data. *Chemometrics and Intelligent Laboratory Systems, 29*(2), 233-241. doi: 10.1016/0169-7439(95)80098-T. Retrieved from http://www.sciencedirect.com/science/article/pii/016974399580098T

Henry, W. B., Shaw, D. R., Reddy, K. R., Bruce, L. M., & Tamhankar, H. D. (2004). Remote sensing to detect herbicide drift on crops. *WEED TECHNOLOGY, 18*(2), 358-368. doi: 10.1614/WT-03-098. Retrieved from http://dx.doi.org/10.1614/WT-03-098

Hilker, T., van Leeuwen, M., Coops, N. C., Wulder, M. A., Newnham, G. J., Jupp, D. L. B., & Culvenor, D. S. (2010). Comparing canopy metrics derived from terrestrial and airborne laser scanning in a Douglas-fir dominated forest stand. *Trees, 24*(5), 819-832. doi: 10.1007/s00468-010-0452-7

Hoffmeister, D., Bolten, A., Curdt, C., Waldhoff, G., & Bareth, G. (2010). *High resolution crop surface models (CSM) and crop volume models (CVM) on field level by terrestrial laser scanning.* In Proc. SPIE 7840, Sixth International Symposium on Digital Earth: Models, Algorithms, and Virtual Reality, 78400E, Beijing, China. Retrieved from https://www.spiedigitallibrary.org/conference-proceedings-of-spie/7840/78400E/High-resolution-Crop-Surface-Models-CSM-and-Crop-Volume-Models/10.1117/12.872315.short

Hosoi, F., & Omasa, K. (2009). Estimating vertical plant area density profile and growth parameters of a wheat canopy at different growth stages using three-dimensional portable lidar imaging. *ISPRS Journal of Photogrammetry and Remote Sensing, 64*(2), 151-158. doi: 10.1016/j.isprsjprs.2008.09.003. Retrieved from http://www.sciencedirect.com/science/article/pii/S0924271608001019

Huang, Y., Reddy, K. N., Thomson, S. J., & Yao, H. (2015). Assessment of soybean injury from glyphosate using airborne multispectral remote sensing. *Pest Management Science, 71*(4), 545-552. doi: 10.1002/ps.3839. Retrieved from http://dx.doi.org/10.1002/ps.3839

Huang, Y., & Thomson, S. J. (2010). *Airborne multispectral and thermal remote sensing for detecting the onset of crop stress caused by multiple factors.* In Proc. SPIE 7824, Remote Sensing for Agriculture, Ecosystems, and Hydrology XII Retrieved from http://proceedings.spiedigitallibrary.org/proceeding.aspx?articleid=724906

Huete, A., Didan, K., Miura, T., Rodriguez, E. P., Gao, X., & Ferreira, L. G. (2002). Overview of the radiometric and biophysical performance of the MODIS vegetation indices. *Remote Sensing of Environment, 83*(1–2), 195-213. doi: 10.1016/S0034-4257(02)00096-2. Retrieved from http://www.sciencedirect.com/science/article/pii/S0034425702000962

Huete, A., Justice, C., & Liu, H. (1994). Development of vegetation and soil indices for MODIS-EOS. *Remote Sensing of Environment, 49*(3), 224-234.

Huete, A. R. (1988). A soil-adjusted vegetation index (SAVI). *Remote Sensing of Environment, 25*(3), 295-309.

Huete, A. R., Liu, H. Q., Batchily, K., & van Leeuwen, W. (1997). A comparison of vegetation indices over a global set of TM images for EOS-MODIS. *Remote Sensing of Environment, 59*(3), 440-451. doi: 10.1016/S0034-4257(96)00112-5. Retrieved from http://www.sciencedirect.com/science/article/pii/S0034425796001125

Hunt, E. R., & Rock, B. N. (1989). Detection of changes in leaf water content using near- and middle-infrared reflectances. *Remote Sensing of Environment, 30*(1), 43-54. doi: 10.1016/0034-4257(89)90046-1. Retrieved from http://www.sciencedirect.com/science/article/pii/0034425789900461

Indahl, U., & Næs, T. (2004). A variable selection strategy for supervised classification with continuous spectroscopic data. *Journal of Chemometrics, 18*(2), 53-61. doi: 10.1002/cem.836. Retrieved from http://dx.doi.org/10.1002/cem.836

Indahl, U. G., Liland, K. H., & Næs, T. (2009). Canonical partial least squares—a unified PLS approach to classification and regression problems. *Journal of Chemometrics, 23*(9), 495-504. doi: 10.1002/cem.1243. Retrieved from http://dx.doi.org/10.1002/cem.1243

Industry Task Force II on 2-4-D Research Data. (2013). *Protecting food crops from yield loss*. Retrieved November 18, 2013 from http://www.24d.org/benefits/default.aspx

János, T. (2011). *Precision agriculture*. Debreceni Egyetem a TÁMOP 4.1.2 pályázat keretein belül. http://www.tankonyvtar.hu/en/tartalom/tamop425/0032_precizios_mezogazdasag/adatok.html. Retrieved from http://www.tankonyvtar.hu/en/tartalom/tamop425/0032_precizios_mezogazdasag/adatok.html

Jensen, J. L. R., Humes, K. S., Vierling, L. A., & Hudak, A. T. (2008). Discrete return lidar-based prediction of leaf area index in two conifer forests. *Remote Sensing of Environment, 112*(10), 3947-3957. doi: 10.1016/j.rse.2008.07.001

Jiang, M., Wang, C., Zhang, Y., Feng, Y., Wang, Y., & Zhu, Y. (2014). Sparse Partial-least-squares discriminant analysis for different geographical origins of *Salvia miltiorrhiza* by 1H-NMR-based metabolomics. *Phytochemical Analysis, 25*(1), 50-58. doi: 10.1002/pca.2461. Retrieved from http://dx.doi.org/10.1002/pca.2461

Jiang, Z., Huete, A. R., Didan, K., & Miura, T. (2008). Development of a two-band enhanced vegetation index without a blue band. *Remote Sensing of Environment, 112*(10), 3833-3845. doi: 10.1016/j.rse.2008.06.006. Retrieved from http://www.sciencedirect.com/science/article/pii/S0034425708001971

Jordan, C. F. (1969). Derivation of leaf-area index from quality of light on the forest floor. *Ecology, 50*(4), 663-666. doi: 10.2307/1936256. Retrieved from http://www.jstor.org/stable/1936256

Kantartzi, S. K., & Stewart, J. M. (2013). Growth and production of cotton. *Encyclopedia of Life support Systems (EOLSS), 2*. http://www.eolss.net/sample-chapters/c10/e1-05a-

20-00.pdf. Retrieved from http://www.eolss.net/sample-chapters/c10/e1-05a-20-00.pdf

Kappler, B., & Namuth, D. (2004). *Herbicide classification*. Plant & Soil Sciences eLibraryPRO, Retrieved March 21, 2013 from http://passel.unl.edu/pages/informationmodule.php?idinformationmodule=1059083105&topicorder=5&maxto=5&minto=1

Kaufman, Y. J., Wald, A. E., Remer, L. A., Bo-Cai, G., Rong-Rong, L., & Flynn, L. (1997). The MODIS 2.1-μm channel-correlation with visible reflectance for use in remote sensing of aerosol. *IEEE Transactions on Geoscience and Remote Sensing, 35*(5), 1286-1298. doi: 10.1109/36.628795

Khanna, S., Palacios-Orueta, A., Whiting, M. L., Ustin, S. L., Riaño, D., & Litago, J. (2007). Development of angle indexes for soil moisture estimation, dry matter detection and land-cover discrimination. *Remote Sensing of Environment, 109*(2), 154-165. doi: 10.1016/j.rse.2006.12.018. Retrieved from http://www.sciencedirect.com/science/article/pii/S003442570700003X

Knight, E., & Kvaran, G. (2014). Landsat-8 operational land imager design, characterization and performance. *Remote Sensing, 6*(11), 10286. doi: 10.3390/rs61110286. Retrieved from http://www.mdpi.com/2072-4292/6/11/10286

Kuhn, M. (2008). Building predictive models in R using the Caret package. *Journal of Statistical Software, 28*(5).

Lagomasino, D., Price, R. M., Whitman, D., Campbell, P. K. E., & Melesse, A. (2014). Estimating major ion and nutrient concentrations in mangrove estuaries in Everglades National Park using leaf and satellite reflectance. *Remote Sensing of Environment, 154*, 202-218. doi: 10.1016/j.rse.2014.08.022. Retrieved from http://www.sciencedirect.com/science/article/pii/S0034425714003198

Landsat. (2017, June 22). *Landsat collections*. U.S. Geological Survey, Retrieved October 19, 2017 from https://landsat.usgs.gov/landsat-collections

Lefsky, M. A., Cohen, W. B., Parker, G. G., & Harding, D. J. (2002). LiDAR remote sensing for ecosystem studies. *BioScience, 52*(1), 19. doi: https://doi.org/10.1641/0006-3568(2002)052[0019:LRSFES]2.0.CO;2. Retrieved from https://academic.oup.com/bioscience/article/52/1/19-30/291259

Li, H., Lascano, R. J., Barnes, E. M., Booker, J., Wilson, L. T., Bronson, K. F., & Segarra, E. (2001). Multispectral reflectance of cotton related to plant growth, soil water and texture, and site elevation. *AGRONOMY JOURNAL, 93*(6), 1327-1337.

LiCOR. (1999). *Using the LI-6400. Portable photosynthesis system*

Liu, L. Y., Zhao, J. J., & Guan, L. L. (2013). Tracking photosynthetic injury of Paraquat-treated crop using chlorophyll fluorescence from hyperspectral data. *European journal of remote sensing, 46*, 459-473. doi:10.5721/EuJRS20134627.

Liu, S., Peng, Y., Du, W., Le, Y., & Li, L. (2015). Remote estimation of leaf and canopy water content in winter wheat with different vertical distribution of water-related properties. *Remote Sensing, 7*(4), 4626. http://www.mdpi.com/2072-4292/7/4/4626. Retrieved from http://www.mdpi.com/2072-4292/7/4/4626

Luo, J., Ying, K., He, P., & Bai, J. (2005). Properties of Savitzky–Golay digital differentiators. *Digital Signal Processing, 15*(2), 122-136. doi: 10.1016/j.dsp.2004.09.008. Retrieved from http://www.sciencedirect.com/science/article/pii/S1051200404000727

Maptek™ I-Site™ Studio 2015, *I-Site Studio Training Manual Version 6.0*, Maptek™.

Marshall, M., & Thenkabail, P. (2015). Advantage of hyperspectral EO-1 Hyperion over multispectral IKONOS, GeoEye-1, WorldView-2, Landsat ETM+, and MODIS vegetation indices in crop biomass estimation. *ISPRS Journal of Photogrammetry and Remote Sensing, 108*, 205-218. doi: 10.1016/j.isprsjprs.2015.08.001. Retrieved from http://www.sciencedirect.com/science/article/pii/S0924271615001926

Martinez-Morales, R. (2012). Using remotely sensed imagery for forest resource assessment and inventory. In Dr Juan A Blanco (Ed.), Forest Ecosystems – More than Just Trees (March 7 ed., 10.5772/30140pp. 165-178). InTech. doi: 10.5772/30140. Retrieved from http://www.intechopen.com/download/get/type/pdfs/id/30811

Merton, R., Sugianto, J. F., & Huntington, J. (2004). *A multi-temporal and multi-angular study of hyperspectral data related to the biophysical properties of cotton crops and soil characteristics, NSW, Australia.* In Proceedings of the 2nd CHRIS/Proba Workshop, ESRIN, Frascati, Italy. Retrieved from http://earth.esa.int/workshops/chris_proba_04/papers/19_merton.pdf

Mevik, B.-H., & Wehrens, R. (2007). The pls package: principal component and partial least squares regression in R. *Journal of Statistical Software, 18*(2), 1-24.

Mevik, B. H., & Cederkvist, H. R. (2004). Mean squared error of prediction (MSEP) estimates for principal component regression (PCR) and partial least squares regression (PLSR). *Journal of Chemometrics, 18*(9), 422-429. doi: 10.1002/cem.887. Retrieved from http://dx.doi.org/10.1002/cem.887

Mewes, T., Franke, J., & Menz, G. (2009). *Data reduction of hyperspectral remote sensing data for crop stress detection using different band selection methods.* In Geoscience and Remote Sensing Symposium,2009 IEEE International,IGARSS 2009 Retrieved from http://ieeexplore.ieee.org/ielx5/5403226/5417750/05418292.pdf?tp=&arnumber=5418292&isnumber=5417750

Miller, H. M., Richardson, L., Koontz, S. R., Loomis, J., & Koontz, L. 2013, *Users, uses, and value of landsat satellite imagery. Results from the 2012 survey of users*, 2013–1269, U.S. Department of the Interior and U.S. Geological Survey. NASA.

Moran, M. S., Inoue, Y., & Barnes, E. M. (1997). Opportunities and limitations for image-based remote sensing in precision crop management. *Remote Sensing of Environment, 61*(3), 319-346. doi: 10.1016/S0034-4257(97)00045-X. Retrieved from http://www.sciencedirect.com/science/article/pii/S003442579700045X

http://ac.els-cdn.com/S003442579700045X/1-s2.0-S003442579700045X-main.pdf?_tid=030cfe26-7cba-11e3-b576-00000aab0f02&acdnat=1389662590_c2debd11c195cf81a1216bbab0598187

http://ac.els-cdn.com/S003442579700045X/1-s2.0-S003442579700045X-main.pdf?_tid=0adf19cc-7cba-11e3-b9de-00000aab0f02&acdnat=1389662604_85ac2ec50c9a694ee95a5ca4d9307137

Muharam, F. M., Bronson, K. F., Maas, S. J., & Ritchie, G. L. (2014). Inter-relationships of cotton plant height, canopy width, ground cover and plant nitrogen status indicators. *Field Crops Research, 169*, 58-69. doi: 10.1016/j.fcr.2014.09.008

Munk, D., Hembree, K., Al-Khatib, K., Hutmacher, B., Munier, D., & Wright, S. (2014). *Synthetic auxin herbicide injury in cotton*. UCCE Cotton Production Guide- lines, (http://cottoninfo.ucdavis.edu/files/149596.pdf). University of California Cooperative Extension.

MyBMP. (2016). *BMP - Best management practices*. Retrieved May 17, 2016 from https://www.mybmp.com.au/What_is_different.aspx

NASA. (2017, May 1). *Operational land imager*. NASA, Retrieved January 3, 2014 from http://landsat.gsfc.nasa.gov/?p=5107

National Cotton Council of America. (2013a). *Growth and Development of a Cotton Plant*. Retrieved 3 July, 2013 from http://www.cotton.org/tech/ace/growth-and-development.cfm

National Cotton Council of America. (2013b). *Plant Growth Regulators (PGRs)*. Retrieved 12 June, 2013 from http://www.cotton.org/tech/ace/growth-and-development.cfm

Nicolai, D., Stahl, L., & Herzfeld, D. (2015). *When is it too windy to spray?* University of Minnesota, Extention, Retrieved January, 2015 from http://blog-crop-news.extension.umn.edu/2015/06/when-is-it-too-windy-to-spray.html

North Carolina State University. (2015). *Herbicide injury factsheets*. NC State Extention, Retrieved May, 2016 from https://content.ces.ncsu.edu/catalog/series/184/

North Carolina State University Extension Service 2010, *2010 Cotton information*, C. o. A. a. L. S. N. C. C. E. Service.

Olivieri, A. C. (2015). Practical guidelines for reporting results in single- and multi-component analytical calibration: A tutorial. *Analytica Chimica Acta, 868*, 10-22. doi: 10.1016/j.aca.2015.01.017. Retrieved from http://www.sciencedirect.com/science/article/pii/S0003267015000537

Omasa, K., Hosoi, F., & Konishi, A. (2007). 3D lidar imaging for detecting and understanding plant responses and canopy structure. *Journal of Experimental Botany, 58*(4), 881-898. doi: 10.1093/jxb/erl142

Oosterhuis, D. M. (1990). Growth and development of the cotton plant. In W. N. M. a. D. M. Oosterhuis (Ed.), *Nitrogen nutrition in cotton: Practical Issues Proc Southern Branch Workshop for Practicing Agronomists.* (pp. 1-24). Madison, WI: Publ. Amer. Soc. Agron.

Oosterhuis, D. M., & Kerby, T. A. (2008). Measures of Cotton Growth and Development. In DM Oosterhuis & TA Kerby (Eds.), COTMAN Crop Management System (pp. 21). Arkansas, USA: Division of Agriculture and Cotton Incorporated, University of Arkansas.

Ortiz, B. V., Thomson, S. J., Huang, Y., Reddy, K. N., & Ding, W. (2011). Determination of differences in crop injury from aerial application of glyphosate using vegetation indices. *Computers and Electronics in Agriculture, 77*(2), 204-213. doi:

10.1016/j.compag.2011.05.004. Retrieved from http://www.sciencedirect.com/science/article/pii/S0168169911001025

Perumal, N. K., Hebbar, K. B., Rao, M. R. K., & Singh, P. 2006, *Physiological disorders in cotton*, Central Institute for Cotton Research. Nagpur, India. Retrieved from http://www.cicr.org.in/pdf/physiological_disorder.pdf

Pimentel, D., Greiner, A., & Bashore, T. (1998). Environmental toxicology current development. In J. Rose (Ed.), Environmental Toxicology (pp. xii , 397, 393 p). Gordon and Breach Science Publishers.

Pinter, P. J., Hatfield, J. L., Schepers, J. S., Barnes, E. M., Moran, M. S., Daughtry, C. S. T., & Upchurch, D. R. (2003). Remote sensing for crop management. *PHOTOGRAMMETRIC ENGINEERING AND REMOTE SENSING, 69*(6), 647-664.

Pinty, B., & Verstraete, M. M. (1992). GEMI: A non-linear Index to monitor global vegetation from satellites. *Vegetatio, 101*(1), 15-20. doi: 10.1007/BF00031911

Plant, R. E., Munk, D. S., Roberts, B. R., Vargas, R. L., Rains, D. W., Travis, R. L., & Hutmacher, R. B. (2000). Relationships between remotely sensed reflectance data and cotton growth and yield. *Transactions of the ASAE, 43*(3), 535-546.

Price, J. C. (1998). An approach for analysis of reflectance spectra. *Remote Sensing of Environment, 64*(3), 316-330. doi: 10.1016/S0034-4257(98)00008-X. Retrieved from http://www.sciencedirect.com/science/article/pii/S003442579800008X

Quinn, J., & Kelly, D. (2011). Crop growth stages (C. E. Team, Trans.)Australian Cotton Production Manual 2011 (2 ed., Australia.

R Core Team. (2014). R: A language and environment for statistical computing. Viena, Austria: R Foundation for Statistical Computing. Retrieved from http://www.R-project.org

R Core Team. (2015). Fitting linear models (Version 3.2.0). Retrieved from https://stat.ethz.ch/R-manual/R-devel/library/stats/html/lm.html

Rama Rao, N. (2008). Development of a crop-specific spectral library and discrimination of various agricultural crop varieties using hyperspectral imagery. *International Journal of Remote Sensing, 29*(1), 131-144. doi: 10.1080/01431160701241779. Retrieved from http://dx.doi.org/10.1080/01431160701241779

Rama Rao, N., Garg, P. K., Ghosh, S. K., & Dadhwal, V. K. (2008). Estimation of leaf total chlorophyll and nitrogen concentrations using hyperspectral satellite imagery. *The Journal of Agricultural Science, 146*(1), 65-75. doi: 10.1017/S0021859607007514. Retrieved from http://dx.doi.org/10.1017/S0021859607007514

Rapaport, T., Hochberg, U., Shoshany, M., Karnieli, A., & Rachmilevitch, S. (2015). Combining leaf physiology, hyperspectral imaging and partial least squares-regression (PLS-R) for grapevine water status assessment. *ISPRS Journal of Photogrammetry and Remote Sensing, 109*, 88-97. doi: 10.1016/j.isprsjprs.2015.09.003. Retrieved from http://www.sciencedirect.com/science/article/pii/S092427161500204X

Rhodes, G. N. J., Israel, T. D., & Steckel, L. 2012, *Diagnosing suspected off-target herbicide damage to cotton*, W 291-B, Institute of Agriculture, The University of Tennessee,.

Retrieved from http://trace.tennessee.edu/utk_agexcrop/?utm_source=trace.tennessee.edu%2Futk_agexcrop%2F137&utm_medium=PDF&utm_campaign=PDFCoverPages

Ritchie, G. L., Bednarz, C. W., Jost, P. H., & Brown, S. M. 2004, *Cotton growth and development*, C. E. Service, The University of Georgia College of Agricultural and Environmental Sciences. Retrieved from http://www.spar.msstate.edu/class/EPP-2008/Chapter%201/Reading%20material/Temperature%20including%20Extremes/cotton_heat_Units1.pdf

Robles, W., Madsen, J. D., & Wersal, R. M. (2010). Potential for remote sensing to detect and predict herbicide injury on waterhyacinth (Eichhornia crassipes). *Invasive Plant Science and Management, 3*(4), 440-450. doi: 10.1614/IPSM-D-09-00040.1

Rodríguez-Gonzálvez, P., Muñoz-Nieto, Á. L., Zancajo-Blázquez, S., & González-Aguilera, D. (2016). *Geomatics and forensic: Progress and challenges* (50528). doi:50528. Retrieved from http://www.intechopen.com/books/export/citation/EndNote/forensic-analysis-from-death-to-justice/geomatics-and-forensic-progress-and-challenges

Rondeaux, G., Steven, M., & Baret, F. (1996). Optimization of soil-adjusted vegetation indices. *Remote Sensing of Environment, 55*(2), 95-107. doi: 10.1016/0034-4257(95)00186-7. Retrieved from http://www.sciencedirect.com/science/article/pii/0034425795001867

Roseboro, K. (2014). *New GMOs, herbicide threaten to force family off organic farm*. The Organic & Non-GMO Report, Retrieved March, 2017 from http://non-gmoreport.com/articles/october-2014/new-GMOs-herbicides-threaten-family-organic-farm.php

Rosell, J. R., Llorens, J., Sanz, R., Arnó, J., Ribes-Dasi, M., Masip, J., . . . Palacín, J. (2009). Obtaining the three-dimensional structure of tree orchards from remote 2D terrestrial LIDAR scanning. *Agricultural and Forest Meteorology, 149*(9), 1505-1515. doi: 10.1016/j.agrformet.2009.04.008. Retrieved from www.sciencedirect.com/science/article/pii/S0168192309000926

Rosell Polo, J. R., Sanz, R., Llorens, J., Arnó, J., Escolà, A., Ribes-Dasi, M., . . . Palacín, J. (2009). A tractor-mounted scanning LIDAR for the non-destructive measurement of vegetative volume and surface area of tree-row plantations: A comparison with conventional destructive measurements. *Biosystems Engineering, 102*(2), 128-134. doi: 10.1016/j.biosystemseng.2008.10.009. Retrieved from www.sciencedirect.com/science/article/pii/S1537511008003231

Roujean, J.-L., & Breon, F.-M. (1995). Estimating PAR absorbed by vegetation from bidirectional reflectance measurements. *Remote Sensing of Environment, 51*(3), 375-384. doi: 10.1016/0034-4257(94)00114-3. Retrieved from http://www.sciencedirect.com/science/article/pii/0034425794001143

Rouse, J. W., Haas, R. H., Schell, J. A., & Deering, D. W. (1974). *Monitoring vegetation systems in the Great Plains with ERTS.* In Third ERTS Symposium, Washington, DC.

San José Alonso, J. I., Martínez Rubio, J., Fernández Martín, J. J., & García Fernández, J. (2011). *Comparing time-of-flight and phase-shift. The survey of the Royal Pantheon in the Basilica of San Isidoro (León)*. Paper presented at the International Archives

of the Photogrammetry, Remote Sensing and Spatial Information Sciences - ISPRS Archives, Trento, Italy.

Schlemmer, M., Gitelson, A., Schepers, J., Ferguson, R., Peng, Y., Shanahan, J., & Rundquist, D. (2013). Remote estimation of nitrogen and chlorophyll contents in maize at leaf and canopy levels. *International Journal of Applied Earth Observation and Geoinformation, 25*, 47-54. doi: 10.1016/j.jag.2013.04.003. Retrieved from http://www.sciencedirect.com/science/article/pii/S0303243413000469

Schmidt, K. S., & Skidmore, A. K. (2004). Smoothing vegetation spectra with wavelets. *International Journal of Remote Sensing, 25*(6), 1167-1184. doi: 10.1080/0143116031000115085. Retrieved from http://dx.doi.org/10.1080/0143116031000115085

Schwartz, A. (1984). Metabolic energy for stomatal opening. Roles of photophosphorylation and oxidative phosphorylation. *Planta, 161*(2), 129-136. doi: 10.1007/BF00395472

Sluijs, M. H. v. d., Long, R. L., & Bange, M. P. (2015). Comparing cotton fiber quality from conventional and round module harvesting methods. *Textile Research Journal, 85*(9), 987-997. doi: doi:10.1177/0040517514540770. Retrieved from http://journals.sagepub.com/doi/abs/10.1177/0040517514540770

Smith, D. T., & Wiese, A. F. (1972). Cotton response to low rates of 2,4-D and other herbicides (http://hdl.handle.net/1969.1/92985pp. 8). Texas Agricultural Experiment Station. Retrieved from http://hdl.handle.net/1969.1/92985

Smith, W. F. (2005). *Experimental Design for Formulation* (Vol. 15). Society for Industrial and Applied Mathematics. https://books.google.com.au/books?id=nIir8fVFgPcC. Retrieved from https://books.google.com.au/books?id=nIir8fVFgPcC

Spiess, A.-N., & Neumeyer, N. (2010). An evaluation of R2 as an inadequate measure for nonlinear models in pharmacological and biochemical research: A Monte Carlo approach. *BMC Pharmacology, 10*, 6-6. doi: 10.1186/1471-2210-10-6. Retrieved from http://www.ncbi.nlm.nih.gov/pmc/articles/PMC2892436/

Stevens, A., & Ramirez-Lopez, L. (2014). *An introduction to the prospectr package*: R package vignette

Straub, P., Shen, Q., & Ho, T.-h. (1994). Structure and promoter analysis of an ABA- and stress-regulated barley gene, HVA1. *Plant Molecular Biology, 26*(2), 617-630. doi: 10.1007/BF00013748. Retrieved from http://dx.doi.org/10.1007/BF00013748

Suarez, L. A., Apan, A., & Werth, J. (2016). Hyperspectral sensing to detect the impact of herbicide drift on cotton growth and yield. *ISPRS Journal of Photogrammetry and Remote Sensing, 120*, 65-76. doi: 10.1016/j.isprsjprs.2016.08.004. Retrieved from http://www.sciencedirect.com/science/article/pii/S0924271616302635

Suarez, L. A., Apan, A., & Werth, J. (2017). Detection of phenoxy herbicide dosage in cotton crops through the analysis of hyperspectral data. *International Journal of Remote Sensing, 38*(23), 6528-6553. doi: 10.1080/01431161.2017.1362128. Retrieved from http://dx.doi.org/10.1080/01431161.2017.1362128

Sullivan, D. G., Fulton, J., Shaw, J., & Bland, G. (2007). Evaluating the sensitivity of an unmanned thermal infrared aerial system to detect water stress in a cotton canopy. *Transactions of the ASABE, 50*(6), 1963-1969.

Sun, S., Li, C., & Paterson, A. (2017). In-field high-throughput phenotyping of cotton plant height using LiDAR. *Remote Sensing, 9*(4), 377. http://www.mdpi.com/2072-4292/9/4/377. Retrieved from http://www.mdpi.com/2072-4292/9/4/377

Swatantran, A., Dubayah, R., Roberts, D., Hofton, M., & Blair, J. B. (2011). Mapping biomass and stress in the Sierra Nevada using lidar and hyperspectral data fusion. *Remote Sensing of Environment, 115*(11), 2917-2930. doi: 10.1016/j.rse.2010.08.027. Retrieved from http://www.sciencedirect.com/science/article/pii/S0034425711001374

Tan, K. P., Kanniah, K. D., & Cracknell, A. P. (2012). A review of remote sensing based productivity models and their suitability for studying oil palm productivity in tropical regions. *Progress in Physical Geography, 36*(5), 655-679. doi: 10.1177/0309133312452187

Teixeira, M. C., Duque, P., & Sá-Correia, I. (2007). Environmental genomics: mechanistic insights into toxicity of and resistance to the herbicide 2,4-D. *Trends in Biotechnology, 25*(8), 363-370. doi: 10.1016/j.tibtech.2007.06.002. Retrieved from http://www.sciencedirect.com/science/article/pii/S0167779907001400

The Australian Cotton Industry Development & Delivery Team 2013, *WATERpak – a guide for irrigation management in cotton and grain farming systems*, Cotton Research and Development Corporation.

Thenkabail, P. S., Smith, R. B., & De Pauw, E. (2000). Hyperspectral vegetation indices and their relationships with agricultural crop characteristics. *Remote Sensing of Environment, 71*(2), 158-182. doi: 10.1016/S0034-4257(99)00067-X. Retrieved from http://www.sciencedirect.com/science/article/pii/S003442579900067X

Thissen, U., Pepers, M., Üstün, B., Melssen, W. J., & Buydens, L. M. C. (2004). Comparing support vector machines to PLS for spectral regression applications. *Chemometrics and Intelligent Laboratory Systems, 73*(2), 169-179. doi: https://doi.org/10.1016/j.chemolab.2004.01.002. Retrieved from http://www.sciencedirect.com/science/article/pii/S0169743904000103

Thorp, K. R., Gore, M. A., Andrade-Sanchez, P., Carmo-Silva, A. E., Welch, S. M., White, J. W., & French, A. N. (2015). Proximal hyperspectral sensing and data analysis approaches for field-based plant phenomics. *Computers and Electronics in Agriculture, 118*, 225-236. doi: 10.1016/j.compag.2015.09.005. Retrieved from http://www.sciencedirect.com/science/article/pii/S016816991500280X

Thulin, S., Hill, M. J., Held, A., Jones, S., & Woodgate, P. (2012). Hyperspectral determination of feed quality constituents in temperate pastures: Effect of processing methods on predictive relationships from partial least squares regression. *International Journal of Applied Earth Observation and Geoinformation, 19*, 322-334. doi: 10.1016/j.jag.2012.06.006. Retrieved from http://www.sciencedirect.com/science/article/pii/S0303243412001341

Tian, P., Zhao, G., Li, J., Gao, J., & Zhang, Z. (2012). Integration of monthly water balance modeling and nutrient load estimation in an agricultural catchment. *International Journal of Environmental Science and Technology, 9*(1), 163-172. doi: 10.1007/s13762-011-0010-x. Retrieved from http://dx.doi.org/10.1007/s13762-011-0010-x

Tian, Y., Zhu, Y., & Cao, W. (2005). Monitoring leaf photosynthesis with canopy spectral reflectance in rice. *Photosynthetica, 43*(4), 481-489. doi: 10.1007/s11099-005-0078-y. Retrieved from http://dx.doi.org/10.1007/s11099-005-0078-y

Tilly, N., Hoffmeister, D., Aasen, H., Brands, J., & Bareth, G. (2014). Multi-temporal crop surface models derived from terrestrial laser scanning for accurate plant height measurement and biomass estimation of barley. In J. Bendig & G. Bareth (Eds.). *Proceedings of the Workshop on UAV-based Remote Sensing Methods for Monitoring Vegetation.* (pp. 83 - 91). Cologne, Germany.

Tivendale, N. D., Le Signor, C., Thompson, R., Horne, J., Reid, J. B., Ross, J. J., . . . Bala, R. K. (2012). Biosynthesis of the halogenated auxin, 4-chloroindole-3-acetic acid. *Plant physiology, 159*(3), 1055-1063. doi: 10.1104/pp.112.198457

Tran, T. N., Afanador, N. L., Buydens, L. M. C., & Blanchet, L. (2014). Interpretation of variable importance in Partial Least Squares with Significance Multivariate Correlation (sMC). *Chemometrics and Intelligent Laboratory Systems, 138*, 153-160. doi: 10.1016/j.chemolab.2014.08.005. Retrieved from http://www.sciencedirect.com/science/article/pii/S0169743914001786

Trenton, J. I. (2012). *Crop stress detection and classification using hyperspectral remote sensing.* (3505368 Ph.D.), Mississippi State University, Ann Arbor. Retrieved from http://search.proquest.com/docview/1013441862?accountid=14647 ProQuest Dissertations & Theses A&I database.

Tucker, C. J. (1979). Red and photographic infrared linear combinations for monitoring vegetation. *Remote Sensing of Environment, 8*(2), 127-150.

U.S. Geological Survey. (2016). *Landsat 8 (L8) data users handbook*. (LSDS-1574). Retrieved from https://landsat.usgs.gov/sites/default/files/documents/Landsat8DataUsersHandbook.pdf

University of Minnesota. (1999). *Herbicide mode of action and injury symptoms*. North Central Regional Extension, Retrieved July, 2014 from http://www.cof.orst.edu/cof/fs/kpuettmann/FS%20533/Vegetation%20Management/Herbicide%20Mode%20of%20Action%20and%20Injury%20Symptoms.htm

Vaiphasa, C. (2006). Consideration of smoothing techniques for hyperspectral remote sensing. *ISPRS Journal of Photogrammetry and Remote Sensing, 60*(2), 91-99. doi: 10.1016/j.isprsjprs.2005.11.002. Retrieved from http://www.sciencedirect.com/science/article/pii/S0924271605001012

Van der Sluijs, R. (2015). Beyond the farm gate, GinningAustralian Cotton Production Manual 2015 (pp. 152).

Vigneau, N., Ecarnot, M., Rabatel, G., & Roumet, P. (2011). Potential of field hyperspectral imaging as a non destructive method to assess leaf nitrogen content in wheat. *Field Crops Research, 122*(1), 25-31. doi: 10.1016/j.fcr.2011.02.003. Retrieved from http://www.sciencedirect.com/science/article/pii/S0378429011000451

Wang, H., Lin, H., Munroe, D. K., Zhang, X., & Liu, P. (2016). Reconstructing rice phenology curves with frequency-based analysis and multi-temporal NDVI in double-cropping area in Jiangsu, China. *Frontiers of Earth Science, 10*(2), 292-302.

doi: 10.1007/s11707-016-0552-9. Retrieved from https://doi.org/10.1007/s11707-016-0552-9

Wang, L., Qu, J. J., Hao, X., & Zhu, Q. (2008). Sensitivity studies of the moisture effects on MODIS SWIR reflectance and vegetation water indices. *International Journal of Remote Sensing, 29*(24), 7065-7075. doi: 10.1080/01431160802226034. Retrieved from http://dx.doi.org/10.1080/01431160802226034

Wang, T.-C., Ma, B. L., Xiong, Y.-C., & Li, F.-M. (2012). A reflectance-based method for estimating transpirational water use efficiency in maize exposed to drought stress. *Journal of Plant Nutrition, 35*(5), 651-663. doi: 10.1080/01904167.2012.636128. Retrieved from http://ezproxy.usq.edu.au/login?url=http://search.ebscohost.com/login.aspx?direct=true&db=a9h&AN=73326821&site=ehost-live

Wilson, J. (n.d.). *Pesticide Drift*. Center for Integrated Pest Management, Retrieved 21 May, 2013 from http://pesticidestewardship.org/drift/Pages/default.aspx

Wold, S., Sjöström, M., & Eriksson, L. (2001). PLS-regression: a basic tool of chemometrics. *Chemometrics and Intelligent Laboratory Systems, 58*(2), 109-130. doi: 10.1016/S0169-7439(01)00155-1. Retrieved from http://www.sciencedirect.com/science/article/pii/S0169743901001551

Yang, C., Everitt, J., & Bradford, J. (2006). Comparison of QuickBird satellite imagery and airborne imagery for mapping grain sorghum yield patterns. *An International Journal on Advances in Precision Agriculture, 7*(1), 33-44. doi: 10.1007/s11119-005-6788-0

Yang, C., Everitt, J., & Bradford, J. (2009). Evaluating high resolution SPOT 5 satellite imagery to estimate crop yield. *Precision Agriculture, 10*(4), 292-303. doi: 10.1007/s11119-009-9120-6

Yang, C., Everitt, J. H., & Bradford, J. M. (2002). Optimum time lag determination for yield monitoring with remotely sensed imagery. *Transactions of the ASAE, 45*(6), 1737. doi: 10.13031/2013.11420

Yang, C., Everitt, J. H., Bradford, J. M., & Murden, D. (2004). Airborne hyperspectral imagery and yield monitor data for mapping cotton yield variability. *Precision Agriculture, 5*(5), 445-461. doi: 10.1007/s11119-004-5319-8. Retrieved from http://dx.doi.org/10.1007/s11119-004-5319-8

Yi, Q.-x., Huang, J.-f., Wang, F.-m., & Wang, X.-z. (2008). Quantifying biochemical variables of corn by hyperspectral reflectance at leaf scale. *Journal of Zhejiang University Science B, 9*(5), 378-384. doi: 10.1631/jzus.B0730019. Retrieved from http://www.ncbi.nlm.nih.gov/pmc/articles/PMC2367376/

Yi, Q., Jiapaer, G., Chen, J., Bao, A., & Wang, F. (2014). Different units of measurement of carotenoids estimation in cotton using hyperspectral indices and partial least square regression. *ISPRS Journal of Photogrammetry and Remote Sensing, 91*, 72-84. doi: 10.1016/j.isprsjprs.2014.01.004. Retrieved from http://www.sciencedirect.com/science/article/pii/S0924271614000082

Yilmaz, M. T., Hunt Jr, E. R., & Jackson, T. J. (2008). Remote sensing of vegetation water content from equivalent water thickness using satellite imagery. *Remote Sensing of*

Environment, 112(5), 2514-2522. doi: 10.1016/j.rse.2007.11.014. Retrieved from http://www.sciencedirect.com/science/article/pii/S0034425707004798

Yu, K., Gnyp, M. L., Gao, L., Miao, Y., Chen, X., & Bareth, G. (2015). Estimate leaf chlorophyll of rice using reflectance indices and partial least squares. *Photogrammetrie - Fernerkundung - Geoinformation, 2015*(1), 45-54. doi: 10.1127/pfg/2015/0253. Retrieved from http://dx.doi.org/10.1127/pfg/2015/0253

Zainol Abdullah, W. N. Z., Apan, A. A., Maraseni, T. N., & Le Brocque, A. F. (2014). Spectral discrimination of bulloak (*Allocasuarina luehmannii*) and associated woodland for habitat mapping of the endangered bulloak jewel butterfly (*Hypochrysops piceata*) in southern Queensland. *Journal of Applied Remote Sensing, 8*(1), 083561-083561. doi: 10.1117/1.JRS.8.083561. Retrieved from http://dx.doi.org/10.1117/1.JRS.8.083561

Zarco-Tejada, P. J., Ustin, S. L., & Whiting, M. L. (2005). Temporal and spatial relationships between within-field yield variability in cotton and high-spatial hyperspectral remote sensing imagery. *AGRONOMY JOURNAL, 97*(3), 641-653. doi: 10.2134/agronj2003.0257. Retrieved from https://dl.sciencesocieties.org/publications/aj/abstracts/97/3/0641?highlight=&search-result=1?access=0&view=article

Zhai, Y., Cui, L., Zhou, X., Gao, Y., Fei, T., & Gao, W. (2013). Estimation of nitrogen, phosphorus, and potassium contents in the leaves of different plants using laboratory-based visible and near-infrared reflectance spectroscopy: Comparison of partial least-square regression and support vector machine regression methods. *International Journal of Remote Sensing, 34*(7), 2502-2518. doi: 10.1080/01431161.2012.746484. Retrieved from http://dx.doi.org/10.1080/01431161.2012.746484

Zhang, B. H., Wang, H. M., Liu, F., Li, Y. H., & Liu, Z. D. (2001). In vitro assay for 2,4-D resistance in transgenic cotton. *In Vitro Cellular & Developmental Biology - Plant, 37*(2), 300-304. doi: 10.1007/s11627-001-0053-7. Retrieved from http://dx.doi.org/10.1007/s11627-001-0053-7

Zhang, H., Lan, Y., Suh, C. P. C., Westbrook, J., Clint, H., W., Yang, C., & Huang, Y. (2013). Fusion of remotely sensed data from airborne and ground-based sensors to enhance detection of cotton plants. *Computers and Electronics in Agriculture, 93*, 55-59. doi: 10.1016/j.compag.2013.02.001. Retrieved from http://www.sciencedirect.com/science/article/pii/S0168169913000288

Zhang, L., & Grift, T. E. (2012). A LIDAR-based crop height measurement system for *Miscanthus giganteus*. *Computers and Electronics in Agriculture, 85*(0), 70-76. doi: 10.1016/j.compag.2012.04.001. Retrieved from http://www.sciencedirect.com/science/article/pii/S0168169912000877

Zhang, X., Liu, F., He, Y., & Gong, X. (2013). Detecting macronutrients content and distribution in oilseed rape leaves based on hyperspectral imaging. *Biosystems Engineering, 115*(1), 56-65. doi: https://doi.org/10.1016/j.biosystemseng.2013.02.007. Retrieved from http://www.sciencedirect.com/science/article/pii/S1537511013000378

Zhao, D., Huang, L., Li, J., & Qi, J. (2007). A comparative analysis of broadband and narrowband derived vegetation indices in predicting LAI and CCD of a cotton canopy. *ISPRS Journal of Photogrammetry and Remote Sensing, 62*(1), 25-33. doi:

10.1016/j.isprsjprs.2007.01.003. Retrieved from http://www.sciencedirect.com/science/article/pii/S0924271607000056

Zhao, D., Reddy, K. R., Kakani, V. G., Read, J. J., & Koti, S. (2007). Canopy reflectance in cotton for growth assessment and lint yield prediction. *European Journal of Agronomy, 26*(3), 335-344. doi: 10.1016/j.eja.2006.12.001. Retrieved from http://www.sciencedirect.com/science/article/pii/S1161030106001626

Zhao, D., Reddy, K. R., Kakani, V. G., & Reddy, V. R. (2005). Nitrogen deficiency effects on plant growth, leaf photosynthesis, and hyperspectral reflectance properties of sorghum. *European Journal of Agronomy, 22*(4), 391-403. doi: 10.1016/j.eja.2004.06.005. Retrieved from http://www.sciencedirect.com/science/article/pii/S116103010400053X

Zhao, K., Valle, D., Popescu, S., Zhang, X., & Mallick, B. (2013). Hyperspectral remote sensing of plant biochemistry using Bayesian model averaging with variable and band selection. *Remote Sensing of Environment, 132*, 102-119. doi: 10.1016/j.rse.2012.12.026. Retrieved from http://www.sciencedirect.com/science/article/pii/S0034425713000047

Zheng, G., & Moskal, L. M. (2012). Spatial variability of terrestrial laser scanning based leaf area index. *International Journal of Applied Earth Observation and Geoinformation, 19*(0), 226-237. doi: 10.1016/j.jag.2012.05.002. Retrieved from http://www.sciencedirect.com/science/article/pii/S0303243412000980

Zimmerman, D., Pavlik, C., Ruggles, A., & Armstrong, M. P. (1999). An experimental comparison of ordinary and universal kriging and inverse distance weighting. *Mathematical Geology, 31*(4), 375-390. doi: 10.1023/a:1007586507433. Retrieved from https://doi.org/10.1023/A:1007586507433

Zub, H. W., Arnoult, S., & Brancourt-Hulmel, M. (2011). Key traits for biomass production identified in different Miscanthus species at two harvest dates. *Biomass and Bioenergy, 35*(1), 637-651. doi: 10.1016/j.biombioe.2010.10.020

Appendices

CHAPTER 4

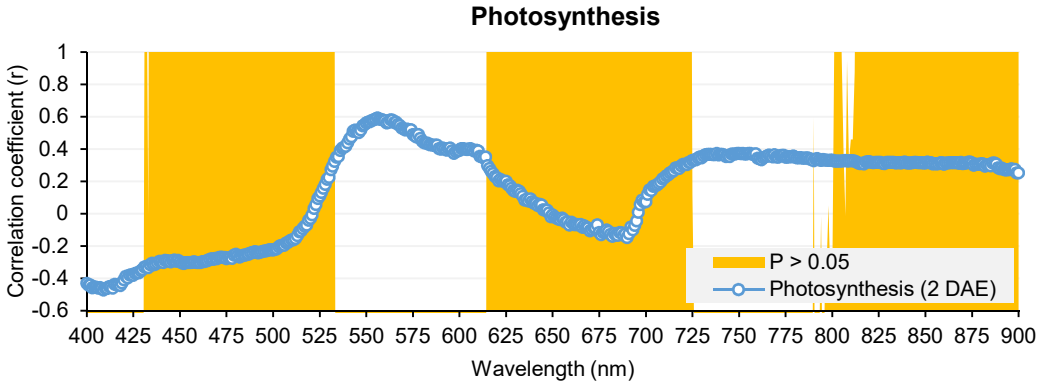

Appendix 4-1. Correlation between photosynthesis and reflectance data at two days after the exposure (2 DAE).

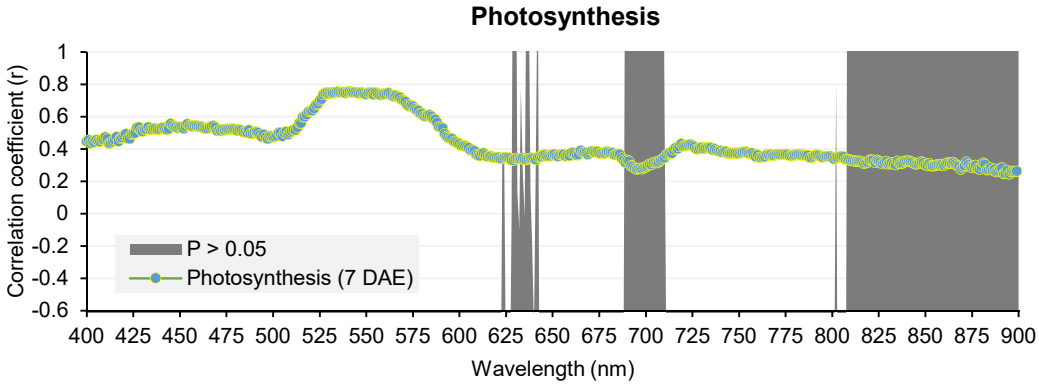

Appendix 4-2. Correlation between photosynthesis and reflectance data at seven days after the exposure (7 DAE).

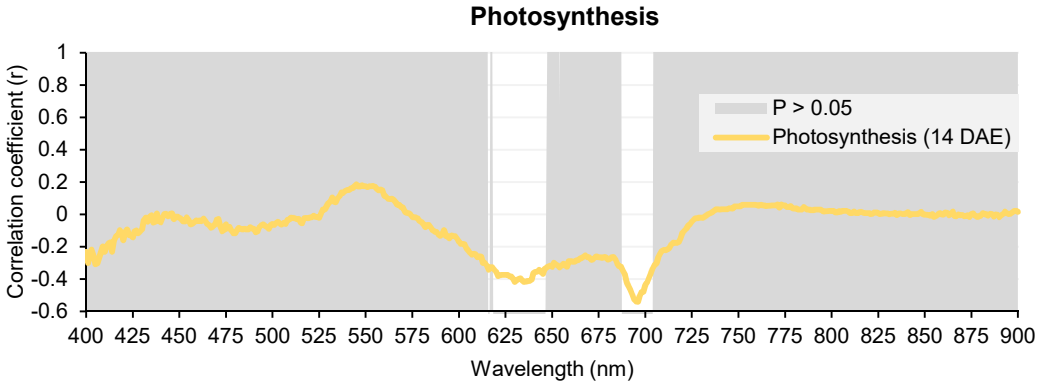

Appendix 4-3. Correlation between photosynthesis and reflectance data at 14 days after the exposure (14 DAE).

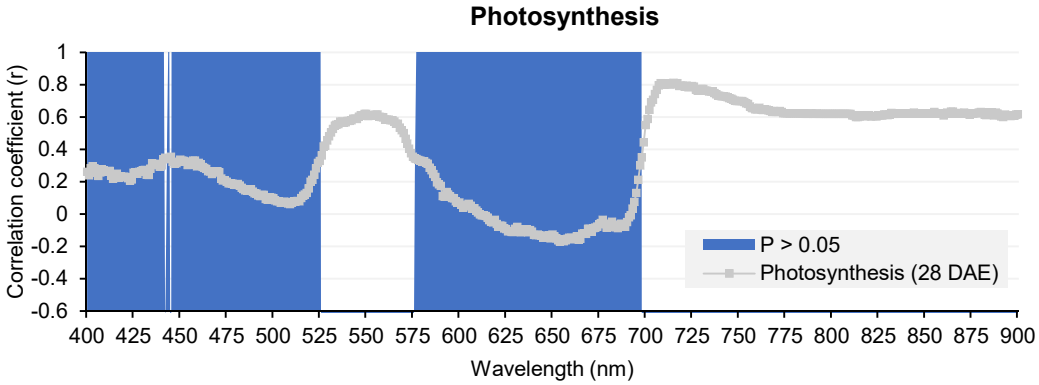

Appendix 4-4. Correlation between photosynthesis and reflectance data at 28 days after the exposure (28 DAE).

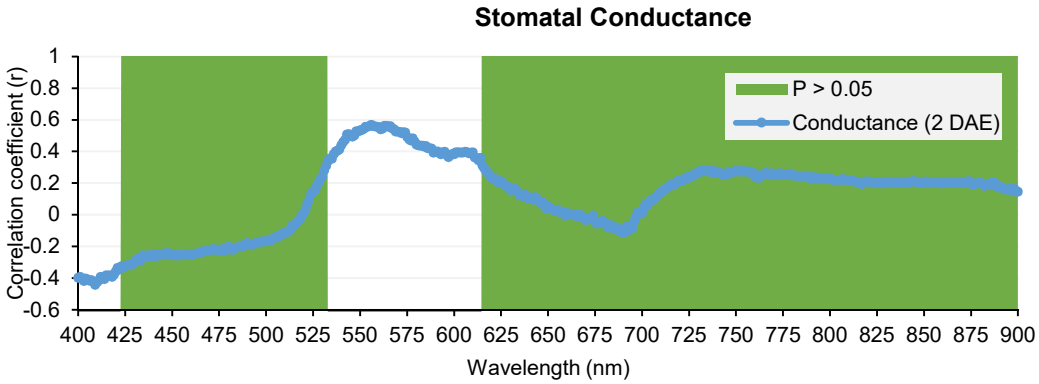

Appendix 4-5. Correlation between stomatal conductance and reflectance data at two days after the exposure (2 DAE).

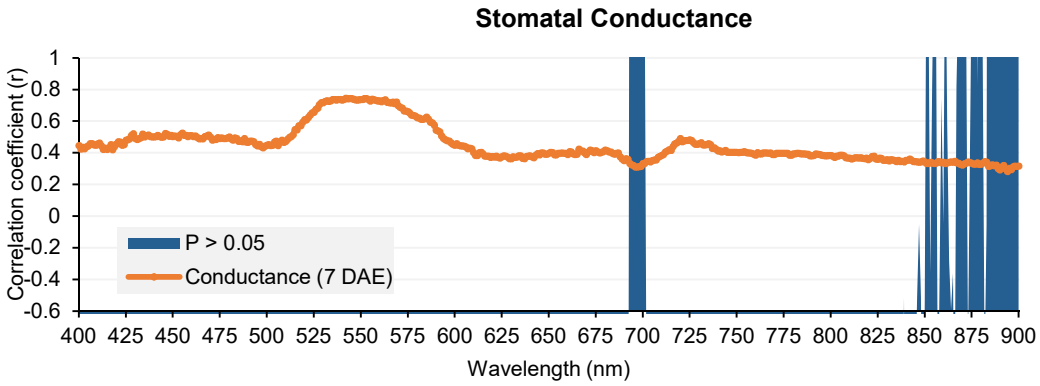

Appendix 4-6. Correlation between stomatal conductance and reflectance data at seven days after the exposure (7 DAE).

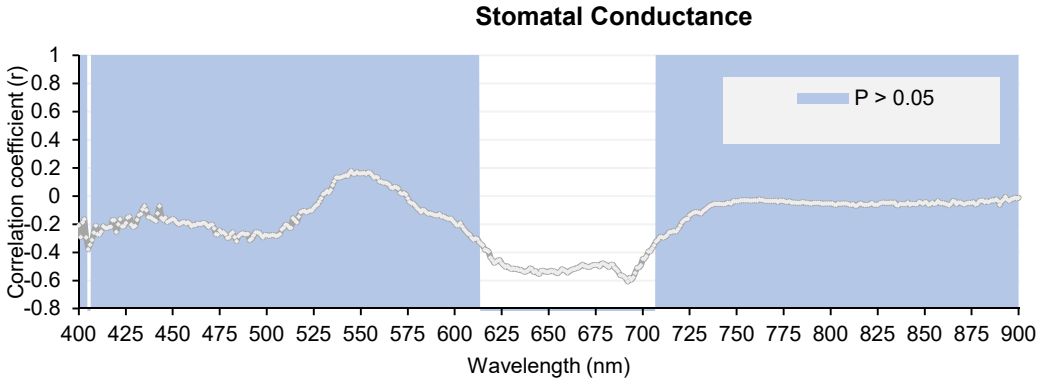

Appendix 4-7. Correlation between stomatal conductance and reflectance data at 14 days after the exposure (14 DAE).

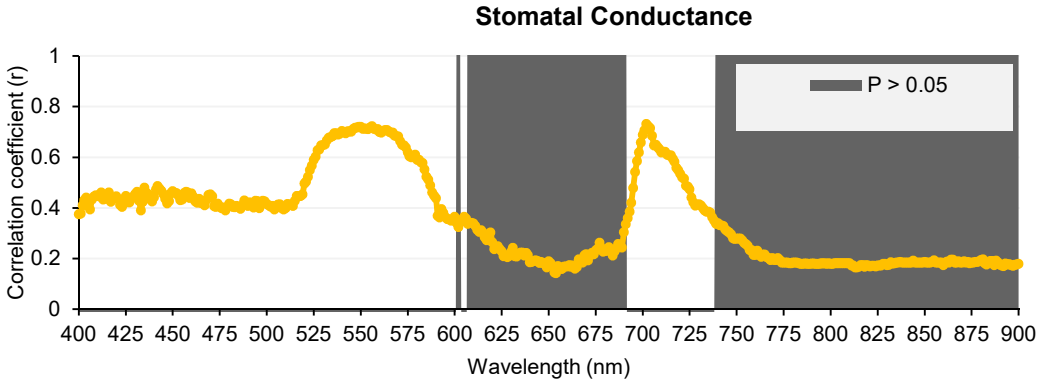

Appendix 4-8. Correlation between stomatal conductance and reflectance data at 28 days after the exposure (28 DAE).

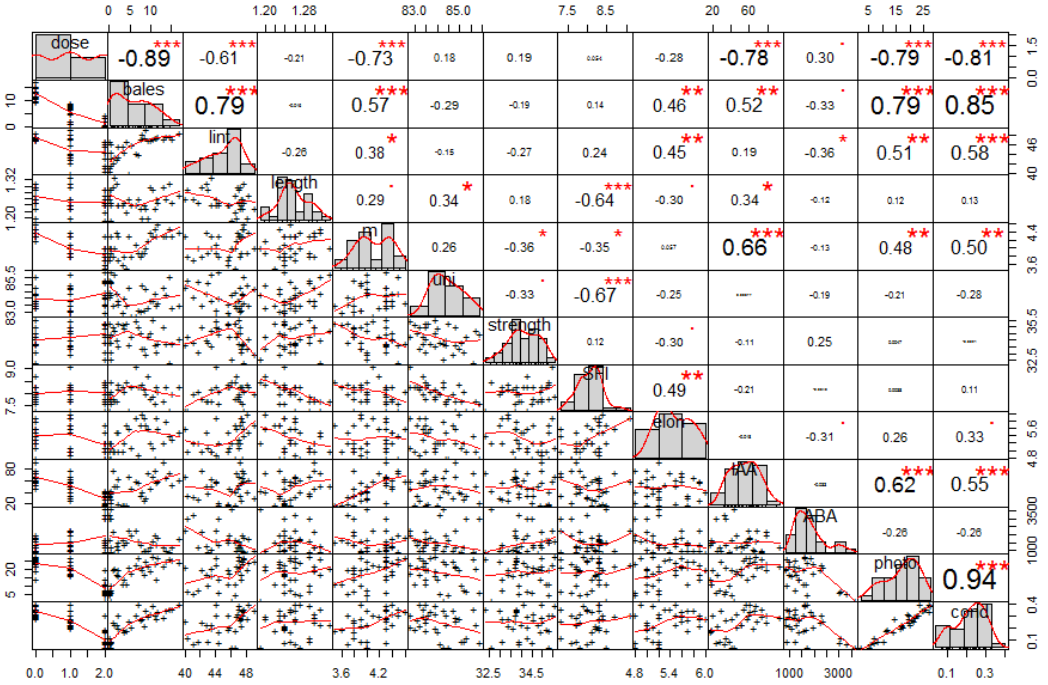

Appendix 4-9. Correlation matrix: dose vs. yield, quality, internal variables and hormone contents.
Dose: Dose; bales: yield (bales/ha); lint: lint turnout percentage, length and strength of fibre, m: micronaire, uni: uniformity; SFI: short fibre index; elon: elongation; photo: photosynthesis and condu: conductance

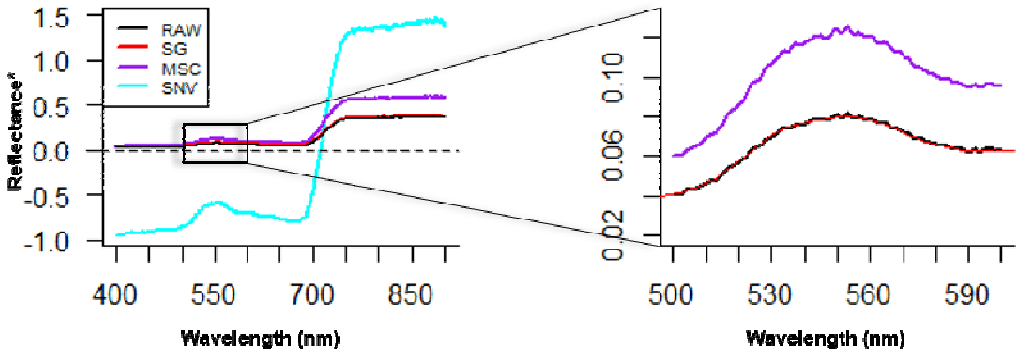

Appendix 4-10. Scatter filters vs. raw spectral data.
Raw spectra (RAW); multiplicative scatter correction (MSC); standard normal variation (SNV); Savitzky-Golay (SG).
* Transformed reflectance for MSC and SNV.

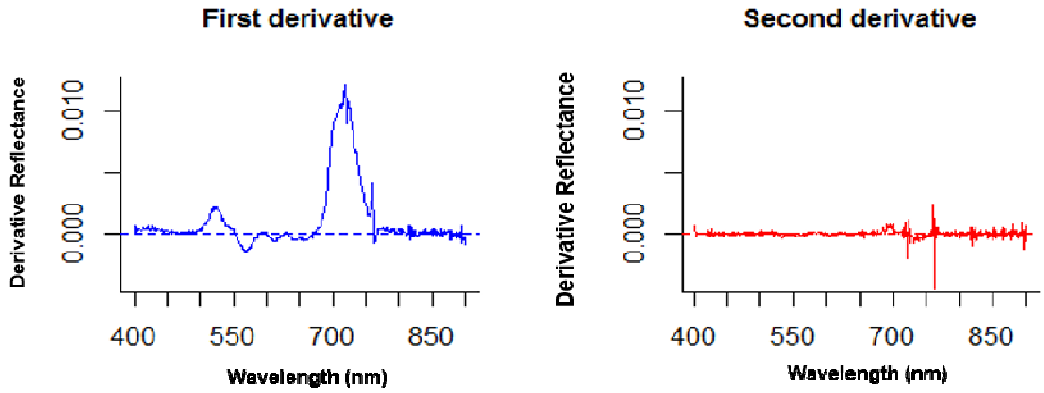

Appendix Error! No text of specified style in document.**-1. Reflectance transformation: First and second derivative algorithms.**

ISPRS Journal of Photogrammetry and Remote Sensing 120 (2016) 65–76

Contents lists available at ScienceDirect

ISPRS Journal of Photogrammetry and Remote Sensing

journal homepage: www.elsevier.com/locate/isprsjprs

Hyperspectral sensing to detect the impact of herbicide drift on cotton growth and yield

L.A. Suarez [a,*], A. Apan [b], J. Werth [c]

[a] International Centre for Applied Climate Sciences, University of Southern Queensland, Toowoomba, QLD 4350, Australia
[b] School of Civil Engineering and Surveying, University of Southern Queensland, Toowoomba, QLD 4350, Australia
[c] Agri-Science Queensland, Department of Agriculture and Fisheries, Leslie Research Centre, 13 Holberton St. PO Box 2282, Toowoomba, QLD 4350, Australia

ARTICLE INFO

Article history:
Received 12 April 2016
Received in revised form 12 August 2016
Accepted 15 August 2016

Keywords:
Cotton
PLS-R
Hyperspectral data
Herbicide drift
Yield

ABSTRACT

Yield loss in crops is often associated with plant disease or external factors such as environment, water supply and nutrient availability. Improper agricultural practices can also introduce risks into the equation. Herbicide drift can be a combination of improper practices and environmental conditions which can create a potential yield loss. As traditional assessment of plant damage is often imprecise and time consuming, the ability of remote and proximal sensing techniques to monitor various bio-chemical alterations in the plant may offer a faster, non-destructive and reliable approach to predict yield loss caused by herbicide drift. This paper examines the prediction capabilities of partial least squares regression (PLS-R) models for estimating yield. Models were constructed with hyperspectral data of a cotton crop sprayed with three simulated doses of the phenoxy herbicide 2,4-D at three different growth stages. Fibre quality, photosynthesis, conductance, and two main hormones, indole acetic acid (IAA) and abscisic acid (ABA) were also analysed. Except for fibre quality and ABA, Spearman correlations have shown that these variables were highly affected by the chemical. Four PLS-R models for predicting yield were developed according to four timings of data collection: 2, 7, 14 and 28 days after the exposure (DAE). As indicated by the model performance, the analysis revealed that 7 DAE was the best time for data collection purposes (RMSEP = 2.6 and R^2 = 0.88), followed by 28 DAE (RMSEP = 3.2 and R^2 = 0.84). In summary, the results of this study show that it is possible to accurately predict yield after a simulated herbicide drift of 2,4-D on a cotton crop, through the analysis of hyperspectral data, thereby providing a reliable, effective and non-destructive alternative based on the internal response of the cotton leaves.

1. Introduction

Cotton crops are one of the most highly susceptible crops to phenoxy herbicides, in particular to the herbicide 2,4-D. Even with genetic modifications, it has not been possible to avoid yield loss caused by the off-target movement of the active ingredients (Charles et al., 2007). Although resistance to damage has been demonstrated, it is naive to believe that cotton crops would not be affected by this herbicide when the extent of injury depends upon the climate and proximity to thousands of cereal and fallow fields where 2,4-D is sprayed to control broad-leaved weeds (Bondada, 2011). Significant inconsistencies in the traditional assessment of damage have been proven in several studies (Everitt and Keeling, 2009), however a more precise technique for prediction of cotton yield loss has not been tested. This limitation prevents the farmers to optimise management practices and mitigate losses.

The phenoxy herbicide 2,4-D is a selective synthetic auxin which causes an uncontrolled production of simulated Indole Acetic Acid (IAA) in broadleaf plants (Bondada, 2011). IAA is considered as a master hormone because it influences every aspect of plant growth and development (Grossmann, 2010). When applied as herbicide, synthetic auxins mimic the deformation and growth-inhibiting effects caused by IAA at a very constant concentration until the growth causes plant death. In contrast, the phytohormone Abscisic Acid (ABA) is important in the adjustment to environmental stress, seed development and dormancy (Straub et al., 1994). The biosynthesis of ABA is over-stimulated by herbicide 2,4-D causing growth inhibitors, morphological abnormalities and senescence (Teixeira et al., 2007).

* Corresponding author.
E-mail address: Luz.suarezcadavid@usq.edu.au (L.A. Suarez).

http://dx.doi.org/10.1016/j.isprsjprs.2016.08.004
0924-2716/

Appendix 4-12. First journal paper published as part of this research study.

INTERNATIONAL JOURNAL OF REMOTE SENSING, 2017
VOL. 38, NO. 23, 6528–6553
https://doi.org/10.1080/01431161.2017.1362128

Detection of phenoxy herbicide dosage in cotton crops through the analysis of hyperspectral data

L. A. Suarez [a,b], A. Apan[c] and J. Werth[d]

[a]International Centre for Applied Climate Sciences, University of Southern Queensland, Toowoomba, Australia; [b]Agricultural Remote Sensing Team, Precision Agriculture Research Group, University of New England, Armidale, Australia; [c]School of Civil Engineering and Surveying, University of Southern Queensland, Toowoomba, Australia; [d]Agri-Science Queensland, Department of Agriculture and Fisheries, Leslie Research Centre, Toowoomba, Australia

ABSTRACT

Although herbicide drifts are known worldwide and recognized as one of the major risks for crop security in the agriculture sector, the traditional assessment of damage in cotton crops caused by herbicide drifts has several limitations. The aim of this study was to assess proximal sensor and modelling techniques in the detection of phenoxy herbicide dosage in cotton crops. *In situ* hyperspectral data (400–900 nm) were collected at four different times after ground-based spraying of cotton crops in a factorial randomized complete block experimental design with dose and timing of exposure as factors. Three chemical doses: nil, 5% and 50% of the recommended label rate of the herbicide 2,4-D were applied to cotton plants at specific growth stages (i.e. 4–5 nodes, 7–8 nodes and 11–12 nodes). Results have shown that yield had a significant correlation (p-values <0.05) to the green peak (~550 nm) and NIR range, as the pigment and cell internal structure of the plants are key for the assessment of damage. Prediction models integrating raw spectral data for the prediction of dose have performed well with classification accuracy higher than 80% in most cases. Visible and NIR range were significant in the classification. However, the inclusion of the green band (around 550 nm) increased the classification accuracy by more than 25%. This study shows that hyperspectral sensing has the potential to improve the traditional methods of assessing herbicide drift damage.

ARTICLE HISTORY
Received 16 October 2016
Accepted 18 July 2017

1. Introduction

Crop stress can be caused by water, nitrogen and nutrient availability in the paddock but also can be due to management practices in surrounding farms, such as herbicide drifts. Herbicide drift can be defined as the movement of chemical particles through the air reaching non-target areas (EPA 2015; Al-Khatib 2016). In other words, drifts happen when the herbicide leaves the intended target site and moves to other places (off-target place). However, this definition also includes the movement of particles through the soil by volatilization or erosion. Herbicide drifts can cause damage not only to crops but also to animals, environment and

CONTACT L. A. Suarez luz.suarezcadavid@usq.edu.au International Centre for Applied Climate Sciences, University of Southern Queensland, Toowoomba, QLD4350,Australia

Appendix 4-13. Second journal paper published as part of this research study.

CHAPTER 5

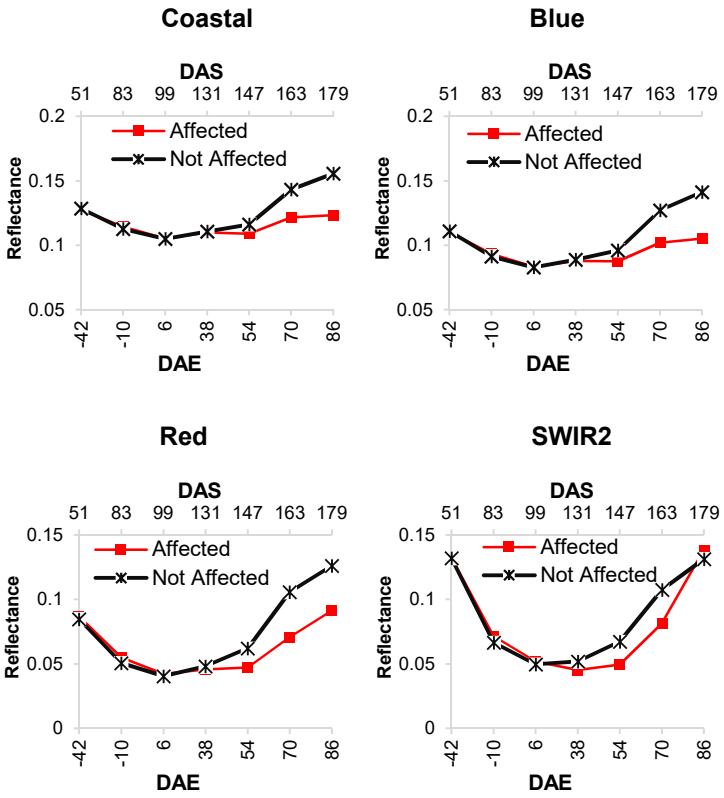

Appendix 5-1. Reflectance variability through time in unaffected and affected areas. DAS: days after sowing; DAE: days after exposure

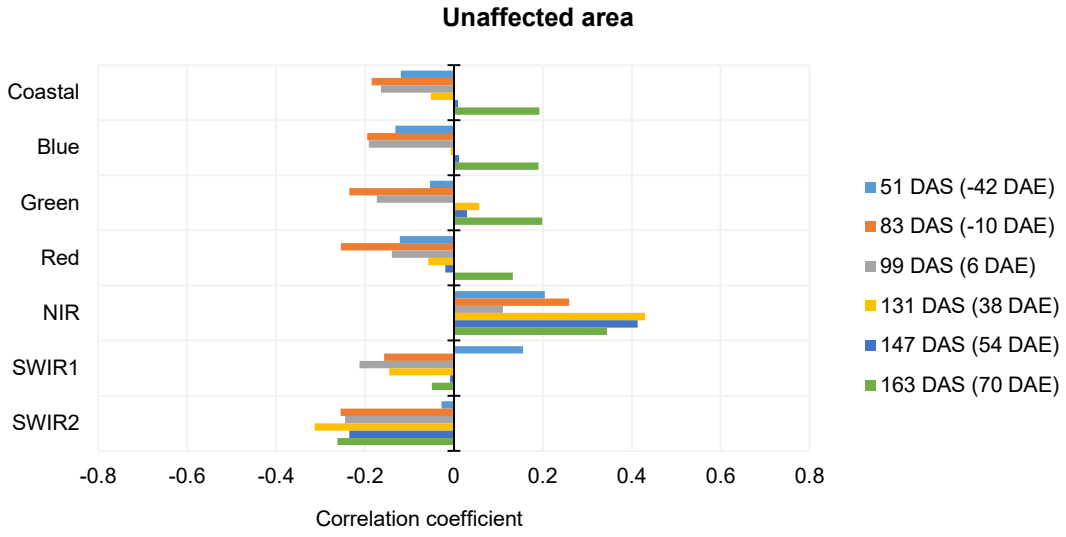

Appendix 5-2. Correlation coefficient variability through time in the unaffected area. Correlation between multispectral bands and yield (bales/ha). DAS = days after sowing; DAE = days after exposure.

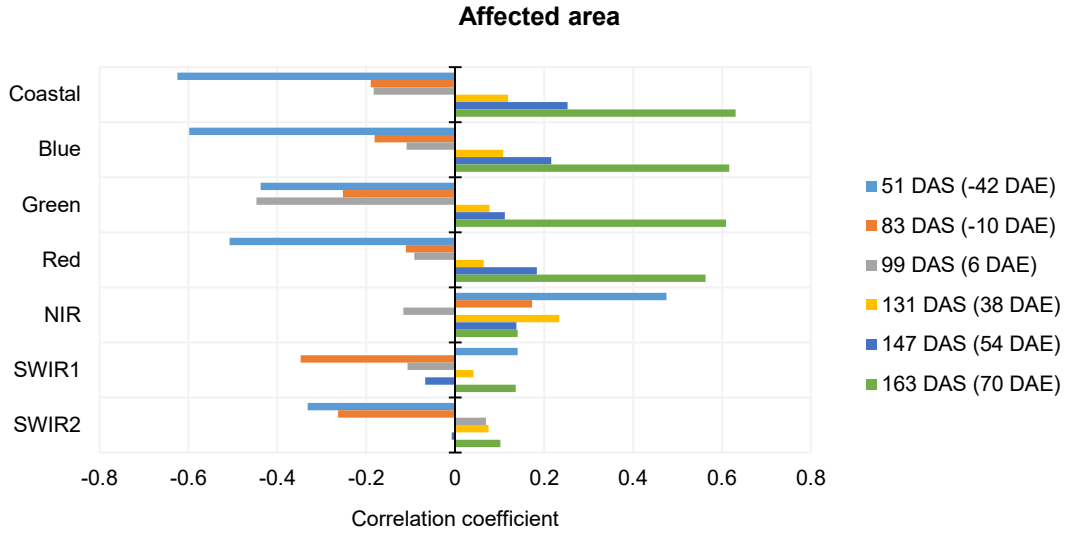

Appendix 5-3. Correlation coefficient variability through time in the affected area. Correlation between multispectral bands and yield (bales/ha). DAS = days after sowing; DAE = days after exposure

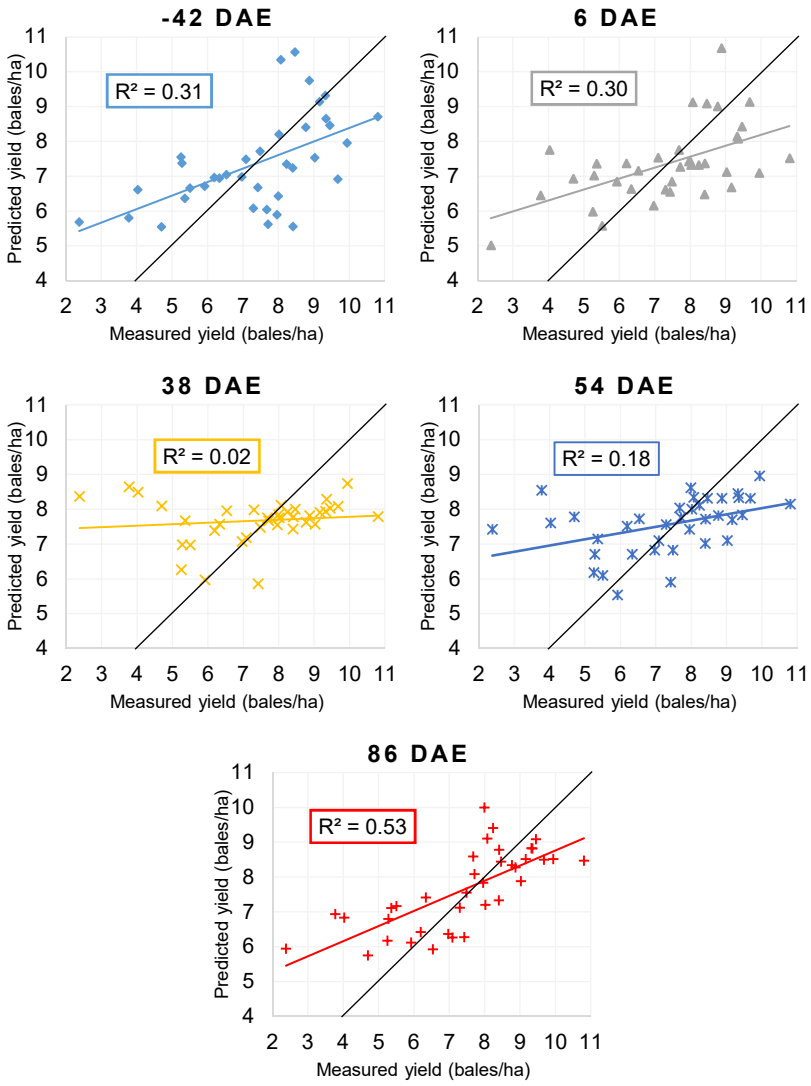

Appendix5-4. Validation performance of PLS-R models with test dataset in the affected area (n = 37). Data collected at -42, 6, 38, 54 and 86 days after the exposure (DAE).